VOLUME 5

Thorax, Abdomen, Blood, Endocrine, and Metabolic Disorders

Atlas of the Newborn

Rudolph

VOLUME 5

Thorax, Abdomen, Blood, Endocrine and Metabolic Disorders

Atlas of the Newborn

Arnold J. Rudolph, M.D.
(1918-1995)
Professor of Pediatrics and
Obstetrics and Gynecology
Baylor College of Medicine
Houston, Texas

VOLUME 5

Thorax, Abdomen, Blood, Endocrine and Metabolic Disorders

Atlas of the Newborn

Arnold J. Rudolph, M.D.
1918-1995

1997
B.C. Decker Inc.
Hamilton • London

B.C. Decker Inc.
4 Hughson Street South
P.O. Box 620, L.C.D. 1
Hamilton, Ontario L8N 3K7
Tel: 905 522-7017
Fax: 905 522-7839
e-mail: info@bcdecker.com

Printed in Canada

97 98 99 00/BP/9 8 7 6 5 4 3 2 1

ISBN 1-55009-035-6

Sales and distribution

United States
Blackwell Science Inc.
Commerce Place
350 Main Street
Malden, MA 02148
U.S.A.
Tel: 1-800-215-1000

U.K., Europe, Scandinavia, Middle East
Blackwell Science Ltd.
c/o Marston Book Services Ltd.
P.O. Box 87
Oxford OX2 0DT
England
Tel: 44-1865-79115

Canada
Copp Clark Ltd.
200 Adelaide Street West
3rd Floor
Toronto, Ontario
Canada M5H 1W7
Tel: 1-800-815-9417

Australia
Blackwell Science Pty, Ltd.
54 University Street
Carleton, Victoria 3053
Australia
Tel: 03 9347 0300
Fax: 03 9349 3016

Japan
Igaku-Shoin Ltd.
Tokyo International P.O. Box 5063
1-28-36 Hongo, Bunkyo-ku
Tokyo 113, Japan
Tel: 3 3817 5680
Fax: 3 3815 7805

India
Jaypee Bros. Medical Publishers (PUT) Ltd.
B-3 EMCA House, 23/23B Ansari Road
Daryaganj
P.B. 7193, New Delhi, -11002 India
Tel: 327 2143, 328 2021
Fax: 327 6490

Foreword

Sir William Osler stated, "There is no more difficult task in medicine than the art of observation." The late Arnold Jack Rudolph was an internationally renowned neonatologist, a teacher's teacher, and, above all, one who constantly reminded us about how much could be learned by simply observing, in his case, the newborn infant.

This color atlas of neonatology represents a distillation of more than 50 years of observing normal and abnormal newborn infants. The *Atlas* begins with a section on the placenta, its membranes, and the umbilical cord. Jack Rudolph delighted in giving a lecture entitled "Don't Make Mirth of the Afterbirth," in which he captivated audiences by showing them how much you could learn about the newborn infant from simply observing the placenta, its membranes, and the umbilical cord.

In a few more than 60 photomicrographs, we learn to read the placenta and gain insight into such disorders as intrauterine growth retardation, omphalitis, cytomegalic inclusion disease, congenital syphilis, and congenital neuroblastoma. Congenital abnormalities of every organ system are depicted along with the appearance of newborn infants who have been subjected in utero to a variety of different drugs, toxins, or chemicals. We also learn to appreciate the manifestations of birth trauma and abnormalities caused by abnormal intrauterine positioning.

More than 250 photographs are used to illustrate the field of neonatal dermatology. The collection of photographs used in this section is superior to that which I have seen in any other textbook or atlas of neonatology or dermatology; this section alone makes this reference a required addition to the library of any clinician interested in the care of infants and children. Photographs of the Kasabach-Merritt syndrome (cavernous hemangioma with thrombocytopenia), Klippel-Trénaunay syndrome, Turner's syndrome, Waardenburg's syndrome, neurocutaneous melanosis, mastocytosis (urticaria pigmentosa), and incontinentia pigmenti (Bloch-Sulzberger syndrome) are among the best that I have seen.

Cutaneous manifestations are associated with many perinatal infections. The varied manifestations of staphylococcal infection of the newborn are depicted vividly in photomicrographs of furunculosis, pyoderma, bullous impetigo, abscesses, parotitis, dacryocystitis, inastitis, cellulitis, omphalitis, and funisitis. Streptococcal cellulitis, *Haemophilus influenzae* cellulitis, and cutaneous manifestations of listeriosis all are depicted. There are numerous photomicrographs of congenital syphilis, showing the typical peripheral desquamative rash on the palms and soles, as well as other potential skin manifestations of congenital syphilis which may produce either vesicular, bullous, or ulcerative lesions. The various radiologic manifestations of congenital syphilis, including pneumonia alba, ascites, growth arrest lines, Wegner's sign, periostitis, and syphilitic osteochondritis, are depicted. Periostitis of the clavicle (Higouménaki's sign) is shown in a photograph that also depicts periostitis of the ribs. A beautiful photomicrograph of Wimberger's sign also has been included; this sign, which may appear in an infant with congenital syphilis, reveals radiolucency due to erosion of the medial aspect of the proximal tibial metaphysis.

The *Atlas* also includes a beautiful set of photographs which delineate the ophthalmologic examination of the newborn. Lesions which may result from trauma, infection, or congenital abnormalities are included. There are numerous photographs of the ocular manifestations of a variety of systemic diseases, such as Tay-Sachs disease, tuberous sclerosis, tyrosinase deficiency, and many more.

Photographs of disturbances of each of the various organ systems, or disorders affecting such organ systems, also are included along with numerous photographs of different forms of dwarfism, nonchromosomal syndromes and associations, and chromosomal disorders. In short, this *Atlas* is the complete visual textbook of neonatology and will provide any physician, nurse, or student with a distillation of 50 years of neonatal experience as viewed through the eyes of a master clinician.

Arnold Jack Rudolph was born in 1918, grew up in South Africa, and graduated from the Witwatersrand Medical School in 1940. Following residency training in pediatrics at the Transvaal Memorial Hospital for Children, he entered private pediatric practice in Johannesburg, South Africa. After almost a decade, he left South Africa and moved to Boston, where he served as a Senior Assistant Resident in Medicine at the Children's Medical Center in Boston, Massachusetts, and subsequently pursued fellowship training in neonatology at the same institution and at the Boston Lying-In Hospital, Children's Medical Center and Harvard Medical School under Dr. Clement A. Smith.

In 1961, Dr. Rudolph came to Baylor College of Medicine in Houston, Texas, the school at which he spent the remainder of his career. He was a master teacher, who received the outstanding teacher award from pediatric medical students on so many occasions that he was elected to the Outstanding Faculty Hall of Fame in 1982. Dr. Rudolph also received numerous awards over the years from the pediatric house staffs for his superb teaching skills.

He was the Director of the Newborn Section in the Department of Pediatrics at Baylor College of Medicine for many years, until he voluntarily relinquished that position in 1986 for reasons related to his health. Nevertheless, Jack Rudolph continued to work extraordinarily long hours in the care of the newborn infant, and was at the bedside teaching both students and house staff, as well as his colleagues, on a daily basis until just a few months before his death in July 1995.

Although Dr. Rudolph was the author or co-author of more than 100 published papers that appeared in the peer-reviewed medical literature, his most lasting contribution to neonatology and to pediatrics is in the legacy of the numerous medical students, house staff, fellows, and other colleagues whom he taught incessantly about how much one could learn from simply observing the newborn infant. This *Atlas* is a tour de force; it is a spectacular teaching tool that has been developed, collated, and presented by one of the finest clinical neonatologists in the history of medicine. It is an intensely personal volume that, as Dr. Rudolph himself states, "is not intended to rival standard neonatology texts," but rather to supplement them. This statement reveals Dr. Rudolph's innate modesty, since with the exception of some discussion on pathogenesis and treatment, it surpasses most neonatology texts in the wealth of clinical information that one can derive from viewing and imbibing its contents. We owe Dr. Rudolph and those who aided him in this work a debt of gratitude for making available to the medical community an unparalleled visual reference on the normal and abnormal newborn infant.

Ralph D. Feigin, M.D.
June 13, 1996

Preface

I first became attracted to the idea of producing a color atlas of neonatology many years ago. However, the impetus to synthesize my experience and compile this current collection was inspired by the frequent requests from medical students, pediatric house staff, nurses and others to provide them with a color atlas of the clinical material provided in my "slide shows." For the past few decades I have used the medium of color slides and radiographs as a teaching tool. In these weekly "slide shows" the normal and abnormal, as words never can, are illustrated.

"I cannot define an elephant but I know one when I see one."[1]

The collection of material used has been added to constantly with the support of the pediatric house staff who inform me to "bring your camera" whenever they see an unusual clinical finding or syndrome in the nurseries.

A thorough routine neonatal examination is the inalienable right of every infant. Most newborn babies are healthy and only a relatively small number may require special care. It is important to have the ability to distinguish normal variations and minor findings from the subtle early signs of problems. The theme that recurs most often is that careful clinical assessment, in the traditional sense, is the prerequisite and the essential foundation for understanding the disorders of the newborn. It requires familiarity with the wide range of normal, as well as dermatologic, cardiac, pulmonary, gastrointestinal, genitourinary, neurologic, and musculoskeletal disorders, genetics and syndromes. A background in general pediatrics and a working knowledge of obstetrics are essential. The general layout of the atlas is based on the above. Diseases are assigned to each section on the basis of the most frequent and obvious presenting sign. It seems probable that the findings depicted will change significantly in the decades to come. In this way duplication has been kept to a minimum. Additional space has been devoted to those areas of neonatal pathology (e.g., examination of the placenta, multiple births and iatrogenesis) which pose particular problems or cause clinical concern.

Obviously, because of limitations of space, it is impossible to be comprehensive and include every rare disorder or syndrome. I have tried to select both typical findings and variations in normal infants and those found in uncommon conditions. Some relevant conditions where individual variations need to be demonstrated are shown in more than one case.

As the present volume is essentially one of my personal experience, it is not intended to rival standard neonatology texts, but is presented as a supplement to them. It seems logical that references should be to standard texts or reviews where discussion on pathogenesis, treatment, and references to original works may be found.

Helen Mintz Hittner, M.D., has been kind enough to contribute the outstanding section on neonatal ophthalmology.

I have done my best to make the necessary acknowledgements to the various sources for the clinical material. If I have inadvertently omitted any of those, I apologize. My most sincere appreciation and thanks to Donna Hamburg, M.D., Kru Ferry, M.D., Michael Gomez, M.D., Virginia Schneider, PA, and Jeff Murray, M.D., who have spent innumerable hours in organizing and culling the material from my large collection. We wish to thank Abraham M. Rudolph, M.D., for his assistance in reviewing the material.

We also wish to thank the following people for their photo contributions to this work: Cirilo Sotelo-Avila, Gerardo Cabrera-Meza, Ed Gonzalez, Vicky Gresik, Claire Langston, Edward Singleton, and Milton Wagner.

It is hoped that this atlas will provide neonatologists, pediatricians, family physicians, medical students and nurses with a basis for recognizing a broad spectrum of normal variations and clinical problems as well as provide them with an overall perspective of neonatology, a field in which there continues to be a rapid acceleration of knowledge and technology. One must bear in mind the caveat that pictures cannot supplant clinical experience in mastering the skill of visual recall.

1. Senile dementia of Alzheimer's type — normal aging or disease? (Editorial) *Lancet* 1989; i:476-477.

Arnold J. Rudolph, M.D.

CONTENTS

Volume 5
Thorax, Abdomen, Blood, Endocrine and Metabolic Disorders

Introduction

Although several texts provide extensive descriptions of the newborn infant, the senses of touch, hearing, and especially sight, create the most lasting impressions. Over a period of almost five decades, my brother Jack Rudolph diligently recorded, in pictorial form, his vast experiences in physical examination of the newborn infant. *Atlas of the Newborn* reflects his selection from the thousands of color slides in his collection. It truly represents the "art of medicine" as applied to neonatology. A number of unusual or rare conditions are included in this atlas. I consider this fully justified, because if one has not seen or heard of a condition, one will never be able to diagnose it.

This fifth volume of the five-volume series covers, in excellent detail, disorders of the cardiorespiratory, gastrointestinal and genitourinary systems, disorders of endocrinology and metabolism, and nutritional disorders. In addition, hematology, jaundice, and oncology are clearly depicted in this volume.

The first chapter of this volume concentrates on disorders of the heart and lungs. It depicts the various factors which cause cyanosis in the neonate, and presents a magnificent collection of radiographs demonstrating specific features of lung disorders peculiar to the newborn infant. Also shown are disturbances of muscle function and bony chest development that may interfere with respiratory function.

The chapters dedicated to the gastrointestinal and genitourinary tracts graphically present both the clinical aspects and the radiological features of numerous congenital anomalies which may occur in these systems. Also included in this chapter are outstanding presentations of the various abnormalities that can affect the male and female genitalia, and ambiguous genitalia.

Although many of the nutritional, hormonal, and metabolic disorders of the newborn are diagnosed by analysis of blood samples, several present with clinical features which are excellently documented in this volume.

Volume V of *Atlas of the Newborn* will be extremely valuable to neonatologists, obstetricians, and nurses involved in perinatal care, and also valuable to pediatric pulmonologists, cardiologists, gastroenterologists, nephrologists, geneticists and surgeons involved in the care of the newborn infant.

Abraham M. Rudolph, M.D.

Chapter 1
Cardiorespiratory System

Following birth, the function of gas exchange is transferred from the placenta to the lungs. Oxygen supply to the newborn infant depends upon the establishment of rhythmic breathing, expansion of the lungs with air, adequate pulmonary blood flow to pick up oxygen from the lungs, and systemic blood flow to transport oxygen to the tissues.

Normal respiration requires that the central and peripheral nervous systems involved in breathing are appropriately developed, that respiratory muscle function, especially of the diaphragm, is normal, and that the bony chest cage is normal both in size and stability. The airways are filled with fluid before birth, and this fluid must be effectively cleared to allow entry of air into the lungs. The presence of pulmonary surfactant is essential to reduce alveolar surface tension and facilitate lung expansion.

Oxygen is predominantly transported in the blood through its attachment to hemoglobin. Hemoglobin deficiency due to blood loss or hemolysis of red cells may thus reduce oxygen transport. Oxygen transport may also be reduced due to hemoglobin abnormalities, such as methemoglobinemia, which impair the oxygen-carrying capacity of the blood.

The proper circulatory pathways must also be established following birth in order to ensure adequate pulmonary blood flow. The normal increase in pulmonary blood flow after birth may be prevented by a failure of pulmonary vascular resistance to fall, as in persistent pulmonary hypertension of the newborn, or in congenital heart disease, where there is an obstruction of systemic venous blood flow into the lungs as occurs in pulmonary atresia. Furthermore, oxygen transport to the tissues may be inadequate because systemic arterial supply is reduced by myocardial failure, or by congenital heart lesions in which left ventricular output is impaired, as with severe aortic stenosis or aortic atresia.

Despite the complexity of these systems, the adaptations to birth usually occur uneventfully. The purpose of the resuscitation team is to prepare for those unusual occasions when the normal transition from intrauterine to extrauterine life does not proceed smoothly.

1.1

Figure 1.1. Acrocyanosis is the blue discoloration of the distal extremities noted in many normal infants, but it can be observed in older babies with cold stress, infection, or heart failure. Peripheral cyanosis of the hands and feet is a common clinical finding in normal infants in the first 24 hours of life, but may be a nonspecific sign of illness. This finding is the result of a combination of high fetal hemoglobin concentrations and relatively sluggish peripheral circulation from arteriolar vasoconstriction. Note that the infant's face, lips, and trunk appear pink. Spontaneous improvement always occurs. Gentle stroking induces a rapid vasomotor reaction resulting in the sudden dispersal of peripheral cyanosis.

1.2

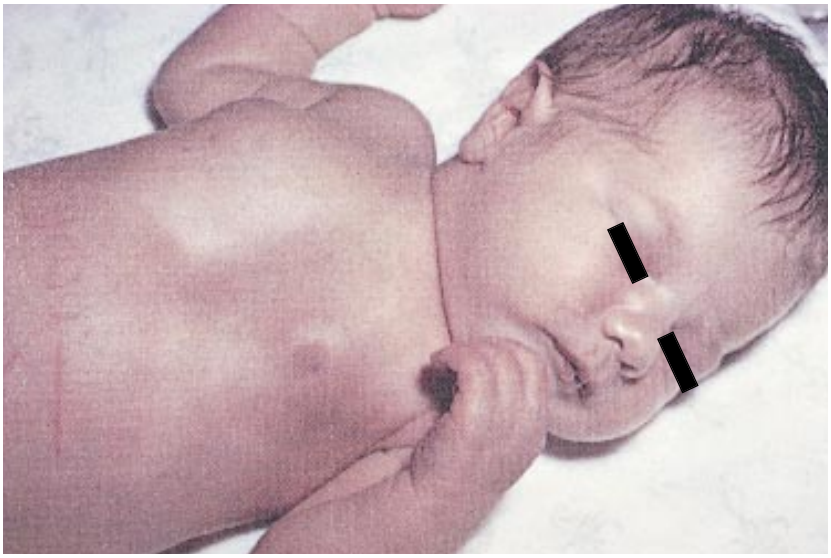

Figure 1.2. This infant's trunk, face and extremities are cyanotic, indicating a reduced hemoglobin oxygen content of at least 5 g/dL. Cyanosis is easier to detect in infants with polycythemia than in those with anemia, although oxygen saturation may be higher in the former and reduced in the latter.

1.3

Figure 1.3. Methemoglobinemia is a condition which results in oxidized iron in hemoglobin being rendered unable to carry oxygen. Though the partial pressure of oxygen may be normal, oxygen content is low. Compare the color of the normal infant on the left with the typical slate grey color of the methemoglobinemic infant on the right. Distress may not be evident in infants until methemoglobin is 50% of the total hemoglobin. Methemoglobinemia is most commonly caused by postnatal exposure to toxins, such as nitrates or aniline dyes, but can also be congenital.

1.4

Figure 1.4. Methemoglobinemia occurred in this infant after the administration of intravenous nitrofurantoin. Methemoglobin was 45% of the total hemoglobin, resulting in the slate grey color. Poor oxygen delivery can lead to severe metabolic acidosis. Treatment is intravenous methylene blue or ascorbic acid.

1.5

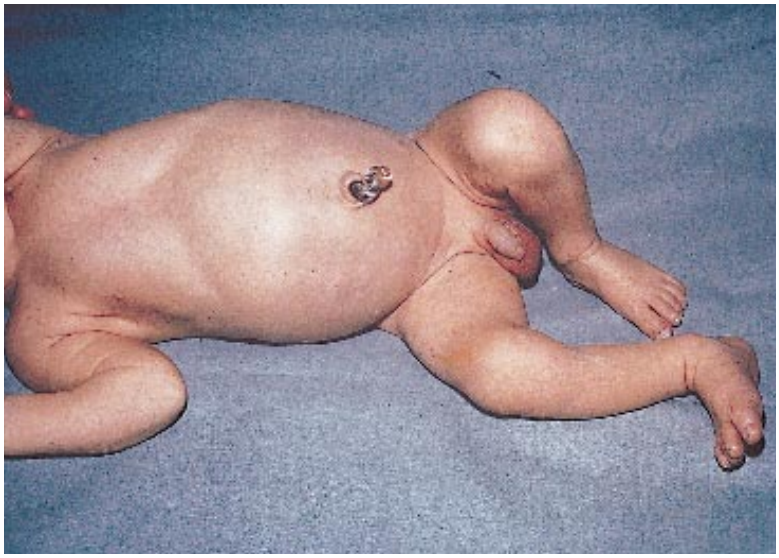

Figure 1.5. Differential cyanosis in an infant with congenital heart disease. Note the line of demarcation in the midabdomen showing the pink body proximally and the cyanosis distally (this infant had pink hands and blue feet). This occurs in infants with aortic obstruction (coarctation of the aorta, interrupted aorta) with a patent ductus arteriosus supplying the descending aorta.

1.6

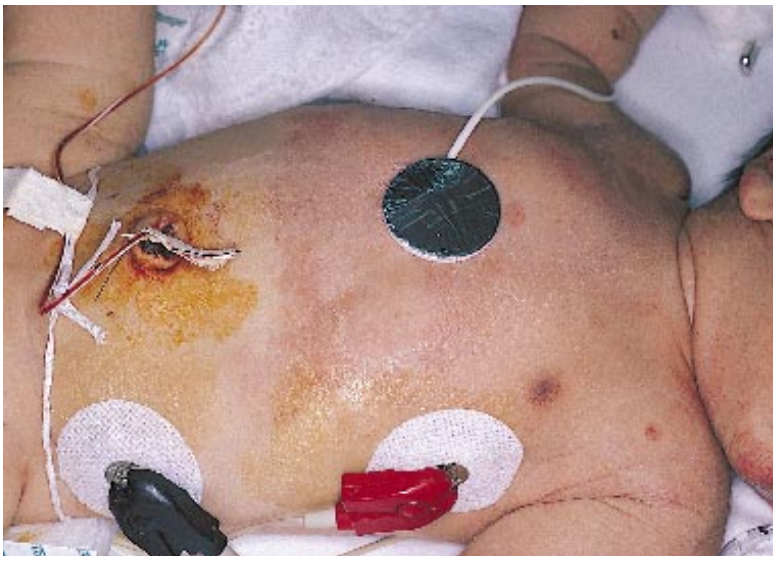

Figure 1.6. Differential cyanosis in an infant with congenital heart disease. Note the demarcation line in the midabdomen, and that the proximal part of the body is cyanotic, but the distal portion is pink (this infant had blue hands and pink feet). In this infant, this was due to aortopulmonary transposition, coarctation of the aorta, patent ductus arteriosus and pulmonary arterial hypertension. Well-oxygenated blood from the pulmonary artery passes through the ductus to the descending aorta, but the ascending aorta receives poorly-oxygenated blood from the right ventricle.

1.7

Figure 1.7. The same infant as in Figure 1.6 showing the differential cyanosis at the mid-abdomen as well as the blue hands and pink feet.

1.8

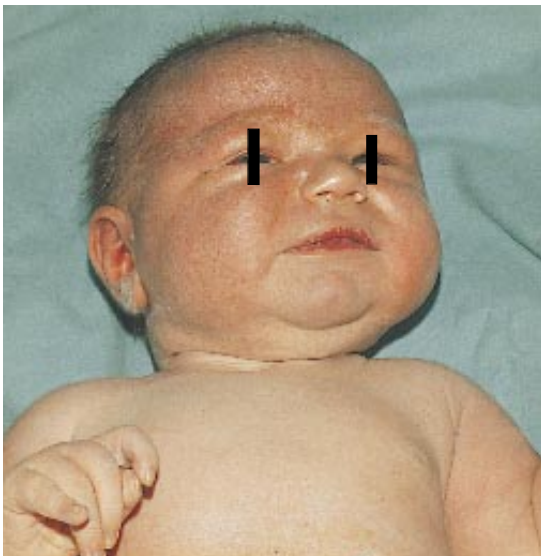

Figure 1.8. This infant developed venous congestion and numerous petechial hemorrhages as a result of a nuchal cord, which is the cause of the red or plethoric face and head. Subconjunctival hemorrhages are also present.

1.9

Figure 1.9. Tight nuchal cords can cause excess venous pressure in the head, and result in the rupture of small capillaries in the face causing petechiae and suffusion. These findings typically resolve spontaneously in a few days.

1.10

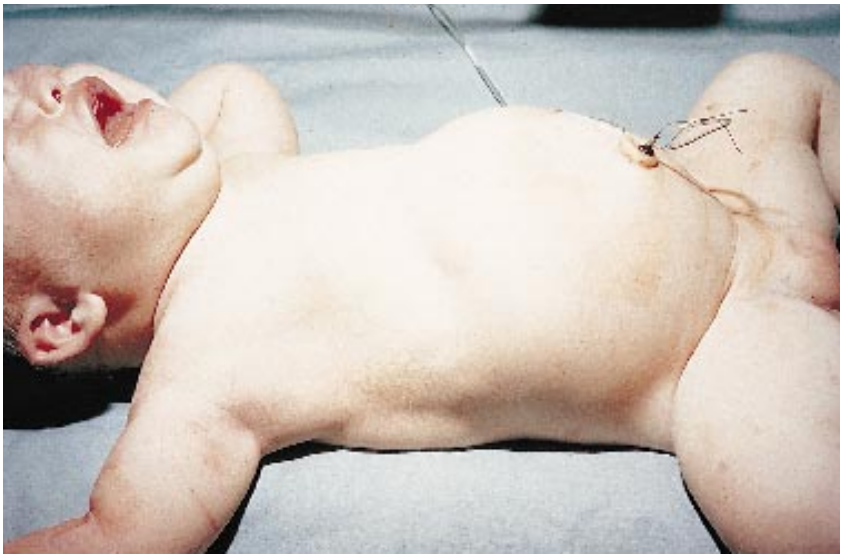

Figure 1.10. Following a difficult breech extraction, there was injury to the spinal cord at C7. This resulted in marked hypotonia (the infant is lying in the "pithed frog" position). Note that the infant is crying, and that a normal infant would usually flex extremities when disturbed. The abdominal distention is due to lack of abdominal muscle tone and an enlarged, paralyzed bladder.

1.11

Figure 1.11. Erb's palsy is the result of trauma to the upper brachial plexus (nerve roots C4–7) at delivery. The infant's left arm is flaccid with the shoulder adducted and the arm internally rotated. The extended elbow follows down to a pronated forearm and flexed wrist. Spontaneous resolution is seen in 70 to 90% of cases within 30 days. Rarely is the injury permanent. Infants with Erb's palsy should have a chest radiograph taken to check for involvement of the ipsilateral diaphragm due to paralysis of the phrenic nerve (C3, 4 and 5).

1.12

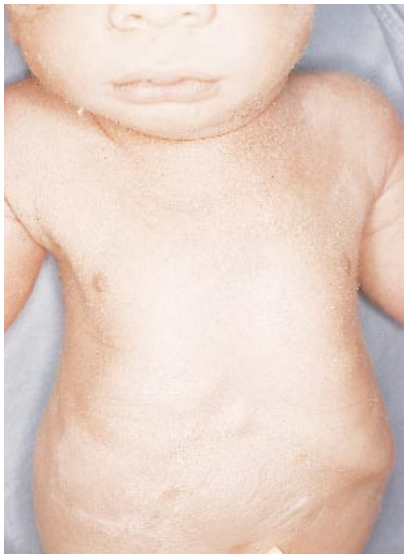

Figure 1.12. Lack of fetal movement in utero can result in positional deformities of the chest wall. Positional deformities, per se, do not cause respiratory distress, but if the changes are due to neuromuscular or osseous problems, respiratory distress may occur.

1.13

Figure 1.13. In the same infant as in Figure 1.12, note how the folded arm compressed the chest causing this change in the chest wall. Decreased fetal movement should alert one to neuromuscular conditions such as spinal muscular atrophy or myotonic dystrophy.

1.14

Figure 1.14. This is an infant with asphyxiating thoracic dystrophy, an autosomal recessive condition which severely restricts chest growth. The congenital deformity of the chest due to the short ribs results in a small chest which limits pulmonary expansion and severely restricts respiration. Because of the small thorax, the whole liver lies in the abdomen, producing the rounded and enlarged appearance seen in this infant.

1.15

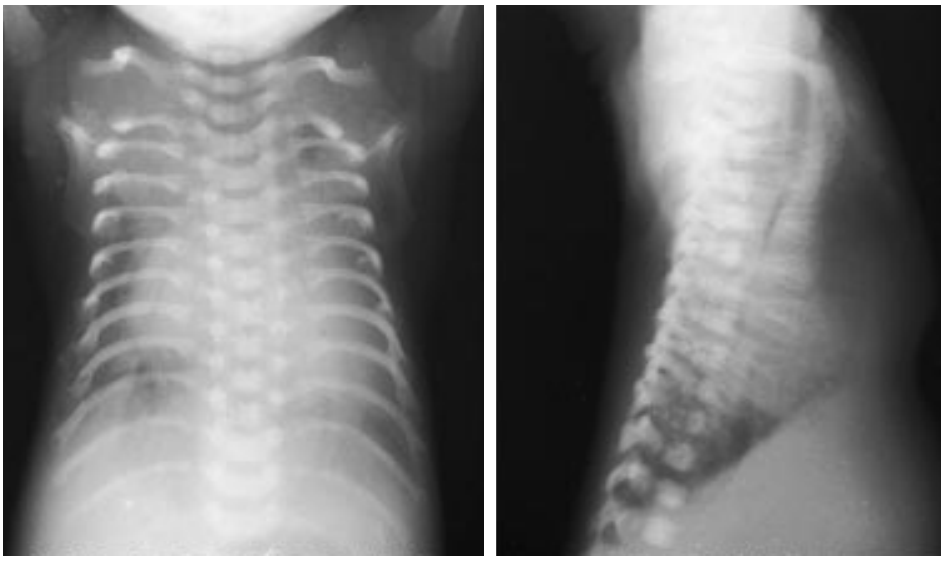

Figure 1.15. In the anteroposterior and lateral radiograph of an infant with asphyxiating thoracic dystrophy, note the thin, abnormally short, straight ribs and small chest wall with protuberant abdomen. This bell-shaped appearance occurs in a variety of conditions because of prenatal weakness of the muscles or a neurologic abnormality.

1.16

Figure 1.16. Nasal obstruction by a glioma in the left nostril caused respiratory distress in this infant. This neural tissue typically comes through the cribriform plate.

1.17

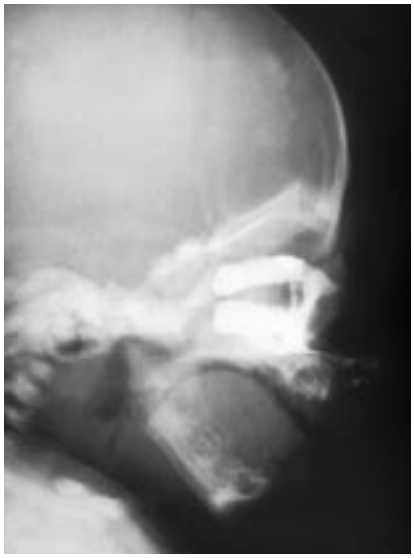

Figure 1.17. Choanal atresia results from blockage of one or both choanae and may present shortly after birth with cyanosis which is relieved when the infant cries. Unilateral choanal atresia may present later in life with the inability to breathe through one side of the nose. Narrowing occurs to some degree within the choanae of many infants. In this radiograph, contrast medium instilled into the nasal cavity did not reach the nasopharynx, indicating obstruction of the choana, most likely from atresia. Atresia is unilateral in 90% of cases (twice as frequent on the right side), and is more common in female infants. Associations occur with facial anomaly syndromes such as Apert's and Treacher-Collins, and with the CHARGE sequence (*c*oloboma, *h*eart disease, *a*tresia of the choanae, *r*etarded postnatal growth and development, *g*enitourinary anomalies, and *e*ar anomalies and deafness).

1.18

Figure 1.18. Macroglossia can result from trauma, hypothyroidism, storage diseases (such as Pompe's), Beckwith-Wiedemann syndrome, hemangiomas, and lymphangiomas, but occurs most often as an idiopathic finding. In the Pierre Robin sequence, the large tongue is exaggerated because of the mandibular hypoplasia.

1.19

Figure 1.19. A lateral radiograph of the head and neck in an infant with Beckwith-Wiedemann syndrome shows the macroglossia which encroaches on the oropharynx with resulting respiratory distress. (Singleton, E., Wagner, M.)

1.20

Figure 1.20. Mandibular hypoplasia, a small underdeveloped mandible, can be an isolated finding or part of a sequence such as Pierre Robin, Treacher-Collins, Hallermann Streiff, or trisomy 18. This may cause severe respiratory distress.

1.21

Figure 1.21. The same infant showing the Pierre Robin sequence: micrognathia, macroglossia, a protruding tongue, and a cleft palate which is often posterior. Cyanosis is often due to the tongue falling back and obstructing the posterior oropharynx. The infant should be managed in a prone position to avoid breathing problems. Micrognathia improves significantly over time.

1.22

Figure 1.22. A lateral radiograph of the head and neck showing mandibular hypoplasia in an infant with trisomy 18. This caused severe respiratory distress because the hypoplastic mandible is associated with narrowing of the nasopharyngeal air passages. (Singleton, E., Wagner, M.)

1.23

Figure 1.23. Congenital goiter is most commonly seen in an infant when there is a history of maternal ingestion of goitrogens such as antithyroid medications or iodides. Goiters can occur endemically in areas with insufficient maternal dietary iodine intake. This neck mass is symmetric about the midline of the neck.

1.24

Figure 1.24. A radiograph of the neck in another infant who developed a very large congenital goiter as a result of maternal use of an iodide-containing medication. It compromised the airway, causing severe respiratory distress.

1.25

Figure 1.25. Cystic hygromas are typically benign unilateral masses in the lateral neck and are lymphatic in origin. They characteristically involve the face and upper trunk. They can occur as an isolated finding or may be associated with Turner's syndrome. The cervical variety can extend into the anterior and middle mediastinum, thus producing respiratory distress.

1.26

Figure 1.26. Transillumination of the cystic hygroma in the same infant as in Figure 1.25 reveals that the hygroma is filled with clear lymphatic fluid.

1.27

Figure 1.27. A branchial cleft cyst is a condition which arises from a persistent cervical sinus or second branchial groove. It is always located along the sternocleidomastoid muscle and is generally painless unless infected. If large, it can cause respiratory distress.

1.28

Figure 1.28. Radiograph of a branchiogenic cyst which is a product of ectopic branchial epithelium. It can be air- or fluid-filled. Enlarging cysts with mucinous secretions can lead to airway compromise. Bronchogenic cysts are most commonly located near the carina.

1.29

Figure 1.29. This anteroposterior radiograph of a normal chest shows the heart on the left, and complete aeration of the lungs with the diaphragm at the level of the 8th intercostal space. The diaphragm of the normal infant is usually rounded smoothly on both frontal and lateral radiographs, and the anterior costophrenic angle is usually quite shallow. The trachea is displaced slightly to the right of the midline by the left aortic arch.

1.30

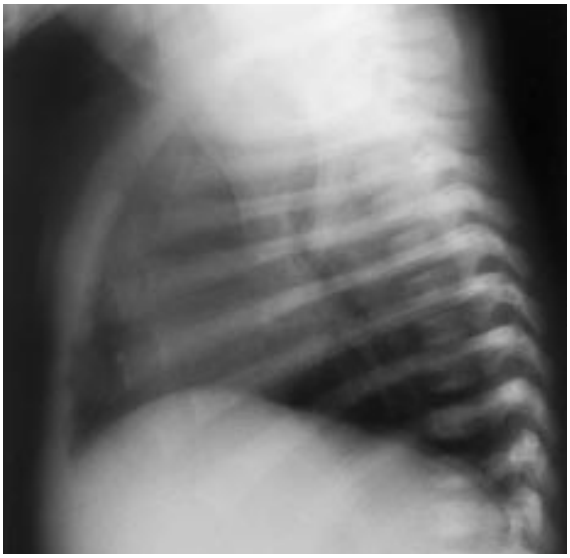

Figure 1.30. A lateral radiograph of a normal chest in an infant showing that the anteroposterior diameter is approximately the same as the thoracic diameter. Note the rounded diaphragm.

1.31

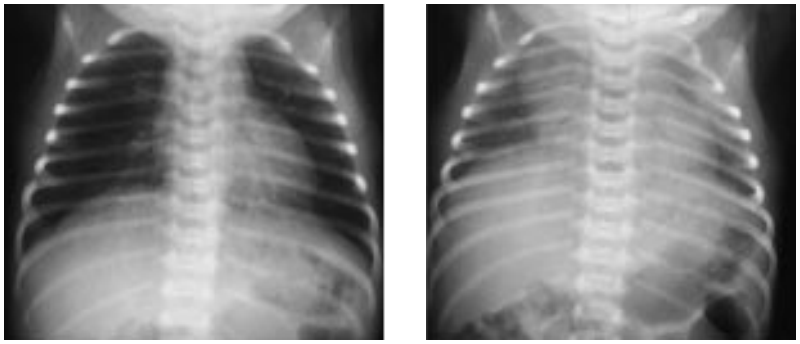

Figure 1.31. Normal chest radiographs of the same infant, showing an inspiratory view on the left and an expiratory view on the right. There can be dramatic differences in chest shape, cardiac and thymic shadow location, and degree of lung expansion, depending on the timing of the exposure. Incomplete aeration of the lungs may simulate pneumonia, and the thymus may appear large. The caliber of the trachea varies with respiration.

1.32

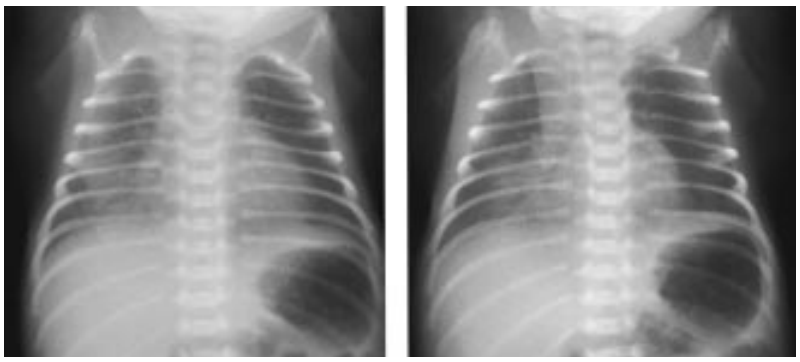

Figure 1.32. Chest radiographs of the same infant as in Figure 1.31 taken in sequence show a skin fold. Note the linear nature of this shadow across the right lung and diaphragm in the view on the left and the normal appearance of the chest in the view on the right. Skin folds should be recognized as normal artifacts and should not be mistaken for pathologic conditions.

1.33

Figure 1.33. This is another example of a skin fold seen on a radiograph of the right chest. Despite the abnormal appearance of the radiograph, the infant was asymptomatic.

1.34

Figure 1.34. The perfect roundness and symmetry of the radiolucent defect in the right hemithorax and diaphragm in this radiograph suggest that this is an artifact created by a hole in the top of the incubator. This is not an uncommon finding when the radiograph is taken through the top of the incubator. (Singleton, E., Wagner, M.)

1.35

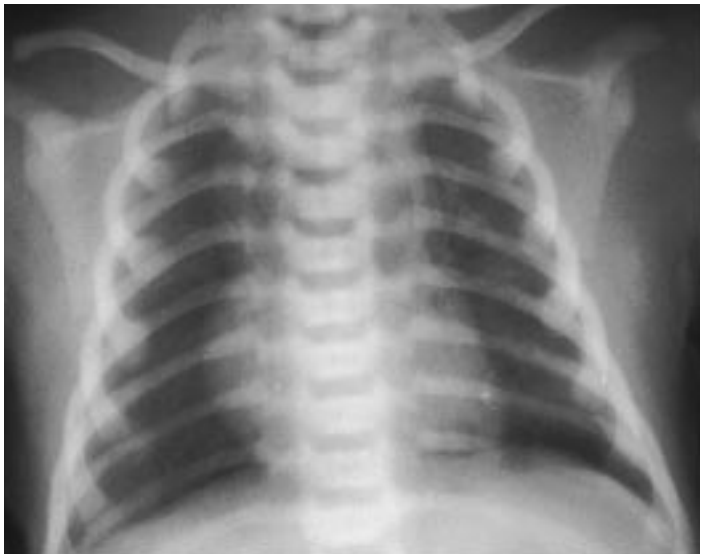

Figure 1.35. This is another example of a chest radiograph showing the "hole" in the incubator. This artifact lies directly over the mediastinum and should not be considered pathologic.

1.36

Figure 1.36. In this chest radiograph there is a symmetric round shadow overlying the mediastinum. This is an artifact caused by a pacifier lying directly on the infant's chest.

1.37

Figure 1.37. Chest radiograph of this infant shows a normal chest, but the scapulae are abnormal and there is amelia of the upper extremities bilaterally. This illustrates the importance of evaluating all osseous structures in any radiograph.

1.38

Figure 1.38. The lack of enamel and tooth buds is noted in this lateral radiograph. This infant had a chest radiograph taken for mild respiratory distress, and when the lack of tooth buds was noted, the diagnosis of ectodermal dysplasia was suspected and later confirmed.

1.39

Figure 1.39. A chest radiograph was taken of this infant with Poland's anomaly to check for any abnormalities of the ribs. Note the increased lucency of the right upper part of the chest and loss of soft tissue shadow caused by the absence of the sternocostal head of the pectoralis muscle. Also note how clearly the scapula can be seen on the right side, also because of the absence of the pectoralis muscle.

1.40

Figure 1.40. A small, bell-shaped thorax is seen in this infant with severe lung hypoplasia. After attempted resuscitation, air leaked into the thoracic and mediastinal spaces. Elevation of the lobes of the thymus created a "butterfly wing" appearance caused by mediastinal air. The abdomen is gasless and the opaque area to the right of the midline above the brim of the pelvis is the umbilical cord. The lung hypoplasia, confirmed at autopsy, occurred as a result of renal agenesis and oligohydramnios.
Difficulty in initiating respiration with minimal chest wall excursion, decreased lung expansion, decreased or absent air entry on auscultation, and persistent cyanosis should alert one to the possibility of lung hypoplasia.

1.41

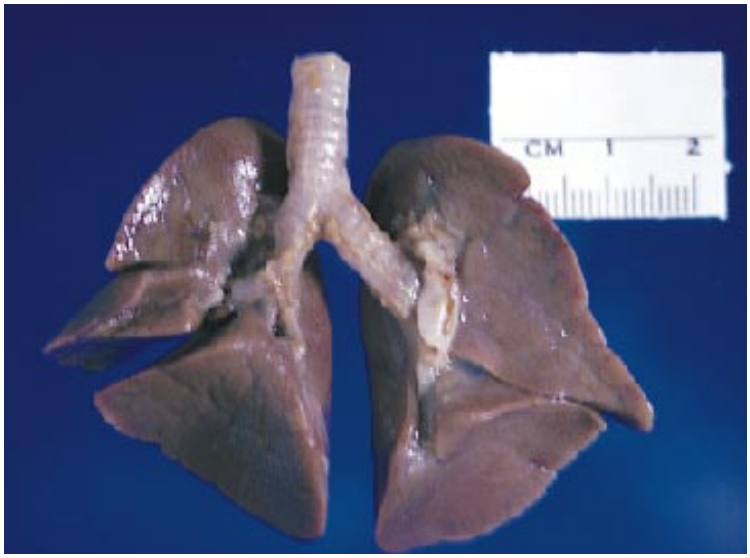

Figure 1.41. The lungs usually comprise 2% of total body weight in infants. This abdominal pregnancy resulted in severe oligohydramnios and severe hypoplasia of the lungs. The lungs weighed only 1% of total body weight in this infant.

1.42

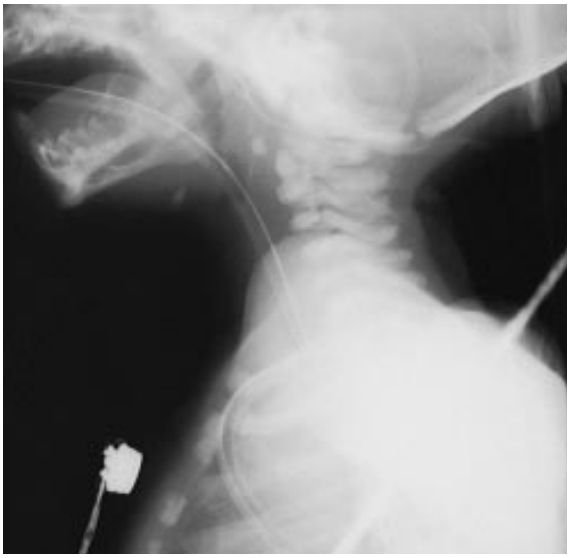

Figure 1.42. Radiograph of the head and neck in an infant with tracheal agenesis. An endotracheal tube could not be passed below the proximal tracheal obstruction. This lethal condition occurs when there is unequal division of the foregut between the esophagus and trachea. Affected infants are usually live-born; they may gasp but cannot introduce air into the lungs. Polyhydramnios is common. The lung architecture below the obstruction is suprisingly normal, and the lungs are typically larger than predicted for age. There may be an associated broncho- or tracheoesophageal fistula. If this is present, the infant may survive for a few hours by exchanging air through the fistula that communicates with the esophagus. Note the tube in the esophagus.

1.43

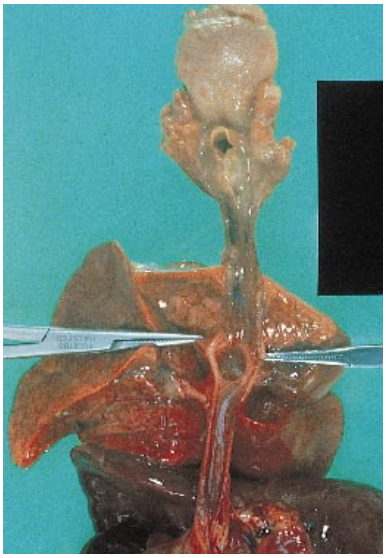

Figure 1.43. In the extremely rare condition of tracheal agenesis, the trachea and esophagus arise from the endoderm of the laryngotracheal tube. Note the communication that abnormally persists between these two structures.

1.44

Figure 1.44. This radiograph depicts a swallowed cuffed endotracheal tube in the stomach. Attempts to resuscitate this infant by endotracheal intubation by the physician in attendance at delivery were unsuccessful. Leaving the tube in place, he called for assistance and the infant was intubated, responding immediately to positive pressure ventilation. In the nursery, attempts to feed the infant resulted in vomiting. This radiograph of the chest was taken and showed the endotracheal tube in the esophagus and stomach. Unbeknownst to the doctors, between attempts at resuscitation, the infant had swallowed the endotracheal tube that had been placed initially in his esophagus. The tube was successfully removed.

1.45

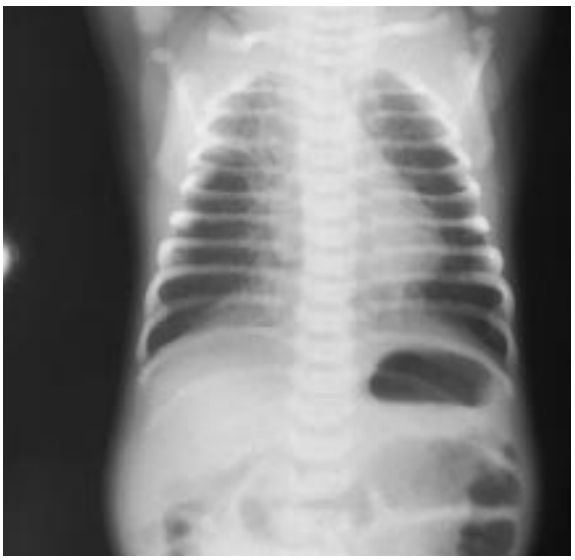

Figure 1.45. This infant presented with respiratory distress, respiratory stridor, and hyperextension of the neck. With these findings, consideration should be given to the diagnosis of vascular ring, which causes compression of the esophagus and trachea. It is most commonly due to a double aortic arch or right aortic arch with a left ductus arteriosus. Dysphagia is not a common presentation in infancy. Rather, it presents with stridor, respiratory distress, and sometimes recurrent pneumonia.

1.46

Figure 1.46. A lateral contrast radiograph of the chest in the same infant demonstrates the indentation of the esophagus by the obstructing vascular ring just below the thoracic inlet. A vascular ring is usually associated with a right-sided or double aortic arch. Usually a right aortic arch exists as an isolated anomaly but it may be associated with congenital heart disease. A double aortic arch which encircles the trachea and esophagus is the type of ring most likely to cause symptoms in early infancy.

1.47

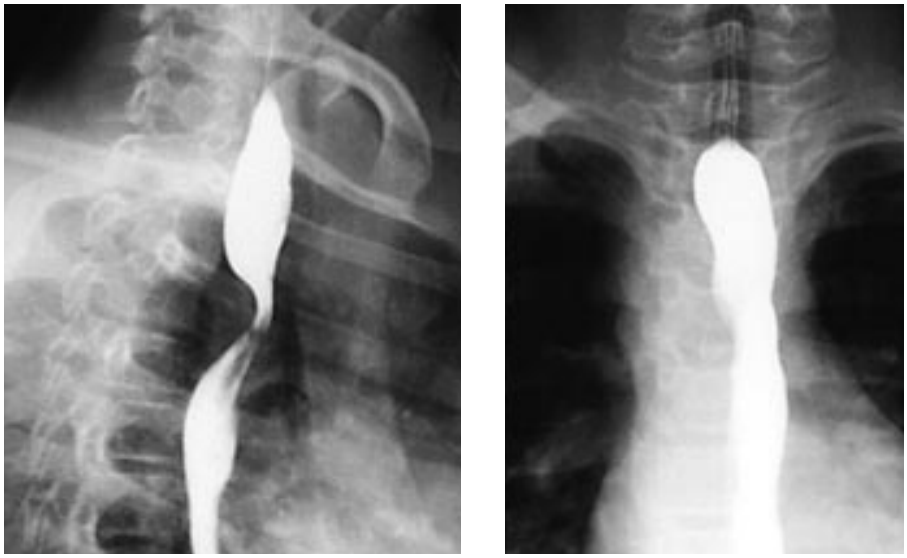

Figure 1.47. Lateral and anteroposterior views of a vascular ring demonstrate how it indents the upper esophagus. The lateral view offers the best opportunity to diagnose this condition. Symptomatic vascular rings should be resected.

1.48

Figure 1.48. In any infant with excess secretions of mucus, the diagnosis of an esophageal atresia with a blind pouch or tracheoesophageal fistula should be considered. Infants may "spit-up" excessive amounts of mucus during normal transition. See this volume, Chapter 2, "Gastrointestinal System," for examples of tracheoesophageal fistulae.

1.49

Figure 1.49. This chest radiograph demonstrates bronchial atresia. The atretic bronchus presents as a fluid-filled density of the area of the left upper lobe of the lung. The absent upper lung is replaced by pleural fluid. (Singleton, E., Wagner, M.)

1.50

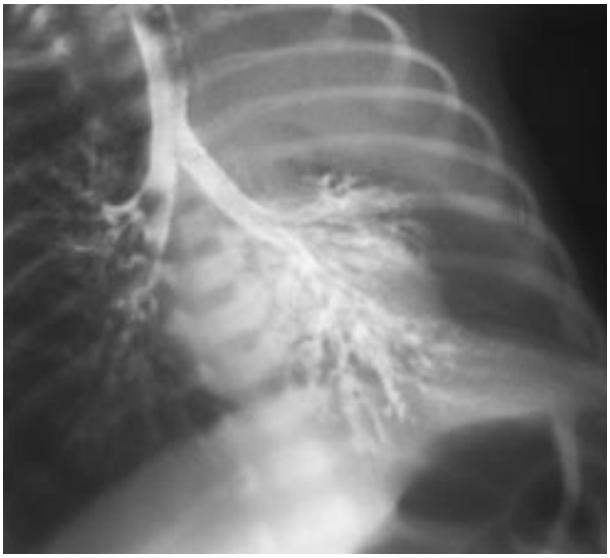

Figure 1.50. Bronchogram of the same infant as in Figure 1.49 demonstrates the normal bronchial segments. Note the normal right lung architecture with three lobes, but only the lower bronchus on the left side. There is an anomalous atretic bronchus with fluid in the lung distal to this. (Singleton, E., Wagner, M.)

1.51

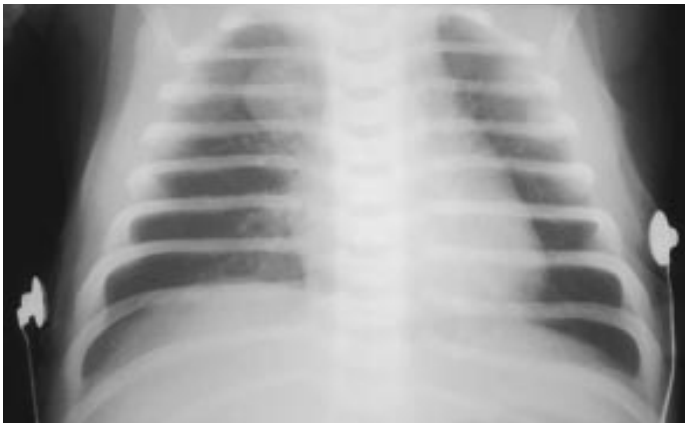

Figure 1.51. Radiograph of the chest shows a bronchogenic cyst on the right side. Such cysts are collections of bronchial epithelial tissue that assume a round, regular appearance. Communication with the large airways can result in spontaneous, intermittent drainage of purulent contents. Congenital bronchogenic cysts arise from abnormal budding of the primitive trachea or abnormal branching of the tracheobronchial tree. They are more common in an area contiguous to the mediastinum, especially in the subcarinal area. If the cyst is completely filled with fluid, it appears as a solid mass.

1.52

Figure 1.52. This chest radiograph demonstrates a lobar sequestration at the right lung base. The infant presented with respiratory distress which did not improve, and the density at the right base remained unchanged. Further work-up was undertaken. In many of these infants, clinical manifestations may not occur early. Pulmonary sequestration is a congenital malformation of the respiratory tract; the sequestered area does not communicate with the normal tracheobronchial tree and has a separate blood supply from systemic arteries. Resection of the sequestered lobe is necessary because it is prone to repeated infection.

1.53

Figure 1.53. Angiography in the same infant as in Figure 1.52 demonstrates the anomalous vascular connection from the aorta to the sequestered lobe of the lung. This is an excellent example of an intralobar sequestration. The sequestered lung segment typically migrates to an improper position in either the chest or abdomen and has an abnormal systemic blood supply from the aorta. Sequestration, especially the more common intralobar type, occurs most often in the lower lobe areas within the normal visceral pleura. The less common extralobar type of lung sequestration, which is accessory lung tissue outside of the normal pleural boundaries, has been reported in nearly every portion of the thorax and even in the upper abdomen.

1.54

Figure 1.54. An angiogram of the same infant as in Figures 1.52 and 1.53 shows the heart on the left with crowding of the pulmonary vessels on the left and the lack of pulmonary vessels in the right lung base. This configuration results in the lack of pulmonary artery blood flow to the right lung base, confirming the diagnosis of sequestration.

1.55

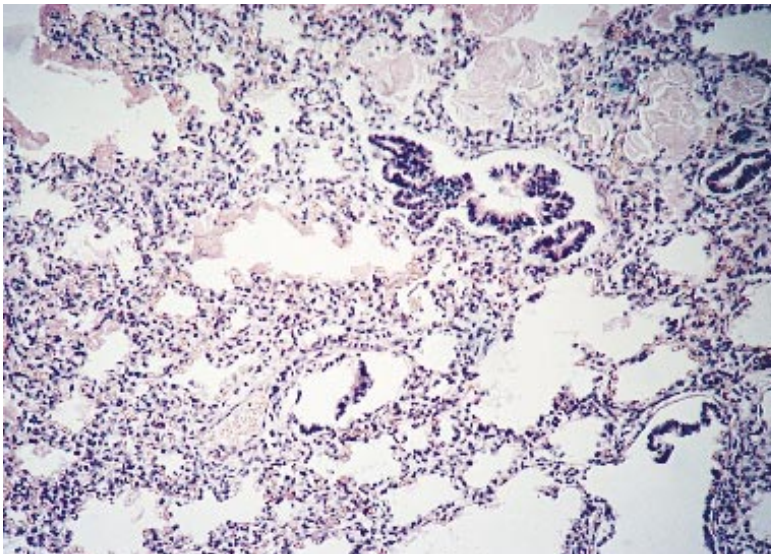

Figure 1.55. In an infant with intralobar sequestration who develops hyaline membrane disease, histologically there is hyaline membrane formation in the nonsequestered lung, but in the sequestered lobe there is no hyaline membrane formation because of its lack of communication with the airway. This photomicrograph shows the hyaline membrane formation in the normal lung, and at the lower right the lack of hyaline membrane in the sequestered lobe. It is possible for partial aeration to occur as a result of fistulous communications with normal lung tissue. This usually occurs following infection.

1.56

Figure 1.56. In this chest radiograph of an infant who presented with severe respiratory distress and congestive heart failure, note the bilateral posterior mediastinal masses and the hyperinflated lungs. These findings are consistent with large airway obstruction from extrapulmonary sequestration.

1.57

Figure 1.57. A contrast study of the chest and abdomen in the same infant as in Figure 1.56 shows that the extrapulmonary sequestration has bronchi originating bilaterally from the esophagus and esophageal bronchi. Both structures have their origin in the tracheoesophageal tube. This anomaly occurs as a result of a congenital foregut malformation.

1.58

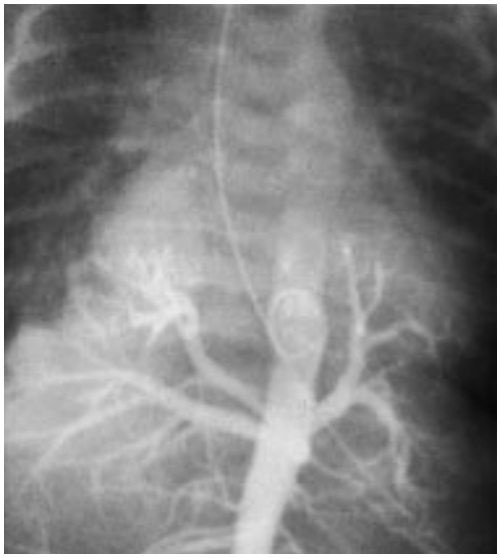

Figure 1.58. An aortogram in the same infant as in Figure 1.56 and 1.57 shows a single systemic artery to the left sequestered lobe and two arteries to the right sequestered lobe.

1.59

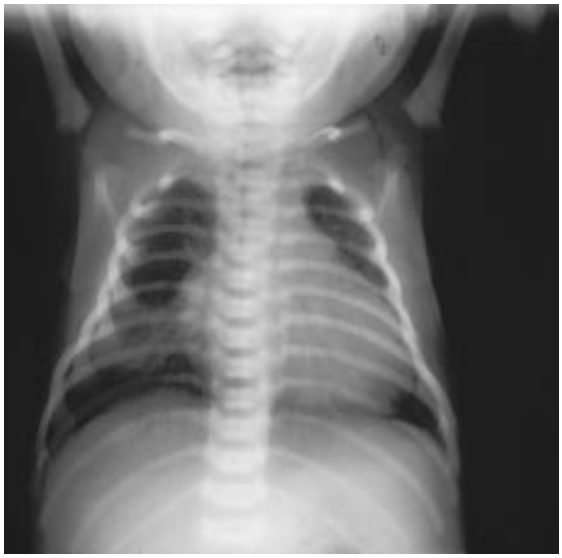

Figure 1.59. In this infant who presented with severe respiratory distress, a radiograph shows a right lower lobe infiltrate which is due to a pulmonary arteriovenous malformation. Congenital pulmonary arteriovenous fistulae may be single or multiple lesions. They present as homogenous densities of variable size and shape and are frequently in continuity with the hilar vascular shadows. They apparently result from persistence of fetal anastamotic capillaries. Frequently there may be associated hemangiomas in other parts of the body.

1.60

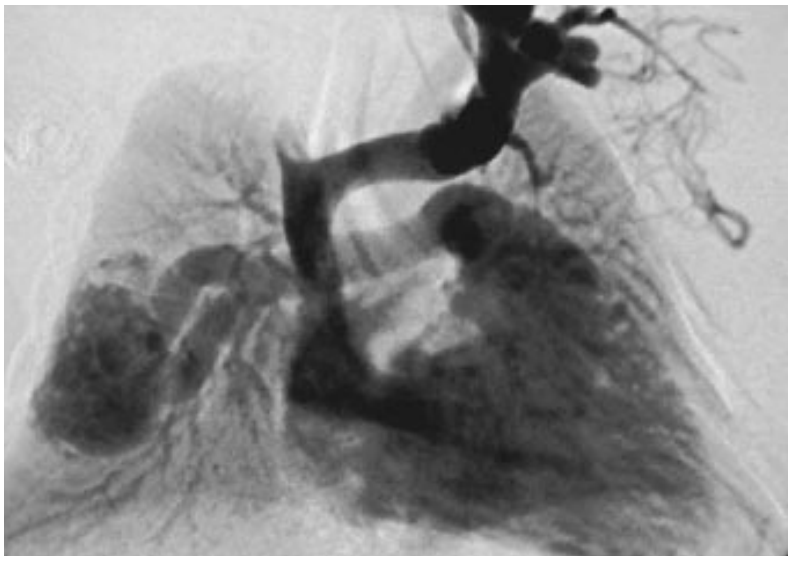

Figure 1.60. Angiography confirms the diagnosis of an arteriovenous malformation of the right lower lobe of the lung. Note the feeder artery from the right pulmonary artery and the direct venous connection going from the malformation into the left atrium. In some of these infants, a continuous bruit may be heard over the site of the arteriovenous malformation.

1.61

Figure 1.61. Congenital lobar emphysema most commonly involves the left upper lobe of the lung (47%). In general, the distribution is slightly greater in the right lung than in the left. The left upper lobe in this infant is hyperinflated and displaces the mediastinum to the right. The left hemithorax is larger than the right, but the absence of increased pulmonary vascular markings on the left and respiratory distress suggests the diagnosis of congenital lobar emphysema. (Singleton, E., Wagner, M.)

1.62

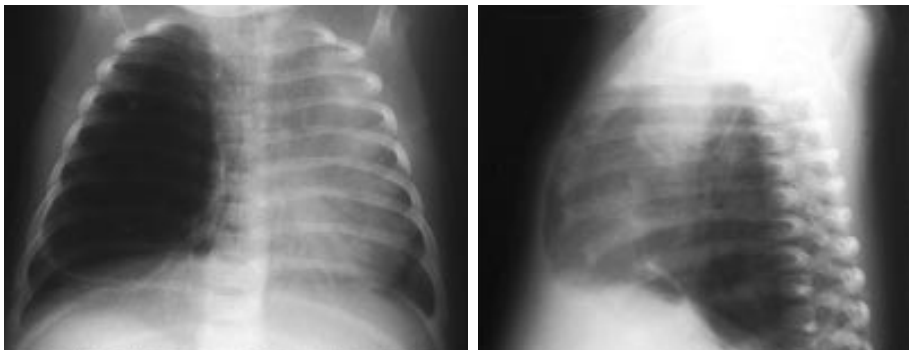

Figure 1.62. Anteroposterior and lateral chest radiographs in an infant with congenital lobar emphysema of the upper lobe of the right lung. Right upper lung lobe involvement occurs in 20% of the cases. Note the hyperinflated right hemithorax with the lack of vascular markings and the displacement of the mediastinum to the left.

1.63

Figure 1.63. At birth, congenital lobar emphysema may present as an opacity due to the presence of retained fetal fluid as noted in this radiograph. When the fluid clears, the typical appearance of lobar emphysema becomes apparent. (Singleton, E., Wagner, M.)

1.64

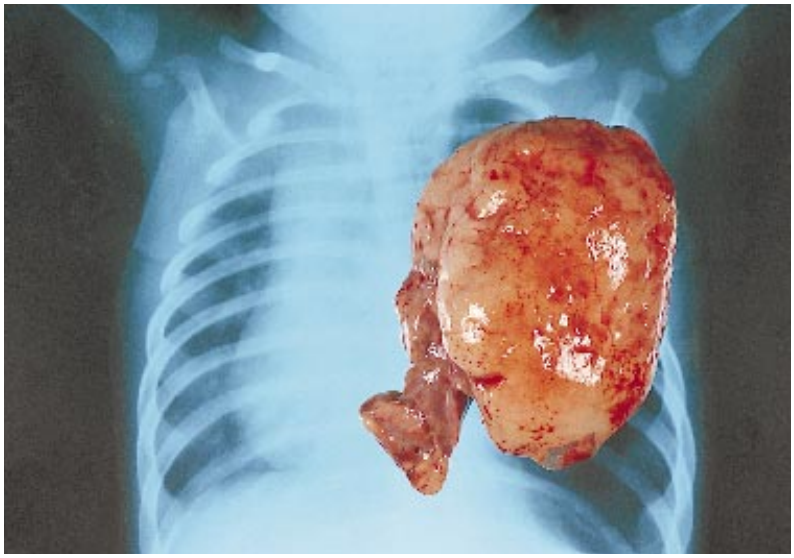

Figure 1.64. The surgical specimen of the emphysematous lobe shows its gross size in comparison to the chest radiograph.

1.65

Figure 1.65. In this infant who presented with mild respiratory distress, note the congenital cyst of the right lung. The cyst has discrete septations, it does not fill the entire hemithorax, and does not appear under pressure as does the lung with lobar emphysema. Many of these infants may be asymptomatic.
Pulmonary cysts are large, thin-walled cysts. They are rare, are more commonly noted in the lung periphery, and probably represent a disorder of bronchial growth at a later stage in fetal life than do the more central bronchogenic cysts.

1.66

Figure 1.66. In infants with congenital cystic adenomatoid malformation of the lung, there may be no or minimal respiratory distress at birth. The respiratory distress becomes progressively worse with gaseous overdistention of the lung and mediastinal shift. In the radiograph of this infant, note the multiple loculi of areas of air in the left hemithorax with gaseous overdistention and the shift of the mediastinum to the right. The areas of loculated air may simulate a diaphragmatic hernia; however, the intestinal gas pattern is normal and the orogastric tube is clearly seen coiled in the stomach. (Singleton, E., Wagner, M.)

1.67

Figure 1.67. Radiograph of another infant with congenital cystic adenomatoid malformation of the lung on the left side. This infant developed increasingly severe respiratory distress within 18 hours of birth as a result of progressive air trapping and hyperinflation. In these infants, surgical removal of the malformation is essential.
Congenital cystic adenomatoid malformation may present initially as an intrapulmonary mass which appears solid or has a few scattered translucent areas, but this progresses to give the typical appearance of congenital cystic adenomatoid malformation.

1.68

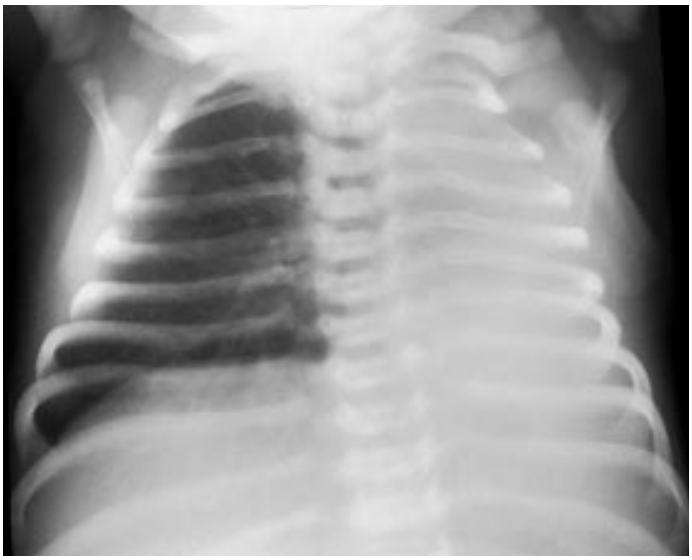

Figure 1.68. This chest radiograph shows pulmonary agenesis on the left side. Note the hyperinflated right lung with widening of the intercostal spaces and splaying of the ribs. The heart is displaced to the left side. In pulmonary agenesis the affected hemithorax is opaque, and the mediastinal structures occupy the airless space. Total agenesis of both lungs is very rare. Absence of the left lung is more frequent than of the right lung. The remaining lung is larger than normal and often herniates into the contralateral chest. Soon after a groove develops in the laryngotracheal tube, the tracheal portion bifurcates into the right and left lung bronchi. Failure to do so may result in agenesis. The presence of another anomaly, such as a vertebral defect, strongly supports the diagnosis of agenesis.

1.69

Figure 1.69. This infant had minimal respiratory distress, but on physical examination was noted to have asymmetry of the chest. A chest radiograph showed a marked difference in the width of the intercostal spaces between the left and right side of the chest. The right lung is opacified and the right hemithorax is small; the left lung is hyperexpanded. Hypogenetic lung syndrome (alveolar hypoplasia) is a variant of pulmonary agenesis. Congenital heart disease is apparently more common with right than with left lung hypogenesis. In this infant there was dextrocardia, pulmonary artery hypoplasia, and anomalous systemic arterial supply to the right lower lobe with anomalous venous drainage.

1.70

Figure 1.70. This infant with a scaphoid abdomen and barrelling of the chest had a diaphragmatic hernia. In any infant with a scaphoid abdomen, two surgical emergencies should be excluded – congenital diaphragmatic hernia, and esophageal atresia with a blind pouch and no communication with the gastrointestinal tract. Normally, the passage of air into the gastrointestinal tract after birth distends the scaphoid abdomen. In severe neuromuscular disease or central nervous system depression, air is not swallowed, hence the abdomen also remains scaphoid.

1.71

Figure 1.71. A radiograph of an infant with a Bochdalek-type congenital diaphragmatic hernia shows a midline abdominal stomach and multiple fluid and air-filled loops of bowel in the left hemithorax. Left-sided herniae occur five times more frequently than right-sided herniae. The incidence of this defect is 1:4000 live births and it constitutes a neonatal emergency if there is severe respiratory distress in the first hour of life. The infant swallows air which inflates the stomach and small bowel, causing collapse of the lung and displacement of the mediastinum. In severe cases, the stomach, small bowel, and left lobe of the liver may lie in the hemithorax during fetal life, resulting in hypoplasia of the lungs.

1.72

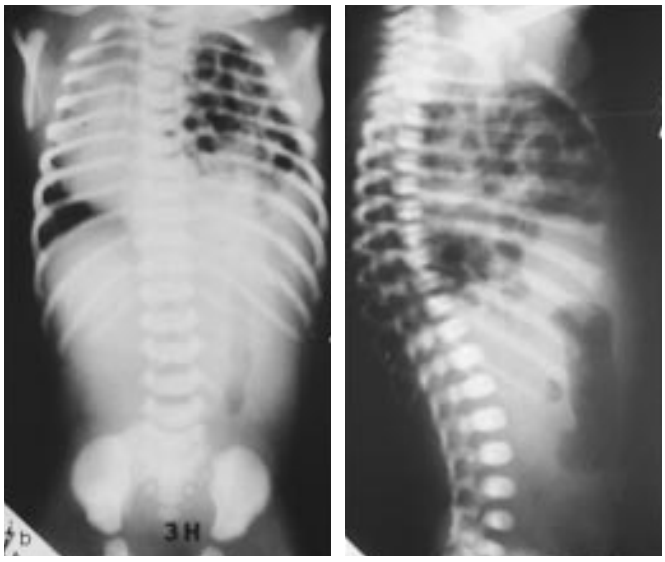

Figure 1.72. Anteroposterior and lateral radiographs of an infant with a diaphragmatic hernia who presented with severe respiratory distress at birth. Note the displacement of the heart to the right and the lack of gas in the gastrointestinal tract. In the lateral view, note the scaphoid appearance of the abdomen.

1.73

Figure 1.73. Infants with diaphragmatic herniae may present with a wide spectrum of symptoms. This infant had minimal respiratory distress, but some abdominal distention and vomiting. A contrast study of the colon demonstrates its location in the left hemithorax, confirming the diagnosis of a congenital diaphragmatic hernia.

1.74

Figure 1.74. In this radiograph note a right-sided diaphragmatic hernia with the liver and bowel in the right side of the chest. Bochdalek-type herniae are typically large and involve a posterolateral defect in the foramen of Bochdalek. Morgagni herniae are retrosternal and involve the foramen of Morgagni. Ninety-eight percent of all defects are the Bochdalek type. Symptoms are generally less severe when the hernia is on the right side.

1.75

Figure 1.75. In this infant with a congenital diaphragmatic hernia, there was vigorous resuscitation at birth. Prolonged bag-mask ventilation can distend the stomach and intestine with air, thus increasing the respiratory distress. Note that the mediastinum and heart are shifted to the right even after decompression and that the markedly distended stomach is in the thoracic cavity. Gastric aspiration relieved the distention as noted in the radiograph on the right. Infants with congenital diaphragmatic hernia often require vigorous resuscitation; thus it is important to place an orogastric tube during resuscitation if diaphragmatic hernia is suspected.

1.76

Figure 1.76. In this infant with Rh isoimmunization and a congenital diaphragmatic hernia, contrast was injected into the amniotic fluid of the fetus to permit swallowing of the contrast for confirmation of the position of the fetal bowel prior to intrauterine transfusion. At birth, the infant was noted to have respiratory distress, and a plain radiograph of the chest and abdomen showed the contrast-filled bowel lying in the chest, confirming the diagnosis of a diaphragmatic hernia. This is of historic interest only because this practice has been replaced by the use of ultrasound during the procedure of intrauterine transfusion.

1.77

Figure 1.77. The asymmetry of the chest in this infant is a result of eventration of the diaphragm. Note the elevation with ballooning of the chest on the right side. Eventration is a congenital thinning of the muscle of the pleuroperitoneal membrane portion of the diaphragm. Thinning allows upward displacement of the liver, thereby elevating the ribs on the affected side. It is usually unilateral, rarely bilateral. If respiratory distress is not severe, these infants may be treated conservatively.

1.78

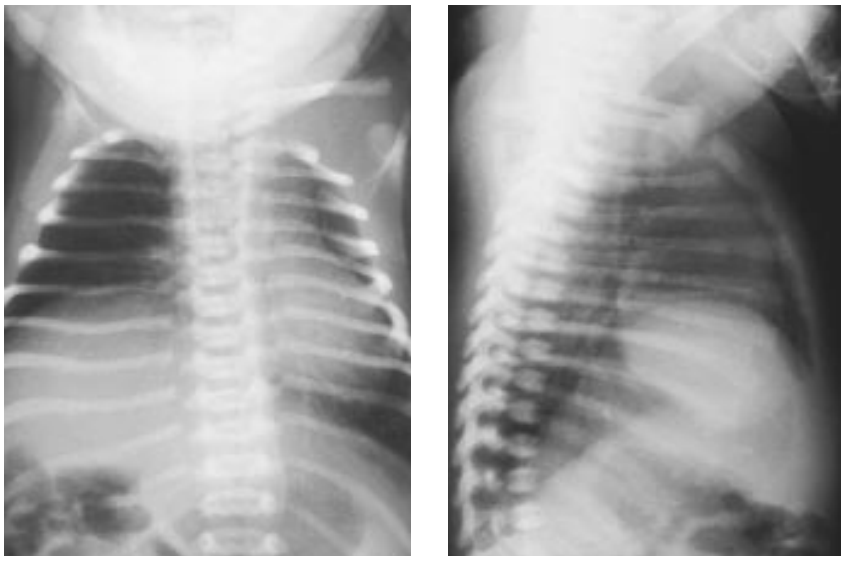

Figure 1.78. An anteroposterior and lateral radiograph of the chest of an infant with eventration of the diaphragm. Note the right diaphragm elevated well above the left with the increased density of the liver below it. Eventration of the diaphragm should be differentiated from paralysis of the diaphragm. On fluoroscopic examination, if the diagnosis is eventration of the diaphragm, there is movement of the diaphragm with respiration whereas, if the diagnosis is paralysis of the diaphragm, there is lack of movement. Currently, the diagnosis is made by ultrasonography.

1.79

Figure 1.79. In this infant with a unilateral paralysis of the right diaphragm, note the elevation of the ribs on the affected side of the chest. The chest is asymmetrical and, with inspiration, chest expansion occurred only on the normal side. In general, this condition is functional and may resolve spontaneously.

1.80

Figure 1.80. A radiograph of an infant with paralysis of the right diaphragm which occurred as a result of phrenic nerve palsy (C3, C4, C5) associated with a right Erb's palsy (C4, C5, C6). If this radiograph is compared with that of an eventration of the diaphragm, it is noted that it is important to do an ultrasonographic study. Paralysis of the diaphragm is more common in large infants and is clearly related to dystocia.

1.81

Figure 1.81. A lateral radiograph shows that the right diaphragm is elevated well above the left. Lack of movement can be appreciated under fluoroscopy or by ultrasonography. Paralysis of the diaphragm occurs on the right side versus the left side at a ratio of 4:1.

1.82

Figure 1.82. A large right pleural effusion obscures most lung markings. Air is appreciated centrally as the infant is supine and the entire hemithorax is not filled with fluid. Note that the cardiac shadow is displaced to the left. The etiology was unknown. Pleural effusions occur with chylothorax, hydrops fetalis, congestive heart failure, transient tachypnea of the newborn, complications of central total parenteral nutrition, and intrauterine viral infections.

1.83

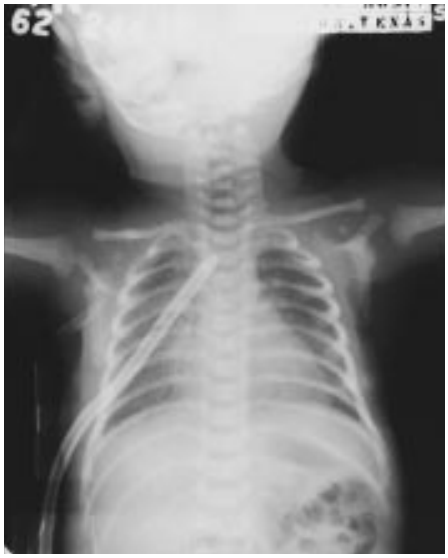

Figure 1.83. The same infant as seen in Figure 1.82 showed rapid improvement after a thoracostomy tube drainage was performed. The lung reinflated and the cardiac shadow returned to its normal position with relief of the respiratory distress.

1.84

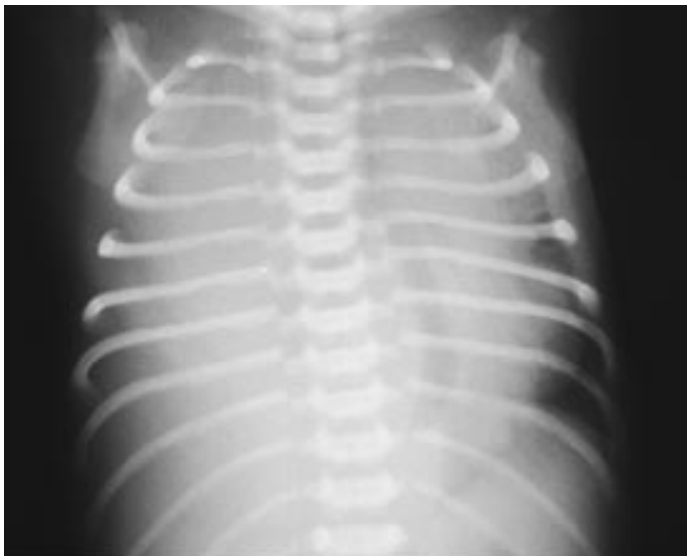

Figure 1.84. This infant presented with severe respiratory distress at birth. A chest radiograph showed marked opacification of the right hemithorax with displacement of the trachea and cardiac shadow to the left. All lung markings were obscured. The appearance was that of a massive pleural effusion, and the diagnosis of congenital chylothorax was made by thoracentesis performed on the right chest with removal of about 300 ml of straw-colored fluid. This resulted in rapid relief of the respiratory distress. Congenital chylothorax results from the leakage of chyle into the pleural space and is presumably caused by congenital defects in the thoracic duct or by trauma. The other lymphatic vessels are usually normal.

1.85

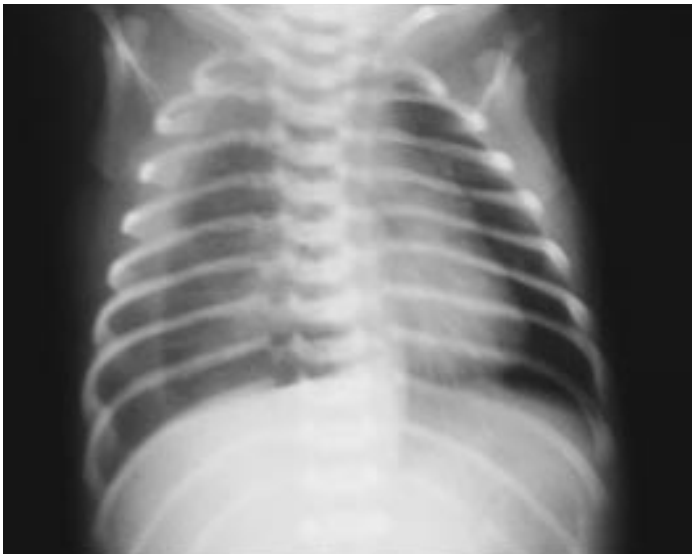

Figure 1.85. Radiograph of the same infant as in Figure 1.84 at the age of eight hours, following thoracentesis at the age of 4 hours. Note marked improvement, although some fluid is still present.

1.86

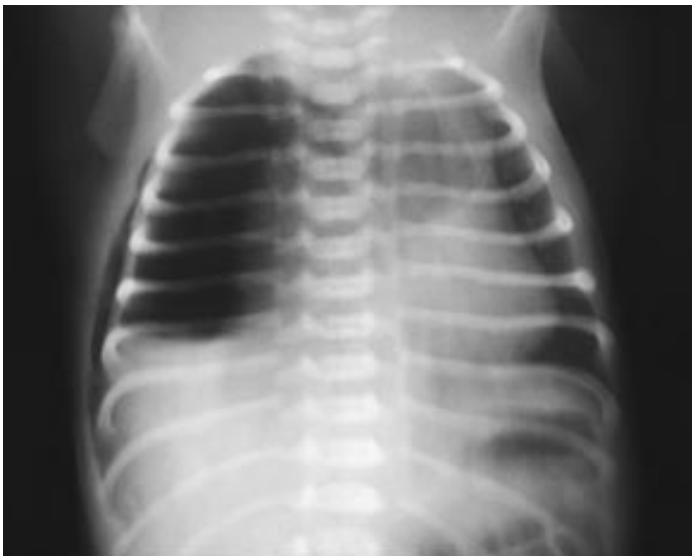

Figure 1.86. The same infant as in Figure 1.84 and 1.85 later required a second thoracentesis at the age of 48 hours. In this chest radiograph following aspiration of the chylothorax, a subcutaneous collection of air and a small residual pneumothorax persisted.

1.87

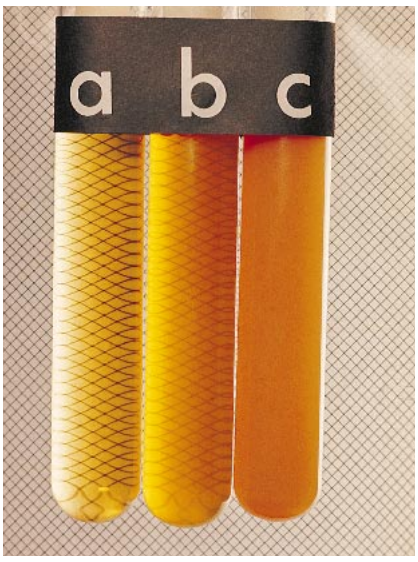

Figure 1.87. Comparisons of the clarity of chylous fluid at (a) the age of 4 hours, and prior to feeding, (b) 48 hours and after several milk feeds, and (c) after feeding has been well established. Note the progressive increase in turbidity associated with appearance of fat-laden chylomicrons after initiation of oral dietary fat intake. Chylous fluid is also high in protein and white blood cells. Management of this infant would include feeds with medium-chain triglycerides and total parenteral nutrition rather than the use of regular formula.

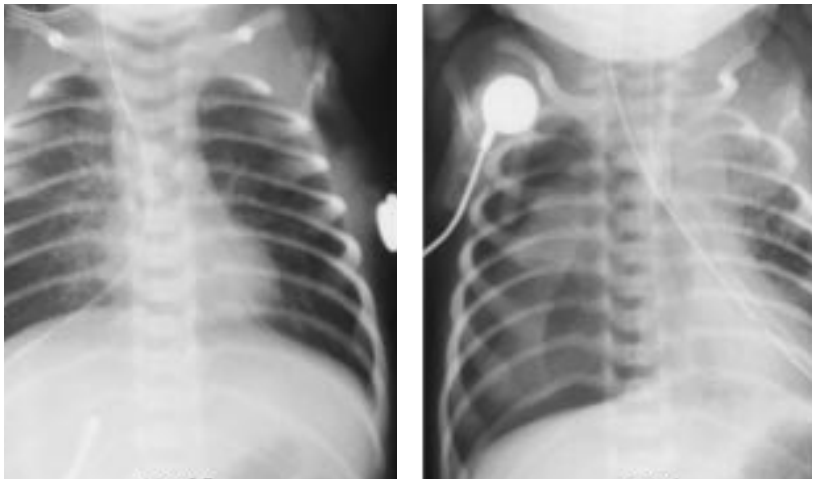

1.88

Figure 1.88. A tear in the hypopharynx of this infant occurred from erosion by a feeding tube. The tube went through a tear in the hypopharynx into the right pleural cavity (left radiograph). The tube was withdrawn and reinserted the following day, going through the tear into the left pleural cavity (right radiograph). Note the pneumothorax in the right chest in the radiograph on the right. A complication of gastric and endotracheal tube placement is a tear in the esophagus that allows the tube to be placed into the mediastinum, often resulting in a pneumothorax.

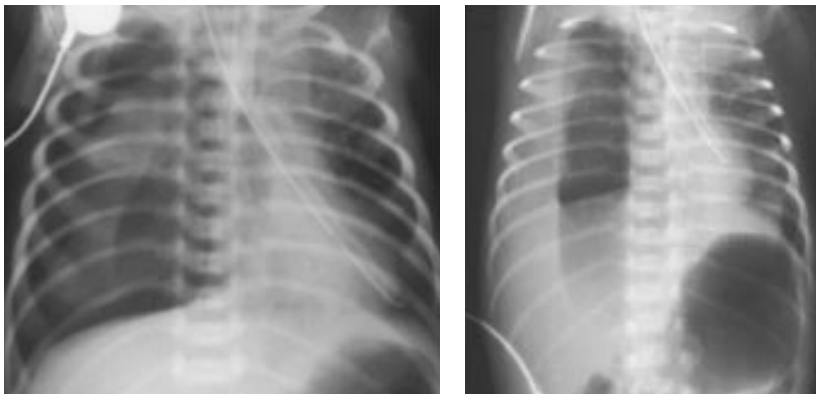

1.89

Figure 1.89. These anteroposterior and left lateral decubitus chest radiographs demonstrate a right hydropneumothorax caused by a malpositioned nasotracheal tube that tore through the hypopharynx.

1.90

Figure 1.90. These twin premature infants with severe hyaline membrane disease developed respiratory distress soon after birth. Note the glistening, gelatinous appearance of the skin due to edema; severe nasal flaring; and intercostal, subcostal, and xyphoid retractions because of the pliability of the chest wall. This reflects the stiffness of the lungs and worsens over the first two to three days. Clinically, the infants have tachypnea with a "see-saw" pattern of breathing and an expiratory grunt.

1.91

Figure 1.91. Severe xyphoid, subcostal, and intercostal retractions are shown in this infant with hyaline membrane disease. The stomach progressively dilates with swallowed air.

1.92

Figure 1.92. In this infant with hyaline membrane disease, the alae nasi are widely flared, the mouth is open, and there are severe retractions of the sternum and intercostal spaces. These reflect the severity of the respiratory distress. With severe distress, the alae nasi remain open and no flaring is noted. The mouth is open because of the infant's lack of tone and, with improvement in the infant's condition, flaring of the alae nasi is again noted.

1.93

Figure 1.93. This radiograph taken at 20 minutes of age in an infant with mild hyaline membrane disease demonstrates that most of the lung fluid has been cleared. It does not yet reflect the volume loss and consolidation of the lung typical of surfactant deficiency and pulmonary edema.

1.94

Figure 1.94. A lateral radiograph of the same infant as in Figure 1.93 shows the sternal retraction, and there is a mild air bronchogram.

1.95

Figure 1.95. Over the ensuing several hours, surfactant deficiency results in severe lung injury with hyaline membrane formation, loss of lung volume, and air bronchograms on the chest radiograph along with the development of a reticulogranular pattern of the lung parenchyma. The reticulogranular pattern consists of diffuse, symmetrical areas of alveolar atelectasis interspersed with aerated bronchioles and alveolar ducts.

1.96

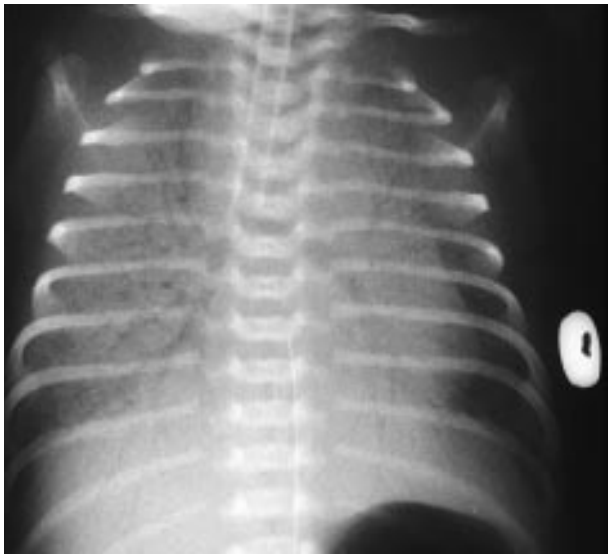

Figure 1.96. Hyaline membrane disease is a heterogeneous process involving only some alveoli while others are unaffected. In this instance, a radiograph demonstrates a more severely affected right lung. The typical radiologic appearance of hyaline membrane disease may vary from the typical reticulogranular ("ground glass") appearance of the lung fields with air bronchograms to complete opacification of the chest.

1.97

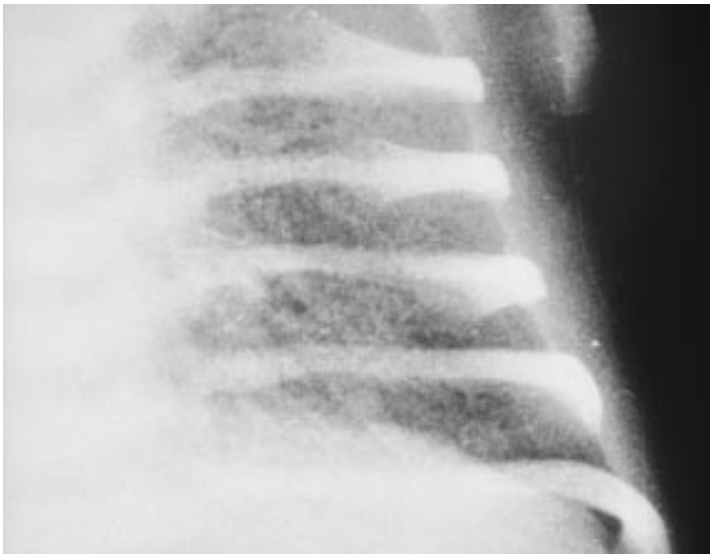

Figure 1.97. A detailed view of the left cardiophrenic angle in this radiograph demonstrates the reticulogranular pattern of the lung parenchyma in hyaline membrane disease. With progression of the disease, the reticulogranular pattern becomes more prominent, and coalescence of many of the small atelectatic areas occurs resulting in more opaque lung fields.

1.98

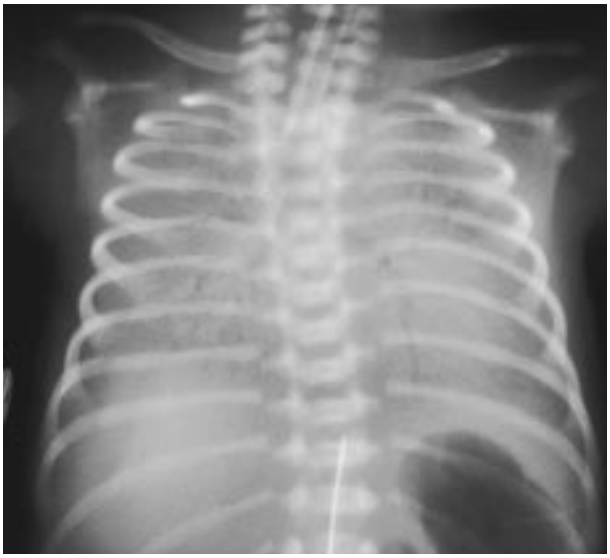

Figure 1.98. Lung volume in hyaline membrane disease is progressively lost, resulting in opacification as seen in this radiograph, and can be difficult to recruit again despite the use of vigorous positive pressure ventilation via an endotracheal tube.

1.99

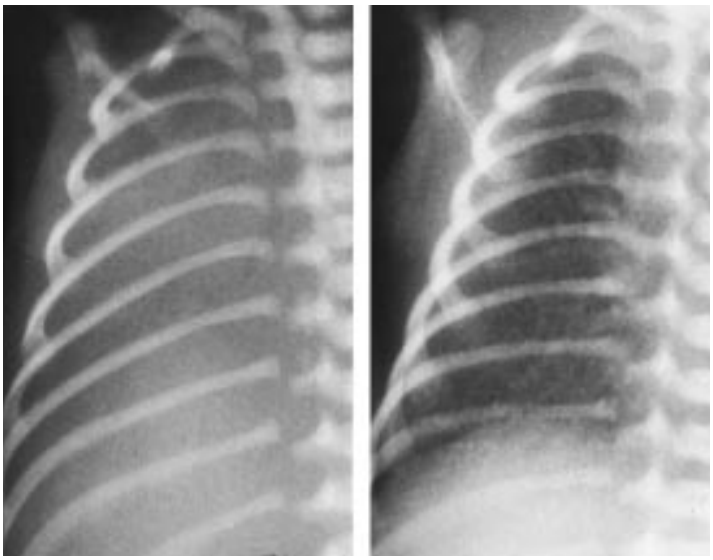

Figure 1.99. The appearance of hyaline membrane disease, seen in the radiograph on the left, can be altered dramatically with the application of positive pressure ventilation (radiograph on the right). The application of continuous positive airway pressure (CPAP) can result in a dramatic increase in lung volume and clearing of fluid from the lung fields. (Singleton, E., Wagner, M.)

1.100

Figure 1.100. Pulmonary interstitial emphysema occurs as a complication in infants with hyaline membrane disease on ventilatory support. This may progress to other manifestations of the airblock syndrome (pneumothorax, pneumomediastinum, etc.). In this radiograph, note the pulmonary interstitial emphysema and pneumothorax on the right. Typically, the "solid lung" of infants with hyaline membrane disease does not collapse if they develop the airblock syndrome. The amount of free air in a pneumothorax may appear to be small because of the inability of the lungs to collapse.

1.101

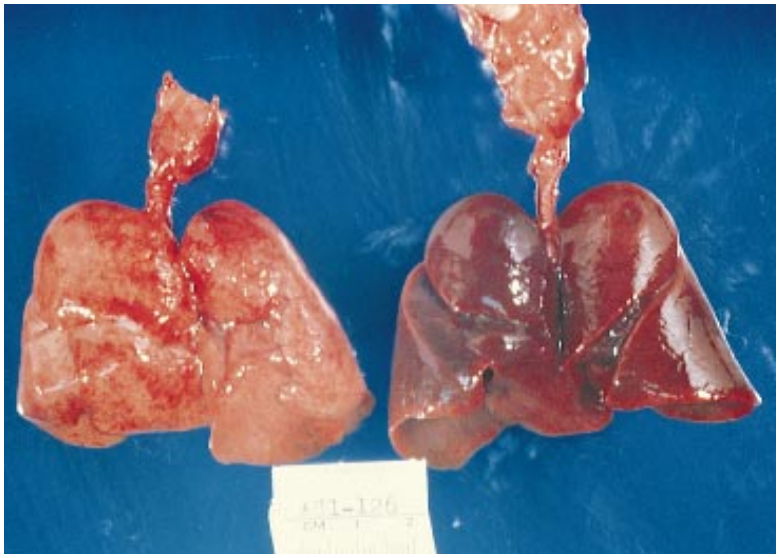

Figure 1.101. These pathologic specimens demonstrate the gross appearance of hyaline membrane disease. The lungs on the left are normal; those on the right are severely affected with hyaline membrane disease. They are cyanotic and engorged with edema fluid and are described as having the consistency and appearance of liver.

1.102

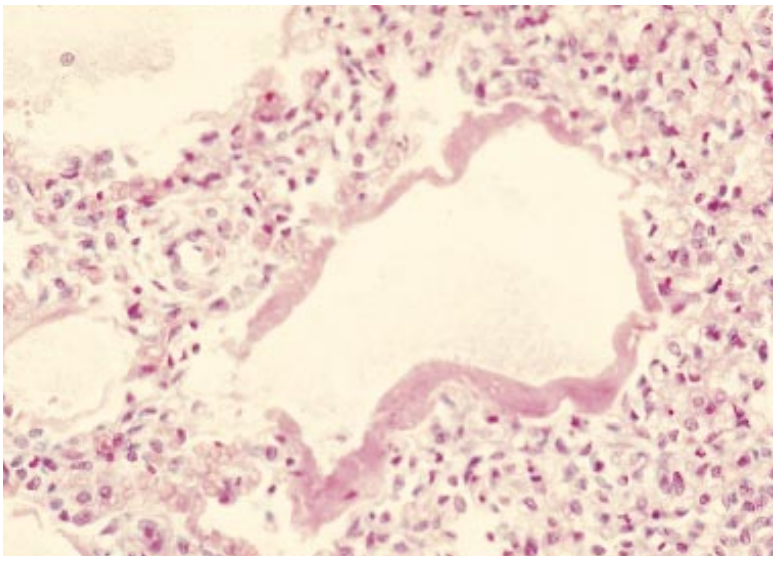

Figure 1.102. This photomicrograph shows hyaline membrane formation and edema fluid within the alveolus. The surrounding alveoli are thickened and atelectatic. Hyaline membranes are proteinaceous exudate from injured type I alveolar cells not lined with surfactant. The lack of surfactant represents immaturity of the type II alveolar cell.

1.103

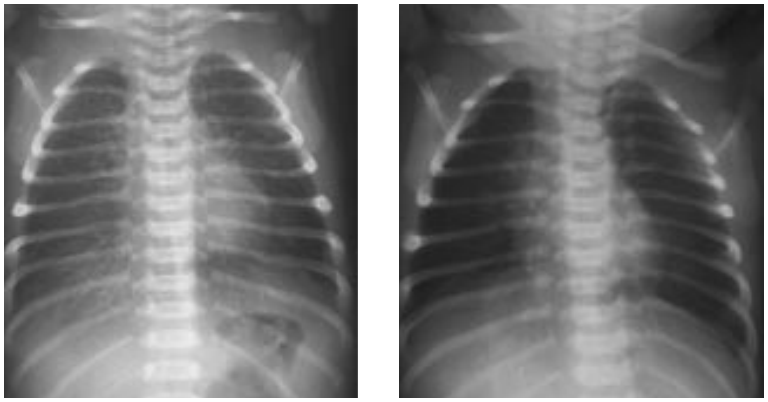

Figure 1.103. Transient tachypnea of the newborn ("wet lung" syndrome) may occur at all gestational ages (most common in term infants) and must be differentiated from hyaline membrane disease. The delayed clearance of excess fetal lung fluid, which normally is partly expelled by the trachea and partly absorbed by the pulmonary lymphatics, describes the physiologic basis for this condition which is most often associated with cesarean births. Prominent vascular markings radiating from the hilar area give rise to the typical "sunburst" appearance. The heart size is borderline or slightly enlarged. In several days (radiograph on the right) the prominence of the pulmonary vascular channels and the heart size decreases.

1.104

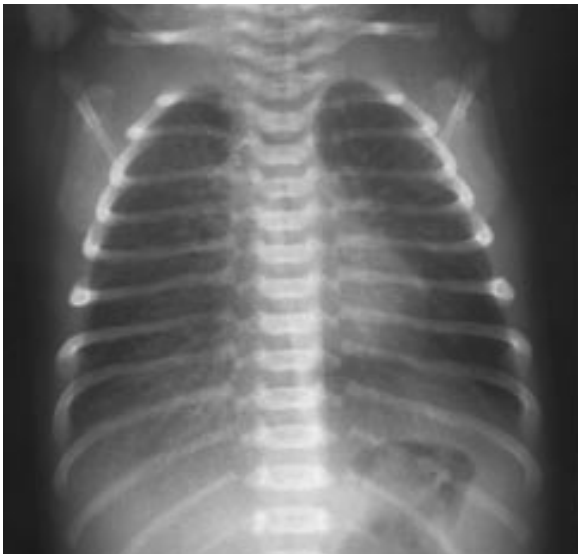

Figure 1.104. An anteroposterior radiograph of another infant with transient tachypnea of the newborn showing, in addition to the "sunburst" appearance, fluid in the transverse fissure and a right pleural effusion. Clearing of fetal lung fluid is probably mediated humorally and not by squeezing of the chest at expulsion during vaginal delivery. Other factors such as prematurity and depression of fetal breathing movements with anesthetics can contribute to this condition.

1.105

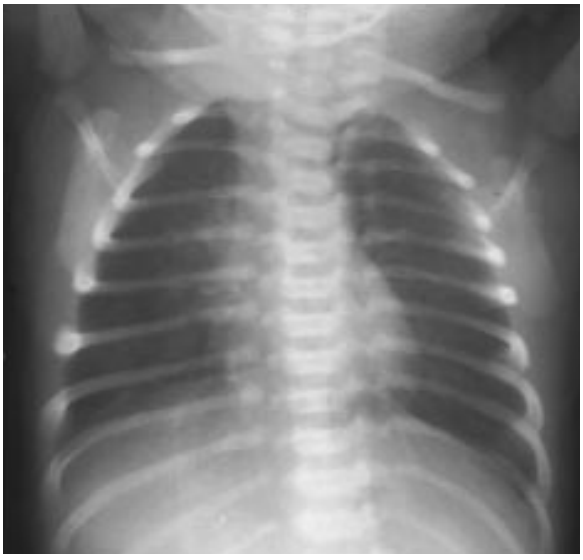

Figure 1.105. The same infant as in Figure 1.104, 24 hours later, showing the rapid improvement in the infant's condition. This was also apparent clinically.

1.106

Figure 1.106. This infant, with meconium aspiration syndrome, has a barrelled chest with increased anteroposterior diameter and increased convexity of the anterior chest wall similar to that seen with other forms of obstructive emphysema. Note the meconium staining of the skin. Aspiration syndrome occurs when amniotic fluid which may or may not be meconium-stained extends into the respiratory tract. A certain amount of particulate matter in the form of squamous cells and lanugo may be aspirated, but these do not cause distress. If the aspiration is associated with meconium, there may be severe fetal distress. Meconium aspiration is more common in term and postmature infants and may cause a severe chemical pneumonitis.

1.107

Figure 1.107. Once the meconium is cleared from the airways, there is generally less hyperinflation and some resolution of the respiratory distress symptoms. Note that the same infant as in Figure 1.106 has improved markedly within 48 hours. The barrelling of the chest and increased anteroposterior diameter are much improved.

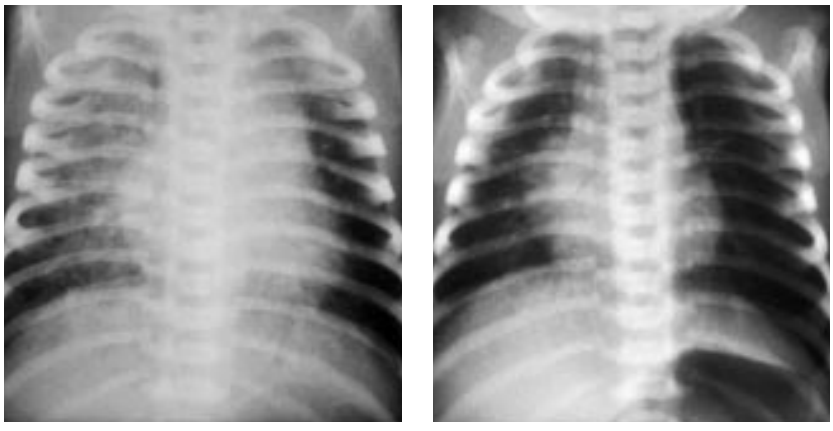

1.108

Figure 1.108. In the radiograph on the left, note the typical appearance of meconium aspiration pneumonia. The radiograph on the right, at 3 days later, shows a marked improvement. Regardless of contents aspirated (meconium, blood, amniotic fluid, or gastric contents), chest radiographs can demonstrate patchy diffuse infiltrates.

1.109

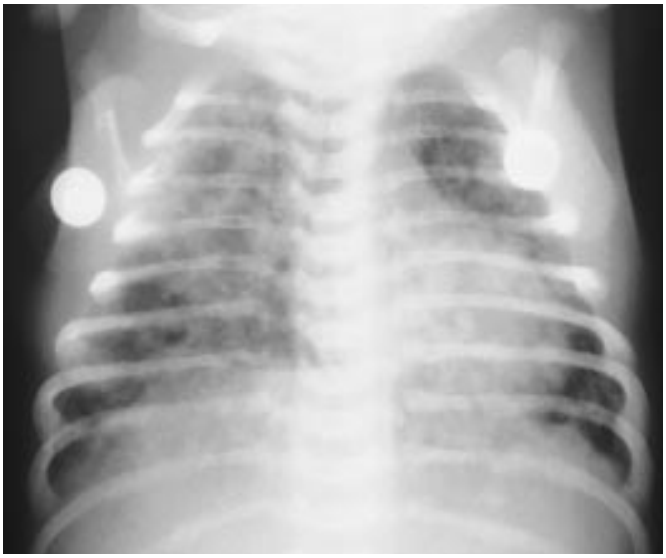

Figure 1.109. Meconium pneumonitis can occur when aspirated contents cause chemical inflammation of portions of the lung, resulting not only in hyperinflation from obstruction of airways but in patchy interstitial infiltrates extending out to the periphery. In meconium aspiration syndrome, the radiologic changes vary from lobar consolidation to widespread opacities involving both lung fields. There may be asymmetry of the patchy densities in both lung fields as seen in this radiograph. The radiologic findings in meconium aspiration syndrome may be identical to those seen in infectious pneumonia of the newborn. Aspiration pneumonitis may be secondary to esophageal atresia, pharyngeal incoordination, a vascular ring, and central nervous system abnormalities.

1.110

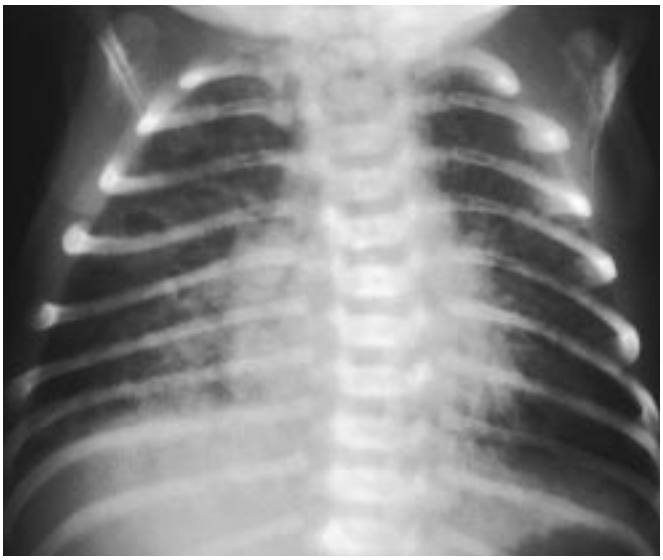

Figure 1.110. The sequelae of meconium aspiration syndrome are noted in this radiograph. There are areas of infiltrate and blebs seen in the right lung field. Pneumothorax and pneumomediastinum are common complications.

1.111

Figure 1.111. Persistent pulmonary hypertension of the newborn (persistent fetal circulation) is a condition in which there is persistence of the fetal high pulmonary vascular resistance. The condition can be primary, but is generally secondary to other causes such as meconium aspiration or diaphragmatic hernia. This chest radiograph shows no significant pulmonary pathology. There is decreased vascularity with mild cardiomegaly. There is severe respiratory distress and cyanosis, and the response to oxygen is initially poor.

1.112

Figure 1.112. Medical therapy of persistent pulmonary hypertension of the newborn can cause severe complications as depicted in this radiograph. Vigorous positive pressure ventilation resulted in the development of interstitial emphysema and bilateral pneumothoraces. Persistent shunt pathways (shunting at the foramen ovale and ductus arteriosus) and high pulmonary vascular resistance make the condition poorly responsive to medical therapy with a mortality of 30 to 50%.

1.113

Figure 1.113. Pulmonary hemorrhage frequently develops in infants with hyaline membrane disease and is common in small-for-date infants. It also occurs with other conditions such as asphyxia, cold stress, or cerebral edema. The clinical picture is that of respiratory distress associated with the coughing or aspiration of frothy bloody mucus from the trachea. Chest radiographs demonstrate homogeneous bilateral hazy infiltrates which may affect one or more pulmonary segments and give the appearance of hyaline membrane disease or consolidation. The combination of hypoxia and increased lung capillary pressure is thought to contribute to the development of this condition.

1.114

Figure 1.114. In this gross specimen is severe hemorrhage with an irregular distribution over the surface of the lung. It may be associated with a bleeding diathesis or can occur independently. In most cases, it reflects the massive accumulation of edema thereby explaining a generally lower hematocrit in the trachea's effluent than in venous blood (about 10% lower). True hemorrhage, however, can occur.

1.115

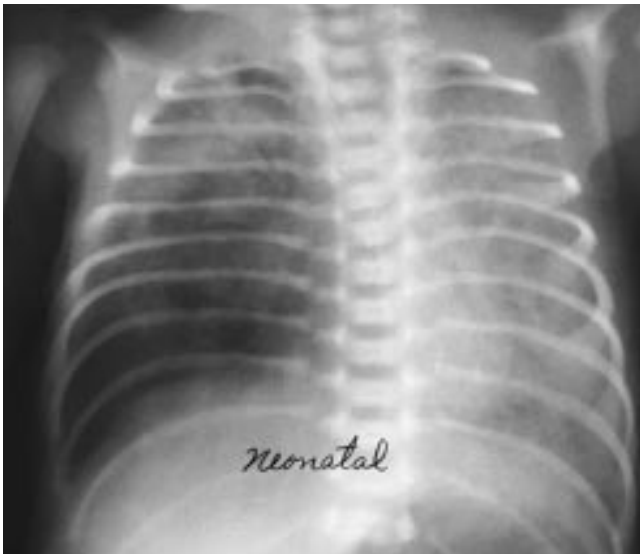

Figure 1.115. Neonatal pneumonia is most commonly caused by group B *Streptococcus*, but can be due to *Escherichia coli*, *Staphylococcus aureus*, or *Listeria monocytogenes*, etc. Ascending infection and aspiration of infected amniotic fluid is the postulated mechanism of infection. The radiographic appearance of intrauterine pneumonia is very similar to that of meconium aspiration syndrome. There are coarse linear areas of density, segmental areas of consolidation, atelectasis, and air trapping. The lungs are overinflated and, consequently, the diaphragm is at a low position. (Singleton, E., Wagner, M.)

1.116

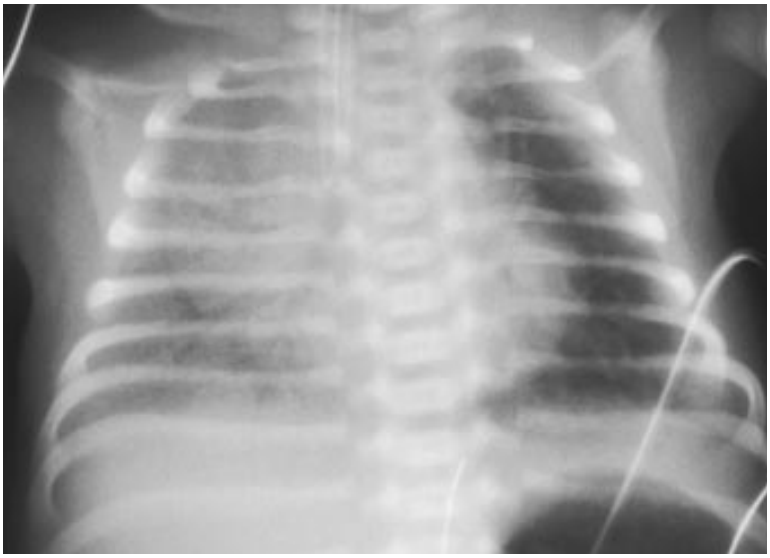

Figure 1.116. This radiograph is an example of group B streptococcal pneumonia. This chest radiograph demonstrates adequate lung expansion, but a diffuse, generalized reticulogranular pattern is noted over the lung fields making the condition difficult to distinguish from hyaline membrane disease.

1.117

Figure 1.117. This radiograph is another example of group B streptococcal pneumonia indistinguishable from hyaline membrane disease. Only 50% of blood cultures are positive with congenital pneumonia. The diagnosis of group B streptococcal pneumonia was suggested by a positive tracheal aspirate and urine counterimmune electrophoresis (CIE).

1.118

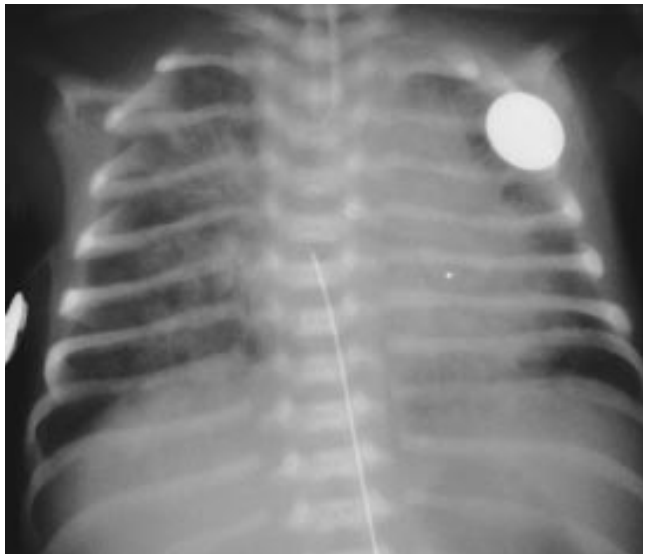

Figure 1.118. In this infant with congenital *Listeria monocytogenes* pneumonia the radiograph is indistinguishable from other types of pneumonia, but the infant had typical listerial skin lesions at birth and positive blood and spinal fluid cultures.

1.119

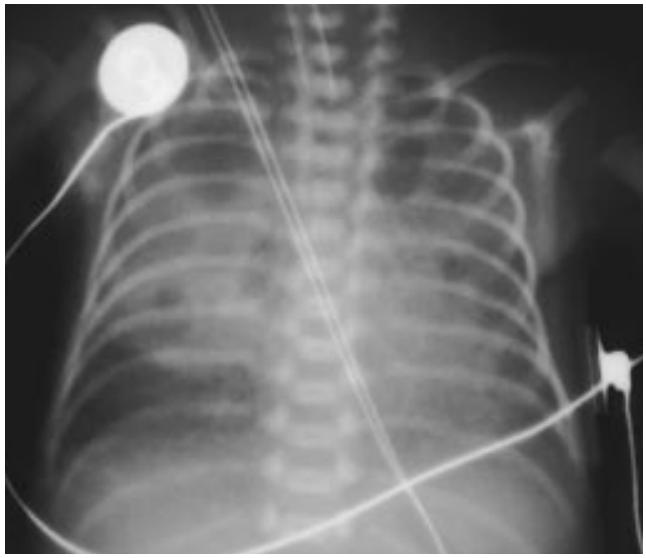

Figure 1.119. This infant with a birth weight of 700 g developed *Staphylococcus aureus* osteomyelitis and pneumonia. In this radiograph of the chest, note the consolidation and early pneumatocele formation. There was improvement with antibiotic treatment. At the present time, staphylococcal pneumonia in the neonate is not a major problem. Large outbreaks of staphylococcal infections in nurseries occurred several decades ago, often causing pneumonia and the development of pneumatoceles. Development of air-filled cystic pneumatoceles is quite characteristic of staphylococcal pneumonia. They generally are a sign of healing and require no specific therapy other than the appropriate antibiotics. Rarely they may rupture into the thorax producing a pneumothorax and the acute onset of distress. This complication suggests that therapy has been inadequate.

1.120

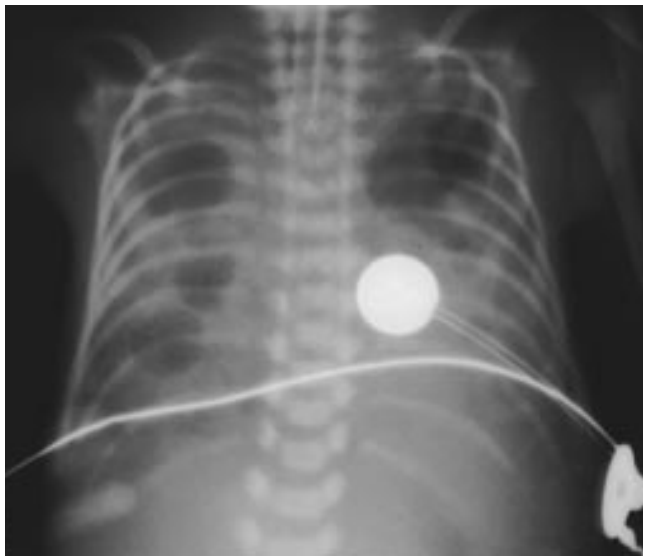

Figure 1.120. A chest radiograph of the same infant as in Figure 1.119 shows the pneumatoceles two days later when the infant generally was improving. Fluid levels may occasionally be seen in pneumatoceles. Residual fluid levels presumably represent persistent infection. Pneumatoceles must be differentiated from cystic emphysema which has developed as a sequel to interstitial emphysema or bronchopulmonary dysplasia. The cysts in these conditions are diffuse and bilateral. Serial films demonstrate evidence of prolonged respirator therapy with interstitial emphysema which then progresses to emphysematous bullae.

1.121

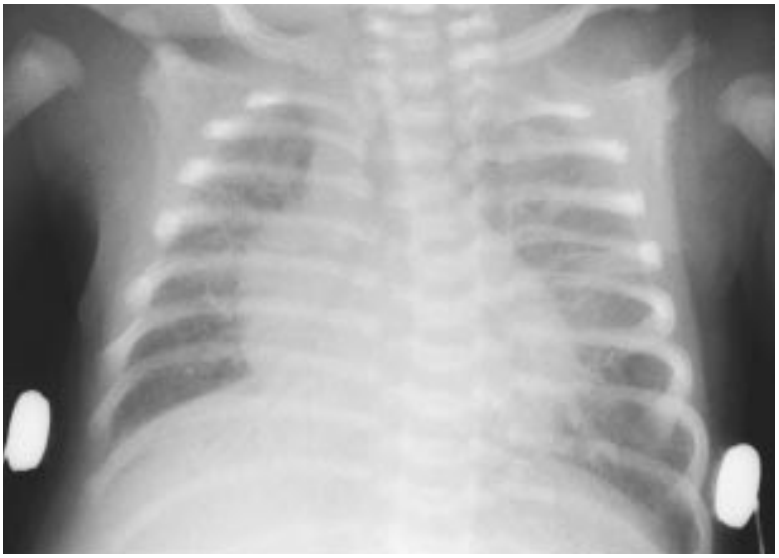

Figure 1.121. A radiograph of the chest of an infant with congenital syphilis demonstrates the typical interstitial pneumonia (pneumonia alba) and the osseous changes of growth arrest lines at the proximal ends of the humeri and periostitis of the clavicles (Higouménakis' sign).

1.122

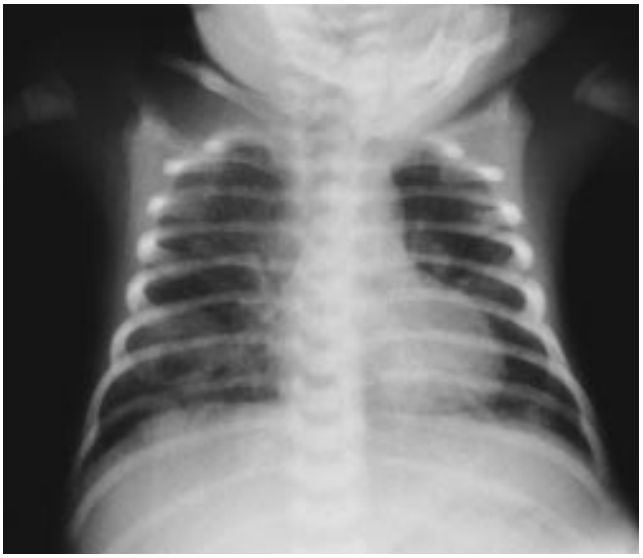

Figure 1.122. This infant who had severe congenital syphilis at birth with generalized osseous changes of all extremities shows pneumonia alba and bony changes in the proximal parts of the humerus in this chest radiograph. This stresses the importance of checking for any skeletal changes when reviewing a chest radiograph. (Singleton, E., Wagner, M.)

1.123

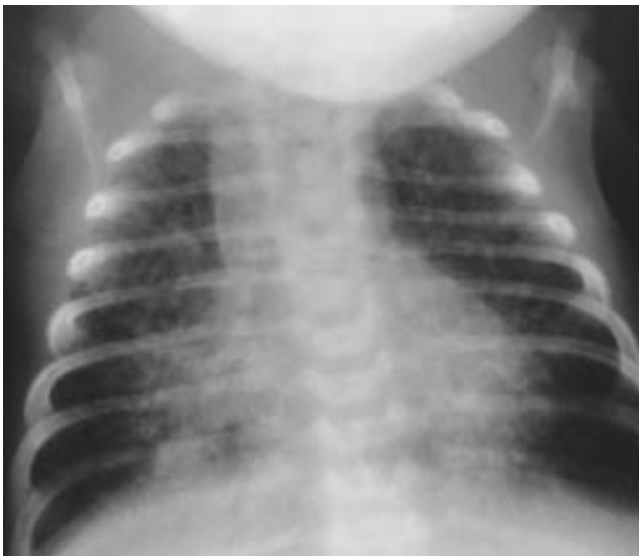

Figure 1.123. In this radiograph of an infant with chlamydia pneumonia note the bilateral interstitial infiltrates. He developed a stacatto cough, low grade fever, and purulent eye drainage at the age of 2 to 3 weeks and had positive cultures for *Chlamydia trachomatis* from the nasopharynx.

1.124

Figure 1.124. Pulmonary lymphangiectasia is a rare condition in which dysplastic, malformed lymphatics of the lungs result in poor lymph drainage with interstitial engorgement and hyperinflation. Lymphatic tissue proliferates in the lungs, thereby compromising the normal pulmonary ventilation. The condition is usually not recognized until later in childhood and, in its severe form, is incompatible with life. Bacterial pneumonias are a common complication. (Singleton, E., Wagner, M.)

1.125

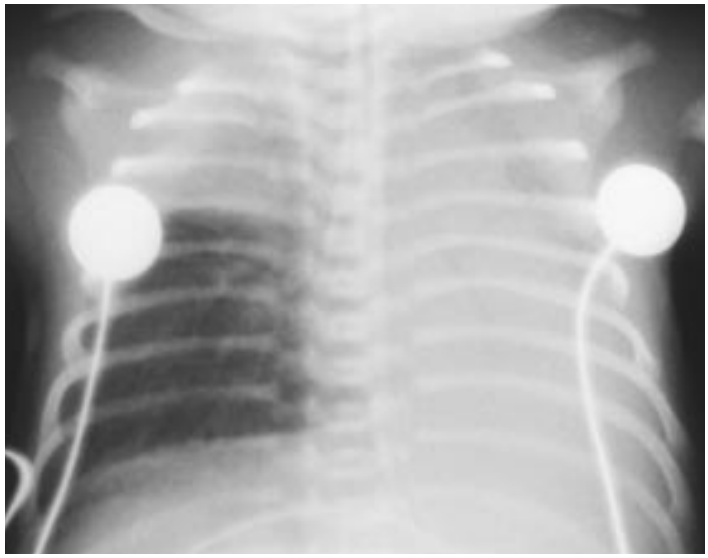

Figure 1.125. This infant had an endotracheal tube placed in his right mainstem bronchus as seen in this radiograph. Note the complete collapse of the left lung and collapse of the upper lobe of the right lung as a result of the obstructed airways.

1.126

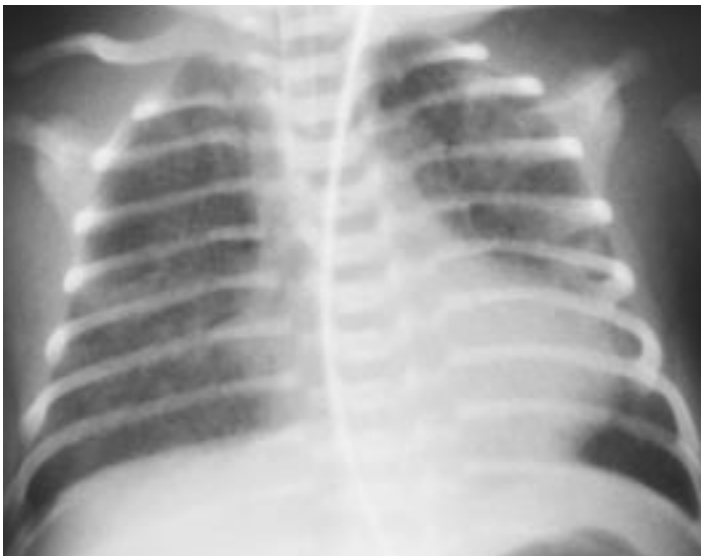

Figure 1.126. The same infant as in Figure 1.125 shows re-expansion 2 hours later of all of the collapsed areas after repositioning the endotracheal tube to the midtrachea.

1.127

Figure 1.127. This infant with severe hyaline membrane disease developed severe diffuse bilateral pulmonary interstitial emphysema (PIE). Clinically, it behaves like other types of airblock-producing hypercarbia initially with hypoxemia and systemic hypotension when severe. The heart may be compressed by severe bilateral pulmonary interstitial emphysema. Systemic venous return and cardiac output may be severely compromised, resulting in a small heart shadow on chest radiograph. Loose connective tissue in the wide interstitial spaces of the preterm lung results in the accumulation of interstitial air. The onset may be gradual or sudden, resulting in decreased chest excursion with thoracic distention.

1.128

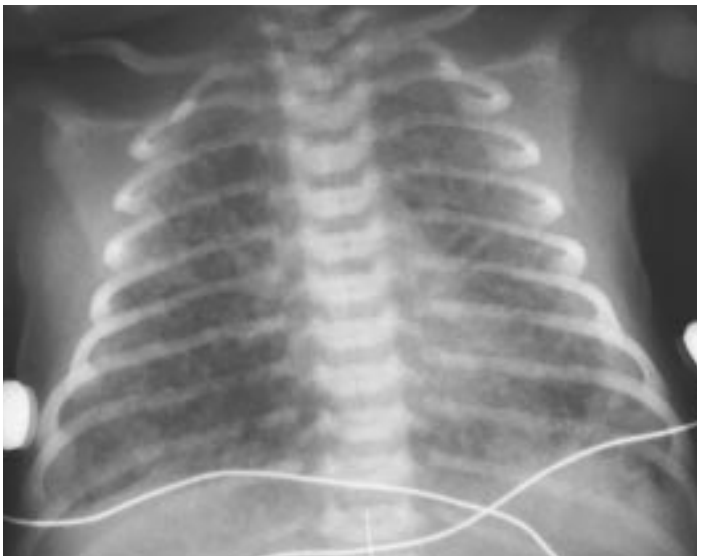

Figure 1.128. Bilateral pulmonary interstitial emphysema in another infant in which the radiograph shows the typical findings of hyperinflation and diffuse hyperlucencies within the lung parenchyma. This complication of hyaline membrane disease occurs most commonly as a complication of mechanically assisted ventilation and rarely occurs spontaneously. There is widespread rupture of alveoli resulting in accumulation of air in the interstitial lung tissue.

1.129

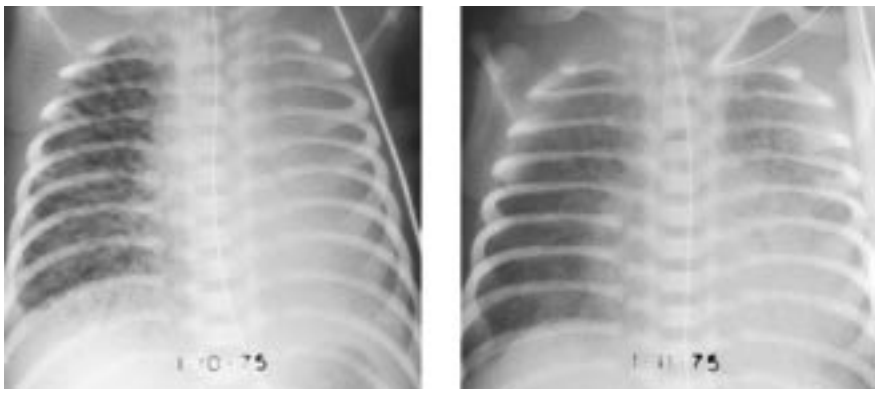

Figure 1.129. The radiograph on the left shows severe hyaline membrane disease in the left lung and pulmonary interstitial emphysema in the right lung. This is an example of unilateral PIE in an infant with hyaline membrane disease. Within 24 hours, the hyaline membrane disease is resolving, as is the PIE. On chest radiograph, the irregular linear streakiness of pulmonary interstitial emphysema is typical of air dissecting into the large interstitial spaces of the lung.

1.130

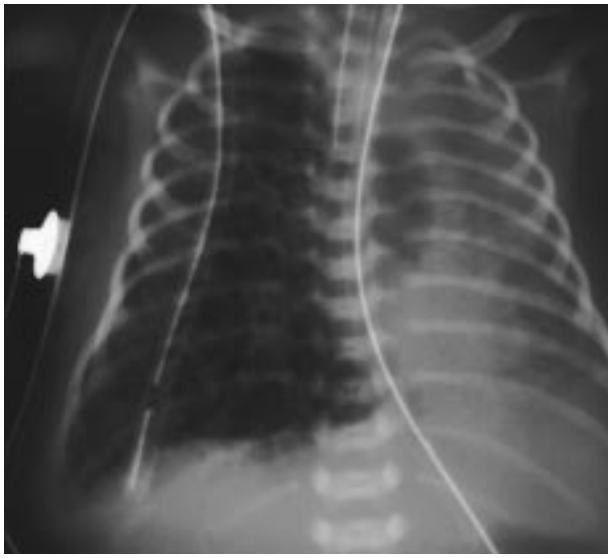

Figure 1.130. In more severe cases of pulmonary interstitial emphysema, air can accumulate in the interstitium to the extent that it causes herniation of an involved lung across the midline. The incidence of severe interstitial emphysema has significantly decreased with widespread use of exogenous surfactant replacement.

1.131

Figure 1.131. In pulmonary interstitial emphysema, the complications of pneumothorax and pneumomediastinum are not uncommon, with the result that air may extend into the pleural spaces, mediastinal space, pericardial space and even dissect down tissue planes into the abdominal cavity. Note the pulmonary interstitial emphysema, pneumomediastinum, and pneumoperitoneum.

1.132

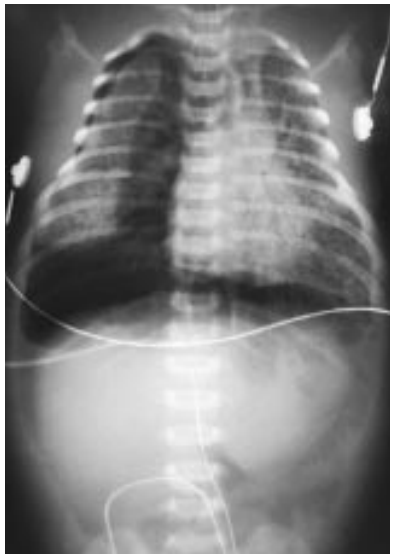

Figure 1.132. Radiograph of the same infant as in Figure 1.131 2 hours later showing the pulmonary interstitial emphysema on the left side and a large pneumothorax on the right side with collapse of the lung and the continued presence of the pneumomediastinum and pneumoperitoneum.

1.133

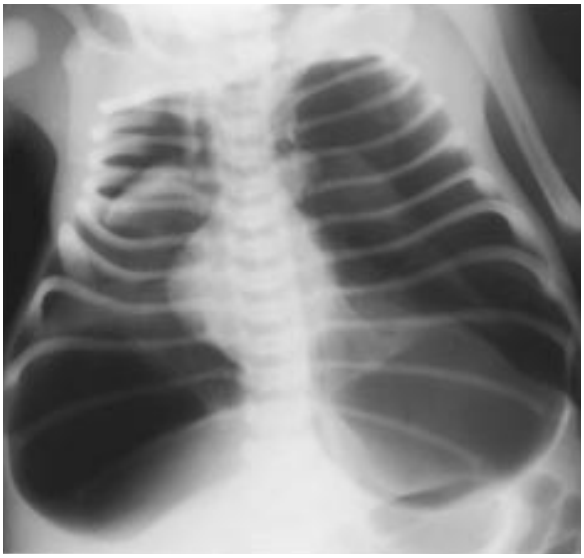

Figure 1.133. This radiograph of the chest shows massive bilateral pneumothoraces after resuscitative efforts. Note that these are both severe tension pneumothoraces in that both lungs have collapsed and both sides of the diaphragm are concave. In general, if the pneumothorax is not severe, there will be no concavity of the diaphragm. (Singleton, E., Wagner, M.)

1.134

Figure 1.134. A gross specimen of the lung shows the severe extent of the pulmonary interstitial emphysema. Note that the upper lobe of the lung appears more affected.

1.135

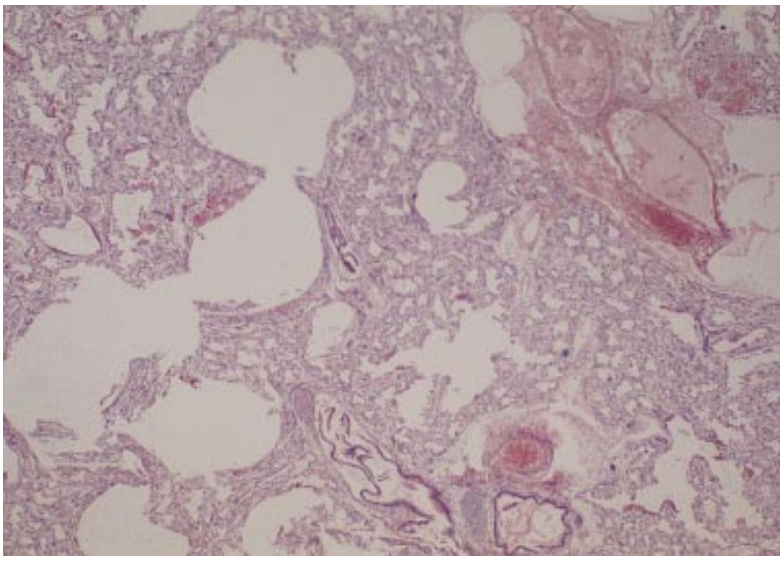

Figure 1.135. Histopathology of the lung shows the massively dilated, air-filled interstitial spaces and markedly thickened alveolar sacs in pulmonary interstitial emphysema.

1.136

Figure 1.136. Clinical findings suggesting the diagnosis of pneumothorax include increasing respiratory distress, a unilateral chest bulge, diminished breath sounds on the affected side, and especially restlessness or irritability. If there is a large tension pneumothorax, there is decreased cardiac output and an elevated central venous pressure with profound circulatory collapse. In this radiograph there is a large left tension pneumothorax pushing the mediastinum and heart to the right. Note the marked depression of the diaphragm.

1.137

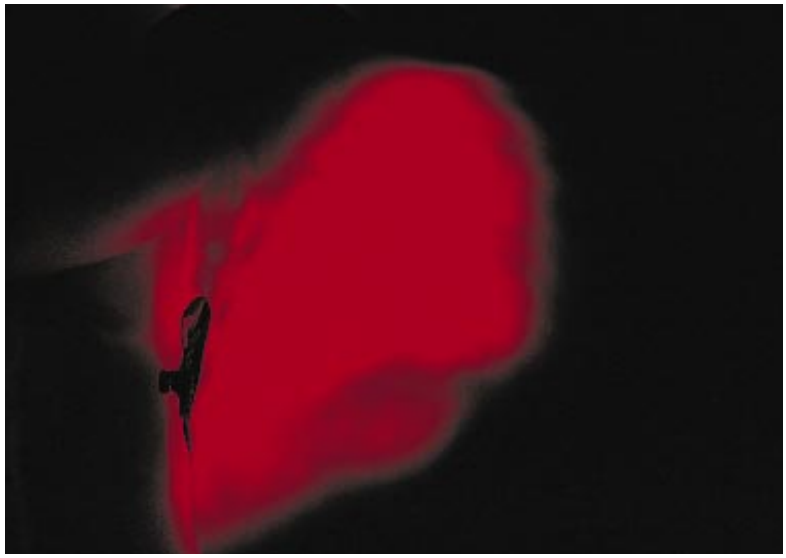

Figure 1.137. The diagnosis of pneumothorax can be rapidly established by the use of a bright light source for transillumination, especially in premature infants. This approach results in prompt recognition of the pneumothorax and can quickly direct appropriate therapy. In this figure, note the outline of the chest wall with the electrode attached and the total collapse of the right lung. Pneumothorax may occur spontaneously in infants who did not receive resuscitative measures or, more commonly, as a complication of assisted ventilation of preterm infants. A large tension pneumothorax should be promptly evacuated with a thoracostomy tube. A small pneumothorax, especially in the absence of symptoms, does not require treatment.

1.138

Figure 1.138. A radiograph of this infant with severe hyaline membrane disease shows the complications of positive pressure ventilation. There is a large right tension pneumothorax, pneumomediastinum, and subcutaneous air in the neck. Note that although there is collapse of lung with a severe pneumothorax, total collapse has not occurred because of the poor compliance of the lung. If the pneumothorax is associated with a positive pressure air leak, there is rapid clinical deterioration with mediastinal shift and collapse of the lungs. Placement of a thoracostomy tube results in rapid clinical improvement.

1.139

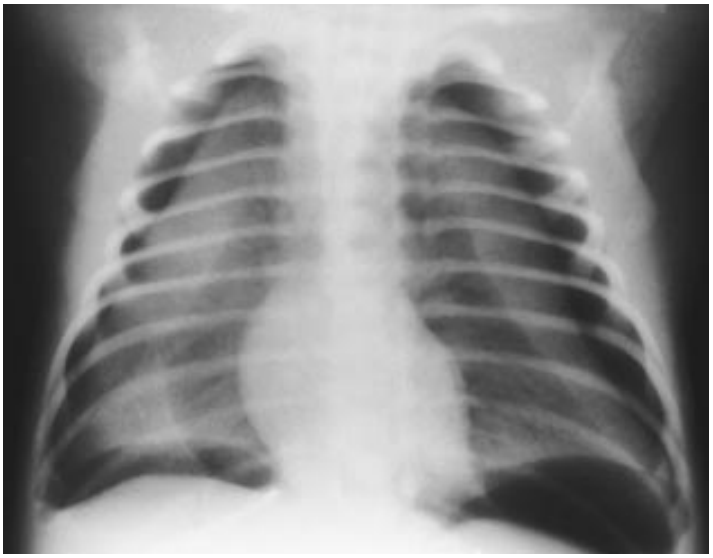

Figure 1.139. This radiograph shows bilateral pneumothoraces with accumulation of air on both the medial and lateral sides of the lung in an infant lying supine. Again, note that the lungs are not completely collapsed because of the severe degree of lung disease.

1.140

Figure 1.140. Air dissecting into the thorax and mediastinum may elevate the lobes of the thymus, resulting in the "butterfly wing" appearance of the lobes of the thymus gland. Clinically, pneumomediastinum is usually asymptomatic but findings may include a sternal bulge, restlessness or irritability, tachypnea, and distant heart sounds. Hamman's sign (a crunchy sound synchronous with the heart beat) is rarely present in the newborn period. Rupture of alveoli into the mediastinal space with accumulation of air around the heart does not usually require active management, except in extreme cases. (Singleton, E., Wagner, M.)

1.141

Figure 1.141. A lateral chest radiograph of the same infant as in Figure 1.140 shows air in the anterior mediastinum behind the sternum with elevation of the thymus. Note the well-outlined thymus gland and the subcutaneous air in the neck. (Singleton, E., Wagner, M.)

1.142

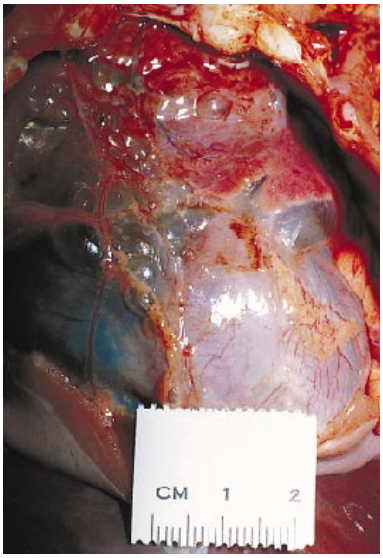

Figure 1.142. In this pathologic specimen note the multiple blebs dissecting through the soft tissue planes of the mediastinum as a result of a pneumomediastinum.

1.143

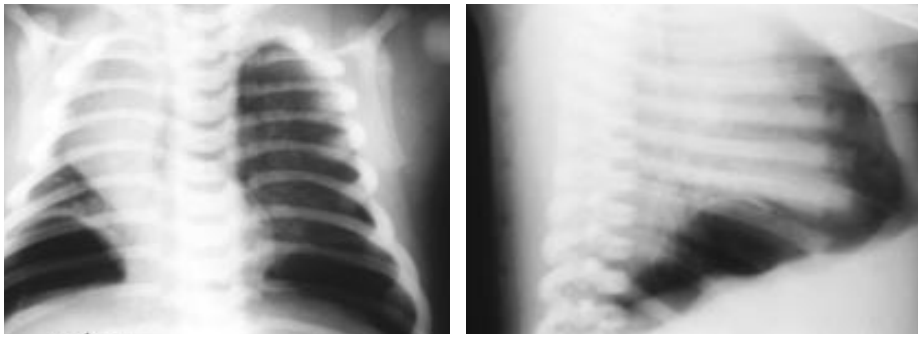

Figure 1.143. A rare complication associated with a pneumomediastinum is a subpleural collection of air. The air tracks between the parietal pleura and the diaphragm as seen in the anteroposterior and lateral radiographs of this infant.

1.144

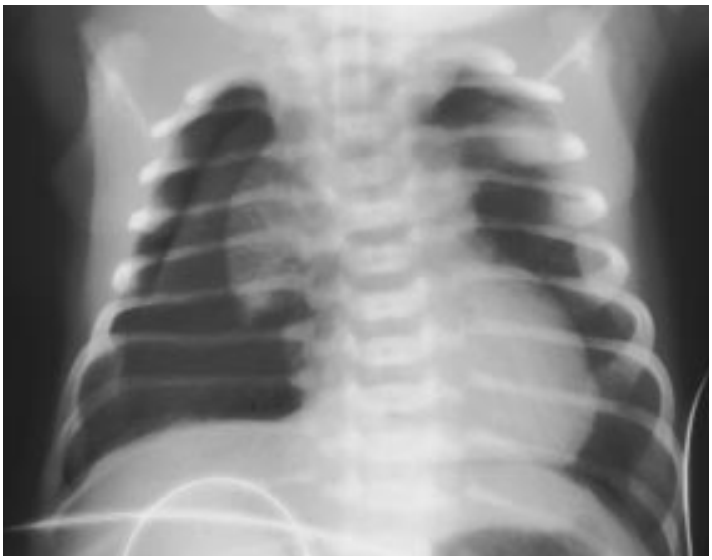

Figure 1.144. The chest radiograph of this infant shows a right pneumothorax and a pneumomediastinum. Note the lobes of the thymus gland displaced superiorly by the pneumomediastinum giving the "butterfly wing" appearance.

1.145

Figure 1.145. Three hours after the radiograph in Figure 1.144 was taken, the infant's condition had deteriorated and a repeat radiograph showed progression of the airblock with the development of a pneumopericardium. Clinically there is sudden deterioration with a marked decrease in peripheral circulation, marked decrease in blood and pulse pressure, and an elevated central venous pressure.

1.146

Figure 1.146. Pneumopericardium is a rare, but potentially fatal, form of airblock with accumulation of air around the heart. There are distant or absent heart sounds. Rupture of alveoli leads to interstitial emphysema and tracking of air along the pulmonary veins into the pericardial sac. This may resolve spontaneously or may result in cardiac tamponade with muffled heart sounds and poor cardiac output. The pericardium is readily seen as a line of increased density between the air surrounding the heart and the air infiltrating the lung.

1.147

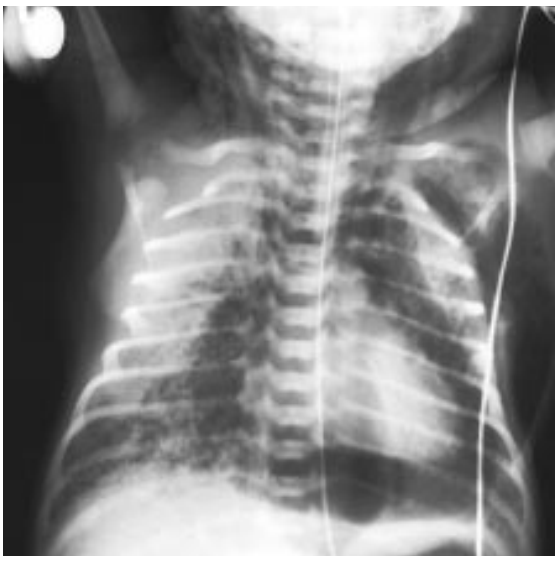

Figure 1.147. This infant on positive pressure ventilation developed a pneumothorax, pneumomediastinum, massive pneumopericardium, and subcutaneous emphysema in the neck, and especially on the left side of the chest. A massive pneumopericardium such as this always results in cardiac tamponade. Subcutaneous emphysema can be recognized clinically by crepitant bulging in the neck or over the chest, and results from the dissection of air from a pneumomediastinum. See Figure 7.71 in Volume I, Chapter 7.

1.148

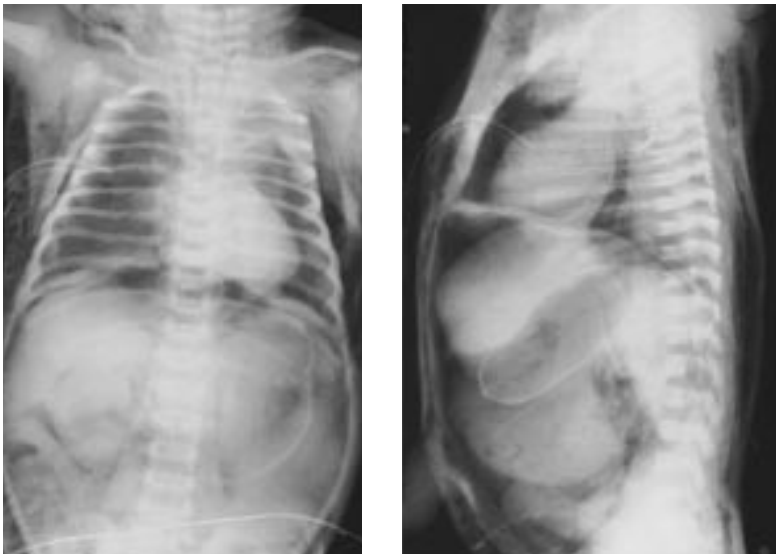

Figure 1.148. Poor lung compliance with hyaline membrane disease and positive pressure ventilation can lead to the development of severe air leaks. In this instance, air has dissected into the mediastinum, the abdominal cavity, and the subcutaneous tissue. In the lateral radiograph, the pneumomediastinum outlines the thymus gland. The air in the peritoneal cavity must be distinguished from that of a ruptured viscus. Thoracic air can dissect through any or all of the diaphragmatic apertures: the vena cava, aorta or esophagus. Especially on the lateral radiograph, note the large amount of subcutaneous air.

1.149

Figure 1.149. Extensive air leaks occurred in this male infant on positive pressure ventilation. Note the subcutaneous air over the scalp, chest and abdominal walls, and in the scrotum. In pneumoperitoneum associated with tracking down of air from a pneumomediastinum, no air/fluid levels are seen in the abdomen. With pneumoperitoneum associated with a perforation, air/fluid levels are present. In a pneumoperitoneum, air enters the scrotum via the patent processus vaginalis.

1.150

Figure 1.150. In the most severe cases, air can dissect into the intravascular spaces. In this radiograph, note that the air has dissected into the venous system causing massive air embolism to the heart. Note that the portal venous system is also filled with air.

1.151

Figure 1.151. Massive air embolism occurs as a result of air dissecting into the vascular system and accumulating in the heart displacing blood. In this infant, note the air in the chambers of the heart and along the vessels in the neck and arms. Sudden fatal extravasation of gas into the circulatory system may occur apparently due to rupture of pulmonary veins in conjunction with high intra-alveolar pressures from positive pressure ventilation.

1.152

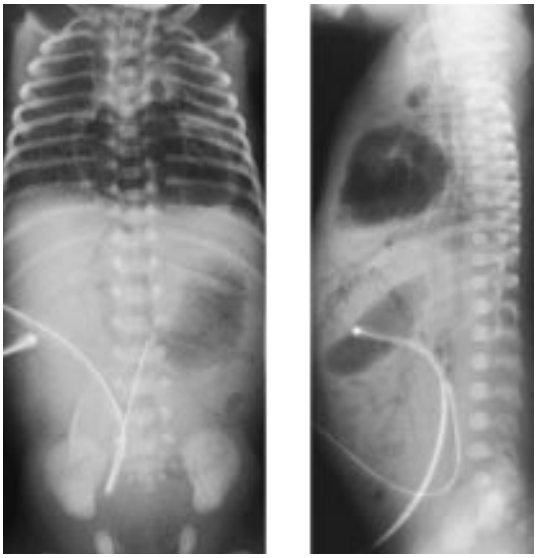

Figure 1.152. This is another example of a massive air embolism showing air dissecting into the vascular system. Note the air not only in the heart but also in the major vessels as clearly seen in the lateral radiograph.

1.153

Figure 1.153. A skull radiograph of the same infant as in Figure 1.152 shows a pneumoencephalogram produced by the massive air embolism introducing air into the ventricular system. There was an associated intraventricular hemorrhage.

1.154

Figure 1.154. Bronchopulmonary dysplasia (BPD) is a form of chronic lung disease which occurs in infants who receive prolonged exposure to oxygen with positive pressure ventilation. There are four radiologic stages. Stage I occurs from 1 to 3 days of age and is indistinguishable from severe hyaline membrane disease. Stage II occurs between 4 to 10 days of age when the lungs become homogeneously opacified. Stage III occurs between 10 to 30 days of age when multiple small rounded areas of radiolucency appear as a result of focal alveolar emphysema somewhat similar to the "bubbly" appearance of the lung in Wilson-Mikity syndrome. Stage IV occurs after 30 days of age when the cystic areas of the lung coalesce into larger cysts particularly in the upper lobes, and streaky, linear areas of scarring appear.

1.155

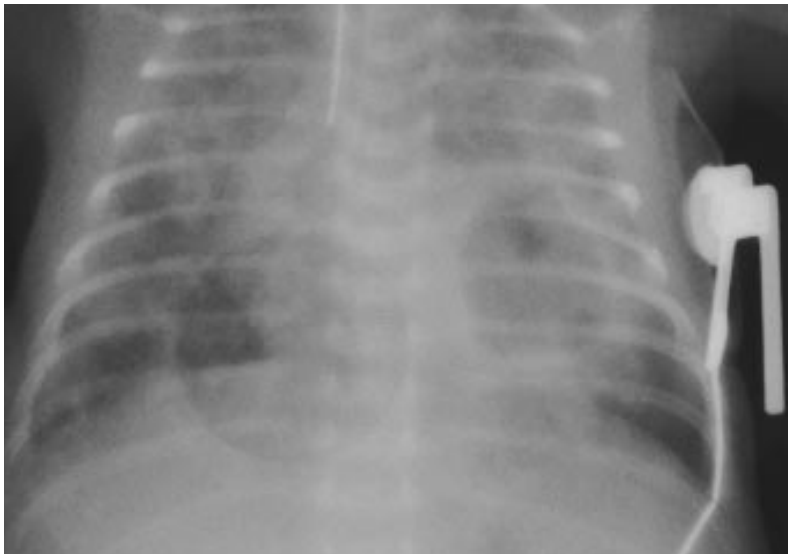

Figure 1.155. This chest radiograph of an infant with Stage IV BPD demonstrates pneumatocele formation in the left chest, prominent interstitial markings, and pulmonary edema. The circular hyperlucency seen over the mediastinum and right chest is an artifact caused by the hole in the incubator when the radiograph is taken from above.

1.156

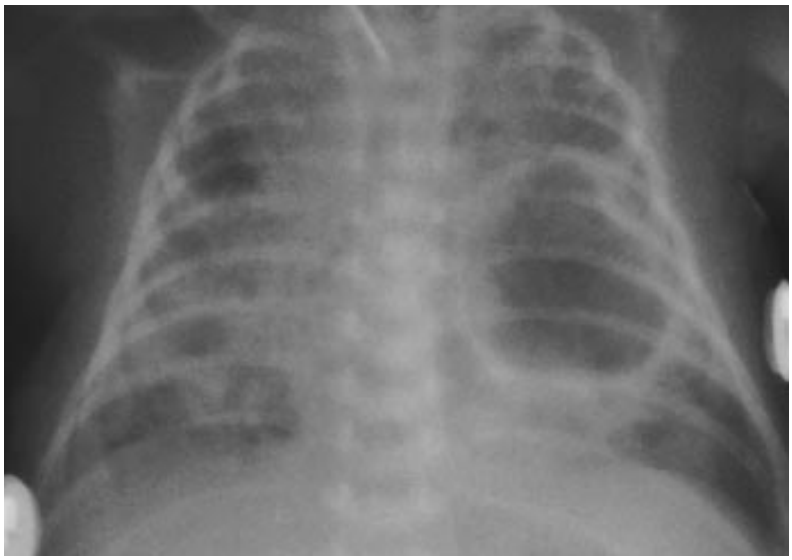

Figure 1.156. Twenty-four hours later, the same infant as in Figure 1.155 had an increase in the cystic areas and the pneumatocele on the left was larger.

1.157

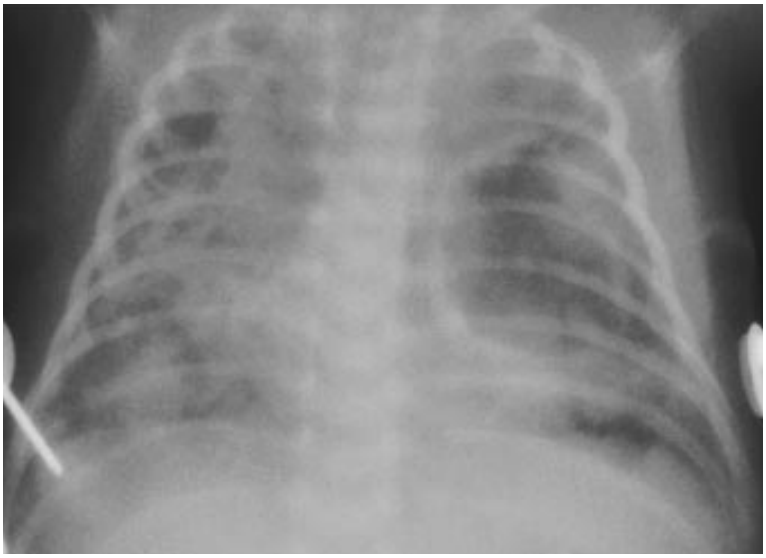

Figure 1.157. A radiograph of the chest of the same infant as in Figure 1.155 and 1.156 5 days later shows progression to the chronic changes of scarring and pulmonary edema. Lung injury this severe is often complicated by cor pulmonale. The overall prognosis for these infants is that approximately one-third recover, one-third develop chronic respiratory disease, and one-third die of respiratory failure.

1.158

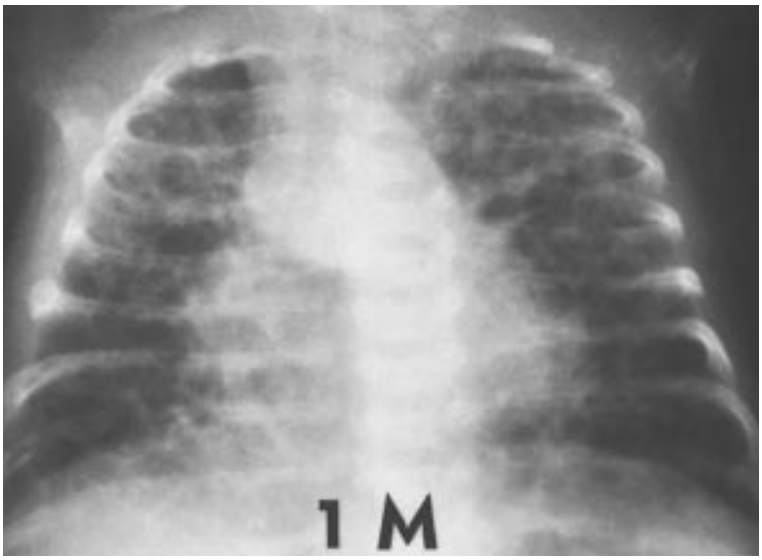

Figure 1.158. Wilson-Mikity syndrome (pulmonary dysmaturity, "bubbly" lung syndrome) shares many of the same radiologic features as Stage III BPD but there is no history of preceding hyaline membrane disease or of excessive oxygen therapy. The lungs are somewhat hyperinflated and there is a prominence of interstitial markings. Wilson-Mikity syndrome is not currently recognized as a disease entity.

1.159

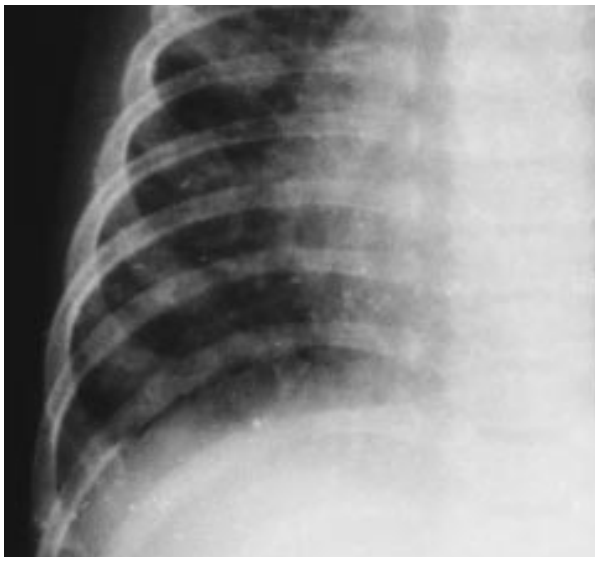

Figure 1.159. In an enlarged radiograph of lung markings at the costophrenic angle in the same infant as in Figure 1.158, the "bubbly" appearance of the lungs is noted. These radiographic features are usually pathognomonic in that they show diffuse linear and reticular areas of density within which are multiple cyst-like areas of hyperaeration.

1.160

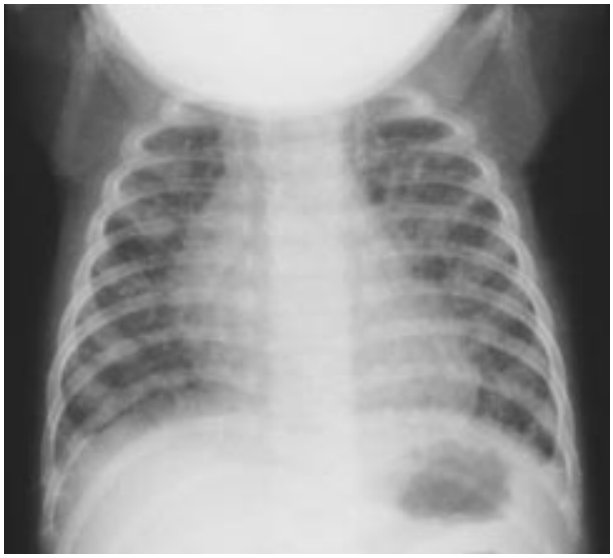

Figure 1.160. Wilson-Mikity syndrome is often confused with BPD because of the similar appearance on chest x-ray. This syndrome typically begins with no sign of respiratory distress. Clinical evidence of respiratory distress may occur in the first few days of life, especially in premature infants. However, the syndrome may not become evident until several weeks after birth, with the onset of respiratory distress which is usually not as severe as is seen in hyaline membrane disease. Oxygen requirements are usually not high.

1.161

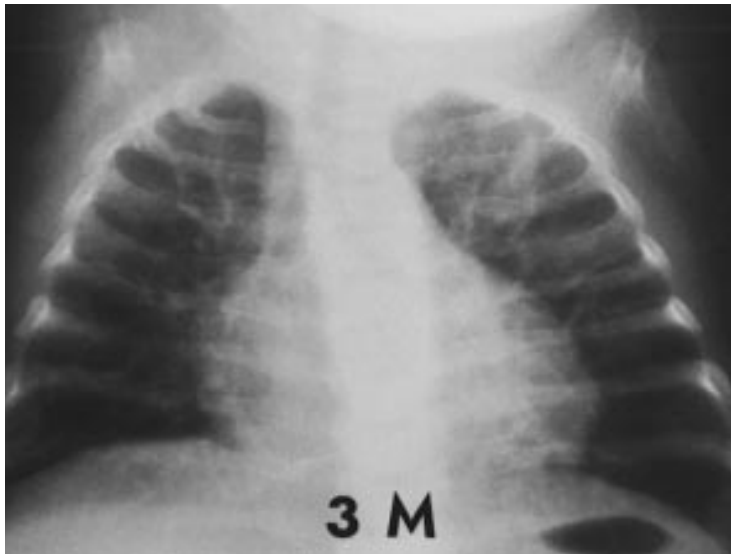

Figure 1.161. This chest radiograph in the same infant as in Figure 1.160 at the age of 3 months demonstrates persistent hyperinflation and prominent lung markings. The infant gradually improved over a period of 6 months and oxygen requirements were minimal.

1.162

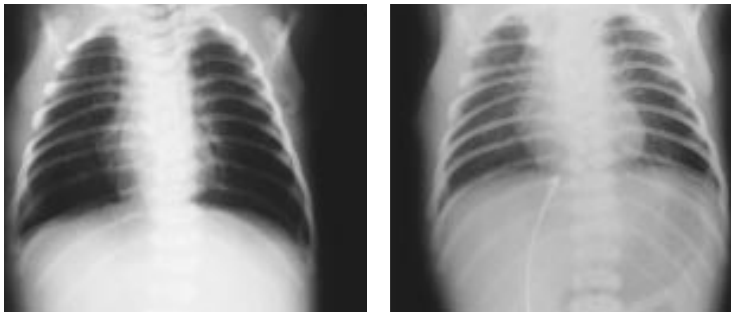

Figure 1.162. This infant was normal at birth, but at 1 week of age developed severe dehydration with cardiovascular symptoms and a severe metabolic acidosis. The chest radiograph on the left shows the markedly hyperinflated lungs with a small cardiac silhouette. The diagnosis of a salt-losing congenital adrenal hyperplasia was established. There was rapid improvement following rehydration and base administration, as noted in the chest radiograph on the right taken 2 hours later in which the lung fields and heart size appear normal. Severe dehydration associated with gastroenteritis can result in a similar problem.

1.163

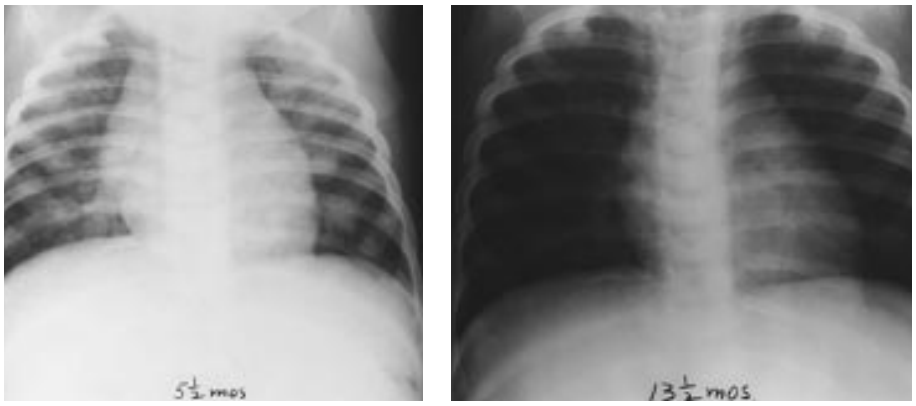

Figure 1.163. Congenital generalized fibromatosis can involve the skin, subcutaneous tissue, muscle, bone and visceral organs. The radiograph on the left demonstrates multiple fibromas in the chest of a 5 1/2-month-old child. There was complete resolution by 13 months of age, as seen in the radiograph on the right. Congenital generalized fibromatosi usually resolves spontaneously but is often fatal when visceral organs are involved, especially the lungs.

1.164

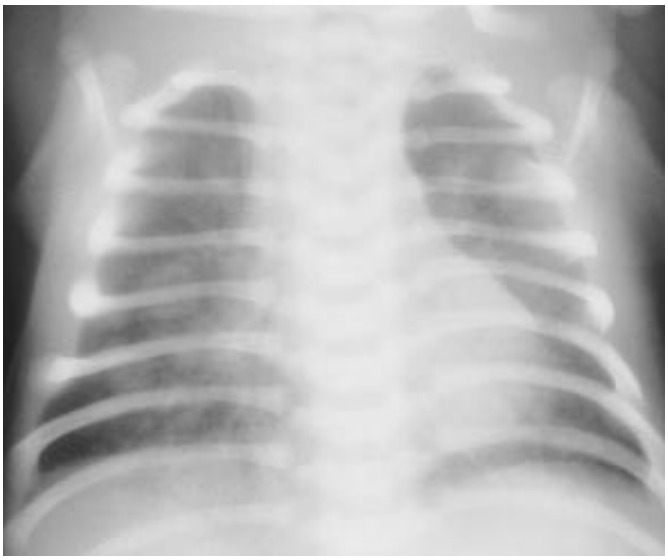

Figure 1.164. Reticuloendothelioses or histiocytosis X represents a variety of conditions which show clinical and pathologic overlap. There is a spectrum of widely disseminated monoblastic leukemia formerly called Letterer-Siwe disease. The lung is involved in only 2% of all cases. In this chest radiograph, note the bilateral lung nodules.

1.165

Figure 1.165. Histiocytosis X skin lesions are discrete, flat macules that occur when the cells invade the papillary dermis as seen in this same infant as in Figure 1.164. The infant did well on therapy.

1.166

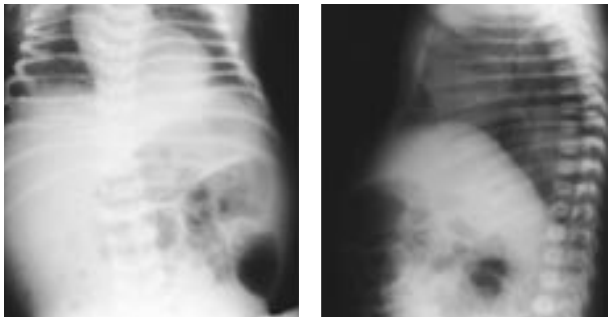

Figure 1.166. A left intrathoracic kidney is noted in this chest radiograph. The kidney arises embryologically from mesodermal tissue in the pelvis. It migrates caudally, passing along its blood supply to progressively higher levels of the aorta. Excessive migration can result in a thoracic location. Intrathoracic kidneys are generally asymptomatic. This infant had a chest radiograph performed at the age of 1 week because he had some abdominal distention.

1.167

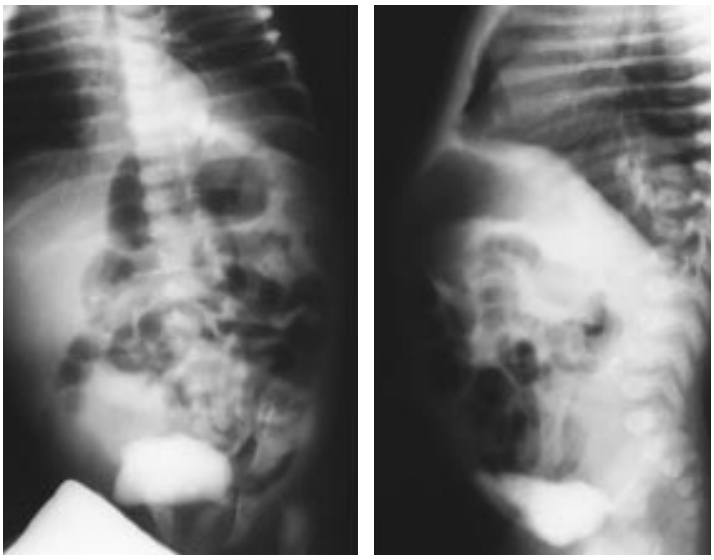

Figure 1.167. An intravenous pyelogram in the same infant as in Figure 1.166 demonstrates the location of the kidney in the thorax. Currently the diagnosis would be confirmed with the use of ultrasonography rather than a pyelogram.

1.168

Figure 1.168. In isolated dextrocardia, the apex of the heart is in the right side of the chest. Situs solitus is the rotation of viscera embryologically so that the heart lies in the left hemithorax and the abdominal organs are in their proper relationships (stomach on the left side and liver on the right). Situs inversus results when the heart and stomach are on the right and the liver is on the left. Infants with isolated dextrocardia have an increased incidence of congenital heart disease.

1.169

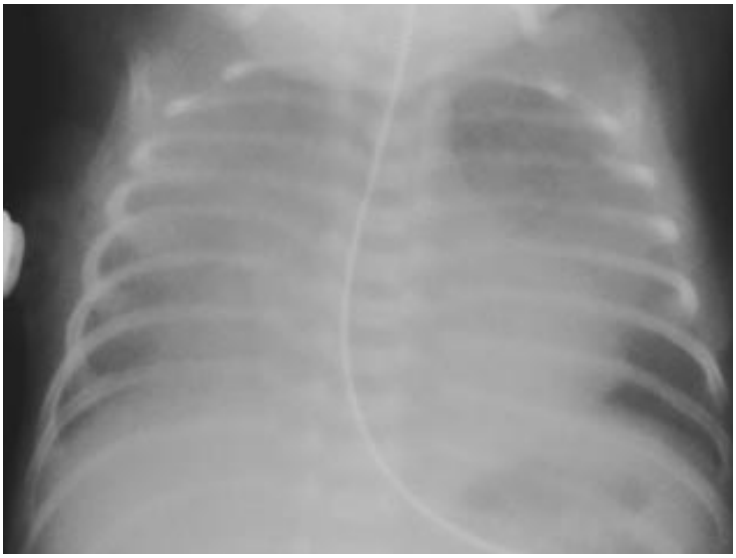

Figure 1.169. Patent ductus arteriosus (PDA) occurs commonly in preterm infants, but is rare in term infants. It can cause severe pulmonary overcirculation and systemic steal of blood flow resulting in shock, pulmonary edema and pulmonary hemorrhage. This radiograph shows an enlarged heart and hazy lung parenchyma because of a PDA and congestive heart failure.

1.170

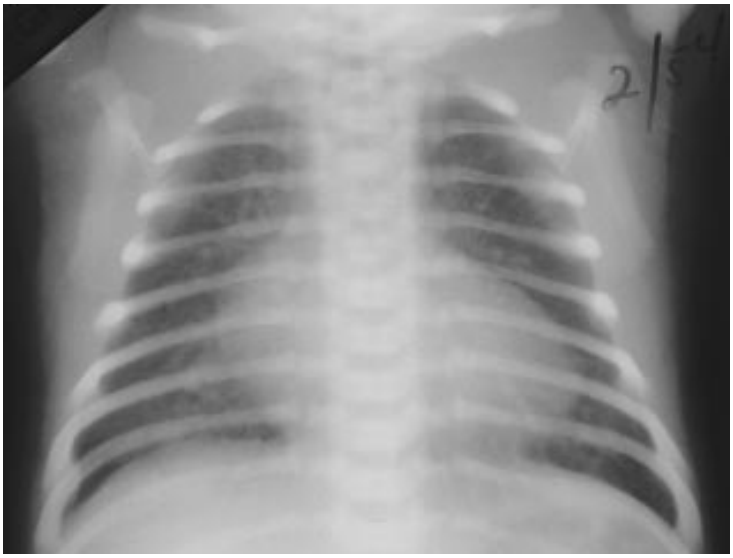

Figure 1.170. This is a chest radiograph of an infant with transposition of the great vessels. The heart is large and egg-shaped and the mediastinum is narrow on the anteroposterior view ("egg on a string"). The pulmonary artery segment is relatively flat and the pulmonary vascular markings are somewhat increased, compatible with the increased pulmonary blood flow in this condition.

1.171

Figure 1.171. In tricuspid atresia, there is a marked decrease in pulmonary artery vascularity, hence the nearly absent lung markings in this chest radiograph. The right heart border is relatively straight, and the cardiac apex is blunt and rounded with a concave pulmonary artery segment.

1.172

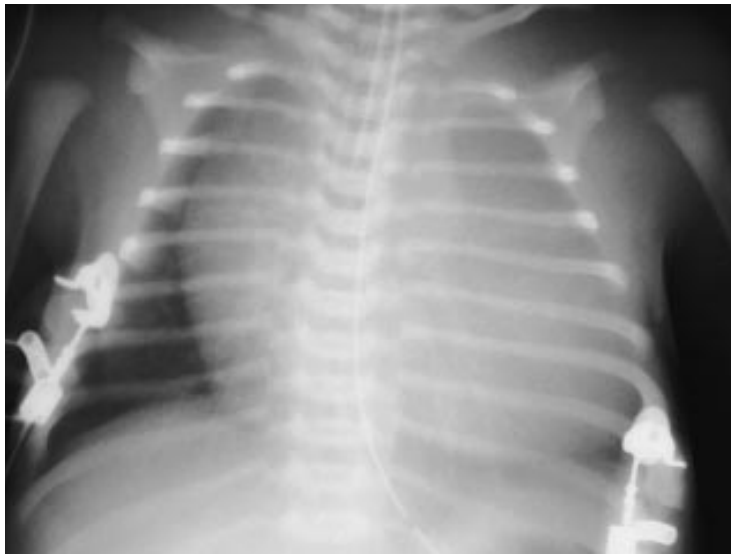

Figure 1.172. Ebstein's anomaly results in a massively dilated heart from tricuspid valve malformation, with tricuspid insufficiency, and sometimes right ventricular outflow tract obstruction. Clinically, the infants are profoundly cyanotic with severe respiratory distress. In Ebstein's anomaly the pulmonary vascularity is decreased and the right atrium is prominent.

1.173

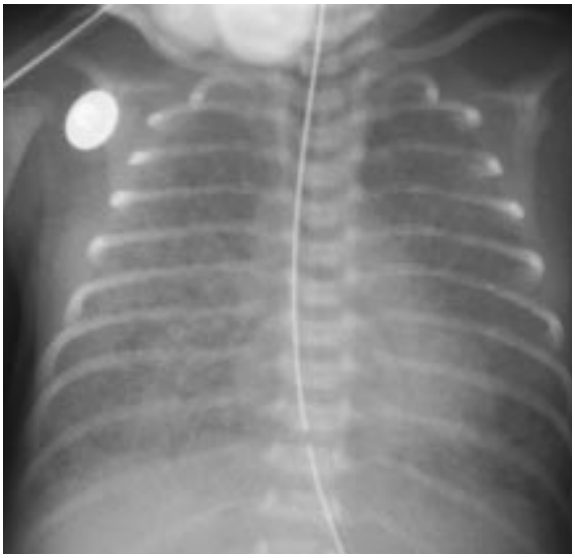

Figure 1.173. Anomalous pulmonary venous return below the diaphragm typically presents with respiratory distress. The infant presents with gross cyanosis, a normal cardiac outline, and plethoric lung fields (pulmonary edema) due to obstruction of the pulmonary venous drainage. The chest radiograph can mimic hyaline membrane disease or, rarely, meconium aspiration syndrome. Lack of improvement over the course of a few days should suggest the diagnosis. Mortality is high when the veins return to the inferior vena cava in a subdiaphragmatic position and are obstructed.

1.174

Figure 1.174. At 1 week of age, there was no clinical or radiographic improvement in the infant shown in Figure 1.173, suggesting the diagnosis of total anomalous pulmonary venous return below the diaphragm with obstruction. This was later confirmed by cardiac catheterization.

1.175

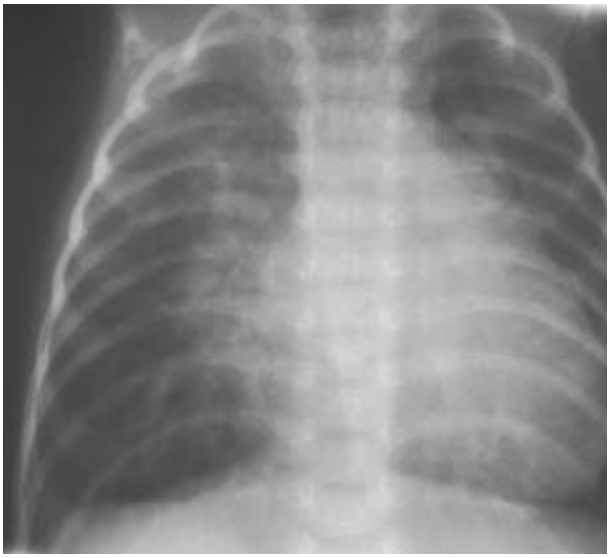

Figure 1.175. This infant with a large ventricular septal defect developed severe congestive heart failure. The cardiac silhouette is markedly enlarged and the lung fields are hazy from pulmonary edema.

1.176

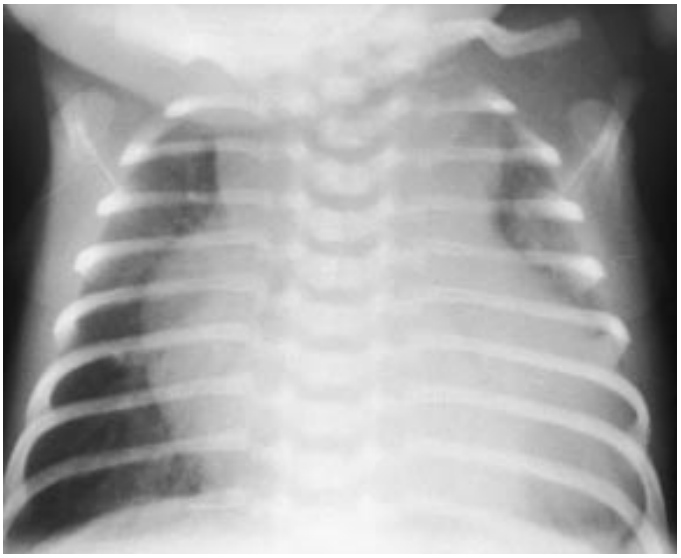

Figure 1.176. This infant presented with marked cardiomegaly and congestive heart failure from an arteriovenous malformation of the liver. In addition to congenital heart disease or myocarditis, the diagnosis of a large arteriovenous malformation should be included in the differential diagnosis of cardiomegaly. Clinical examination should include a careful auscultation for bruits over the skull, liver, and lungs and examination of the skin for shunts in large hemangiomas.

1.177

Figure 1.177. In the same infant as in Figure 1.176, angiography demonstrates venous filling of the arteriovenous malformation with rapid run-off of systemic arterial blood to the low resistance venous vessels. A bruit over the liver may not be heard on auscultation in every case.

1.178

Figure 1.178. Congestive heart failure due to a large arteriovenous malformation of the vein of Galen resulted in massive cardiomegaly as noted in the angiograph on the left. The angiograph on the right demonstrates the massive aneurysmal dilatation 1.3 seconds after an arterial injection. Arteriovenous malformations are now recognized prenatally with the use of fetal ultrasonography, and the diagnosis can be made postnatally with ultrasonography and computed tomography.

1.179

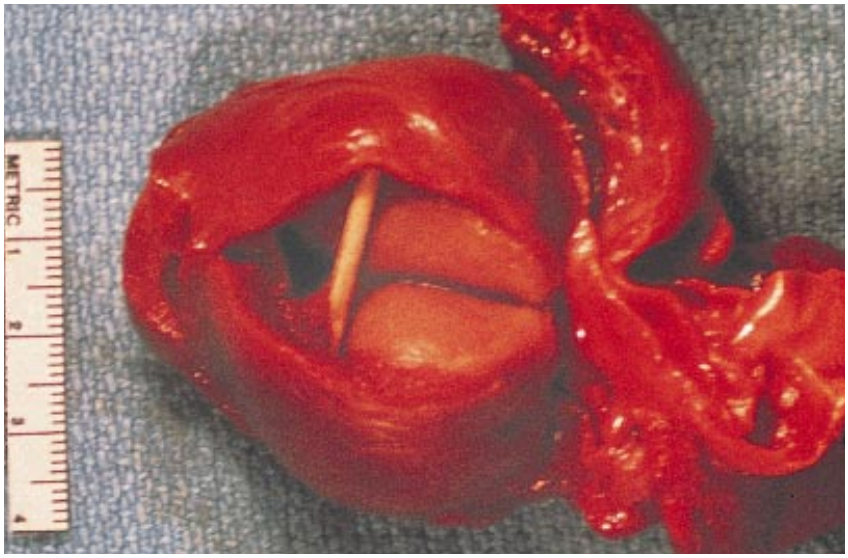

Figure 1.179. Tuberous sclerosis is a neurocutaneous syndrome in which there are skin lesions, as well as tumors of the brain, kidney, and the heart. This gross pathologic specimen shows a large rhabdomyoma lying within the atria. This syndrome may be recognized prenatally with the use of fetal ultrasonography.

1.180

Figure 1.180. A diverticulum of the left ventricle presented as a thoracoabdominal swelling in this infant. Cardiac activity was visible through the skin.

1.181

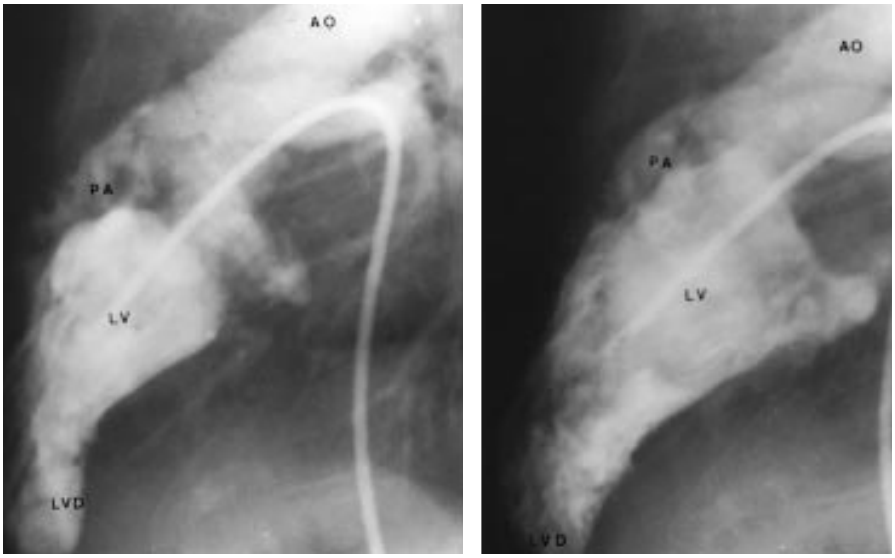

Figure 1.181. In the same infant as in Figure 1.180, the diagnosis of diverticulum of the left ventricle was confirmed by angiogram.

1.182

Figure 1.182. In this stillborn infant with ectopia cordis, the heart lies outside the thoracoabdominal wall. The heart typically has severe defects, such as in this case, with tetralogy of Fallot, secundum atrial septal defect, persistent left superior vena cava, and absent ductus arteriosus.

1.183

Figure 1.183. In another view of the same infant as in Figure 1.182, the heart is lying outside the skin over the chest and abdominal wall and is connected to the infant's circulation by a single small vessel. Attachment of the umbilical cord is also abnormal as there are severe circulatory anomalies. Surgical correction is not possible due to the small thoracic cavity and the possibility of compromising blood flow to the great vessels.

Chapter 2
Gastrointestinal System

The gastrointestinal tract absorbs and digests nutrients, maintains fluid and electrolyte balance, and protects the newborn from pathogens and toxins. Anatomic malformations of this system may be numerous and affect the pharynx, diaphragm, esophagus, stomach, small or large bowel, pancreas, liver, and spleen. The development of the gastrointestinal system is in close proximity and timing to the development of the respiratory and urogenital systems, and frequently malformations occurring in these systems are related. Normally the fetus is able to swallow and move amniotic fluid through the gastrointestinal tract at 12 weeks gestation, helping to regulate the amount of fluid in the amniotic sac. Maternal polyhydramnios may indicate that this regulation is not taking place and suggests a high intestinal obstruction in the fetus. Imaging studies, including radiographs, ultrasound, contrast, and magnetic resonance, may be necessary to define these disorders of the newborn gastrointestinal tract. During the second and third trimester, the fetal gut elongates and its glandular and functional development continues. Premature birth interrupts this development and poses special problems for the feeding, growth, and development of the infant.

2.1

Figure 2.1. Excess mucus secretion in an infant with esophageal atresia. The diagnosis of esophageal atresia or tracheoesophageal fistula should be considered in any infant spitting up a lot of mucus. During transition, normal infants may spit up a lot of mucus.

2.2

Figure 2.2. Radiograph of the chest of an infant showing esophageal atresia with a blind pouch. Note the tip of the catheter in the blind esophageal pouch. A gasless abdomen, which remains scaphoid, typically is seen in esophageal atresia because of the lack of communication between the respiratory and gastrointestinal tract.

2.3

Figure 2.3. Radiograph of the chest and abdomen in an infant with esophageal atresia. Note the coiled catheter in the air-filled blind pouch in the upper mediastinum and the excessive amount of gas in the abdomen. Lack of abdominal gas would, therefore, suggest the diagnosis of an esophageal atresia with a blind pouch; whereas air in the stomach and abdomen indicates communication between the trachea and esophagus, suggesting the diagnosis of tracheoesophageal fistula.

2.4

Figure 2.4. Radiograph of the chest and abdomen in an infant with a tracheoesophageal fistula and a double bubble of duodenal atresia. This combination of malformations is not uncommon in that both defects involve disorders of cannulation of the respective anlage. This infant had a type A tracheoesophageal fistula. These comprise 90% of tracheoesophageal fistulae.

2.5

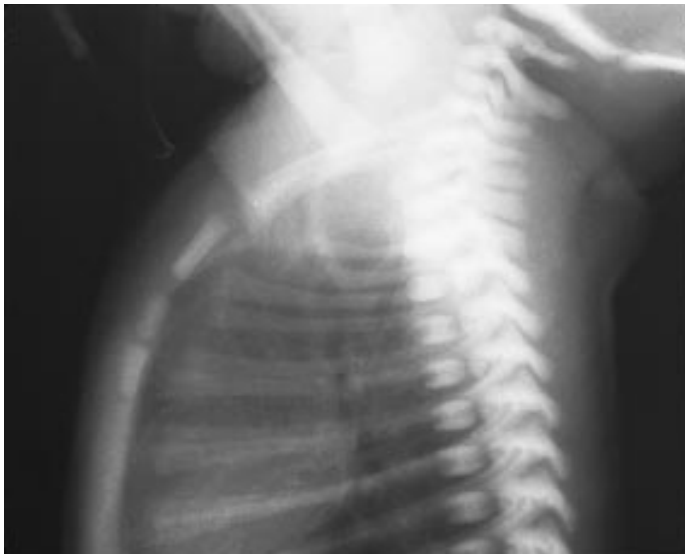

Figure 2.5. Lateral chest radiograph view of the same infant as in Figure 2.4 clearly demonstrates the blind pouch of the tracheoesophageal fistula. Note that the tracheal air column is present, but the esophageal air column is absent.

2.6

Figure 2.6. Contrast study of the blind pouch in an infant with a type A tracheoesophageal fistula.

2.7

Figure 2.7. Contrast study more clearly delineates the abnormal pouch. This procedure is often not needed and carries increased risk. Note the communication with spillage of barium into the respiratory tract as an excessive amount of contrast was used. This aspiration of contrast into the lungs via the tracheoesophageal connection is typical of type C and D tracheoesophageal fistulae, but can occur with any type.

2.8

Figure 2.8. Contrast study showing the typical H-type fistula (type B tracheoesophageal fistula). Note that the "H" looks like a reversed "N." This occurs as a result of unequal growth of the trachea and esophagus. This type is rare and occurs in less than 5% of cases.

2.9

Figure 2.9. In infants with tracheoesophageal fistula, consideration should be given to whether this is a part of the VACTERL (*v*ertebral defects, imperforate *a*nus, *c*ardiac defects, *t*racheoesophageal fistula, *r*enal anomalies, and *l*imb defects) or VATER (*v*ertebral defects, imperforate *a*nus, *t*racheoesophageal fistula, and *r*adial and *r*enal dysplasia) syndrome. This chest radiograph shows an infant with the VACTERL syndrome. Note the vertebral and rib anomalies, the blind pouch and gasless abdomen associated with esophageal atresia, and the dextrocardia. The infant also had an imperforate anus.

2.10

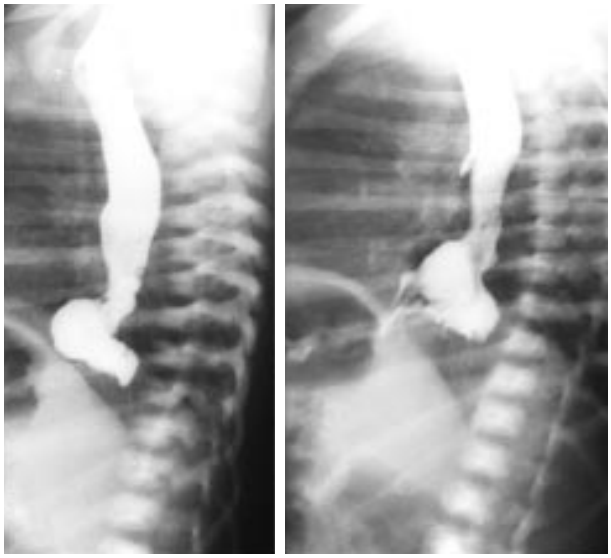

Figure 2.10. In a neonate who was vomiting at 4 days of age, the barium study demonstrates a hiatal hernia (congenital short esophagus).

2.11

Figure 2.11. Intestinal obstruction beyond the ampulla of Vater should be excluded in any neonate with bile-stained vomitus. Bile-stained vomitus can also occur in infants with sepsis or necrotizing enterocolitis.

2.12

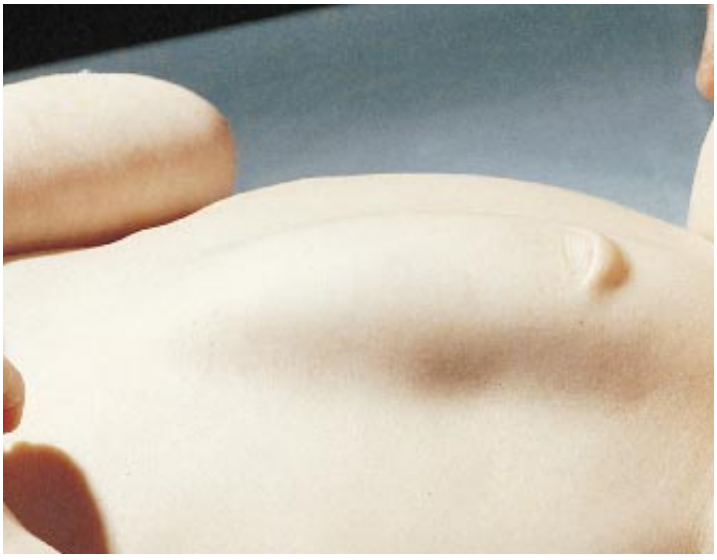

Figure 2.12. Diastasis recti (divarication of the recti muscles) in a term infant. This is a widened space between the rectus abdominis muscles. Lying between the umbilicus and the xiphoid process, it presents as a bulge especially with straining or crying. Varying degrees of separation may be found in nomal infants.

2.13

Figure 2.13. Diastasis recti in a premature infant. This condition is more frequently observed in low-birthweight infants and improves with maturation.

2.14

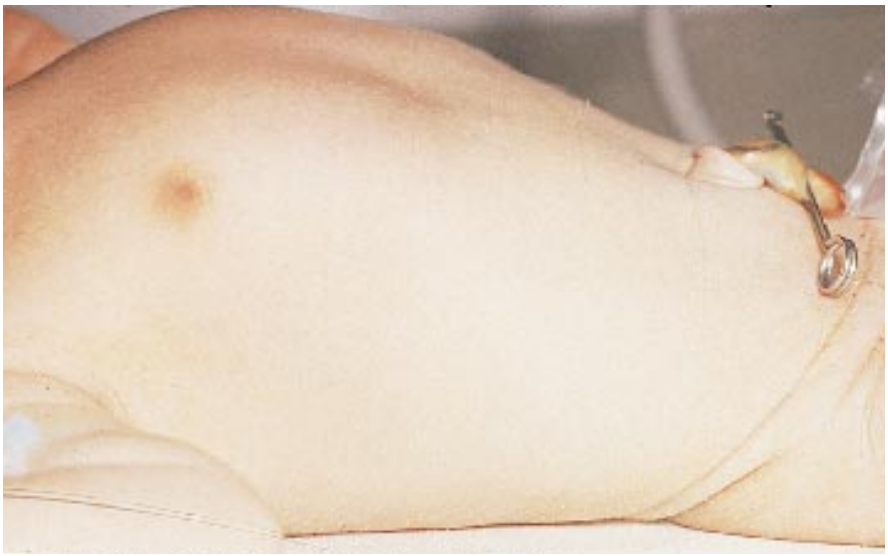

Figure 2.14. The abdomen is usually scaphoid at birth but as loops of bowel are filled with gas from swallowed air and the liver is displaced downward by postnatal expansion of the lungs, the abdomen soon becomes moderately protuberant. In this infant with a scaphoid abdomen, a diaphragmatic hernia was present. Differential diagnosis of a scaphoid abdomen includes severe CNS depression, congenital diaphragmatic hernia, and esophageal atresia with a blind pouch.

2.15

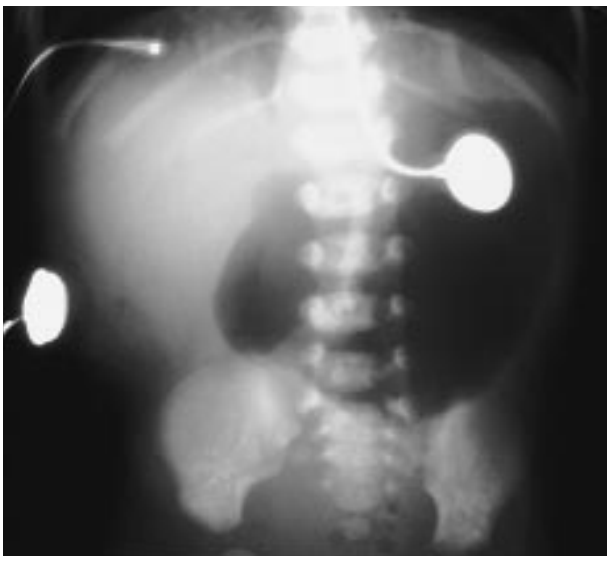

Figure 2.15. Radiograph of an infant with pyloric atresia. Note the large dilated stomach ("single bubble") with no gas distal to the obstruction. There is an association of pyloric atresia with epidermolysis bullosa.

2.16

Figure 2.16. Note the typical gastric peristalsis in a 10-day-old infant with pyloric stenosis. There was a history of projectile vomiting, constipation, and an "olive" was palpable. It is unusual for pyloric stenosis to present at this early age.

2.17

Figure 2.17. Radiograph of the same infant as in Figure 2.16 with pyloric stenosis. Note the large dilated stomach which is typical unless the infant has vomited recently. Note the gas in the gastrointestinal tract distal to the stomach as compared with the infant with pyloric atresia shown in Figure 2.15.

2.18

Figure 2.18. Contrast radiograph in a 3-day-old infant who presented with projectile vomiting. Pyloric stenosis generally does not present at this early age. At surgery a pyloric membrane was found. Note the "string" sign at the pylorus.

2.19

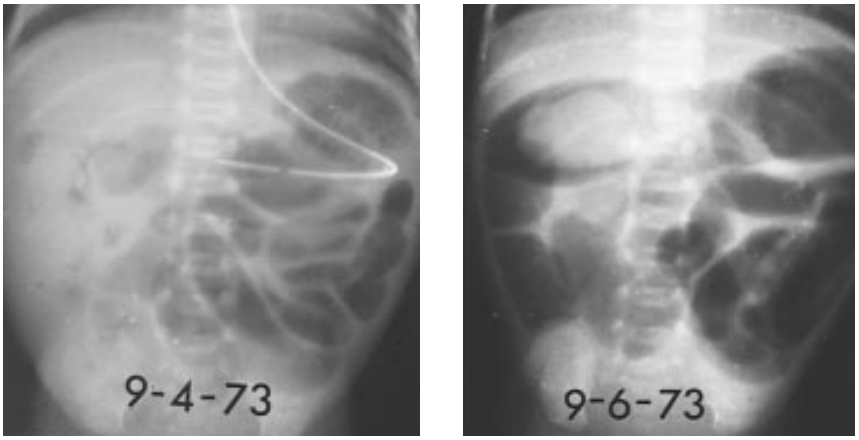

Figure 2.19. Radiograph of an infant with the inspissated milk syndrome. Note the multiple air fluid levels. This probably occurs with the use of formula containing excess long-chain fatty acids which form insoluble soaps resulting in indigestible milk curds. Note the lactobezoar with a marked increase in the size of the lactobezoar over the course of 2 to 3 days.

2.20

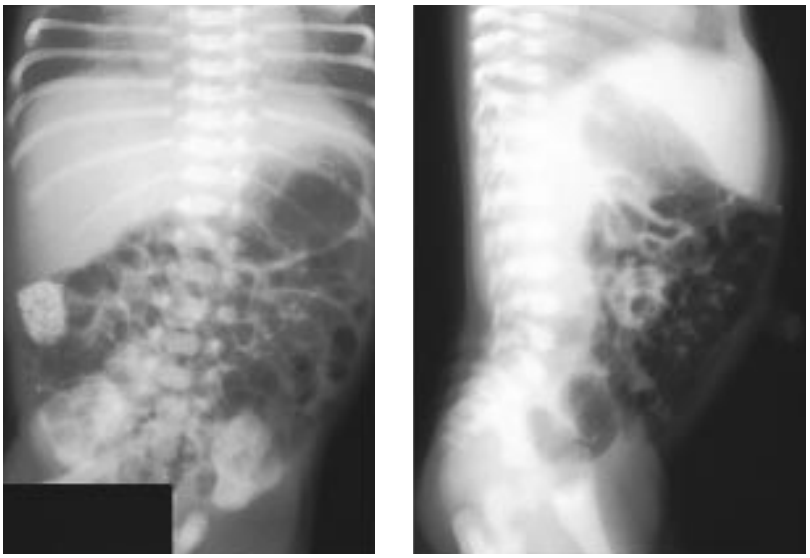

Figure 2.20. Anteroposterior and lateral radiograph showing a lactobezoar in an infant with the inspissated milk syndrome.

2.21

Figure 2.21. Duodenal atresia observed clinically in an infant at the age of 6 hours. Note the dilated stomach and dilated proximal duodenum giving rise to the "double bubble" appearance. At this early age, the infant also has a scaphoid lower abdomen. Thirty percent of infants with duodenal atresia will have other major anomalies, especially chromosomal abnormalities (e.g., Down syndrome).

2.22

Figure 2.22. Radiograph of the same infant as in Figure 2.21 with duodenal atresia showing the classic "double bubble" appearance. Note that there is no gas distal to the obstruction at the duodenum. The opacity in the right lower quadrant represents the soft tissue shadow of the umbilical cord. This shadow is normally obscured in a gas-filled abdomen.

2.23

Figure 2.23. Radiograph of a normal infant at the age of 2 hours. The appearance suggests a "double bubble." This is an artifact as the radiograph was taken through the top of the incubator. The very circular lucency seen in the right abdomen represents the hole in the incubator.

2.24

Figure 2.24. Radiograph of an infant with a duodenal web and windsock deformity resulting in the typical "double bubble" appearance. One can see a similar appearance in an annular pancreas causing complete obstruction.

2.25

Figure 2.25. Radiograph of infant with duodenal stenosis. Note the presence of gas distal to the "double bubble." This appearance is also seen in infants with annular pancreas and malrotation with Ladd's bands.

2.26

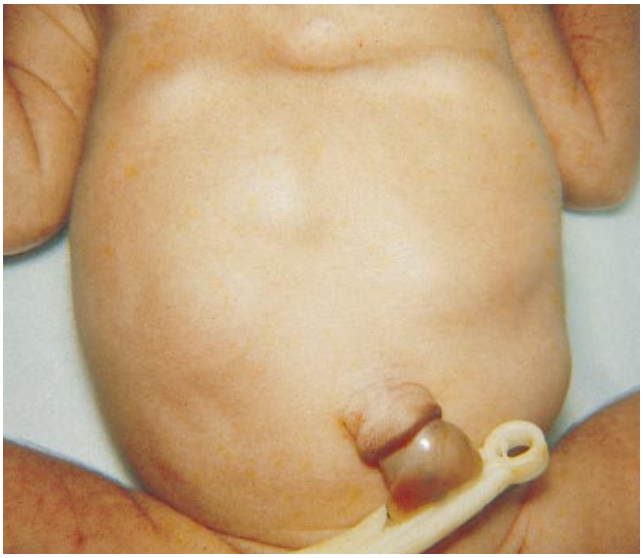

Figure 2.26. Clinical appearance of an infant at the age of 8 hours with jejunal atresia. Note the dilated stomach, dilated duodenum and dilated proximal jejunum giving the typical "triple bubble" appearance. Since jejunal and ileal atresias are due to vascular accidents, they are rarely associated with anomalies.

2.27

Figure 2.27. Lateral view of the same infant as in Figure 2.26 showing the typical "triple bubble" appearance. Note the scaphoid appearance of the lower abdomen in the infant at this early age.

2.28

Figure 2.28. Radiographic appearance of jejunal atresia showing the typical "triple bubble." The dilated stomach, dilated duodenum and dilated proximal part of the jejunum are easily observed.

2.29

Figure 2.29. Barium contrast enema in the same infant with jejunal atresia as in Figure 2.28. Note the "triple bubble" in the background and the microcolon demonstrated by the contrast medium. The microcolon is due to the lack of passage of bowel contents distal to an intestinal obstruction. It may occur in distal jejunal atresia, ileal atresia, or atresia of the proximal colon. Following relief of the obstruction, the caliber and function of the colon are normal.

2.30

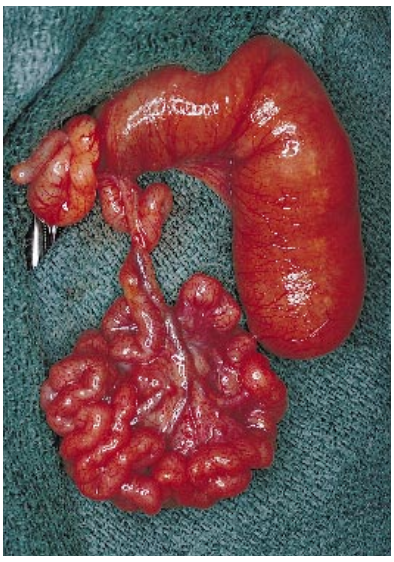

Figure 2.30. Surgical specimen in an infant with jejunal atresia showing the "Christmas tree" deformity (also called "apple peel" deformity). The loops of small bowel encircle a very short mesentery the way lights are draped on a Christmas tree. Note that there is no intestinal continuity and the proximal jejunum is approximately five times the size of the colon.

2.31

Figure 2.31. Marked abdominal distension in an infant with aganglionosis (Hirschsprung's disease) at the age of 4 days. Differential diagnosis includes intestinal obstruction, sepsis (ileus), ascites, and abdominal masses (hydronephrosis, ovarian tumors, etc.).

2.32

Figure 2.32. Abdominal radiograph of an infant who presented with marked distension and failure to pass stool due to ileal atresia. Note the large dilated loops of bowel. Differential diagnosis includes atresia of the colon and imperforate anus. It may be difficult to differentiate between loops of small and large bowel radiographically in a neonate since haustrations are not present at this early age.

2.33

Figure 2.33. Barium enema in the same infant as in Figure 2.32, showing a typical microcolon. Microcolon occurs as a result of lack of passage of bowel contents distal to the obstruction.

2.34

Figure 2.34. Barium enema in an infant with a normal colon. Note the difference in the caliber compared to that of a microcolon (Fig. 2.33). Note the isolated dextrocardia.

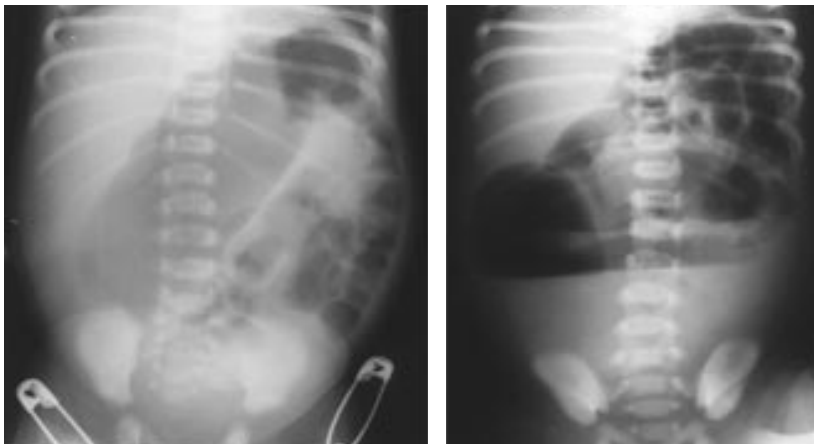

2.35

Figure 2.35. Abdominal radiograph in an infant who presented at the age of 3 days with massive abdominal distension, lack of stool, and vomiting. This infant has atresia of the colon. Note the large distended loop of bowel in the radiograph on the left. The upright radiograph on the right demonstrates air/fluid levels due to the obstruction. (Singleton, E., Wagner, M.)

2.36

Figure 2.36. Barium enema in the same infant as in Figure 2.35 shows a microcolon with abrupt termination at the splenic flexure, confirming the diagnosis of atresia of the colon. (Singleton, E., Wagner, M.)

2.37

Figure 2.37. Appearance of atresia of the colon at surgery in the same infant as in Figures 2.35 and 2.36. Note the large dilated colon proximal to the atresia. Compare this with the preceding radiograph in Figure 2.29. Note the distal microcolon. The vascular insult in this infant resulted in complete separation of the proximal and distal segments of the colon. Decompression and colostomy permitted successful re-anastomosis one week postoperatively.

2.38

Figure 2.38. Radiograph of an infant with aganglionosis (Hirschsprung's disease). Massive dilated loops of bowel are seen on the flat plate film on the left and the upright film on the right. Upright films reveal no gas visible in the rectum.(Singleton, E., Wagner, M.)

2.39

Figure 2.39. Radiograph of another infant with Hirschsprung's disease. Note the markedly dilated loops of bowel, particularly the transverse and descending colon. This infant presented with severe abdominal distension (see Figure 2.31) and delayed passage of meconium.

2.40

Figure 2.40. Barium enema of the same infant as in Figure 2.39 showing the gross dilatation of the large bowel proximal to the short aganglionic segment.

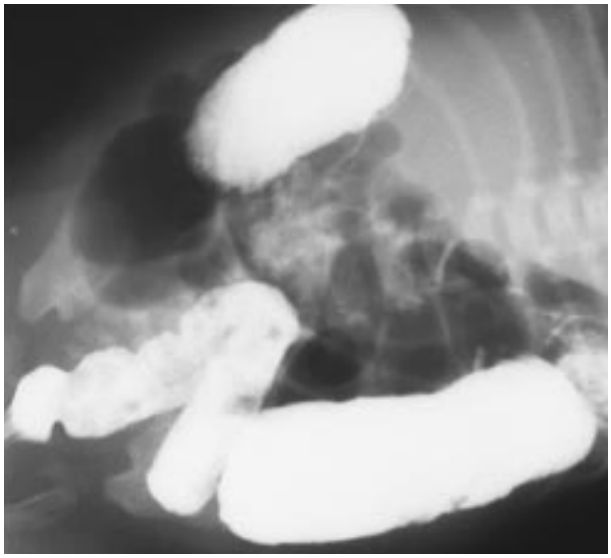

2.41

Figure 2.41. Oblique view of the barium study in the same infant as in Figures 2.39 and 2.40 better demonstrates the aganglionic segment.

2.42

Figure 2.42. Barium enema in an infant of a diabetic mother with the small left colon syndrome. In the small left colon syndrome, there is a microcolon distal to the splenic flexure. Note the lack of haustrations which is normal for an infant. (Singleton, E., Wagner, M.)

2.43

Figure 2.43. Another example of a barium enema in an infant with the small left colon syndrome. This condition is commonly seen in infants of diabetic mothers. Note the microcolon distal to the splenic flexure. Management of this condition is nonoperative, with slow enteral feedings and total parenteral nutrition support until the colon dilates to a more functional size.

2.44

Figure 2.44. Abdominal distension with prominent loops of the bowel in a premature infant. This so-called "pseudoparalytic ileus" of prematurity occurs as a result of poor muscle development in both the abdominal wall and intestinal wall. The infants develop temporary distention with prominent loops of bowel, especially at feeding times. The condition improves with increasing maturity. Persistent distention in a premature infant could be associated with delay in passing meconium.

2.45

Figure 2.45. Intestinal obstruction in a term infant. Note the "ladder pattern" of the dilated loops of bowel. Distention and dilated loops of bowel can occur with any type of intestinal obstruction. In this instance they are secondary to a meconium plug. This appearance is pathologic as compared with the "pseudoparalytic ileus" of prematurity.

2.46

Figure 2.46. Lateral view of the same infant as in Figure 2.45. Note the abdominal distention and the "ladder pattern" of the dilated loops. Differential diagnosis includes other forms of intestinal atresia or obstruction.

2.47

Figure 2.47. Abdominal radiograph of an infant with the meconium plug syndrome. Note the generalized distention due to the dilated loops of bowel and the lack of gas in the pelvis. This would suggest the presence of an obstruction in the distal part of the large bowel.

2.48

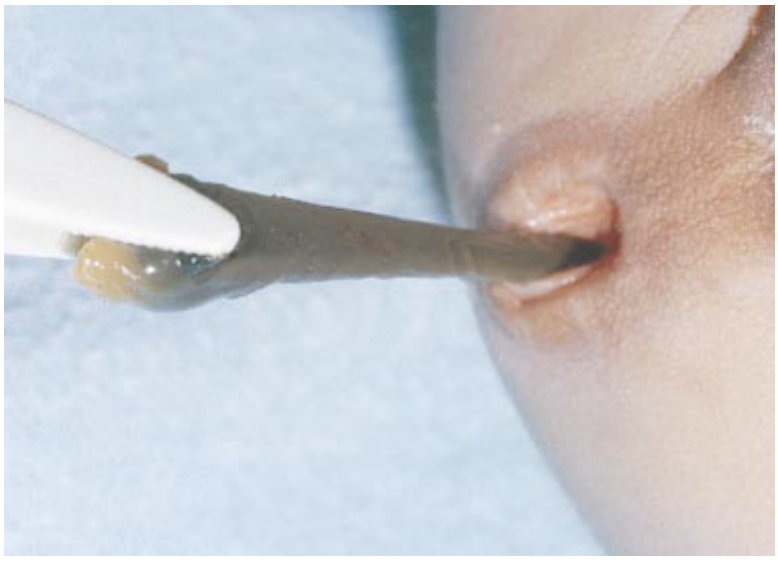

Figure 2.48. The same infant as in Figure 2.47, after a gentle saline enema, passed a large meconium plug. This meconium plug consists of inspissated meconium which obstructs the bowel lumen. In infants with meconium plug syndrome, the differential diagnosis includes meconium ileus (cystic fibrosis) and Hirschsprung's disease. Meconium plugs have also been reported in infants born to mothers treated with magnesium sulfate for toxemia of pregnancy.

2.49

Figure 2.49. Mucous and meconium plug in an infant. A mucous plug forms earlier in gestation and is gray to greenish in appearance. This occurs because of lack of bile formation early in gestation. The true meconium plug occurs later in gestation. This figure demonstrates a combination of a mucous and meconium plug. With passage of the plug, the mucous portion of the plug appears first because it develops earlier.

2.50

Figure 2.50. Pathologic appearance of a large meconium plug in the mid-jejunum. The plug was associated with intraluminal hemorrhage and colitis. This infant died of necrotizing enterocolitis.

2.51

Figure 2.51. Radiographs of an infant with abdominal distention as a result of meconium ileus. Note the opacification of the bowel lumen with relative paucity of air because of the presence of a large amount of inspissated meconium. In infants with meconium ileus, the diagnosis of cystic fibrosis and Hirschsprung's disease should always be excluded. (Singleton, E., Wagner, M.)

2.52

Figure 2.52. Differential diagnosis of abdominal distention at birth includes ascites due to multiple causes, meconium peritonitis, and abdominal masses. In this infant the abdominal distention was due to meconium peritonitis, which arises in utero when there is a perforation of the bowel wall with passage of meconium into the peritoneal cavity. The infant also had severe respiratory distress due to pressure on the diaphragm. The classic association is with either perforation and meconium ileus or perforation with bowel atresia. Often no cause is found.

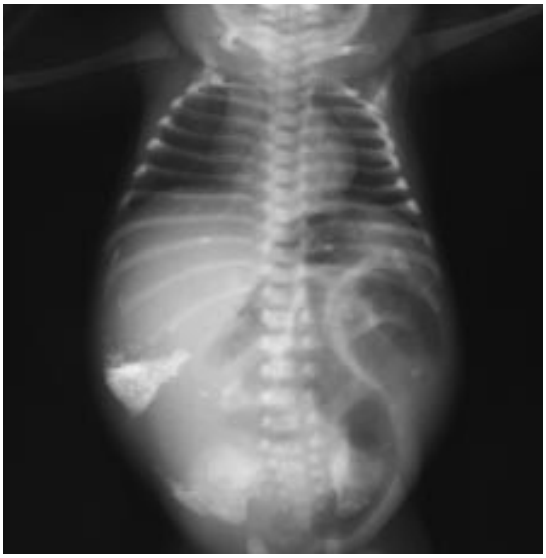

2.53

Figure 2.53. Radiograph of an infant with meconium peritonitis. Note the diffuse calcifications in the peritoneal cavity. This is a classic radiographic sign of this condition. As the bowel perforation occurs in utero, on rare occasions the meconium tracks down the inguinal canal into the scrotum and areas of calcification may be seen in the scrotum.

2.54

Figure 2.54. Lateral view of the same infant as in Figure 2.53 with meconium peritonitis. Note the abdominal distention with diffuse calcifications.

2.55

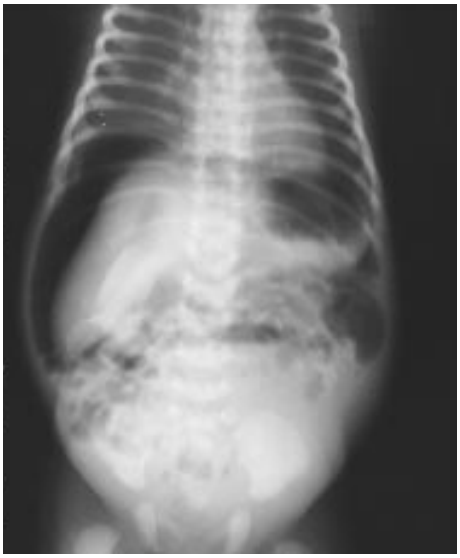

Figure 2.55. Upright radiograph of an infant with meconium peritonitis associated with perforation of the colon and pneumoperitoneum. Also note the diffuse calcification especially over the area of the liver.

2.56

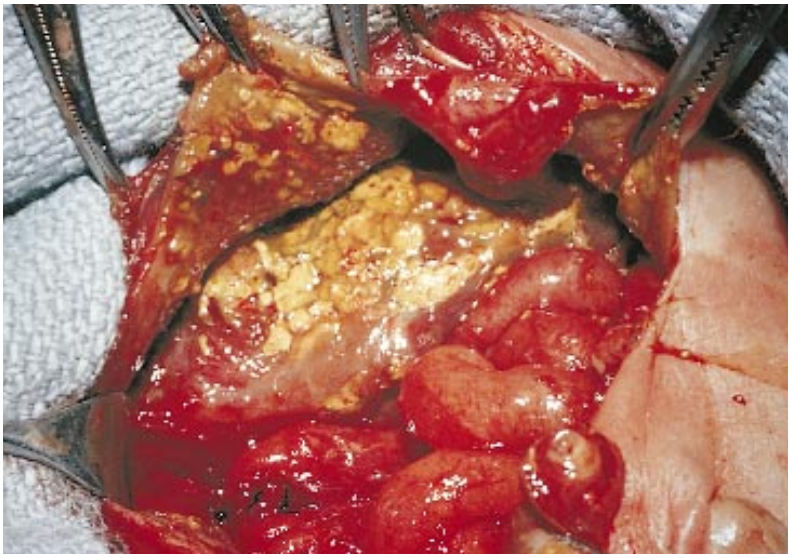

Figure 2.56. Surgical appearance of meconium peritonitis. Note the areas of calcification over the liver and in the peritoneal cavity.

2.57

Figure 2.57. This infant presented with severe abdominal distention at birth. The diagnosis of a giant cystic meconium peritonitis was confirmed radiologically and at surgery. A meconium pseudocyst occurs as a result of a late intrauterine perforation with pouring of meconium into the peritoneal cavity.

2.58

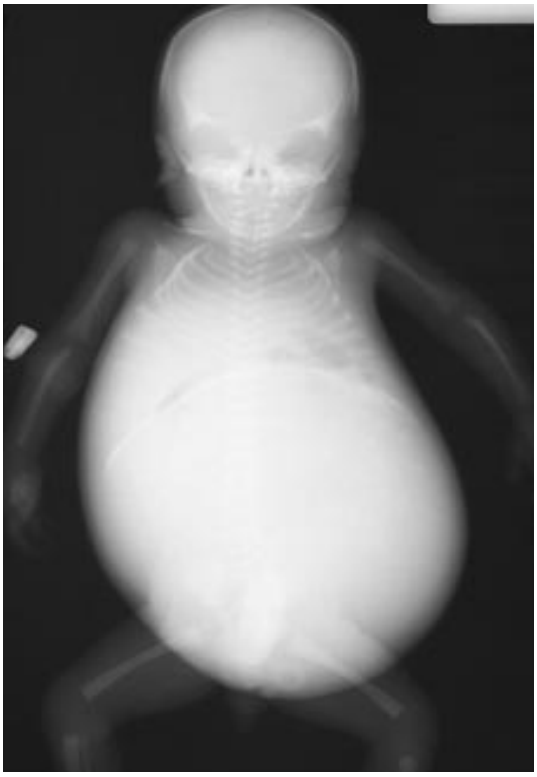

Figure 2.58. Radiograph of the same infant as in Figure 2.57 showing the rim of calcification outlining the giant meconium pseudocyst. There may be large air/fluid levels.

2.59

Figure 2.59. Imperforate anus (anal atresia) in an infant. Imperforate anus may appear in two forms: the rare membranous atresia, which probably results from failure of perforation of the anal membrane early in gestation; and the much more common anorectal atresia, in which the rectum ends blindly some distance above the perineum. In this type a fistula usually joins the blind pouch to the skin and the anal sphincter is usually intact and in its normal location. On the surface a remnant of the anal canal may be seen as a shallow dimple as in this infant.

2.60

Figure 2.60. Extension of the median raphe in an infant with imperforate anus. In low anal atresias there may be a fistula to the anal cleft. Location may be "high" or "low" depending on whether the atresia is above ("high") or below ("low") the puborectalis muscle.

2.61

Figure 2.61. Median raphe with small inclusion cysts and an imperforate anus. Without careful examination, the diagnosis of imperforate anus may easily be missed.

2.62

Figure 2.62. This is another example of an infant with imperforate anus. Note the anal dimple and in addition there is a hypospadias involving the glans. Anal atresia is often associated with other anomalies, primarily genitourinary tract or vertebral anomalies. It is also observed in the VACTERL syndrome.

2.63

Figure 2.63. Imperforate anus with a superficial fistula running anteriorly from the anus along the midline of the perineum to the scrotum.

2.64

Figure 2.64. Imperforate anus with a rectoperineal fistula from which there was passage of meconium and later stool.

2.65

Figure 2.65. Imperforate anus with a rectourethral fistula. The majority of high anal atresias have a fistulous connection with the bladder or urethra in males or the vagina in females. This leads to passage of meconium from the urethra or from the vagina. If there is a fistulous connection to the bladder (rectovesical) the urine is mixed with meconium on voiding. If the fistulous connection is to the urethra (rectourethral), meconium trickles out of the urethra.

2.66

Figure 2.66. This infant with an imperforate anus has a rectovaginal fistula. In addition note the imperforate hymen. Because meconium may be passed through the fistula and out through the vagina, the diagnosis may be missed without careful inspection.

2.67

Figure 2.67. Imperforate anus with a rectovaginal fistula. The large fistulous tract allows for free passage of meconium hence this infant had no abdominal distention.

2.68

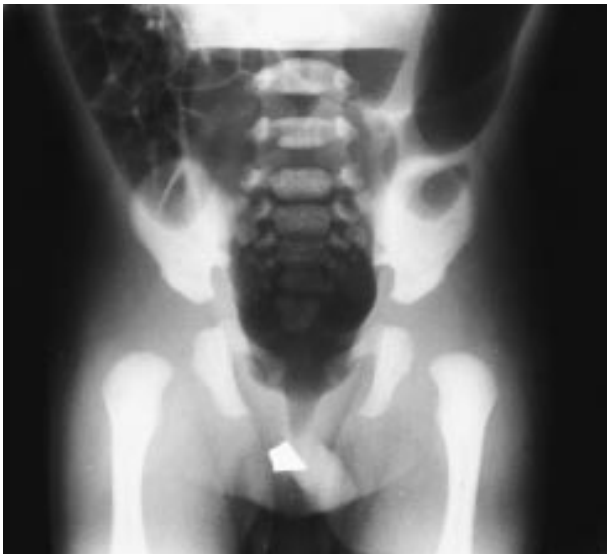

Figure 2.68. Radiograph of an infant with imperforate anus. The Wangensteen technique for diagnosis of high or low location of an imperforate anus places the infant in a head-down position using air as a contrast medium. A radio-opaque marker is placed over the external anal dimple. Presence of an air column, as this figure demonstrates, shows a "low" imperforate anus. Failure of gas to fill the rectum and anal canal demonstrates a "high" imperforate anus. (Singleton, E., Wagner, M.)

2.69

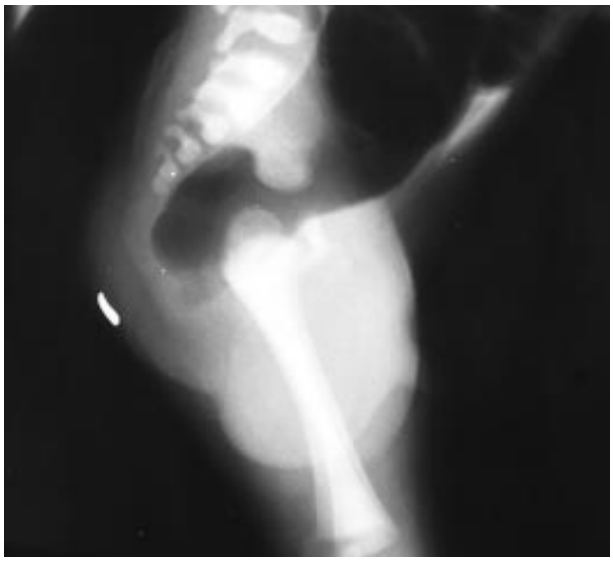

Figure 2.69. Lateral radiograph of the same infant as in Figure 2.68 shows the marker placed over the imperforate anus superficially with the air column demonstrating a "low" obstruction, as the air column is distal to the anatomic position of the puborectalis muscle. This technique may not demonstrate a fistulous tract. (Singleton, E., Wagner, M.)

2.70

Figure 2.70. Imperforate anus with a large left obstructed colon. Note the anomalies of the lumbosacral spine. The spinal column should be checked in any infant with anal atresia.

2.71

Figure 2.71. Contrast radiograph of an infant with an imperforate anus. The fistulous tract may be visualized under fluoroscopy. The technique is to inject a small amount of contrast medium (using the anal dimple as a marker) into the distal rectum from the skin. (Singleton, E., Wagner, M.)

2.72

Figure 2.72. Radiograph of a male infant with an imperforate anus and a rectovesical fistula. Note the calcifications in the abdomen. Urine passage into the colon results in the typical "popcorn" calcifications which are contained in the colon. This differs from the extraluminal calcification seen in patients with meconium peritonitis. Also note the opacity in the left lower abdomen which is the umbilical cord being visualized on an opaque background.

2.73

Figure 2.73. Autopsy specimen of the colon in an infant who had anal atresia with a rectovesical fistula. Note the colonic contents showing calcified meconium due to the anomalous communication between the bowel and genitourinary tract. This infant had caudal regression syndrome. (Langston, C.)

2.74

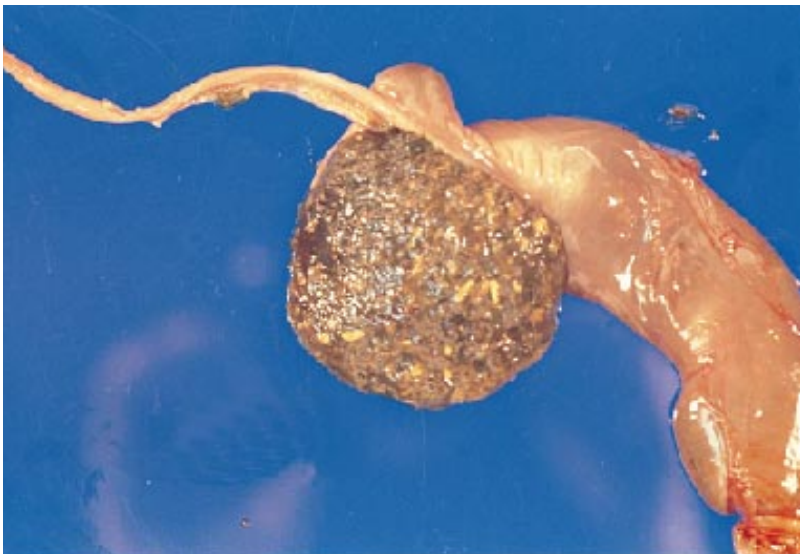

Figure 2.74. Appearance of calcified colonic contents after dissection of the bowel. (Langston, C.)

2.75

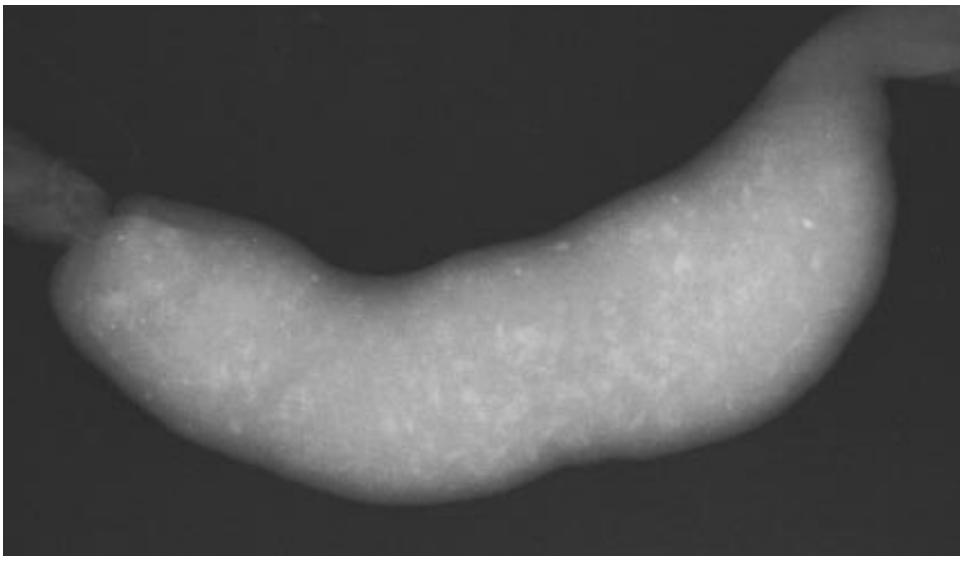

Figure 2.75. Radiograph of the autopsy specimen seen in Figure 2.73, showing the calcified colonic contents ("popcorn" appearance). (Langston, C.)

2.76

Figure 2.76. This infant presented with a patulous appearance of the anal sphincter. This may denote an abnormality of the innervation to the perineum. On rectal examination an obstruction was detected approximately 1 cm from the anal orifice as the result of an imperforate anal membrane.

2.77

Figure 2.77. Following puncture of the membrane with a hemostat in the same infant as in Figure 2.76, there was rapid passage of meconium with no further problems.

2.78

Figure 2.78. Failure of fusion of the perineal raphe involving the rectal sphincter.

2.79

Figure 2.79. Anterior placement of the anus in an infant. This occurs when there is an abnormality of fusion between the urorectal septum and the cloacal membrane. If there is inadequate development of the urorectal septum and if its junction with the cloacal membrane is too far anteriorly, the anus is displaced forward and may open anywhere along the perineum. The anal opening is generally much smaller than normal.

2.80

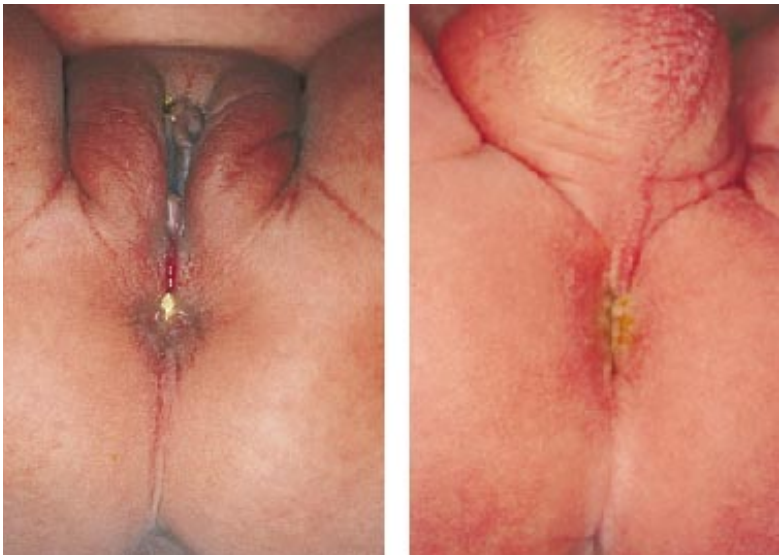

Figure 2.80. Anterior placement of the anus in a female infant on the left and in a male infant on the right. Ectopic anus may rarely be seen in the form of posterior displacement of the anus producing an abnormally long perineum.

2.81

Figure 2.81. Anal skin tags are small outgrowths of the mucosa arising from the anal margin. They are relatively common and have no pathologic significance.

2.82

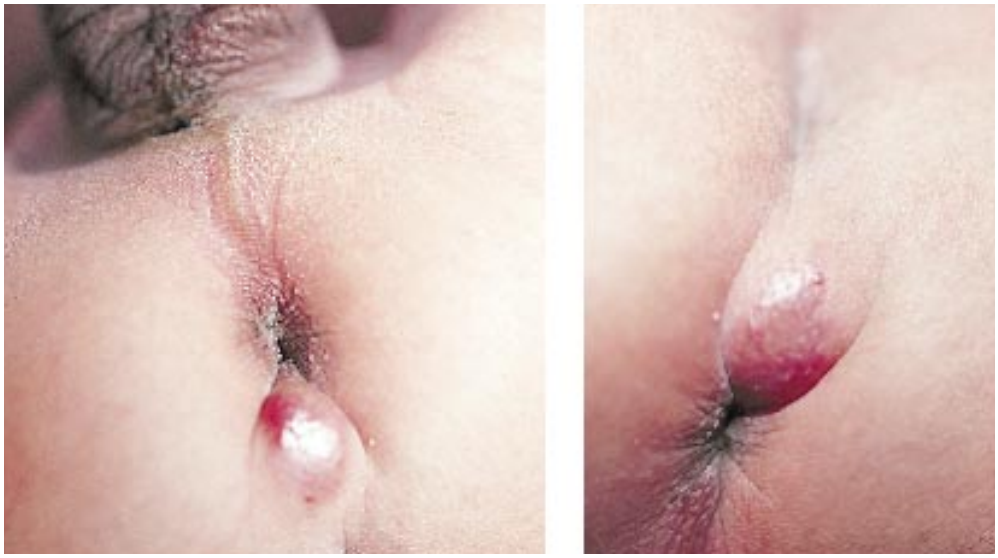

Figure 2.82. Perianal abscess in a neonate at 10 days of age. The etiology was undetermined but it healed rapidly following drainage.

2.83

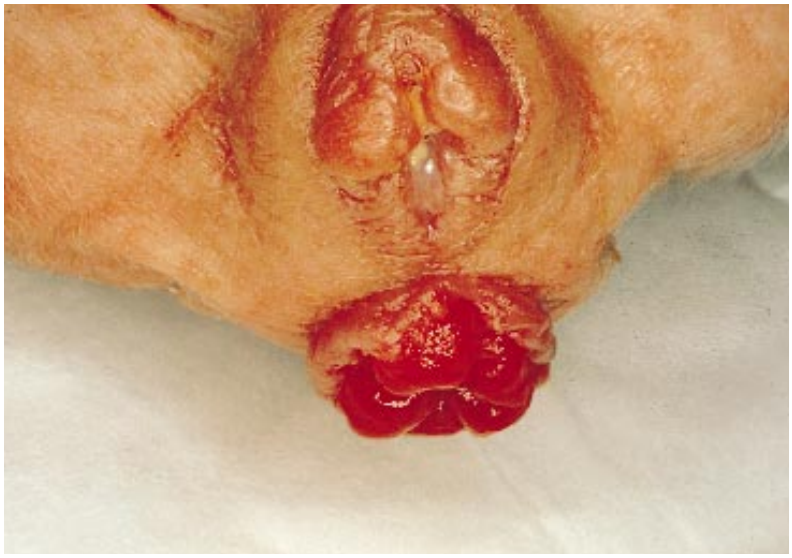

Figure 2.83. Coincidental rectal prolapse in a severely growth-retarded infant with leprechaunism. Rectal prolapse is very rare in a neonate, but if it occurs in the first few months of life a diagnosis of cystic fibrosis should be excluded. It may be seen in association with anomalies such as bladder exstrophy or any other condition causing raised intra-abdominal pressure and usually improves spontaneously.

2.84

Figure 2.84. Barium enema in an infant with malrotation and volvulus. Note the anterior placement of the descending colon with failure to fill the ascending colon as a result of the volvulus.

2.85

Figure 2.85. Contrast radiograph of an infant with a sigmoid volvulus. Note the failure of passage of barium into the descending and transverse colon with proximal dilated air-filled loops. It occurs as a result of a mesenteric abnormality in which the bowel is not attached to the posterior abdominal wall except at the duodenum and proximal colon. Consequently, the bowel may twist on itself resulting in obstruction and possible gangrene. (Singleton, E., Wagner, M.)

2.86

Figure 2.86. This infant presented at the age of 6 days with jaundice and vomiting. Clinically, note the mass in the right upper quadrant. At surgery a diagnosis of duodenal duplication was made.

2.87

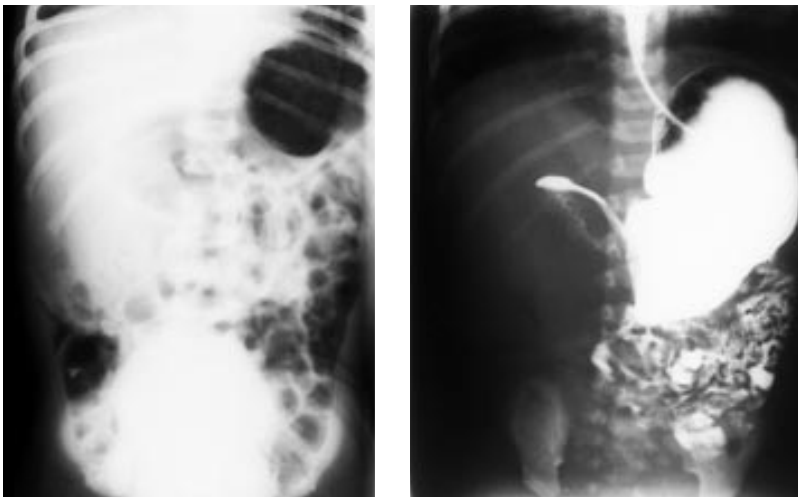

Figure 2.87. Radiographs from the same infant as in Figure 2.86. The flat film on the left shows displacement of the bowel gas to the left. The barium contrast study shows that there is upper displacement of the gastric antrum and duodenal bulb by a large mass. Differential diagnosis includes duodenal duplication and choledochal cyst which displaces the gastric antrum and duodenal bulb downward and medially. On plain radiographs, duplications within the abdomen often appear as soft tissue masses displacing the adjacent bowel. They are more commonly cystic rather than solid masses. (Singleton, E., Wagner, M.)

2.88

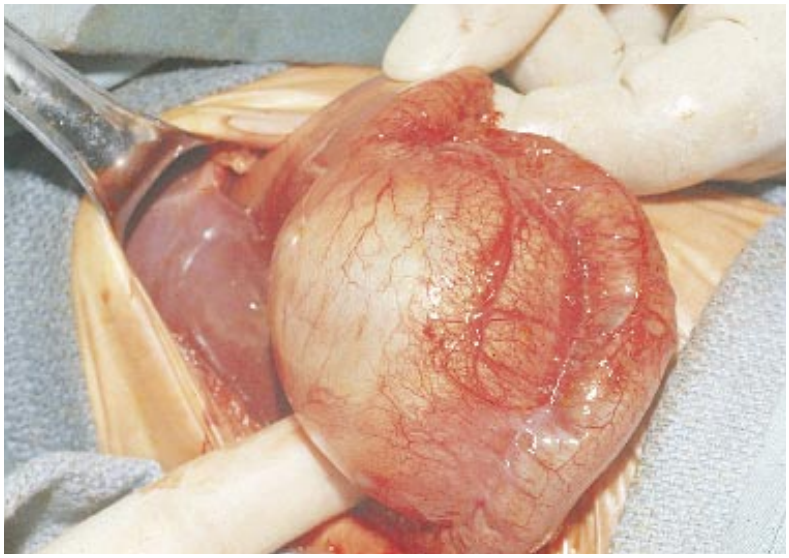

Figure 2.88. Duplication of the duodenum at surgery of the same infant as in Figure 2.87. The duodenum per se is not visible, and note the colon on the left. Duplications of foregut derivation may have associated skeletal malformations (thoracic and cervical vertebrae). With duplications of midgut and hindgut derivation, there are often associated anomalies of the gastrointestinal and genitourinary tracts but *no* skeletal abnormalities.

2.89

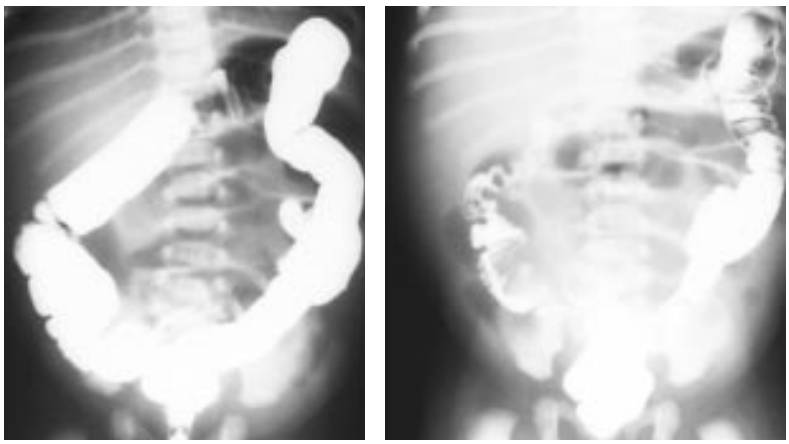

Figure 2.89. This infant presented with vomiting at the age of 5 days. Radiographs with contrast medium demonstrate the duplication of the ileum. Duplications may accumulate secretions in the closed lumen. This leads to distention and consequent obstruction of the normal neighboring bowel. Occasionally the torsion produced by the weight of the duplication leads to small bowel volvulus. (Singleton, E., Wagner, M.)

2.90

Figure 2.90. This infant presented with melena at the age of 3 days. Differential diagnosis includes ingested maternal blood, hemorrhagic disease of the newborn, infection with colitis (e.g., salmonella, shigella), necrotizing enterocolitis, and Meckel's diverticulum. Intussusception is very rare in the neonate.

2.91

Figure 2.91. Melena neonatorum occurred in this infant at 24 hours of age. The most common cause of melena neonatorum is ingested maternal blood, and the diagnosis can be confirmed by the Apt test.

2.92

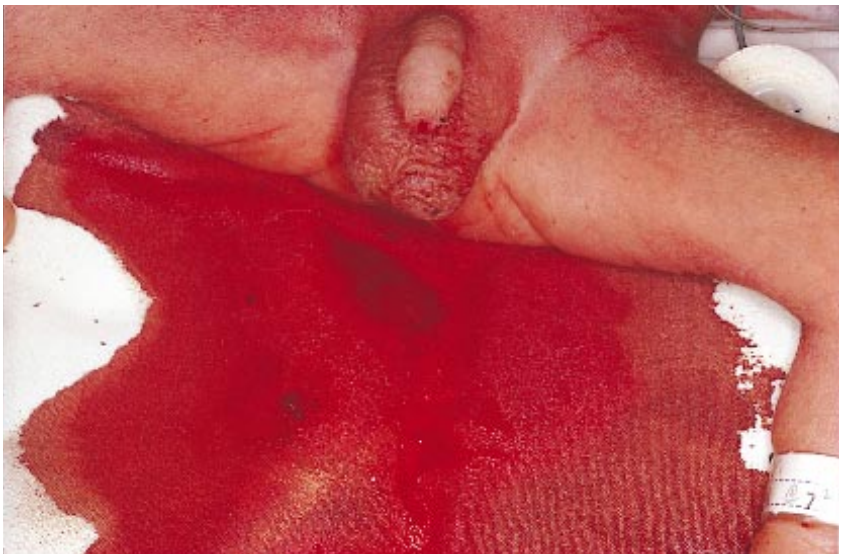

Figure 2.92. Bloody stools in an infant at the age of 3 days showing the gross bleeding from the rectum and the urethra. The etiology in this infant was hemorrhagic disease of the newborn. A vitamin K injection was not given at birth, and the infant developed hypoprothrombinemia.

2.93

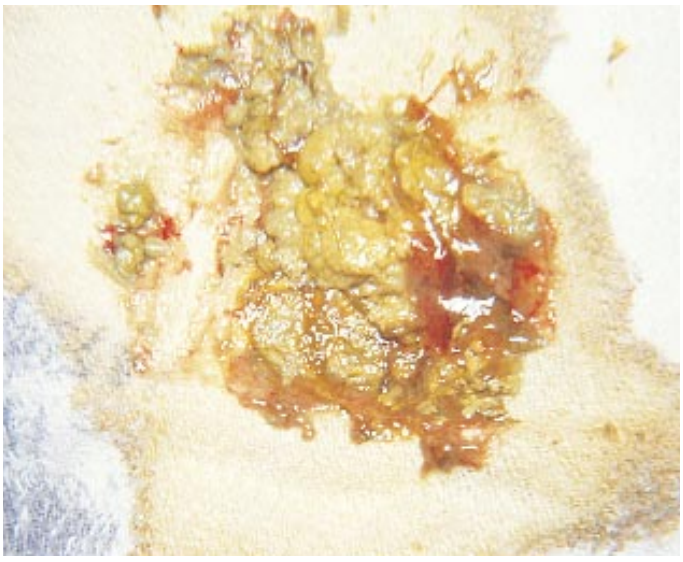

Figure 2.93. Bloody stools in this otherwise normal infant at the age of 48 hours were not caused by ingested maternal blood. Differential diagnosis includes infection, necrotizing enterocolitis, and anal fissure. Etiology was not determined and the infant did well.

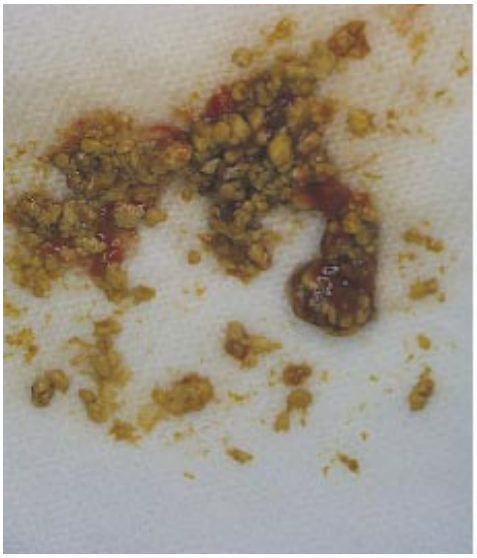

2.94

Figure 2.94. This premature infant with no symptoms at 3 weeks presented with blood in the stool. Note that the blood is not mixed in the stool. Inspection of the anal mucosa revealed fissures which caused the presence of blood in the stool. The most common cause of blood in the stool in the neonate is ingested maternal blood; the next most common cause is an anal fissure.

2.95

Figure 2.95. Normal appearance of the anus of a premature infant with bloody stools. As noted in the figure on the right, it is extremely important to spread the buttocks to permit careful inspection of the anus. Multiple fissures are noted in this same infant.

2.96

Figure 2.96. Bloody stools in an infant with necrotizing enterocolitis. Note the marked abdominal distention and the bile-stained gastric drainage.

2.97

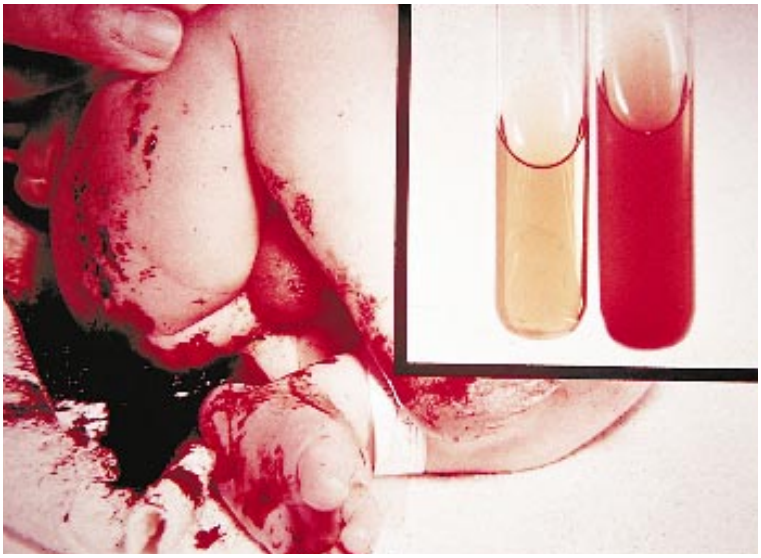

Figure 2.97. The Apt test diagnoses melena neonatorum caused by ingested maternal blood (see inset). Fetal hemoglobin in the presence of alkali remains pink and is not denatured. Adult hemoglobin in the presence of alkali denatures and changes to a yellow-brown color. Note the inset with adult hemoglobin on the left and fetal hemoglobin on the right.

2.98

Figure 2.98. Surgical removal of a Meckel's diverticulum in an infant that presented with bloody stools. Meckel's diverticulum is rarely symptomatic in the neonate. It occurs when the proximal part of the mesenteric duct fails to obliterate. The diverticulum usually arises from the ileum and occurs in 1 to 2% of the population. Of these patients, 1 to 2% may be symptomatic in that there may be hemorrhage or perforation. Ectopic gastric mucosa is commonly present in the diverticulum and, hence, technetium studies may be used in making the diagnosis. (Langston, C.)

2.99

Figure 2.99. Radiograph of an infant with early signs of necrotizing enterocolitis. Clinically these include abdominal distention and blood in stool which may initially be microscopic. Radiographically there is paucity of bowel gas and separation of loops of bowel due to edema of the bowel wall. Late clinical signs include vomiting, ileus, and abdominal tenderness.

2.100

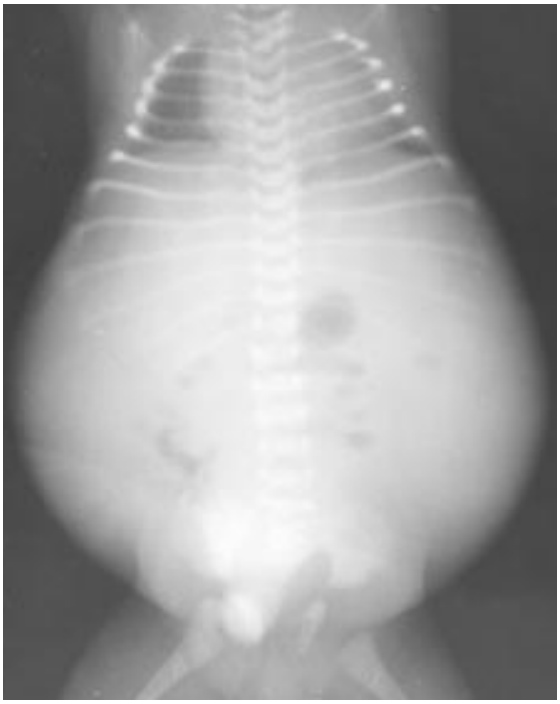

Figure 2.100. Radiograph of another infant with necrotizing enterocolitis. Note the subserosal and submucosal accumulation of gas (pneumatosis cystoides intestinalis) with associated portal gas. The gas in the wall of the intestine is mainly hydrogen and this most commonly reabsorbs without bowel perforation.

2.101

Figure 2.101. Severe pneumatosis cystoides intestinalis in an infant with necrotizing enterocolitis. Note that this clearly shows the subserosal air. (Singleton, E., Wagner, M.)

2.102

Figure 2.102. Lateral radiograph of the same infant as in Figure 2.101 with subserosal pneumatosis cystoides intestinalis in necrotizing enterocolitis. (Singleton, E., Wagner, M.)

2.103

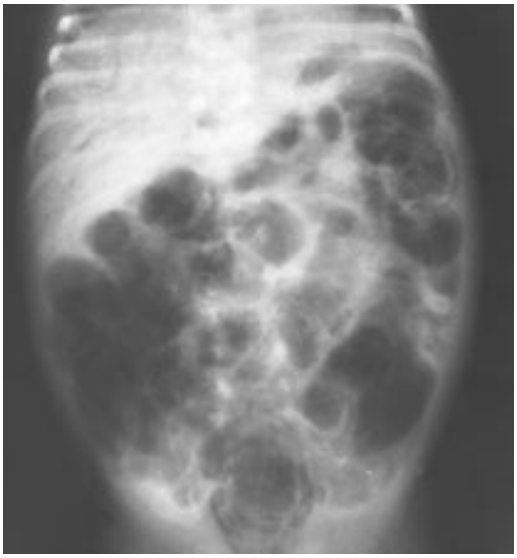

Figure 2.103. Radiograph of an infant with necrotizing enterocolitis. Gas is seen in the portal venous system. This occurs in more severe cases but often resolves spontaneously. In addition note the subserosal pneumatosis cystoides intestinalis.

2.104

Figure 2.104. Upright abdominal radiograph of an infant with necrotizing enterocolitis. Note both the submucosal and subserosal pneumatosis cystoides intestinalis in the bowel. Submucosal pneumatosis characteristically gives the appearance of little bubbles as demonstrated in this figure, especially in both lower quadrants. Subserosal pneumatosis presents as linear areas in the wall of the bowel.

2.105

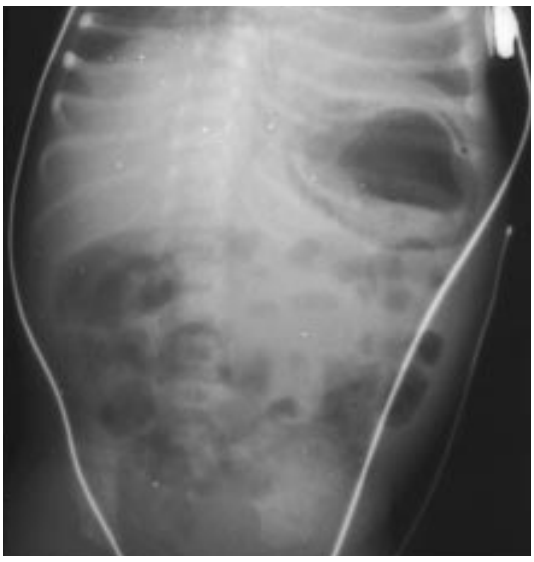

Figure 2.105. Abdominal radiograph of an infant with necrotizing enterocolitis showing gastric pneumatosis. This is not as common as pneumatosis cystoides intestinalis.

2.106

Figure 2.106. Surgical appearance of the bowel of an infant with necrotizing enterocolitis. There is discoloration of the bowel wall as a result of impairment of the vascular supply. Note the subserosal cysts which correlate with the pneumatosis cystoides intestinalis seen in radiographs.

2.107

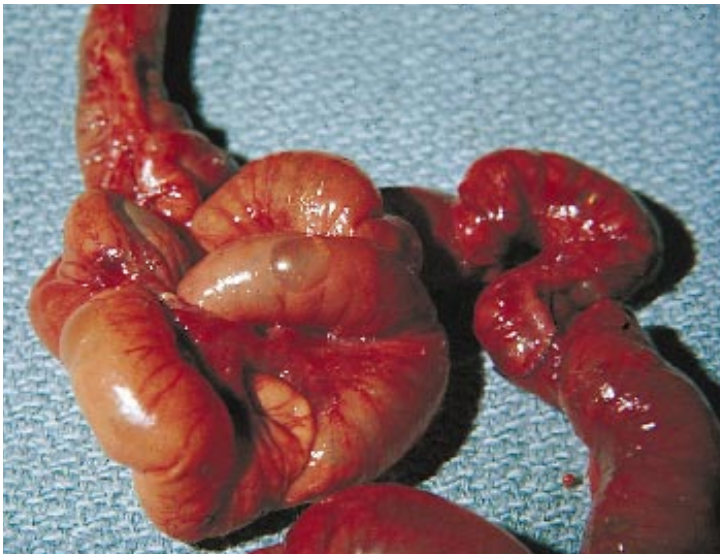

Figure 2.107. Another example of the surgical appearance of the bowel showing the subserosal cysts in an infant with necrotizing enterocolitis.

2.108

Figure 2.108. Pathologic specimen of the small bowel of an infant who had necrotizing enterocolitis. Note the submucosal blebs with a scattered distribution.

2.109

Figure 2.109. A contrast enema in an infant who had recovered from necrotizing enterocolitis. Note the stricture formation in the descending colon with proximal bowel dilatation. This has been reported to occur in about 20% of infants who recover from necrotizing enterocolitis, but the majority of these infants do not develop obstruction. The strictures may occur in the large or small bowel.

2.110

Figure 2.110. Following perforation of the bowel and resulting peritonitis, this infant developed marked abdominal distention and edema of the abdominal wall. This may occur in an infant with a perforated viscus or in low birthweight infants with necrotizing enterocolitis.

2.111

Figure 2.111. Cellulitis and edema of the abdominal wall in an infant with peritonitis which developed after perforation of the ileum.

2.112

Figure 2.112. Lateral view of the abdomen in the same infant as in Figure 2.111, demonstrating the marked abdominal distention and cellulitis.

2.113

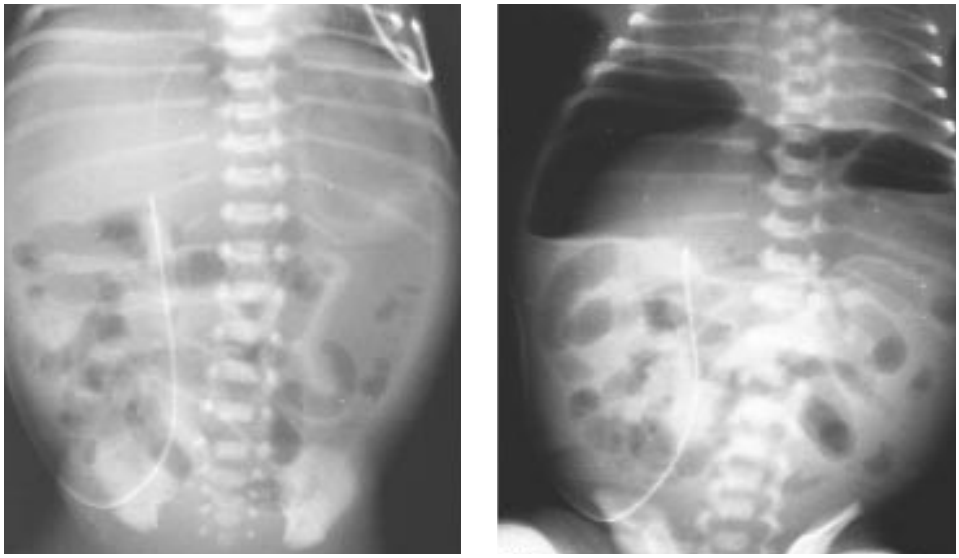

Figure 2.113. Abdominal radiographs of an infant with bowel perforation. In the flat plate film on the left, note the decreased density especially over the liver due to the presence of free air (free air floats to the top). The diagnosis may be easily missed on this film. In the upright plate on the right, the pneumoperitoneum, with subdiaphragmatic air and air/fluid level, is easily appreciated. (Singleton, E., Wagner, M.)

2.114

Figure 2.114. Pneumoperitoneum in an infant with perforation of the colon. Note the large central translucent collection of air referred to as the "football sign" with sharp demarcation of the falciform ligament.

2.115

Figure 2.115. Flat abdominal radiograph in an infant with perforation of the colon, showing the marked pneumoperitoneum. The liver and gallbladder are well outlined in this film, and the subdiaphragmatic air is apparent. The diagnosis of free air is apparent on the flat plate film but is more dramatic in the upright film.

2.116

Figure 2.116. Upright abdominal radiograph of the same infant as in Figure 2.115. Note the subdiaphragmatic air and presence of air/fluid levels.

2.117

Figure 2.117. Abdominal radiograph of an infant with pneumoperitoneum due to perforation of the bowel. Note the subdiaphragmatic air, and in this infant the free air has also tracked down into the scrotum.

2.118

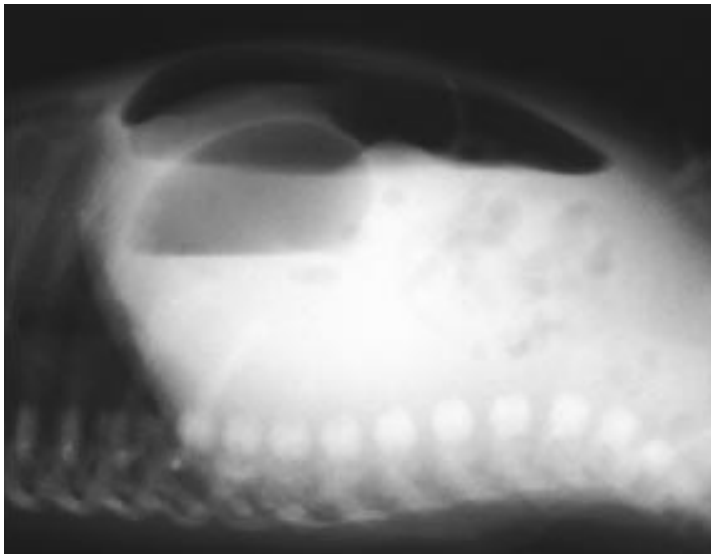

Figure 2.118. Cross-table lateral radiograph of an infant with pneumoperitoneum. This view may be of value in making the diagnosis when other radiographs are inconclusive. Note the lucent area below the abdominal wall superior to the gastric air bubble and bowel gas pattern.

2.119

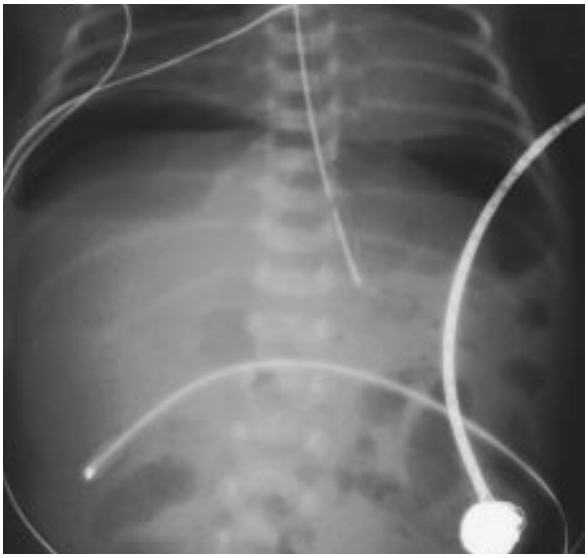

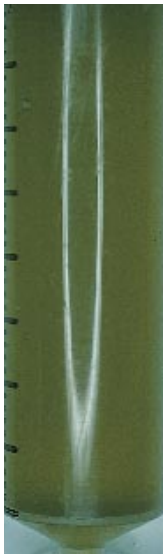

Figure 2.119. Abdominal radiograph of another infant with pneumoperitoneum. Note the subdiaphragmatic collection of free air. Photograph on the right shows the green urine voided by this infant. This association has been reported in cases of bowel perforation.

2.120

Figure 2.120. This infant presented with abdominal distention. A physician in a small community hospital performed a contrast enema which he accomplished by instilling barium into the rectum using a balloon catheter. This caused an iatrogenic perforation of the rectum with spillage of barium into the peritoneal cavity, resulting in barium peritonitis. Note the radiographic shadow of the catheter and balloon in the rectum.

2.121

Figure 2.121. A follow-up contrast radiograph of the same infant as in Figure 2.120, demonstrating the extraluminal barium, particularly in the area of the liver and subdiaphragmatically. The technique of instilling barium with a ballon catheter is inappropriate; however, the infant did well following surgery.

2.122

Figure 2.122. Radiograph of an infant with pulmonary interstitial emphysema, pneumomediastinum, and pneumoperitoneum. Air can track down from the respiratory system to the peritoneum without the perforation of an abdominal viscus. The pneumoperitoneum present in this infant is not the result of perforation. In pneumoperitoneum due to tracking down of air there are *no* air/fluid levels, whereas if it is associated with bowel perforation, air/fluid levels are present. If gas is present in the thorax with a pneumoperitoneum, surgery may not be indicated.

1.123

Figure 2.123. Marked abdominal distention present at birth in an infant with chylous ascites. Ascites may be caused by many conditions such as chylous ascites, urinary ascites, biliary ascites, hydrops fetalis, and infection.

2.124

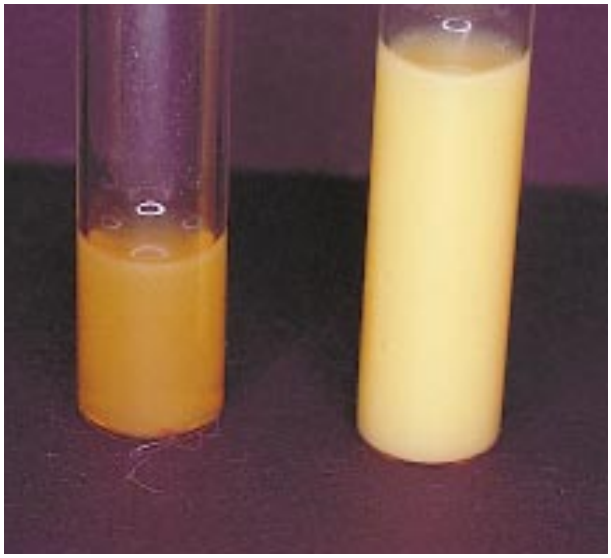

Figure 2.124. Ascitic fluid obtained before (left) and after (right) feedings. The change from a straw-colored fluid to a milky-white opaque fluid after feeds is consistent with a diagnosis of chylous ascites. Today, such an infant would not be placed on regular feedings but would be fed formula containing medium-chain triglycerides and these changes would not occur.

2.125

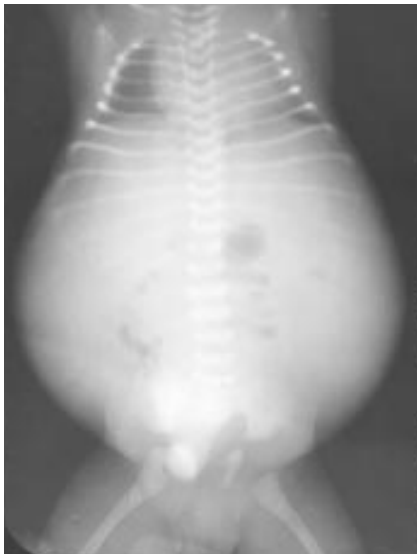

Figure 2.125. Radiograph of an infant with syphilitic ascites. Note the opacification of the abdomen with marked bulging of the flanks and central pooling of bowel gas. The loops of intestine "float" in the middle portion of the abdomen because of the large volume of ascitic fluid. Note the decrease in lung volume as a result of ascites.

2.126

Figure 2.126. Umbilicus cutis or skin navel ("outie") in a normal neonate. Note the tubular projection of the skin up to about 2.5 cm in length. The hard stump is the remnant of the cord covered with skin. Normally the cord is a bluish-white color at birth, or sometimes faintly yellow, especially in postmature infants.

2.127

Figure 2.127. Superior and lateral view of umbilicus cutis in another infant. "Outies" or skin navels are more common in black infants. This protrusion is not reducible in contrast to infants with umbilical herniae. Umbilical herniae arise due to separation of the rectus muscles with herniation of the omentum and, on some occasions, bowel. Umbilical herniae resolve spontaneously as the rectus muscles become stronger, usually by the age of 18 months to 2 years.

2.128

Figure 2.128. Umbilicus amnioticus or amniotic navel ("innie") in an infant at the age of 5 days. This is less common. The amniotic portion of the umbilical cord extends to the abdominal wall and this results in a true belly button.

2.129

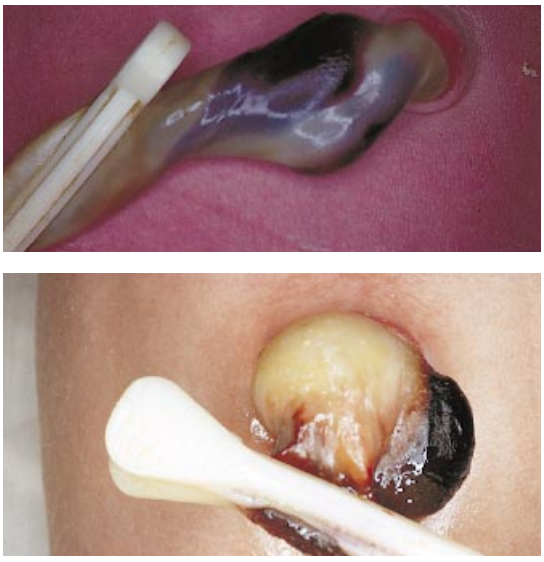

Figure 2.129. Examples of hematoma of the umbilical cord as a result of trauma. These can be a source of significant blood loss if rupture occurs early in the neonatal period.

2.130

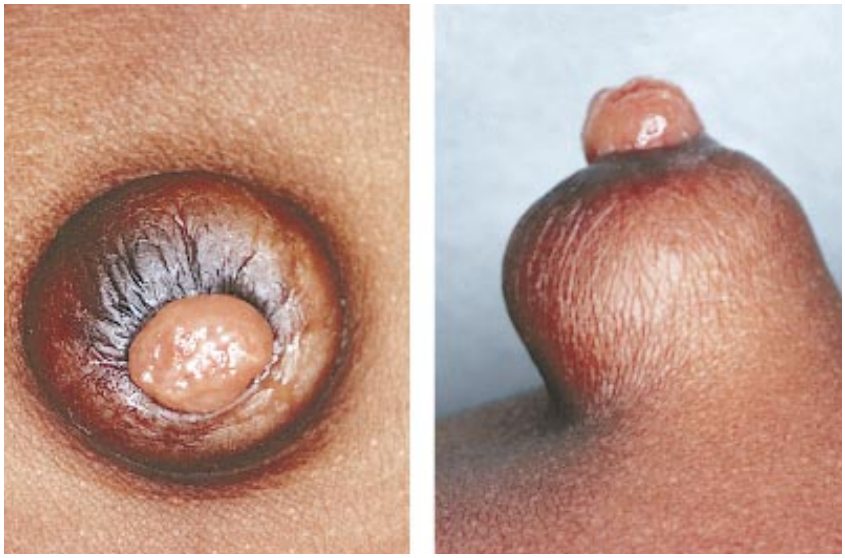

Figure 2.130. Umbilical granuloma in an infant with umbilicus cutis. This results from overgrowth of granulomatous tissue at the umbilicus when the cord separates. These occur more commonly in infants with large, thick umbilical cords. The tissue may be friable and bleeds easily. This can be treated with silver nitrate cauterization. Infants who have discharge or foul odor at the umbilicus may have umbilical granulomas or a patent omphalomesenteric duct (patent vitellointestinal duct).

2.131

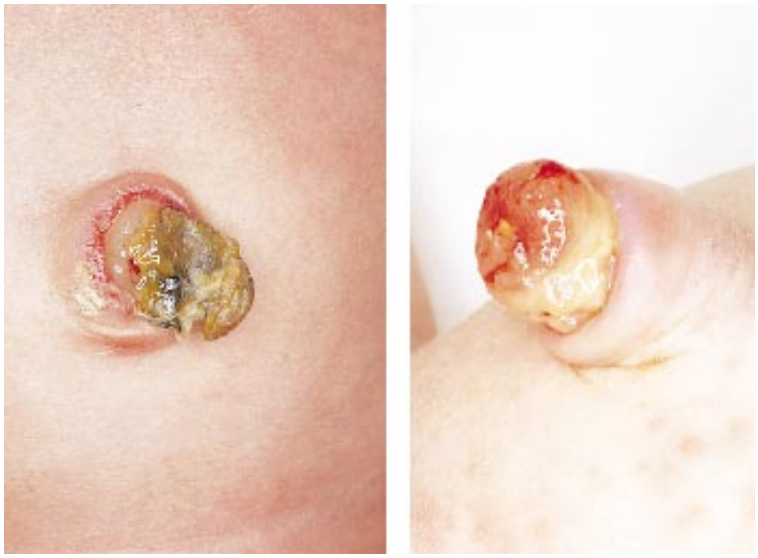

Figure 2.131. Patent omphalomesenteric duct in an infant with stool draining at the umbilicus. During early embryonic life the vitelline duct connects the yolk sac to the primitive bowel. It normally obliterates and atrophies in the course of fetal development. If it persists, it may present as a lumen through which intestinal contents pass from the umbilicus.

2.132

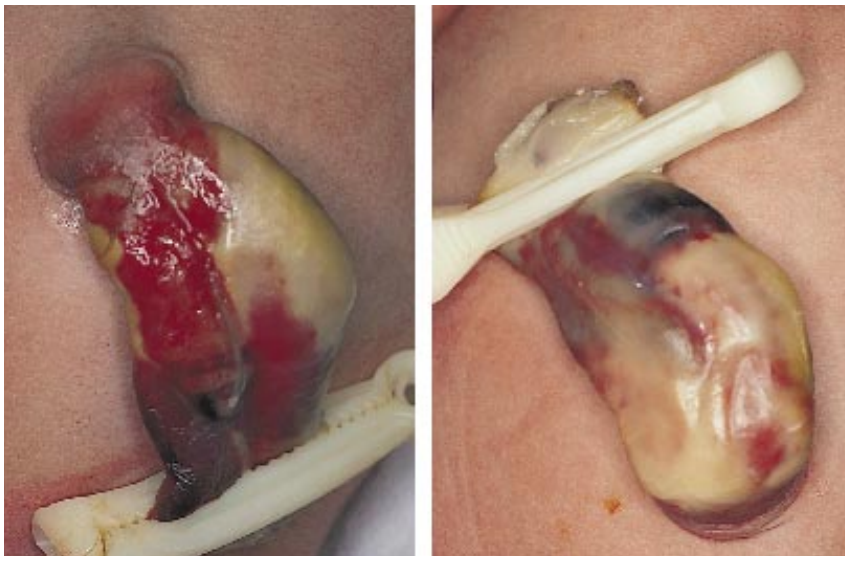

Figure 2.132. This abnormal appearance of an umbilical cord which showed a bright red surface was shown histologically to be a granulomatous omphalomesenteric duct remnant.

2.133

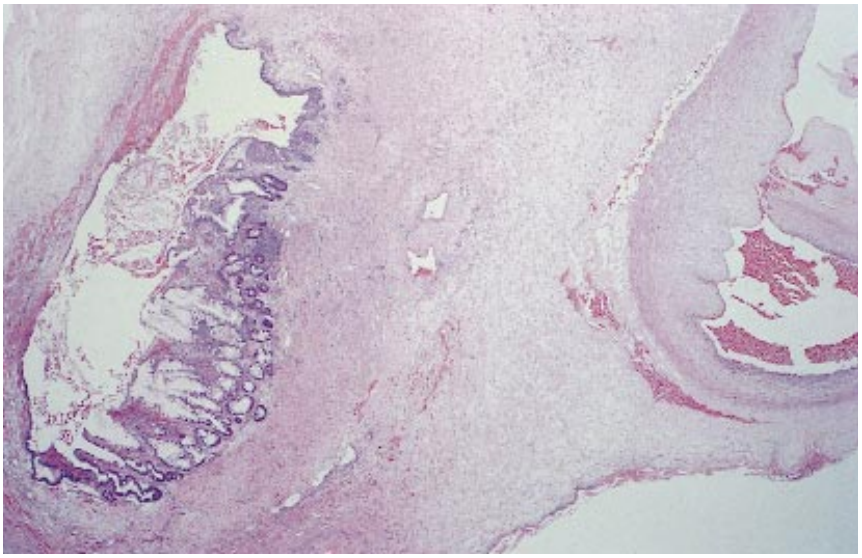

Figure 2.133. Histologic specimen of the same umbilical cord as in Figure 2.132 showing the omphalomesenteric duct remnant. Note the presence of columnar epithelium as seen elsewhere in the intestinal wall.

2.134

Figure 2.134. Note drainage of urine from the umbilicus due to a patent urachus. The marked abdominal distention in this infant was associated with absence of the abdominal musculature.

2.135

Figure 2.135. Umbilical hernia in a black infant at the age of 3 days. Umbilical herniae arise due to a separation of the rectus muscle with herniation of the omentum and, on some occasions, bowel.

2.136

Figure 2.136. Omphaloceles can be quite small in infants and can resemble a Wharton's jelly cyst. The sac may contain a single loop of bowel as noted in this infant. Because of this risk of an omphalocele, the cord should not be cut or clamped close to its insertion.

2.137

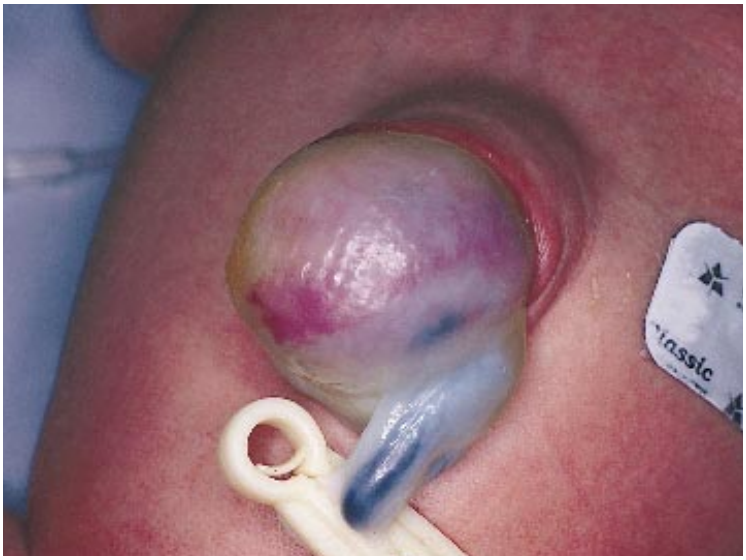

Figure 2.137. This infant has a moderate-sized omphalocele. The sac may contain a single loop of bowel or most of the intestine and liver. An omphalocele is caused by failure of the complete return of intestines to the abdominal cavity in early fetal life (10 weeks). Extra-abdominal contents are positioned midline. The umbilical cord is incorporated and a sac is present. Intestinal malrotation is a frequent associated finding. Omphaloceles may occur as isolated findings or can be associated with other congenital and chromosomal abnormalities. It is frequently seen in trisomy 13 and in Beckwith-Wiedemann syndrome.

2.138

Figure 2.138. Infant with Beckwith-Wiedemann syndrome with an omphalocele. As noted in the preceding photographs of infants with omphaloceles, the defect is covered only by peritoneum without overlying skin. Note the many loops of bowel. This thin membranous sac may rupture.

2.139

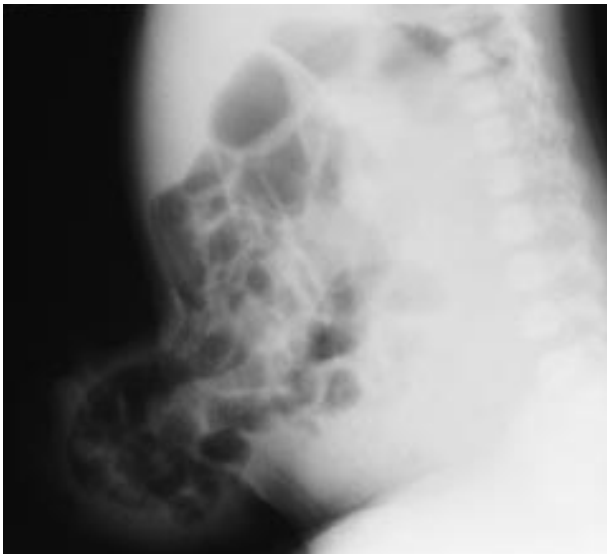

Figure 2.139. Lateral radiograph showing the omphalocele with bowel contents in an infant with Beckwith-Wiedemann syndrome.

2.140

Figure 2.140. This infant has a giant omphalocele. Note that in addition to bowel the liver is present in the omphalocele and that the overlying membranous sac has ruptured. The incorporation of umbilical cord differentiates this from gastroschisis.

2.141

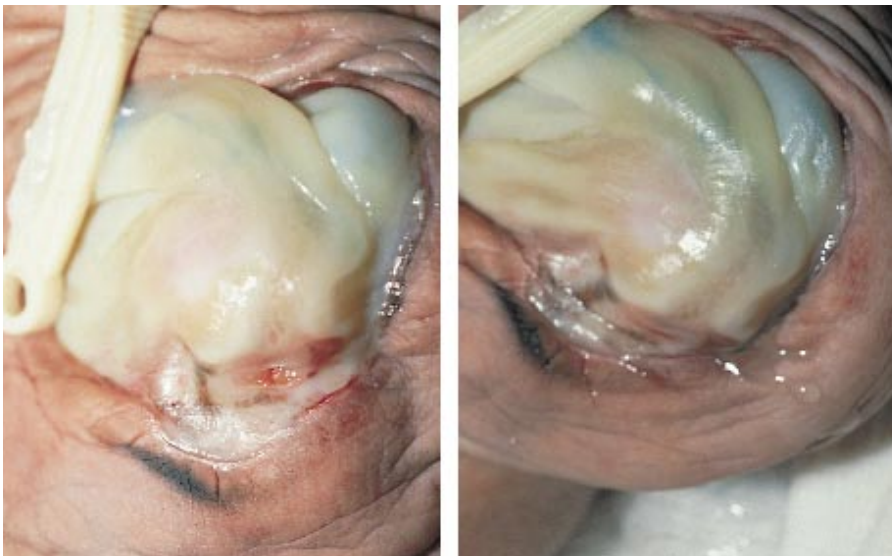

Figure 2.141. This infant with absence of the abdominal musculature (prune belly syndrome) had both an omphalocele and a patent urachus. On the left note the omphalocele with the opening of the urachus in the lower portion. On the right note the omphalocele and drainage of urine from the patent urachus.

2.142

Figure 2.142. In gastroschisis there is no covering membrane. Gastroschisis is the result of an anterior abdominal wall defect which is usually paramedian to the right of the umbilical cord insertion. Gastroschisis is rarely associated with other congenital anomalies. There may be an associated intestinal malrotation and occasionally there are atretic portions of the extra-abdominal bowel. The stomach, bowel, and bladder may be outside the abdomen and completely uncovered. Note that the liver is *never* outside the abdominal cavity in an infant with gastroschisis.

2.143

Figure 2.143. In this infant with gastroschisis note the dilated and thickened loops of bowel. This is common in infants with gastroschisis since the loops of bowel lie free in the amniotic fluid.

2.144

Figure 2.144. A left inguinal hernia which was present at birth in a male infant. Herniae are usually indirect, and are much more common in male and in premature infants. The risk of non–surgically-treated hernias include inability to reduce herniated bowel contents leading to potential strangulation and incarceration.

2.145

Figure 2.145. Abdominal radiograph of an infant with intestinal obstruction as the result of an incarcerated inguinal hernia. Note the bowel gas in the scrotum. It is important to examine the scrotum of male infants who present with abdominal distention due to intestinal obstruction.

2.146

Figure 2.146. Marked abdominal distention in an infant with multiple hemangiomatosis. The abdominal distention was due to massive enlargement of the liver. This infant also had numerous hemangiomas of the skin.

2.147

Figure 2.147. The multiple massive hemangiomas involving the liver are noted at surgery.

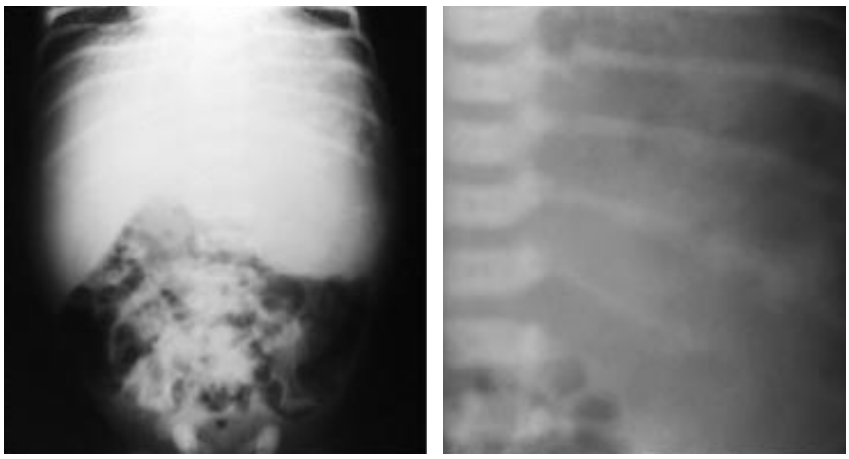

2.148

Figure 2.148. Radiograph of an infant who presented with abdominal distention. On the left note the marked enlargement of the liver and on the right note the calcifications in the right upper quadrant with inferior displacement of the normal bowel gas. This infant had a large hemangioma involving the left lobe of the liver.

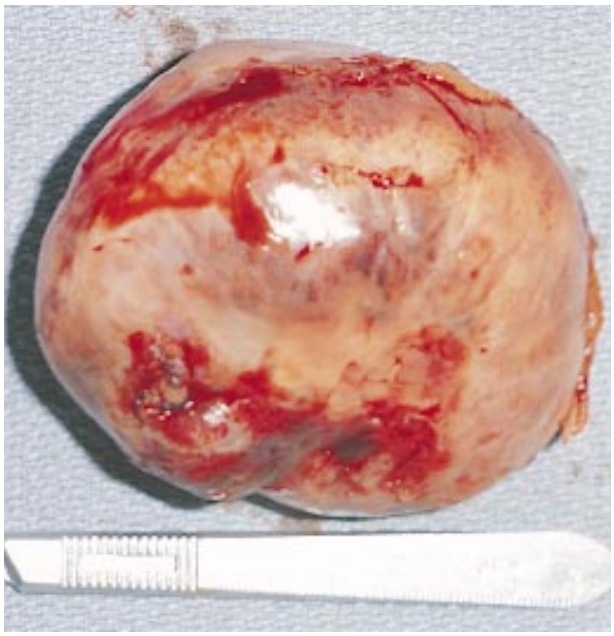

2.149

Figure 2.149. Pathologic specimen from the liver of the same infant as in Figure 2.148 showing the large hemangioma which was successfully removed.

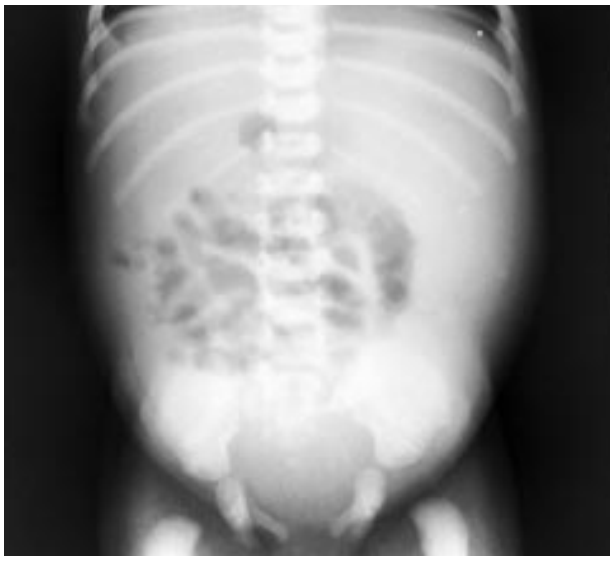

2.150

Figure 2.150. Radiograph of an infant who presented with marked abdominal distention and pallor at 3 days of age associated with a rupture of the spleen. The radiograph shows the marked diffuse opacification of the abdomen with central pooling of the bowel gas associated with a large hemoperitoneum. Pooling of gas is due to loops of bowel floating in the fluid in the peritoneal cavity and, thus, is seen most commonly with ascites.

2.151

Figure 2.151. Lateral radiograph of the same infant as in Figure 2.150 demonstrating abdominal distention and pooling of bowel gas. The pooling of the gas in this infant was due to a hemoperitoneum rather than ascites.

2.152

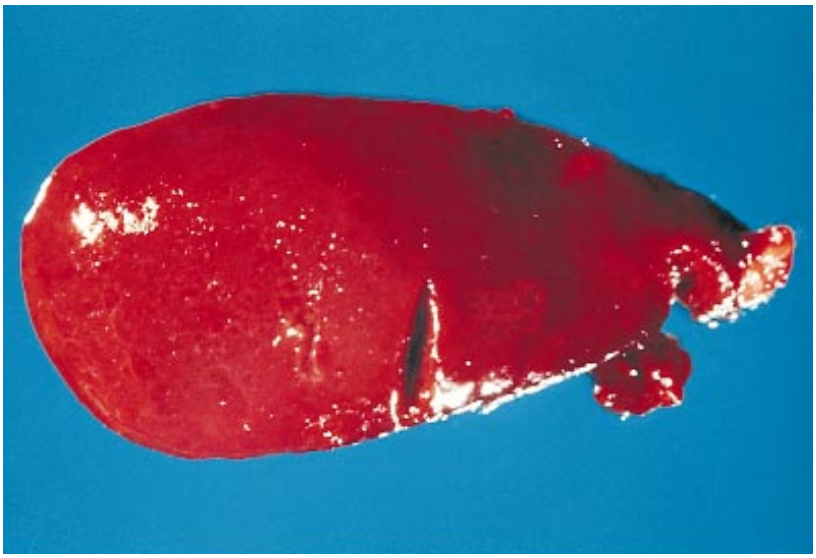

Figure 2.152. Surgical specimen of the spleen of the same infant as in Figure 2.150 and 2.151. Note that the rupture has occurred in the right inferior portion of the spleen. The midline defect is iatrogenic. Hemoperitoneum may occur as the result of rupture of a subcapsular hematoma of the liver and is more common in premature infants, especially with breech delivery. Rupture of the spleen in a normal term infant is rare.

Chapter 3
Nutritional Disorders

The gastrointestinal tract of the newborn must process a relatively large amount and variety of foods soon after birth. The average term infant takes about 540 cc (18 ounces) of food daily by two weeks of age. In adults, correcting for body surface area, this would equal approximately 10 liters of fluid per day. In proportion to its size, the premature infant processes an even greater load. The infant's diet must contain the appropriate quantity of protein, carbohydrates, fats, minerals, vitamins, trace elements and water. The complexity of this task is especially obvious in the premature infant where the child's nutritional reserves are limited and the margin for error is small. Advances in perinatal medicine have resulted in the increased survival of smaller and smaller infants. This poses several special considerations when designing a nutritional plan for these infants, including: the need for rapid growth, the immature functional development of the gut, and the presence of diseases that add additional stress or needs.

3.1

Figure 3.1. Severe intrauterine growth retardation (IUGR) in a post-term baby with a birth weight of 1800 g. Note the typical wizened appearance. The hyperalert expression is also common in postmaturity.

3.2

Figure 3.2. These discordant dizygotic twins demonstrate the condition of unequal size. One twin weighed 3200 g; the other twin weighed 2040 g.

3.3

Figure 3.3. Protein calorie malnutrition (kwashiorkor). This premature infant developed the typical appearance of kwashiorkor at the age of 3 months while in the nursery. She was treated in the pre-parenteral nutrition era.

3.4

Figure 3.4. A close-up of the face of the same infant as in Figure 3.3 showing the earliest appearance of nutritional dermatitis with the copper color and blanching on pressure. Also note the edema, especially of the hand.

3.5

Figure 3.5. In the same infant as in Figure 3.3 and 3.4, note the frank desquamation with raw areas and edema.

3.6

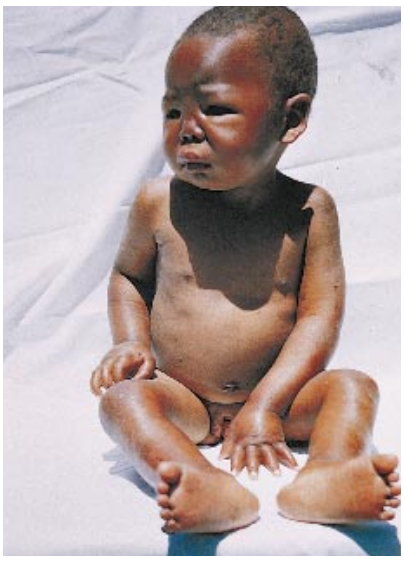

Figure 3.6. Protein calorie malnutrition in an infant. Note the marked edema, the picture of abject misery, and the "pot belly." No dermatitis is present.

3.7

Figure 3.7. The infant on the left with protein calorie malnutrition shows the characteristic gray and atrophic hair. The infant on the right has lost most of his hair, but there are still patches of both atrophic and healthy hair attached to the skin by thin atrophic roots.

3.8

Figure 3.8. The characteristic hair changes are compared. Note the head of a normal infant, one with patchy alopecia, and one with gray and atrophic hair.

3.9

Figure 3.9. A 6-week-old premature infant (birth weight 1400 g) developed marked hyperpigmentation and desquamation of the skin while in the nursery. She was being treated for bronchopulmonary dysplasia with oxygen by cannula and receiving peripheral parenteral nutrition. Her condition improved when trace elements were added to her diet.

3.10

Figure 3.10. Another view of the same infant as in Figure 3.9 shows the marked hyperpigmentation and desquamation of the skin on the abdomen and lower extremities.

3.11

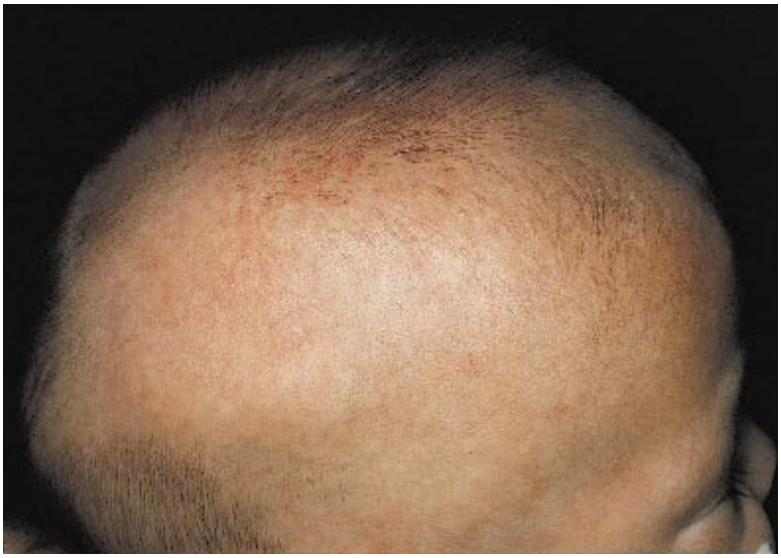

Figure 3.11. A low birthweight infant during the course of her treatment for bronchopulmonary dysplasia developed rickets at the age of 3 months. Note the typical "hot cross bun" head.

3.12

Figure 3.12. A radiograph of the skull of the same infant as in Figure 3.11 showing the marked lack of mineralization of the skull.

3.13

Figure 3.13. This infant with rickets shows the typical rachitic rosary (beading of the ribs at the costochondral junctions). This occurred as a result of prolonged furosemide use for bronchopulmonary dysplasia. Beaded ribs are also seen in hypophosphatasia and chondrodystrophia.

3.14

Figure 3.14. The wrist of the same infant as in Figure 3.13 demonstrates the very obvious broadening of the long bone epiphyses following the use of parenteral nutrition with insufficient vitamin D supplementation and the use of furosemide.

3.15

Figure 3.15. A radiograph of the lower extremities of a premature infant who developed rickets. Note the marked flaring and the ragged appearance of the epiphyses of the distal end of the long bones with widening of the joint space and demineralization.

3.16

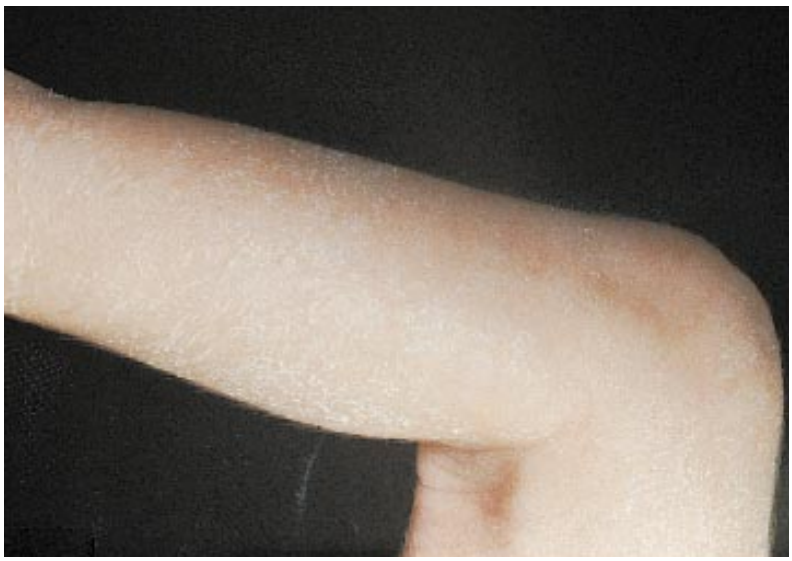

Figure 3.16. Linoleic acid deficiency. Note the fine branny desquamation in this infant with essential fatty acid deficiency.

3.17

Figure 3.17. This infant with cystic fibrosis presented with perforation of the bowel and meconium peritonitis. He was treated for a prolonged period on parenteral nutrition. His abdominal wound healed poorly and he developed a perioral and perianal rash. He also had loose stools. The diagnosis of acrodermatitis enteropathica was confirmed by the addition of zinc to the parenteral nutrition, resulting in clinical improvement. At the time of this infant's hospitalization, trace minerals were not routinely added to parenteral nutrition.

3.18

Figure 3.18. Note the poor healing of the surgical wound in the same infant as in Figure 3.17.

3.19

Figure 3.19. A close-up view of the same infant as in Figures 3.17 and 3.18 shows the perioral lesions in acrodermatitis enteropathica. There are extensive, sharply outlined, erythematous areas of skin partially covered with scales and crusts. Typically the lesions are located in the areas of the mouth, nose, and anogenital region. Initially the skin changes are vesicular or bullous. This condition must be distinguished from epidermolysis bullosa and impetigo.

3.20

Figure 3.20. A close-up view shows the perianal lesions in the same infant as in Figures 3.17 to 3.19. Secondary infection with *Candida* is common in this condition.

Chapter 4
Genitourinary System

The genitourinary system excretes waste products, helps maintain fluid and electrolyte balance, and is the basis for later normal sexual development. Anatomic malformations of this system may be numerous and include the kidneys, ureters, bladder, urethra, or external and internal genitalia. Normally, the fetus is able to urinate into the amniotic sac by 10 weeks gestation. Maternal oligohydramnios may indicate that this is not occurring, and suggests an obstruction of the fetal genitourinary system. Failure to urinate by 24 hours of age may indicate an anatomic or functional disorder in the neonate. Acute and chronic renal dysfunction must also be considered in infants with excessive or decreased urinary excretion. Imaging studies, including radiographs, contrast studies (e.g., intravenous pyelogram, voiding cystourethrogram), ultrasonography, or radionucleotide scan may be necessary to define disorders of this system. Analysis of the urine, including microscopic, biochemical and culture, may also be necessary to delineate some of these disorders. Finally, evaluation of ambiguous genitalia may require complex endocrine evaluation as well as chromosomal analysis.

4.1

Figure 4.1. Frontal view of an infant with renal agenesis showing the typical Potter facies. The facies results from oligohydramnios causing prolonged intrauterine compression on the entire face. The nose is flattened, there are large vertical creases below the eyes, the ears are low set and dysplastic, and there is mild micrognathia.

4.2

Figure 4.2. Lateral view of another infant with renal agenesis causing the Potter facies. Note the flattening of the nose and the low-set ears. Pressure deformity from the oligohydramnios in these infants may cause limb deformities (congenital dislocation of the hips, genu recurvatum, talipes equinovarus). The oligohydramnios may result in pulmonary hypoplasia, and amnion nodosum may be present on the fetal surface of the placenta.

4.3

Figure 4.3. This infant with sirenomelia ("mermaid fetus") has the typical Potter facies, as renal agenesis with resulting oligohydramnios is always present. Sirenomelia is characterized by fusion of all or part of the lower limbs and is a condition incompatible with life.

4.4

Figure 4.4. Fetal surface of the placenta showing amnion nodosum. Note the small nodules which occur as a result of the oligohydramnios. The nodules consist of vernix caseosa, lanugo, and squamous epithelial cells from the fetal skin. (Sotelo-Avila, C)

4.5

Figure 4.5. Abdominal distention with a large mass on the left side. This was a large multicystic kidney. Differential diagnosis of abdominal masses includes hydrometrocolpos, ovarian masses, sacrococcygeal teratoma, urinary tract abnormalities, and neuroblastoma.

4.6

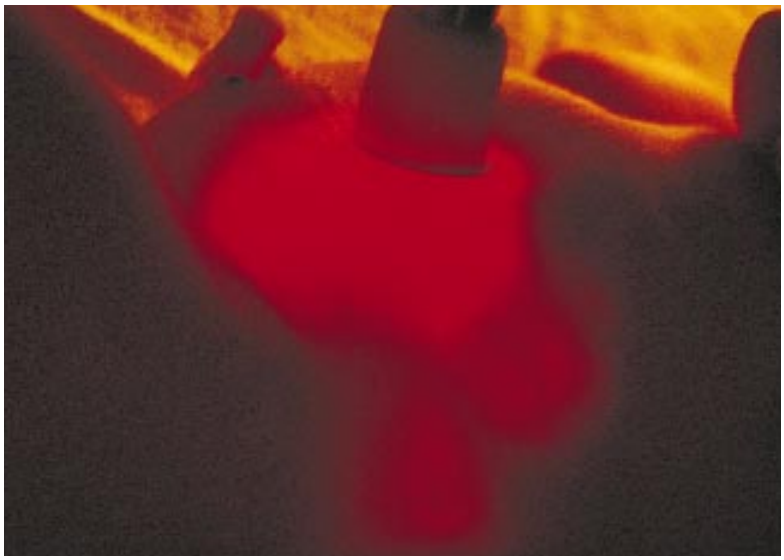

Figure 4.6. Transillumination of the abdomen in the same infant as in Figure 4.5 shows a large cystic mass on the left side. Abdominal masses in the newborn are most commonly cystic rather than solid.

4.7

Figure 4.7. Abdominal radiograph of the same infant as in Figures 4.5 and 4.6 showing the opacity on the left caused by a multicystic kidney. Note the displacement of the normal bowel gas pattern to the right.

4.8

Figure 4.8. Surgical specimen of a large multicystic kidney. Note the numerous multiloculated cysts. Multicystic kidneys show no renal function and are generally unilateral but, on occasion, there may be bilateral involvement. Dysplastic kidneys may have delayed function.

4.9

Figure 4.9. Marked abdominal distention in an infant with urinary ascites and bilateral multicystic kidneys.

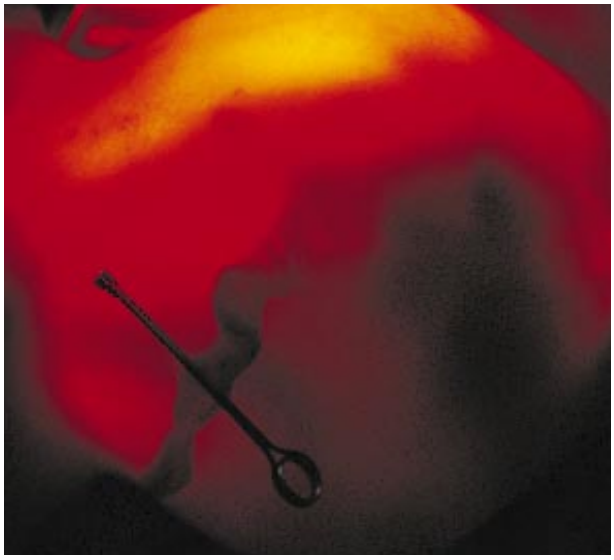

4.10

Figure 4.10. Transillumination of the abdomen in the same infant as in Figure 4.9 showing the large amount of ascitic fluid.

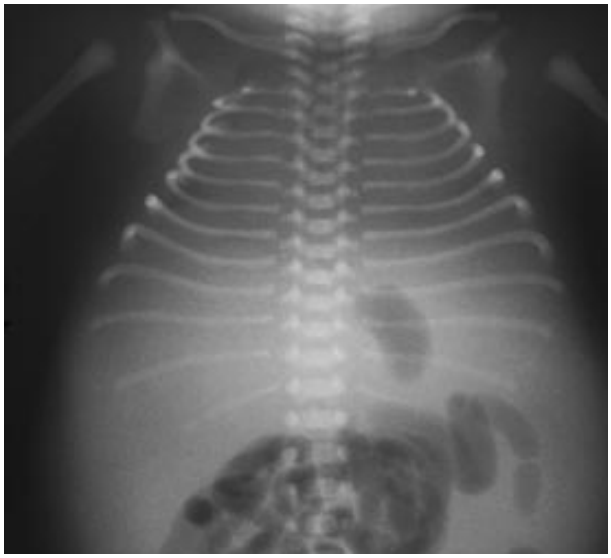

4.11

Figure 4.11. Radiograph showing the marked abdominal distention with bulging opacified flanks and central pooling of the loops of bowel. This radiograph is characteristic of any infant with ascites of any etiology.

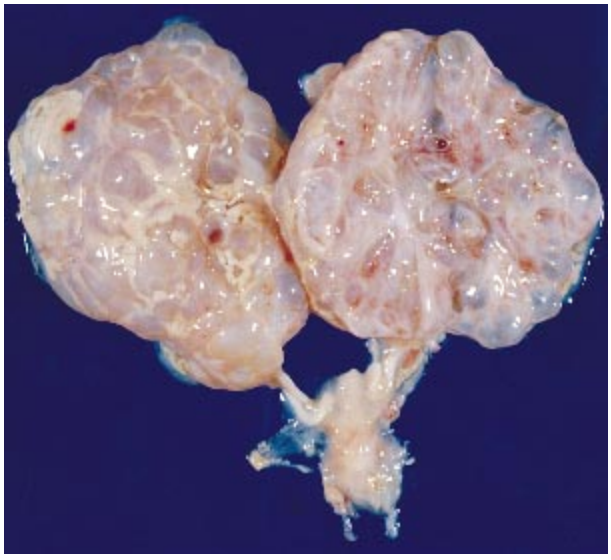

4.12

Figure 4.12. Pathologic specimen of the same infant as in Figure 4.11 with bilateral multicystic kidneys.

4.13

Figure 4.13. Marked abdominal distention in an infant with massive polycystic kidneys. This infant died soon after birth. Infants with polycystic kidneys typically have an autosomal dominant pattern of inheritance in contrast to the autosomal recessive pattern in adult polycystic kidney disease. If little urine is produced, the fetus may exhibit the Potter sequence with fetal compression and pulmonary hypoplasia.

4.14

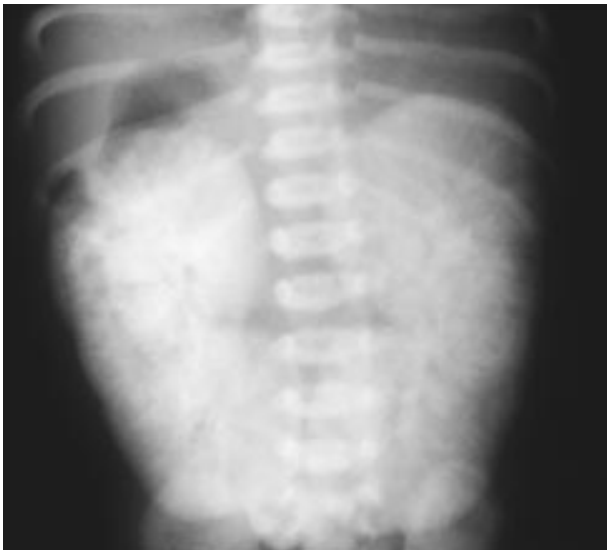

Figure 4.14. Radiograph taken 24 hours after contrast medium was given for an intravenous pyelogram. The contrast dye is contained in the hyperplastic dilated tubules without dye noted in the calyces or bladder. The dye was finally excreted several days later.

4.15

Figure 4.15. An autopsy specimen of a large infantile polycystic kidney. Note the fetal lobulation of the kidney with the visible cysts.

4.16

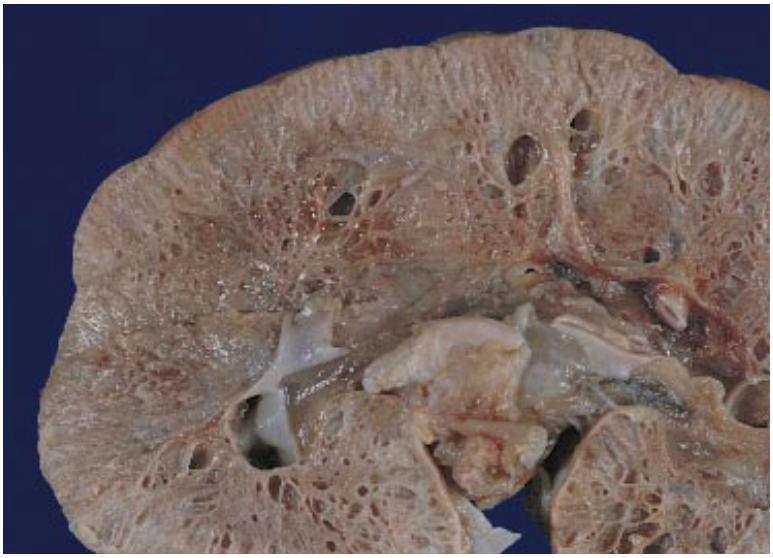

Figure 4.16. A sagittal section through the same specimen as in Figure 4.15. Cysts are noted throughout the whole kidney with the highest concentration in the medulla. This is the anatomic location of the hyperplastic tubules.

4.17

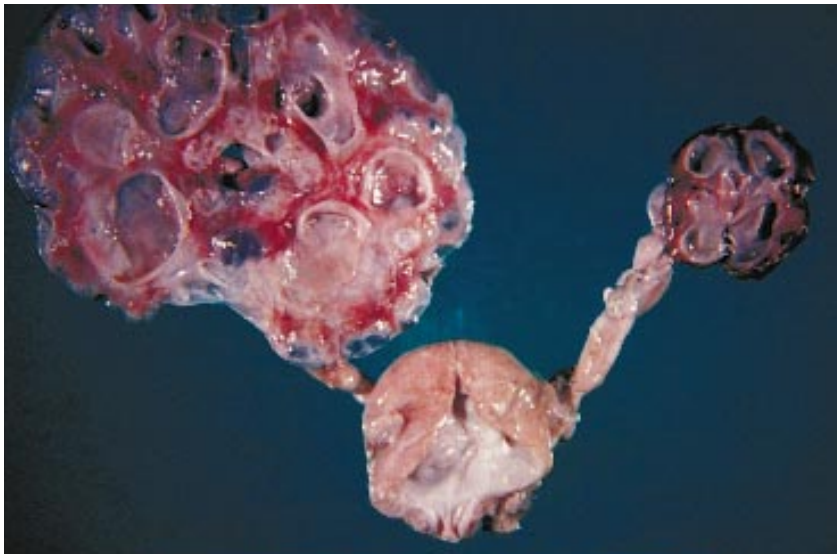

Figure 4.17. Autopsy specimen of an infant showing cystic dysplasia of the kidneys. As compared to multicystic kidneys where there is no renal function, dysplastic kidneys may show some delayed renal function.

4.18

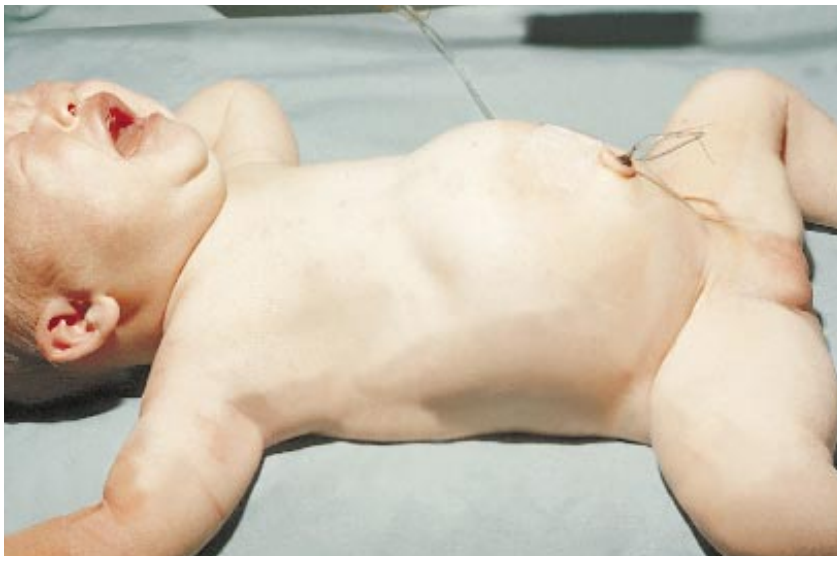

Figure 4.18. This term infant, the product of a breech extraction, presented with marked abdominal distention and respiratory distress. Note the marked hypotonia and "pithed-frog" appearance in a crying infant. Normally, a crying infant does not lie motionless. On examination of the abdomen, a markedly enlarged neurogenic bladder was palpable. This infant had a cervical cord injury at C7 to T1 with associated quadriplegia.

4.19

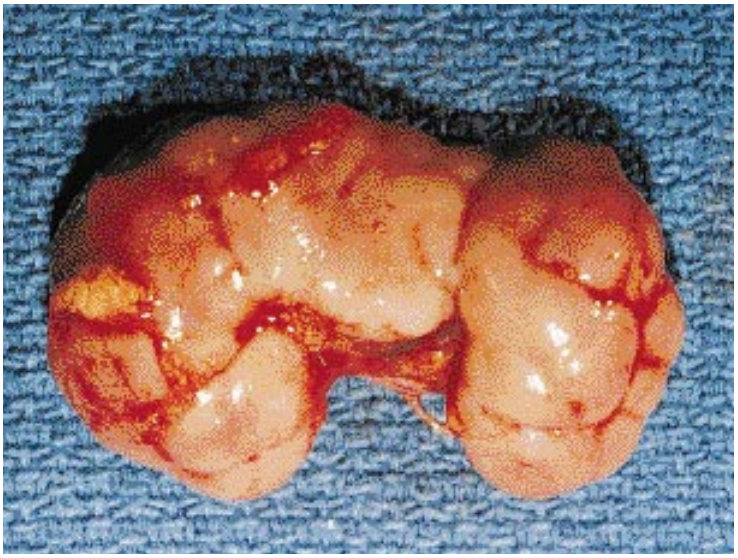

Figure 4.19. Pathologic specimen of a horseshoe kidney. This is not uncommon and is usually asymptomatic. Note the normal fetal lobulation.

4.20

Figure 4.20. An autopsy specimen of "doll's" kidneys. Doll's kidneys refer to hypoplastic kidneys that function well. The cause of death in this infant was unrelated to renal function. This infant had intrauterine growth retardation, a birthweight of 1600 g, and a gestational age of 42 weeks.

4.21

Figure 4.21. Sagittal section through an abnormal kidney. Note the urate deposits which are present as crystals in the collecting tubules and form golden brown aggregates described as "uric acid infarcts." They are obvious to the naked eye in about 15 to 20% of autopsies, but are washed out when the kidneys are fixed. Uric acid infarcts in neonatal kidneys are frequent in dehydration, sepsis, and erythroblastosis fetalis.

4.22

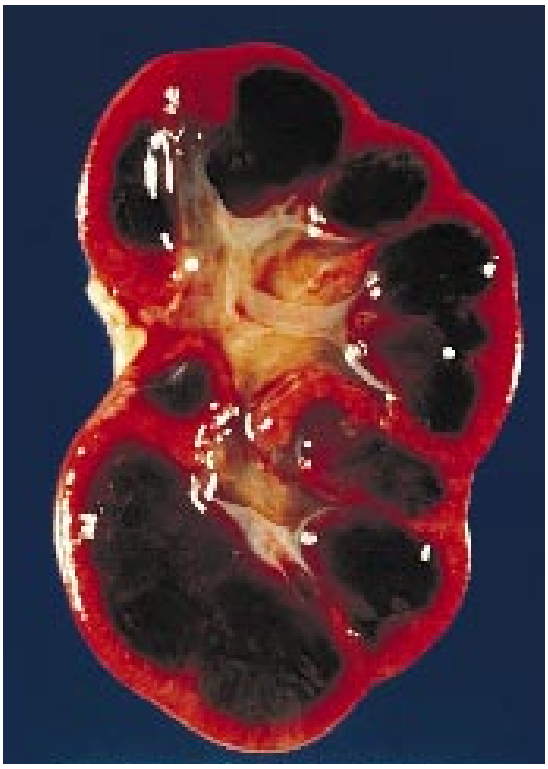

Figure 4.22. Sagittal section of an infant's kidney showing severe medullary hemorrhage secondary to hypoperfusion.

4.23

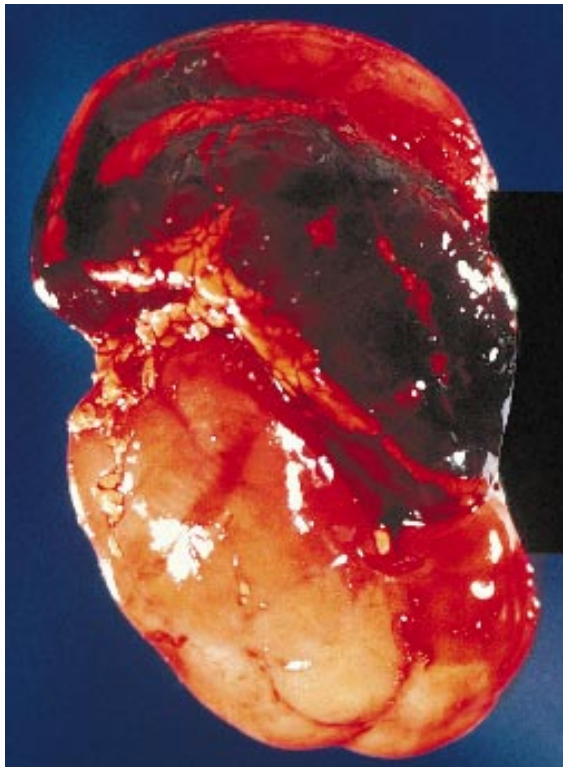

Figure 4.23. Autopsy specimen of the right kidney and adrenal gland in an infant who died from early onset group B streptococcal sepsis with disseminated intravascular coagulopathy. There is a massive adrenal hemorrhage which completely destroyed the adrenal gland by hemorrhagic necrosis. Note the normal kidney with fetal lobulation and the markedly enlarged adrenal gland.

4.24

Figure 4.24. Radiograph showing a large distended abdomen secondary to urinary ascites. Note the bulging flanks with lack of definition of structures and the centralized pooling of bowel gas. Urinary ascites may be due to a traumatic tear in the calyx of the kidney or due to pyelolymphatic backflow. (Singleton, E.)

4.25

Figure 4.25. The intravenous pyelogram in this infant shows a left-sided ureterovesical obstruction resulting in a left hydroureter and severe left hydronephrosis. The radiograph was taken 3 hours after injection of the dye. Note that the calyceal pattern on the right side is normal and the bladder is not very enlarged. Hydronephrosis in the newborn is most commonly due to obstruction at the bladder neck or at the ureterovesical junction. With the advent of ultrasonography, intravenous pyelograms now are rarely performed. (Singleton, E.)

4.26

Figure 4.26. This infant with massive abdominal enlargement, especially on the right side, had congenital posterior urethral valves causing bilateral hydronephrosis and hydroureter, both more severe on the right side. Urethral atresia could give the same appearance of gross distention of the bladder, ureters, and kidneys.

4.27

Figure 4.27. The intravenous pyelogram in this infant with congenital posterior urethral valves demonstrates bilateral hydronephrosis, bilateral hydroureters, and a large dilated bladder. Obstructions at the ureterovesical junction result in unilateral involvement of the ureter and kidney and a normal bladder, whereas obstruction in the urethra results in bilateral involvement of the ureters and kidneys and bladder enlargement. (Singleton, E.)

4.28

Figure 4.28. A cystogram in the same infant as in Figure 4.27 with posterior urethral valves shows extensive vesicoureteral reflux and bilateral hydroureter and hydronephrosis.

4.29

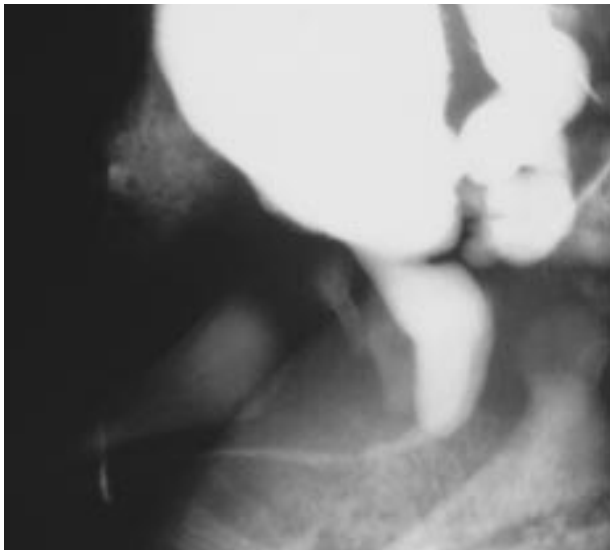

Figure 4.29. Lateral excretory contrast radiograph in an infant with posterior urethral valves. Note the markedly enlarged bladder and large dilated prostatic urethra proximal to the urethral valve. (Singleton, E.)

4.30

Figure 4.30. This infant with urinary ascites had congenital posterior urethral valves. In the cystogram study note the traumatic rupture of the calyx with extravasation of dye from the renal pelvis. (Singleton, E.)

4.31

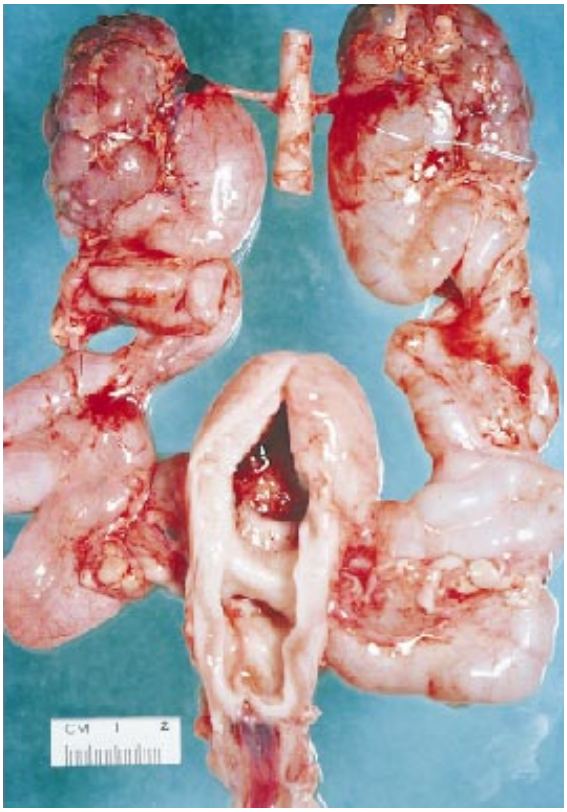

Figure 4.31. Autopsy specimen of the same infant as in Figure 4.30 with congenital posterior urethral valves. Note the urethral valves, enlarged bladder, bilateral hydroureter, and bilateral hydronephrosis.

4.32

Figure 4.32. An infant with the prune belly syndrome (Eagle-Barrett syndrome; triad syndrome) shows the marked wrinkling of the skin and flaccid abdominal wall which bulges laterally as a result of lack of the underlying abdominal muscles. The triad of findings include absence of the abdominal muscles, urinary tract abnormalities, and cryptorchidism. The abdomen has a doughy consistency on palpation, and the abdominal viscera can be felt with unusual ease.

4.33

Figure 4.33. Another example of the prune belly syndrome showing the outlines of loops of bowel. The genitourinary tract findings are most frequently the result of obstruction of the distal urethra which causes marked distention of the bladder, and the ureters are dilated and tortuous. Currently it is thought that the marked distention of the bladder and ureters and renal involvement result in the ablation of the abdominal muscles, especially the recti. The kidneys may be hypoplastic or severely hydronephrotic as a result of the obstruction.

4.34

Figure 4.34. Patent urachus in an infant with absence of the abdominal musculature. The urachus is a persistence of the embryologic tract between the fundus of the bladder and the allantoic sac. A patent urachus results from failure of the tract to close and should be suspected when there is urinary drainage through the umbilicus. This finding is not uncommon in the prune belly syndrome.

4.35

Figure 4.35. Abdominal radiograph in an infant with the prune belly syndrome. Note the marked asymmetrical bulging of the flanks.

4.36

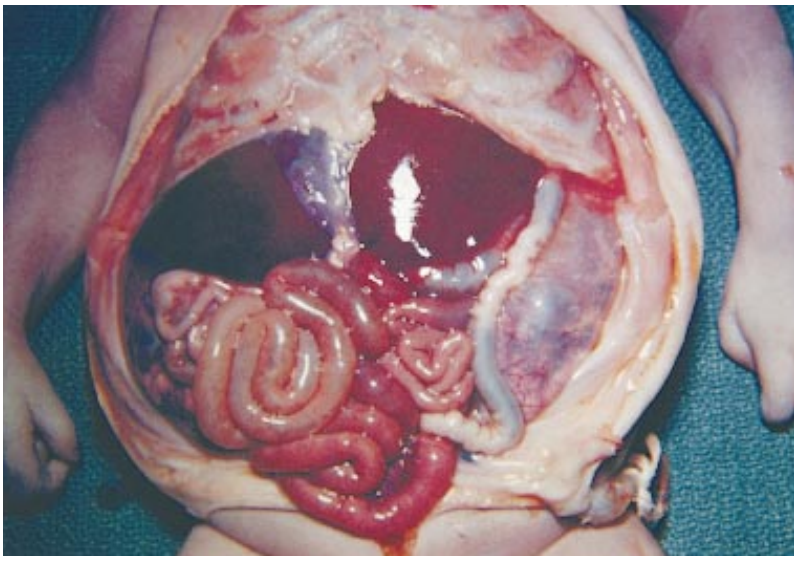

Figure 4.36. Autopsy specimen in an infant with the prune belly syndrome showing the marked bulging of the flanks, lack of abdominal muscles, and bilateral polycystic kidneys.

4.37

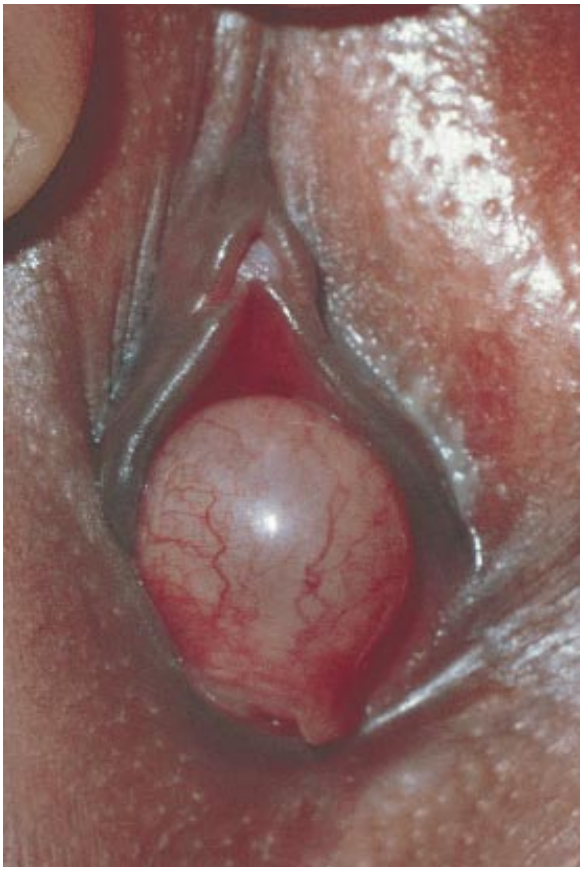

Figure 4.37. This female infant presented with a genital mass superior to the vaginal introitus. The mass is a large ureterocele coming out of the vagina. (Gonzalez, E.)

4.38

Figure 4.38. The mass is raised superiorly in the same infant as in Figure 4.37 to demonstrate a normal vaginal introitus. (Gonzalez, E.)

4.39

Figure 4.39. Gentle traction on the urethra of the same infant as in Figures 4.37 and 4.38 delineates the association of the cystic mass arising from the floor of the urethra. (Gonzalez, E.)

4.40

Figure 4.40. The genitalia of the normal female infant gape, partially revealing the labia minora and, perhaps, the clitoris. The labia majora are full, and the thickened labia minora protrude between them. The mucosa normally is pink and a mucoid vaginal secretion is common.

4.41

Figure 4.41. Normal external female genitalia in a premature infant. Note the prominence of the labia minora. The clitoris is large in preterm babies with the result that the inexperienced physician may suspect ambiguous genitalia.

4.42

Figure 4.42. Marked swelling and bruising of the external genitalia in a normal female infant born via breech extraction. Some of the trauma may occur during vaginal exam of the mother during labor. This usually improves rapidly.

4.43

Figure 4.43. Normal mucoid vaginal discharge in a normal female infant. This results from the "withdrawal effect" from the in utero environment.

4.44

Figure 4.44. "Withdrawal" bleeding in a normal female neonate. Vaginal bleeding is not uncommon in the first week of life. It is caused by the withdrawal of the high maternal estrogen level to which the baby has been exposed in utero. Vaginal bleeding is self-limited in that transplacental hormone withdrawal effect starts on the third to fourth day of life and continues for 2 to 3 days.

4.45

Figure 4.45. This normal female infant has a hymenal tag, which is a protrusion of redundant vaginal mucosa. Hymenal tags are a common finding and usually resolve spontaneously.

4.46

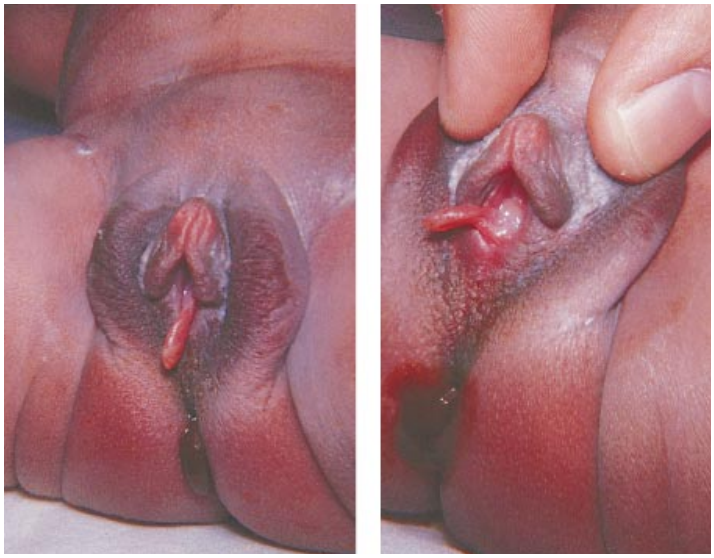

Figure 4.46. Another variant of a hymenal tag in a normal female infant. Hymenal remnants usually resolve spontaneously.

4.47

Figure 4.47. Clitoral hypertrophy giving the appearance of ambiguous genitalia. Potentially life-threatening adrenal abnormalities must be ruled out. Clitoral hypertrophy is the result of increased androgen stimulation as a result of a luteoma of pregnancy. This resolves after pregnancy. There was no adrenal anomaly in this infant.

4.48

Figure 4.48. Abnormal female genitalia in this infant with prominent labia minora, clitoral enlargement, and anterior placement of the anus. Hypoplasia of the labia majora may give rise to the false impression of a large clitoris.

4.49

Figure 4.49. Abnormal anus as the result of failure of the fusion of the perineal raphe involving the external sphincter. The labia majora are very prominent and give the impression of scrotalization.

4.50

Figure 4.50. Absence of the labia majora in an infant with the popliteal pterygium syndrome.

4.51

Figure 4.51. This female infant shows, on the left, adhesions of the labia minora (synechia of the labia). On the right the adhesions have been separated. These adhesions are sometimes present at birth and often can be separated, as in this infant, by gentle traction with the fingers. They are thought to occur as a result of maternal hormone effect.

4.52

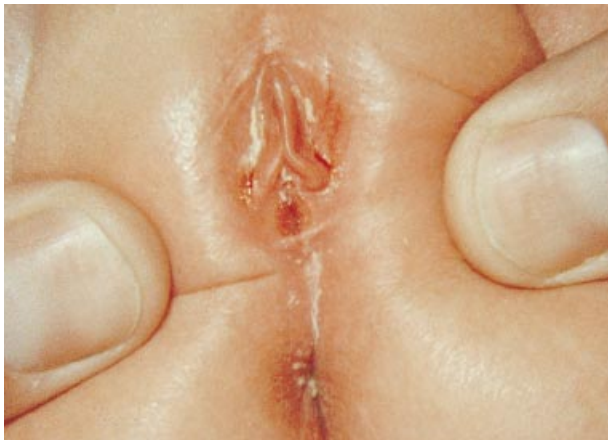

Figure 4.52. Adhesions of the labia minora (synechia of the labia) with some associated normal mucoid vaginal secretions. These adhesions could not be separated readily by the fingers. Separation was accomplished by inserting a probe behind the fusion and pulling forward.

4.53

Figure 4.53. Close-up view of labial adhesions in another newborn infant. Rarely complete closure of the vaginal orifice can result in urinary retention.

4.54

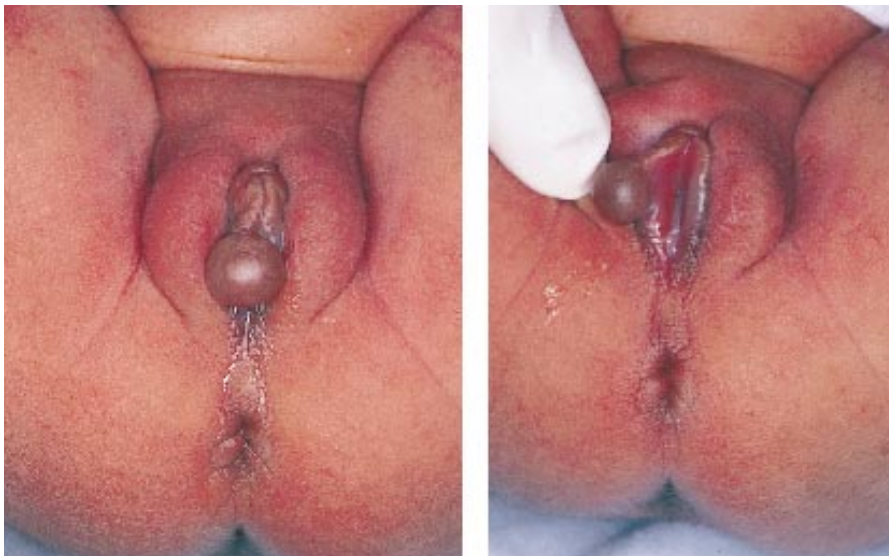

Figure 4.54. A cyst arising in the wall of the right labium minora. The cyst was removed and identified as a retention cyst.

4.55

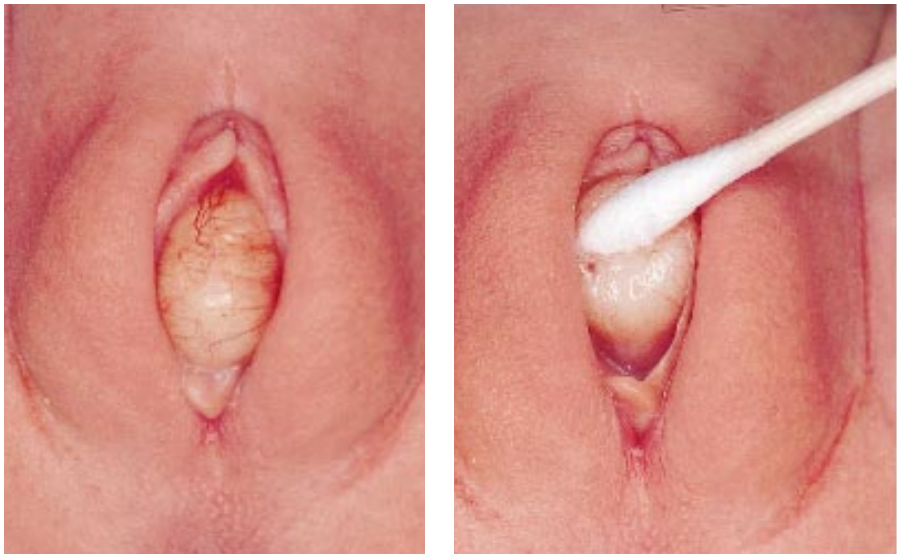

Figure 4.55. A left-sided Skene's gland cyst. In the figure on the left this appears to be midline and would raise concerns about the diagnosis of hydrocolpos. In the figure on the right, the diagnosis of a Skene's gland cyst on the left side is confirmed by the inability to pass a cotton-tip swab on the left side.

4.56

Figure 4.56. Involvement of Bartholin's gland is extremely rare in the neonate. This infant at the age of 2 weeks developed a Bartholin's cyst abscess.

4.57

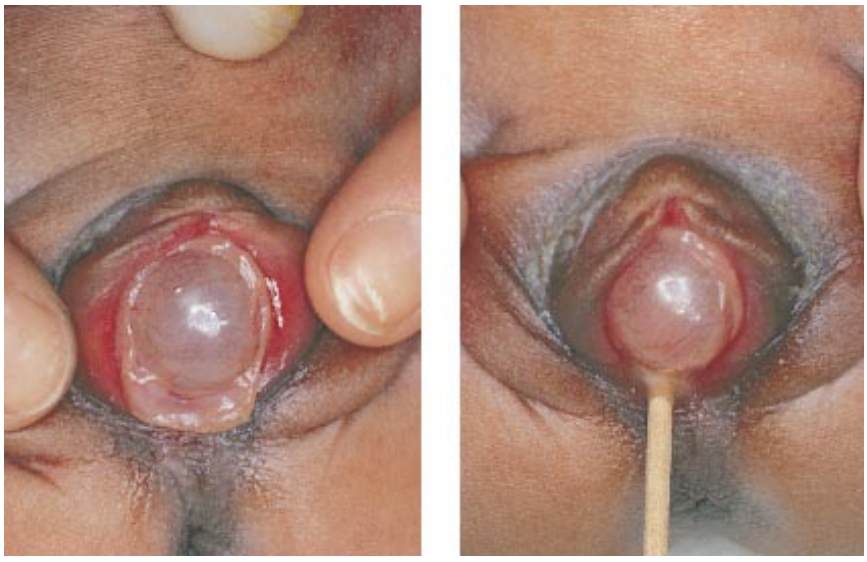

Figure 4.57. This infant presented with a swelling in the vagina. On the left note the typical appearance of a hydrocolpos. On the right, the use of the blunt end of a cotton tip swab demonstrates no obstruction on either side of the cystic swelling; therefore the cyst did not arise from the vaginal wall and the diagnosis is hydrocolpos.

4.58

Figure 4.58. Normal appearance of the external female genitalia in an infant who presented with abdominal distention. The infant had hydrometrocolpos. The diagnosis can be missed if the external genitalia are not carefully examined. This stresses the importance of doing a careful examination on the external female genitalia.

4.59

Figure 4.59. In the same infant as in Figure 4.58, with application of external abdominal pressure and spreading of the labia majora, a large cystic mass is revealed at the introitus. The abdominal distention is the result of hydrometrocolpos. Hydrocolpos is caused by a firm membrane (imperforate hymen) that covers the vaginal outlet, preventing drainage and thus resulting in accumulation of vaginal secretions in the vagina. If the secretions extend into the uterine cavity causing uterine enlargement, the diagnosis is hydrometrocolpos. Occasionally, maternal hormone secretion may cause pseudomenses, resulting in a reddish- or bluish-colored material behind the membrane (hematocolpos or hematometrocolpos).

4.60

Figure 4.60. An abdominal radiograph of an infant with hydrometrocolpos. Note the superior and lateral displacement of the normal loops of bowel and the associated central opacification due to the enlarged uterus. Diagnosis is confirmed by examining the vagina.

4.61

Figure 4.61. Contrast dye study in the same infant as in Figure 4.60 with hydrometrocolpos. Note the outline of the enlarged uterine cavity. This can cause pressure on the ureters, resulting in hydroureter and hydronephrosis.

4.62

Figure 4.62. Autopsy specimen of an infant with bilateral hydronephrosis and hydroureter as a result of severe hydrometrocolpos causing pressure on both ureters. Note the markedly enlarged uterus.

4.63

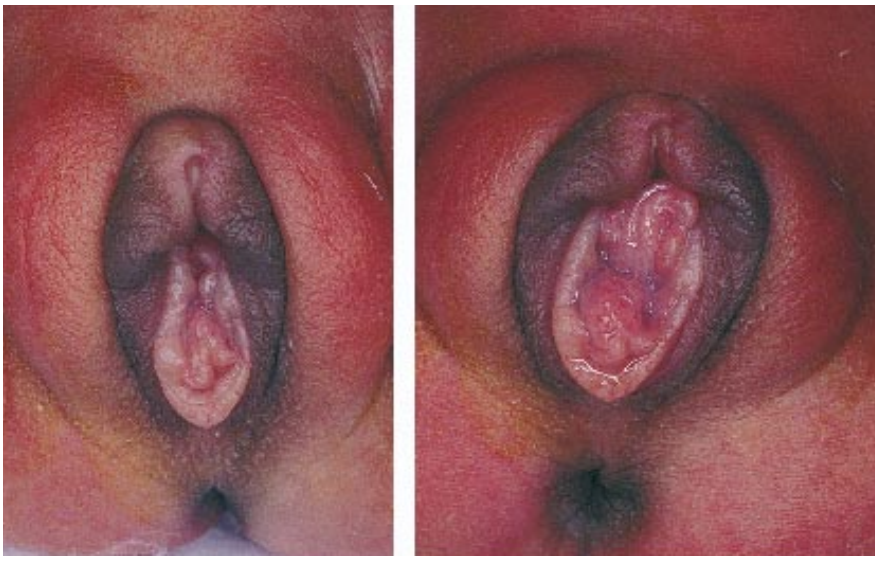

Figure 4.63. Mild procidentia (prolapse of the uterus) in an otherwise normal newborn.

4.64

Figure 4.64. This neonate has a severe procidentia (prolapse of the uterus) to such a degree that the cervix protrudes from the vaginal outlet. The infant had an associated meningomyelocele. Procidentia in the newborn is almost invariably associated with neural tube defects.

4.65

Figure 4.65. In this infant there is duplication of the external genitalia. Note the two vaginal orifices. Duplication of the external genitalia is extremely rare. It has been reported as part of an apparent sagittal mirror-image doubling of the posterior axis of the embryo. Partial or complete duplication of the vagina, labia, penis or scrotum may be caused by inadequate androgenic stimulation or end-organ unresponsiveness during late fetal life.

4.66

Figure 4.66. This infant has duplication of the external female genital tract with other associated anomalies which include omphalocele, absent rectus muscle, and congenital heart disease.

4.67

Figure 4.67. Normal external genitalia in a term male infant. In the newborn male, the relatively large size of the phallus gives the baby the appearance of being "well-endowed." On examination note the size of the phallus and the presence or absence of testes in the scrotum. An unusually large phallus for age usually indicates abnormal androgenic stimulation of testicular or adrenal origin. A true micropenis may represent either deficient hormonal stimulation during growth or a failure of early morphogenesis. Midline hypopigmentation may be noted on the gonads of dark-skinned newborn infants. They may have no other areas of hypopigmentation.

4.68

Figure 4.68. Normal male genitalia in a premature infant with a gestational age of 34 weeks. Note the lack of fullness of the scrotum due to the undescended testes. Note the presence of few rugae which are only on the undersurface of the scrotum. This appearance is consistent with the gestational age of 34 weeks.

4.69

Figure 4.69. Bilateral undescended testes with an empty scrotum in a term male infant.

4.70

Figure 4.70. Bilateral hydroceles in a term male infant. Hydroceles arise from an abnormal collection of fluid in the tunica vaginalis which has failed to invaginate following descent of the testis. This is recognized clinically as a scrotal mass that transilluminates. At birth, up to 15 to 20% of male infants may have some degree of hydrocele. Complete spontaneous resolution is to be expected over a period of a few weeks to months.

4.71

Figure 4.71. Bilateral hydroceles in a term infant with micropenis. The diagnosis of micropenis should be made after careful examination, as a normal penile shaft may be partially buried in the pubic fat pad in a neonate. Micropenis denotes a truly hypoplastic penile shaft.

4.72

Figure 4.72. Large bilateral hydroceles in a premature infant with a normal-sized penis. In infants with hydrocele of the spermatic cord, the swelling is also noted in the groin and thus a hydrocele of the cord must be distinguished from an inguinal hernia.

4.73

Figure 4.73. Transillumination of bilateral hydroceles in a term infant. In the case of an indirect hernia, transillumination is negative.

4.74

Figure 4.74. Massive bilateral inguinal herniae in a 10-week-old (weight 1900 g) premature infant with a birthweight of 700 g. Inguinal herniae occur commonly in neonates but rarely are present at birth. They are much more common in male infants and premature infants, and there is a risk of irreducibility and strangulation.

4.75

Figure 4.75. A unilateral right inguinal hernia in a male infant with trisomy 13.

4.76

Figure 4.76. Large left-sided inguinal hernia in a 9-week-old (weight 1800 g) female premature infant with a birthweight of 750 g. Inguinal herniae are much less common in female infants. Prematurity and increased abdominal pressure increase the incidence. A mass, which is usually an ovary, may be present in the hernial sac.

4.77

Figure 4.77. Marked edema and bruising of the external genitalia of a male infant delivered as a breech presentation. This infant had problems with voiding for the first 48 hours of life and required catheterization.

4.78

Figure 4.78. This infant, delivered as a breech presentation, developed marked swelling of the right side of the scrotum. There was a purplish-blue discoloration and a hard firm tender mass was palpated. The differential diagnosis included torsion of the testis and hematoma. Note that the swelling and discoloration extend beyond the midline to a portion of the left side of the scrotum. This would exclude the diagnosis of torsion of the testis and confirm a diagnosis of hematoma.

4.79

Figure 4.79. Another infant with a hematoma of the right side of the scrotum. In this case, note that the purplish-blue discoloration and swelling do not cross the midline. It would be more difficult to exclude a torsion of the testis in this case. The diagnosis of hematoma was confirmed at surgery.

4.80

Figure 4.80. Torsion of the left testis which was present at birth. The left side felt firm and tender and there was purplish scrotal discoloration which did not cross the midline. The testicular scan may show the characteristic "bull's eye" sign of the vascular supply. With the advent of ultrasonography, the diagnosis is readily confirmed and a scan is not required. This represents a surgical emergency, but the testis usually sustains too much vascular compromise and cannot be salvaged.

4.81

Figure 4.81. This infant has a torsion of the right testis. Note the purplish-blue appearance of the right testis which was firm and tender. The testis usually "rides high" with a torsion. The infant has a hydrocele on the left side. Torsion can lead to irreversible damage of the testis within 6 hours of the occurrence. Testicular salvage is almost unheard of because the torsion often occurs prenatally during the process of testicular decent.

4.82

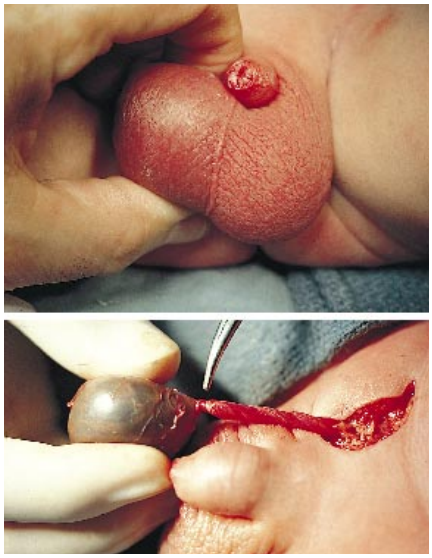

Figure 4.82. At surgery in this same infant as in Figure 4.81, note the gangrene of the right testis and its spermatic cord. It is impossible to salvage such a testis. (Gonzalez, E.)

4.83

Figure 4.83. This infant has a left ectopic testis located in the perineum. The testes migrate from the abdominal cavity to the scrotum in the last trimester of pregnancy. Occasionally one testis fails to descend normally and migrates to an abnormal site. Note the emptiness of the left scrotal sac.

4.84

Figure 4.84. There is an ectopic testis on the right side in this infant. Note the normal scrotal sac on the left with a palpable testis. There was an empty scrotal sac on the right side and the testis was palpable in the perineum.

4.85

Figure 4.85. Bilateral cryptorchidism in a term infant with a normal penis. Note the empty scrotal sacs and the median raphe which traverses the underside of the penile shaft and scrotum. Babies of the youngest gestational ages have the highest rate of undescended testes or cryptorchidism. Even at term, about 3% of male infants have an incompletely descended testis on one side (nearly twice as often on the right as on the left). The majority descend within the first year.

4.86

Figure 4.86. Cryptorchidism in an infant with prune belly syndrome. This is part of the triad of absence of abdominal musculature, genitourinary tract abnormalities, and cryptorchidism.

4.87

Figure 4.87. Cryptorchidism in an infant with Prader-Willi syndrome. This finding and hypotonia should alert one to consideration of the diagnosis of Prader-Willi syndrome in the neonatal period.

4.88

Figure 4.88. Hypogonadism in a term infant. Note the small penis and empty scrotal sacs.

4.89

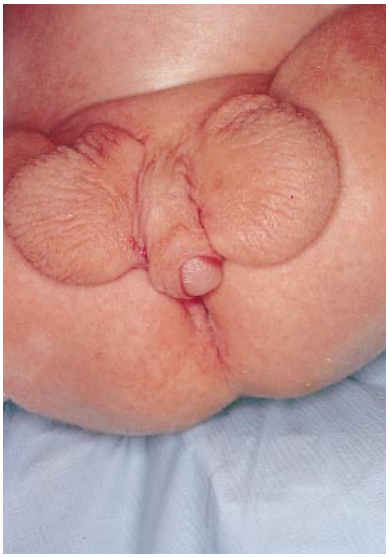

Figure 4.89. This infant has a bifid scrotum which indicates failure of the testosterone-induced fusion of the two labioscrotal folds at about 10 to 11 weeks of gestation with partial penoscrotal transposition. The scrotum is divided into two halves, each containing a testis; this condition may be associated with other perineal abnormalities such as hypospadias or imperforate anus.

4.90

Figure 4.90. Another view of the same infant as in Figure 4.89 with the infant lying on his abdomen showing the bifid scrotum and penoscrotal transposition. Genitalia in which the urethral meatus opens between the two halves of a bifid scrotum (sacral hypospadias) constitute one form of ambiguous genitalia. This is especially worrisome if the testes cannot be palpated.

4.91

Figure 4.91. A right-sided ectopic scrotum with left hemiscrotum in an infant with the popliteal pterygium syndrome. The scrotum is thus divided and there is cryptorchidism on the right. The testis is palpable on the left side.

4.92

Figure 4.92. In this male infant there is a urethral retention cyst (Epstein's pearl) with a hooded foreskin. Epstein's pearls are small retention cysts most commonly found on the palate but also seen on the penis or scrotum or the nipples. The hooded foreskin should not be confused with a shawl scrotum.

4.93

Figure 4.93. Another example of a male infant with urethral retention cysts. These do not interfere with micturition and resolve spontaneously.

4.94

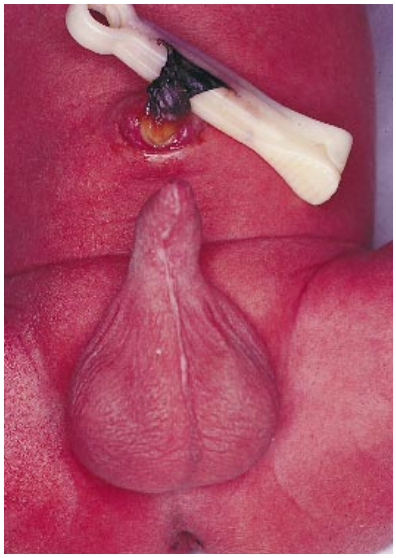

Figure 4.94. In this infant there is a white ridge on the scrotal raphe which probably represents retention cysts.

4.95

Figure 4.95. Redundant normal foreskin in a premature infant. The glans is normal and redundant foreskin is a frequent normal finding. Phimosis (narrowing of the opening of the foreskin preventing retraction) is physiologic in the normal neonate. Normal development releases the adhesions by the age of 2 to 3 years when the foreskin can be fully retracted. Parents should be told not to retract the foreskin in a normal newborn.

4.96

Figure 4.96. Balanoposthitis causing erythema and swelling of the prepuce and glans secondary to inflammation. Balanitis is inflammation of the glans and posthitis is inflammation of the foreskin. This change is frequently due to *Candida* infection but can occur with *Trichomonas* or herpes simplex virus infection. Balanitis should not be confused with a meatal ulceration, which is usually seen in circumcised male infants. In infants with meatal ulceration there is superficial ulceration often resulting from ammoniacal dermatitis. These usually heal spontaneously, but meatal stenosis may result.

4.97

Figure 4.97. This infant has an isolated epispadias. Note that in epispadias the urethral opening is on the dorsal aspect of the phallus. The opening may be either small or large enough to form a furrow bisecting the glans and penis. This is rarely seen as an isolated anomaly, but is more frequently seen in association with extrophy of the bladder.

4.98

Figure 4.98. Epispadias in an infant with bilateral hydroceles.

4.99

Figure 4.99. In this infant who has a mild glanular hypospadias, the prepuce has failed to fuse, resulting in a "hooded" penis. Hypospadias is the second most common genital abnormality (after cryptorchidism) in males. The incidence varies from 0.5 to 0.75% and it occurs much less frequently in black infants. The types of hypospadias are comprised of 87% glanular or coronal, 10% penile, and 3% penoscrotal and perineal.

4.100

Figure 4.100. A glanular hypospadias in an infant with Russell-Silver dwarfism. This type of hypospadias is of minimal significance.

4.101

Figure 4.101. This 4-day-old term infant has a glanular hypospadias with an incomplete prepuce and has developed balanoposthitis (inflammation of the glans and prepuce).

4.102

Figure 4.102. Glanular hypospadias with a hooded foreskin in a term infant. Circumcision is contraindicated in any infant with hypospadias as the foreskin may be required to repair the hypospadias.

4.103

Figure 4.103. Glanular hypospadias with a hooded prepuce (incomplete foreskin) with chordee. Note that the whole ventral surface of the glans is uncovered, with prepuce covering only the dorsum of the glans like a hood. This defect invariably has an accompanying hypospadias. Chordee refers to the ventral curvature of the penile shaft. Severe hypospadias with chordee has more important implications both for its association with other malformations and for urologic repair. The pathogenesis of hypospadias is essentially the same for all degrees of severity in that there is a failure of complete fusion of the margins of the urogenital folds to form the penile urethra.

4.104

Figure 4.104. A premature infant with a glanular hypospadias and chordee in the act of voiding. Note that the chordee results in a stream of urine always pointing downward, hence the importance of correcting this defect. Note the normal appearance of the developing premature scrotum.

4.105

Figure 4.105. A coronal hypospadias. Note that the urethral sulcus is between the glans and the penile shaft.

4.106

Figure 4.106. Penoscrotal hypospadias occurring in the mid or distal penile shaft in a male infant. Infants with penoscrotal or perineal hypospadias may present with the diagnosis of ambiguous genitalia. Both penoscrotal and perineal hypospadias have a strong association with other structural abnormalities of the genitourinary tract.

4.107

Figure 4.107. In this infant with a penoscrotal hypospadias with chordee and some bifurcation of the scrotum, the diagnosis of ambiguous genitalia needs to be considered. The upper portion of the figure shows the genitalia which appear to be fairly normal. In the lower figure, elevation of the penis and separation of the scrotal sacs show the penoscrotal hypospadias. Beware of assuming the gonads are testes in patients in whom the external genitalia are not totally normal. Karyotyping is essential. In this infant the karyotype was XY.

4.108

Figure 4.108. In agenesis of the phallus, there is no urethral meatus or anal opening. Note the single scrotal sac with rugal folds. Autopsy findings included renal agenesis, high anal atresia, small bladder, and no urethra.

4.109

Figure 4.109. Penile agenesis with anterior displacement of an empty scrotum. The urethra appears at the top of the scrotal raphe. Agenesis of the phallus occurs as a result of failure of formation of the genital tubercle. The scrotum is usually present but may lack rugae, and descent of the testes is variable. This malformation has been reported most commonly in sirenomelia.

4.110

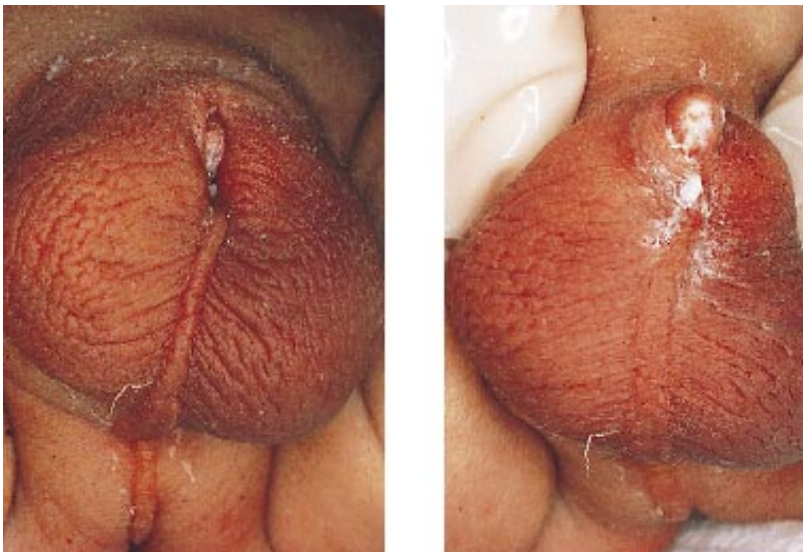

Figure 4.110. Ambiguous genitalia in a male infant with bilaterally descended testes and micropenis. The testosterone level was within normal limits for the newborn. Human chorionic growth hormone stimulation test (performed to see if the testes could respond to and produce testosterone) revealed inadequate testicular function. Exogenous administration of testosterone gave a good response with normal development of male genitalia.

4.111

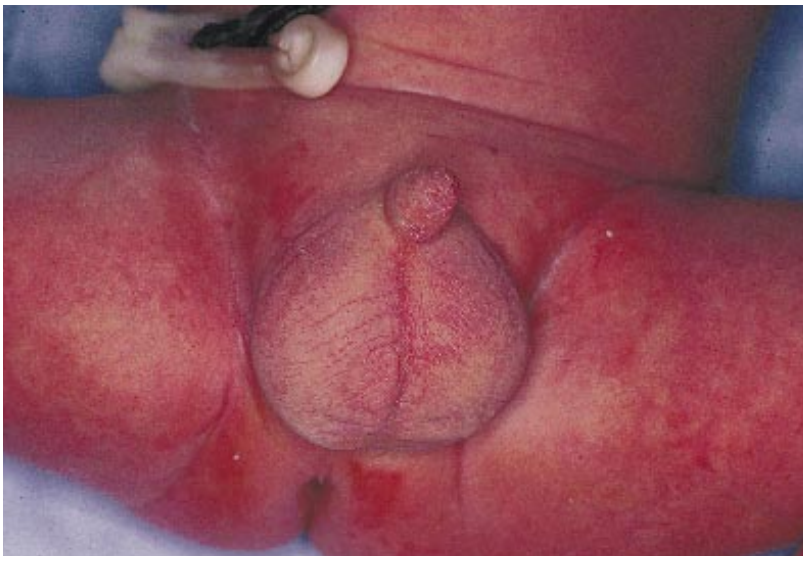

Figure 4.111. This infant presented with severe hypoglycemia and a micropenis with a normal scrotum. The diagnosis of hypopituitarism should always be considered in an infant with micropenis and hypoglycemia. Endocrine studies confirmed the diagnosis of hypopituitarism in this infant.

4.112

Figure 4.112. Enlargement of the penis. Minimal length of the normal stretched penis is 2.5 cm with a maximum length of 4.0 cm.

4.113

Figure 4.113. There is a markedly enlarged penis in this infant. In these infants the diagnosis of megalourethra should be considered.

4.114

Figure 4.114. This infant has a large penis (8 cm) with left cryptorchidism. Note that the scrotal sac is full on the right and empty on the left.

4.115

Figure 4.115. If there is a markedly enlarged penis and bifid scrotum, the diagnosis of megalopenis and megalourethra should be considered. In the more common variety of this unusual anomaly, the corpus spongiosum is absent and the abnormally large penis has a scaphoid shape. The upturned glans penis is normally formed and the urethral meatus is normal in site and in size, without demonstrable obstruction to voiding.

4.116

Figure 4.116. In this infant with a markedly enlarged penis and urethra (megalopenis and megalourethra), the penile urethra forms a large flabby sac on the ventrum of the penis which balloons in a striking fashion during micturition. This condition is non-obstructing and is present at birth as a swelling of variable size. The urine accumulated in about two hours, could be expressed easily, and then reaccumulated. Other abnormalities often coexist (e.g., bilateral refluxing mega-ureters, vesical diverticulum, and defective abdominal wall musculature). In this type of megalourethra, both the corpora cavernosa and corpus spongiosum are absent and the dilated penile urethra has a fusiform shape. There is a danger of infection of the stagnant urine in the dilated urethra.

4.117

Figure 4.117. The same infant as in Figure 4.117 with megalopenis and megalourethra. After the infant voided, the penile size was more normal until the urine reaccumulated. As a rule, the enlarged penis does not grow proportionately with the child, and its proportions may appear relatively normal with time.

4.118

Figure 4.118. Duplication of the glans penis (diphallus) with a fused penile shaft in an infant. (Gonzalez, E.)

4.119

Figure 4.119. Duplication of the male genitalia. There were two bladders with one ureter going into each bladder from the two kidneys, and there was duplication of the urethras with three corpora spongiosum. (Gonzalez, E.)

4.120

Figure 4.120. A term infant with abnormal penile foreskin and glans caused by a rhabdomyosarcoma involving the penile skin, rectal and bladder muscles, and mucous membranes.

4.121

Figure 4.121. The same infant as in Figure 4.120 with rhabdomyosarcoma, showing the abnormal appearance of the glans and foreskin.

4.122

Figure 4.122. Ambiguous genitalia in a monozygotic female twin infant (the other twin was normal). There is imperforate anus and a blind vaginal pouch. This is an example of a "doughnut scrotum" which encircles the phallus. It is a form of penoscrotal transposition and is not of great consequence. This should be distinguished from a shawl scrotum which appears to represent a mild deficit in the full migration of the labioscrotal folds and may be accompanied by other signs of incomplete masculinization of the external genitalia. It is seen in Aarskog syndrome.

4.123

Figure 4.123. Congenital adrenal hyperplasia in a female infant with 21 hydroxylase deficiency. Examples of ambiguous genitalia are presented in Chapter 5.

4.124

Figure 4.124. Bladder exstrophy (ectopia vesicae) in a female infant. This results from failure of midline fusion of the lower half of the abdominal wall, including the deep structures such as the symphysis pubis and anterior bladder wall. The trigone is exposed and inappropriate fusion may result in synechia vulva in the female infant or in associated epispadias in the male infant.

4.125

Figure 4.125. Ectopia vesicae (bladder exstrophy) in a male newborn infant. Note the exposed bladder and epispadias. Ectopia vesicae is most commonly seen in male infants. In the female it involves the bladder and vagina, and the labia are widely split.

4.126

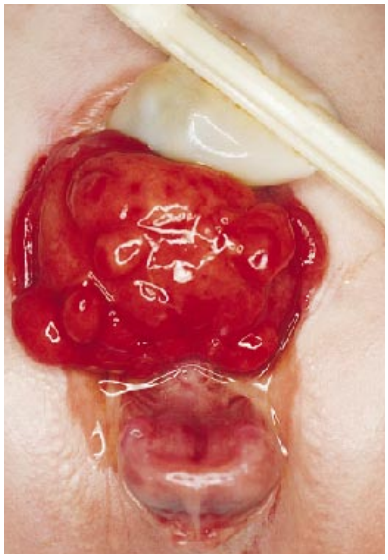

Figure 4.126. Close-up of exstrophy of the bladder in a male infant with a severe epispadias. The anterior wall of the bladder is absent and the posterior wall is exposed to the surface. The posterior wall is seen as a reddened granulomatous mass lying just above the pubic symphysis. The ureteral orifices can often be discerned laterally exuding urine onto the surface of the thickened and hypertrophic bladder mucosa. There is complete epispadias with the urethral opening on the dorsal side of an abnormally short penis.

4.127

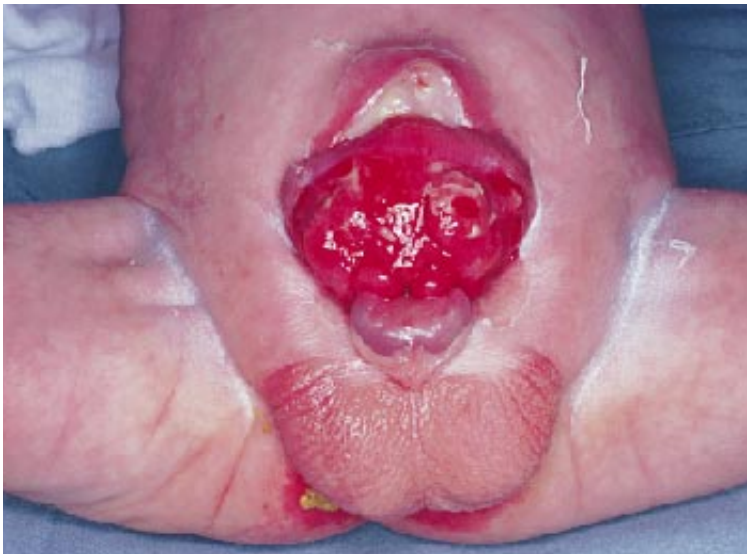

Figure 4.127. Another example of exstrophy of the bladder in a male infant who had meningomyelocele and developed an associated arthrogryposis.

4.128

Figure 4.128. The cloacal dysgenesis sequence which represents a complete urogenital sac defect with a vesicointestinal fissure resulting from abnormal development of the lower half of the abdominal wall.

4.129

Figure 4.129. A urogenital sac defect which resulted in cloacal dysgenesis with anterior placement of the anus is present in this female infant. The features of cloacal dysgenesis include omphalocele, bladder exstrophy, and a blind colon which is associated with anorectal agenesis.

4.130

Figure 4.130. Ambiguous genitalia in a female infant with VACTERL syndrome. Note the cloacal sac with a single urogenital opening. The bladder is in free communication with the rectum. This infant also had congenital heart disease, a tracheoesophageal fistula, imperforate anus, and a right hydronephrosis. Karyotype was XX.

4.131

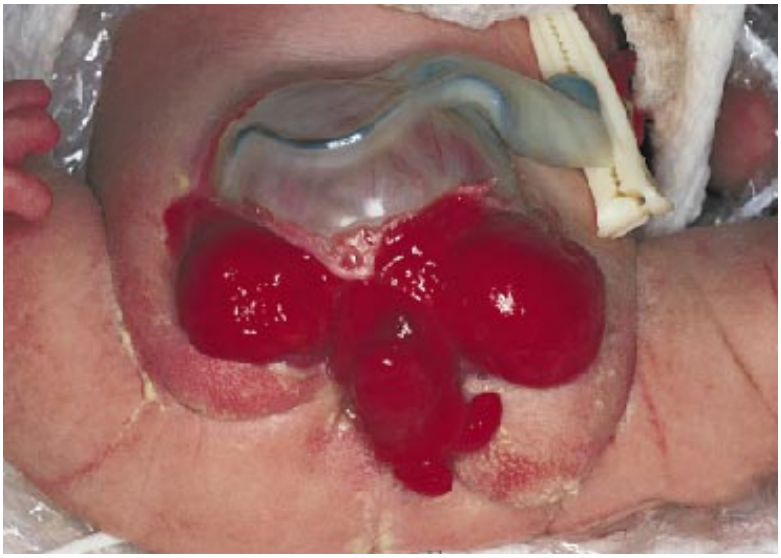

Figure 4.131. This infant has an omphalocele and exstrophy of the cloaca. The etiology for exstrophy of the cloaca (ectopia cloacae, vesicointestinal fissure) is similar to that of exstrophy of the bladder but the deficiency of mesenchymal migration is more severe and occurs before partitioning of the cloaca. Thus, the bladder is present only as lateral remnants which, along with the interior of the rectum, are exposed on the surface of the lower abdomen. The abdominal viscera, including the liver, may herniate through the intra-abdominal defect, and there is a wide gap between the pubic bones.

4.132

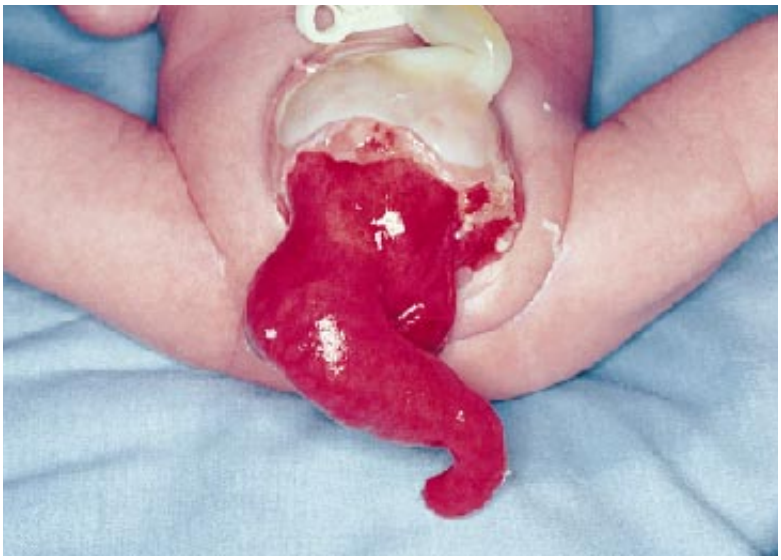

Figure 4.132. Exstrophy of the cloaca is a severe defect of the lower abdominal wall in which the exstrophic bladder is divided into a right and left half between which a field of intestinal mucosa is seen. The prolapsed ileum hangs like a trunk from the exposed field, the so-called "elephant trunk" deformity. In such cases the colon is short and ends blindly in an imperforate anus. This infant demonstrates an omphalocele, bladder exstrophy, a blind colon which is associated with anorectal agenesis, and the "elephant trunk" deformity.

4.133

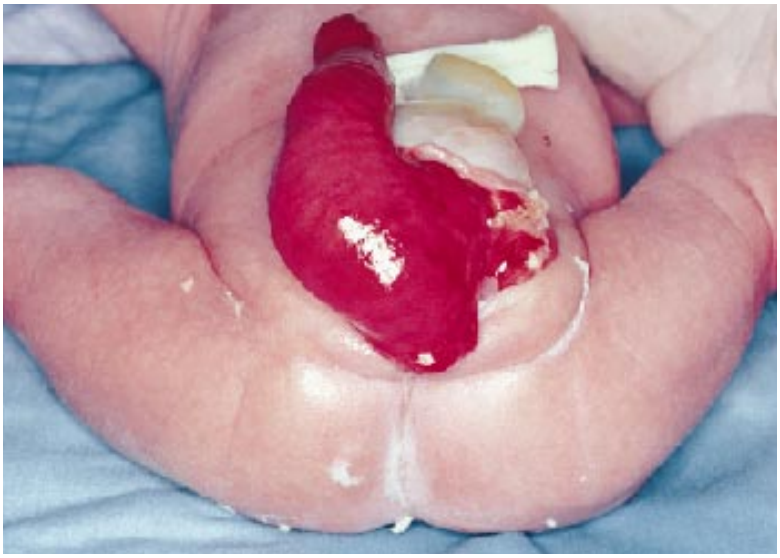

Figure 4.133. The same infant as in Figure 4.132 with exstrophy of the cloaca. Note the absence of an anal opening, the small omphalocele superiorly, and the "elephant trunk" deformity raised superiorly.

4.134

Figure 4.134. This female infant has exstrophy of the cloaca sequence which includes cloacal exstrophy with imperforate anus, ambiguous genitalia, and a lumbosacral myelocystocele (hydromelia). In addition to the exstrophy, the urinary tract may be involved by various anomalies such as hydronephrosis or cystic or absent kidney.

4.135

Figure 4.135. Another example of the exstrophy of the cloaca sequence. Note the exstrophy of the cloaca and hydromelia. This infant also developed an in utero amputation of the right lower extremity, probably from an amniotic band and had a gangrenous skin tag on the buttock. The left foot shows severe talipes equinovarus.

Chapter 5
Endocrine and Metabolic Disorders

Endocrine and metabolic processes are actively involved in the growth and development of the fetus from conception. Clinical disorders of endocrine and metabolic function in the neonate are most often based upon abnormal physiologic function in either the fetus or mother during gestation. The timing of these disturbances during gestation can result in varying clinical presentations. Endocrine system involvement may include the thyroid, pituitary, hypothalamus, parathyroid, testes, ovaries, and adrenal glands. Metabolic disorders may include carbohydrate, amino acid, fatty acid, calcium, phosphorus, and magnesium metabolism. Advances in the recognition, treatment and prevention of many endocrine and metabolic disorders make it imperative that the clinician be familiar with these disorders. Although screening programs exist for many of these disorders, many children remain undiagnosed. Clinicians must remain aware of these conditions so that infants may be diagnosed early and the condition treated, or genetic counseling can be provided to parents.

Endocrine Disorders

5.1

Figure 5.1. Midline neck mass in an infant with congenital goiter. Goiter may occur in the newborn period as a result of maternal iodine deficiency, drug ingestion (e.g., iodide during pregnancy for treatment of maternal asthma), maternal thyrotoxicosis, or inborn errors of thyroxine synthesis. The pressure effect of the enlarged thyroid on the trachea may result in respiratory distress. Medical treatment depends on whether the infant has hypothyroidism or hyperthyroidism.

5.2

Figure 5.2. Left, radiograph of the long bones of the lower extremity in a term infant with congenital hypothyroidism. Note the lack of the ossification centers. The distal femoral ossification center usually appears at 36 weeks gestational age and the proximal tibial ossification center usually appears at 38 weeks gestational age. Right, lateral radiograph of the neck of the same infant showing the presence of a large congenital goiter which caused severe respiratory distress.

5.3

Figure 5.3. This 5-week-old infant with congenital hypothyroidism has generalized myxedema, dry skin, hoarse low-pitched cry, low body temperature, and constipation. Note the characteristic facies with enlarged tongue (macroglossia) and the protuberant abdomen ("pot belly") with umbilical hernia.

5.4

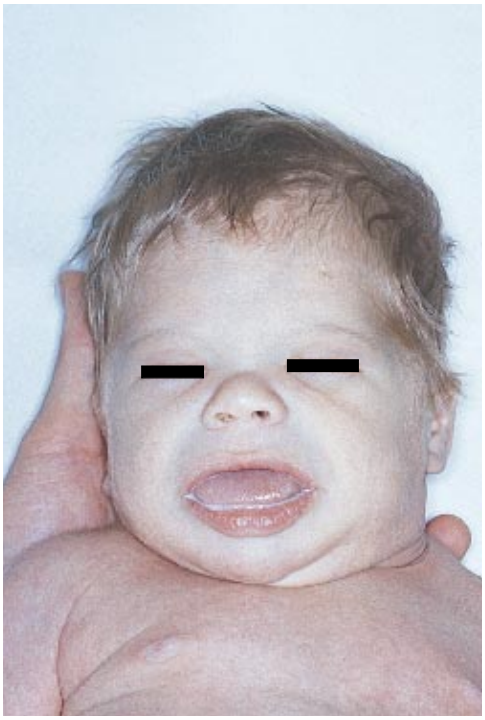

Figure 5.4. Typical facies of the same infant as in Figure 5.3 with congenital hypothyroidism. Note the coarse facial features with the macroglossia and the mottling of the skin (cutis marmorata). At birth there are usually no abnormal signs; the characteristic features of hypothyroidism develop at a few weeks to a few months of age. At the present time, neonatal screening has been invaluable in making an early diagnosis. The diagnosis must be considered in infants with persistent jaundice or constipation.

5.5

Figure 5.5. The face of another infant with congenital hypothyroidism. Note the coarse facies, coarse hair, puffiness of the eyes, and the macroglossia.

5.6

Figure 5.6. Lateral view of the head and face of the same infant as in Figure 5.5. Note the coarse facies, edema of the eyelids, and the macroglossia.

5.7

Figure 5.7. This infant with a goiter had decreased tone as the result of hypothyroidism.

5.8

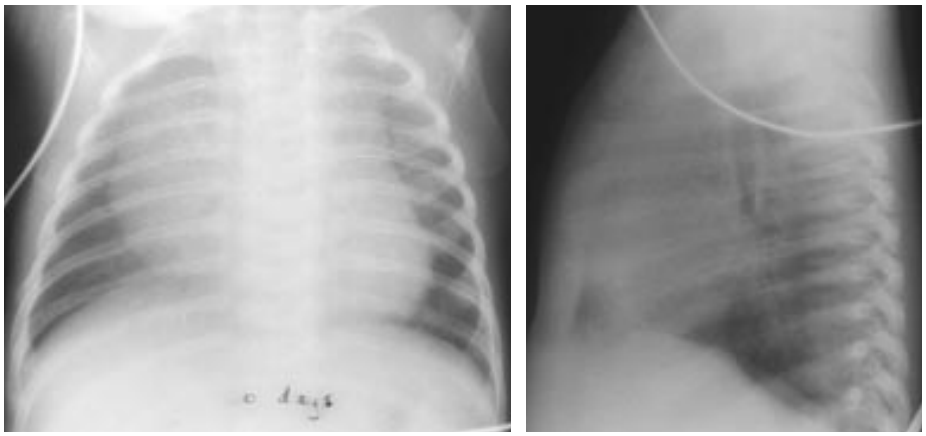

Figure 5.8. Antero-posterior and lateral radiographs of an infant with congenital hypothyroidism. Note the marked cardiomegaly as the result of congestive heart failure.

5.9

Figure 5.9. Typical appearance of infant at the age of 9 days with congenital hypothyroidism (coarse facial features, puffiness of the eyelids, macroglossia, and coarse hair). Infant presented at birth with cardiogenic shock. Hospital course was remarkable for seizures and death at age 12 days from a pulmonary hemorrhage. Infant had a low T4 (thyroxine) and increased TSH (thyroid-stimulating hormone). Autopsy findings revealed the presence of inflammation involving the heart, brain, liver, and kidneys. The thyroid gland was normal histologically. Adenovirus was detected with polymerase chain reaction (PCR) technology.

5.10

Figure 5.10. The same infant as in Figure 5.9 had marked cutis marmorata and non-pitting edema (myxedema) of the face, of the dorsum of the hand, and of the external genitalia.

5.11

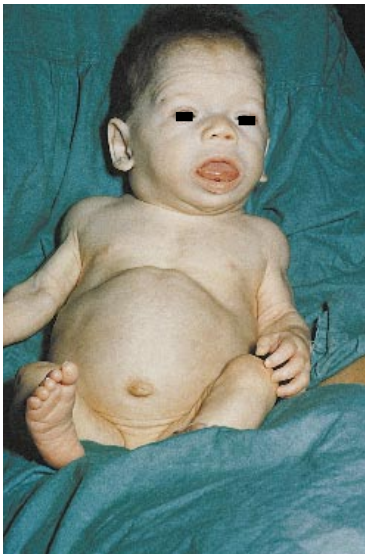

Figure 5.11. Congenital hypothyroidism. Note the classic facial features in association with generalized muscle hypertrophy. These are rare but classic findings in infants with the Kocher-Debré-Sémélaigne syndrome ("wrestler's" syndrome).

5.12

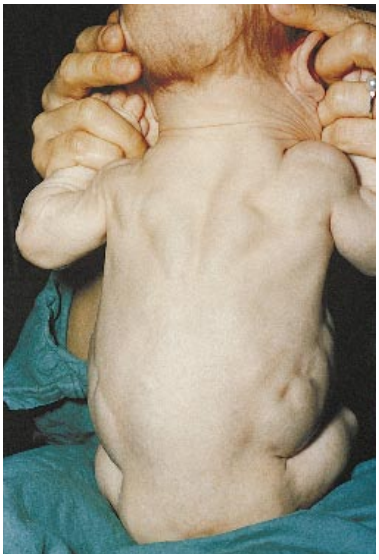

Figure 5.12. Posterior view of the same infant as in Figure 5.11 clearly demonstrating the generalized muscular hypertrophy.

5.13

Figure 5.13. This infant with congenital hyperthyroidism had a large midline neck mass due to a congenital goiter. Congenital goiter can occur when there is a defect in the synthesis of thyroid hormone (due to fetal TSH stimulation causing intrauterine growth of the thyroid gland) or in cases of maternal hyperthyroidism (due to long-acting thyroid stimulator [LATS]) antibody crossing the placenta.

5.14

Figure 5.14. This hyperactive, term male infant with transient congenital hyperthyroidism had severe growth retardation. This infant's mother suffered from Graves' disease, and the maternal LATS antibodies were transmitted to the child. The symptoms include tachycardia, cardiac failure, abnormal eagerness for feedings, enlargement of the thyroid gland, and exophthalmos. Symptoms usually subside 4 to 6 weeks following birth concordant with the disappearance of maternal IgG antibodies. The onset of symptoms may be delayed for about a week as a result of prenatal therapy given to the mother.

5.15

Figure 5.15. The same infant as in Figure 5.14 with congenital hyperthyroidism with exophthalmos and an alert expression failed to gain weight. Birth weight was 1560 g. At 5 weeks of age, this infant weighed 1655 g in spite of adequate caloric intake.

5.16

Figure 5.16. A close-up of the face of the same infant with congenital hyperthyroidism. Note the exophthalmos with retraction of the upper lids (Stellwag's sign).

5.17

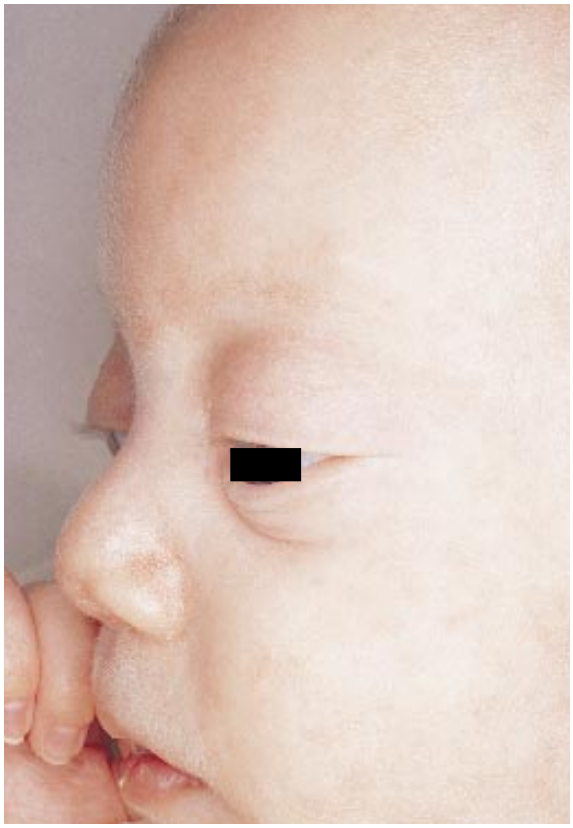

Figure 5.17. Lateral view of the face of the same infant as in Figure 5.16 with exophthalmos. Stellwag's sign is demonstrated in this view.

5.18

Figure 5.18. Unilateral exophthalmos can occur in infants with hypothyroidism. This infant had normal thyroid studies and an MRI of the orbit was normal. Differential diagnosis includes hemangioma, lymphangioma, anterior encephalocele, and intraorbital tumors (rhabdomyosarcoma, metastatic neuroblastoma, dermoid cysts).

5.19

Figure 5.19. Micropenis with a normal scrotum in an infant who presented with severe hypoglycemia. This combination should alert one to the diagnosis of hypopituitarism. There is a higher incidence of hypopituitarism in patients with a variety of midline defects. Hypopituitarism was confirmed in this infant.

5.20

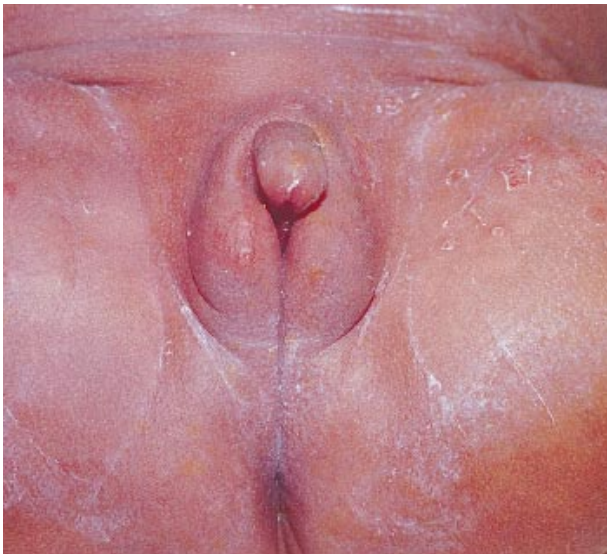

Figure 5.20. This female infant has ambiguous genitalia. The karyotype was XX. Difficulties in determining the sex of an infant may arise from abnormalities of the external genitalia. Ambiguous genitalia encompass a wide range of abnormalities having their origin before the 12th week of gestation. The phallus commonly shows hypospadias with chordee formation and appears large in proportion to the persisting labioscrotal folds which may or may not contain gonads (testis, ovotestis, or rarely a well-defined ovary). In females, the labia may be fused and the clitoris hypertrophied. This condition is known as pseudohermaphroditism.

5.21

Figure 5.21. Lateral view of the same infant as in Figure 5.20 with ambiguous genitalia showing the marked clitoromegaly. Hermaphroditism (intersex) includes 1) true hermaphroditism, 2) female pseudohermaphroditism (virilizing adrenal hyperplasia), 3) male pseudohermaphroditism (the syndrome of incomplete testicular feminization; masculinization with 3-ß-hydroxysteroid dehydrogenase deficiency), 4) pseudohermaphroditism in syndromes (feminizing adrenal tumors).

5.22

Figure 5.22. Ambiguous genitalia in a male pseudohermaphrodite with a karyotype of XY. Note the rugae in the labioscrotal folds. Gonads were not palpable.

5.23

Figure 5.23. Another example of ambiguous genitalia in a male pseudohermaphrodite. Note the marked labioscrotal folds, absence of testes and presence of hypospadias.

5.24

Figure 5.24. This infant with ambiguous genitalia is an example of incomplete testicular feminization in that there are normal-appearing female genitalia except for clitoral hypertrophy and a sinus urogenitalis. Because of the swelling of both labia majora an inguinal hernia may be suspected. At surgery the hernial sac was found to include both testes; no uterus was present. Karyotype was XY.

5.25

Figure 5.25. Another example of incomplete testicular feminization. Note the hypospadias. Karyotype was XY. In the syndrome of testicular feminization, the infants are genetic males: testes are located in the inguinal canal or in the labial folds. The external genitalia are female in configuration, and occasionally the clitoris is slightly enlarged; labioscrotal folds are partially fused and characteristically there is a blind vaginal pouch. The uterus may be rudimentary or absent. Incomplete variants of the syndrome do occur.

5.26

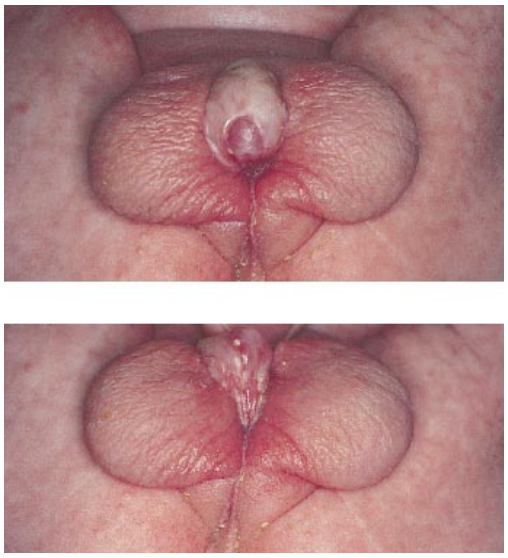

Figure 5.26. Ambiguous genitalia in an infant with a severe penoscrotal hypospadias. Karyotype was XY.

5.27

Figure 5.27. This infant with ambiguous genitalia had an XY karyotype and, thus, was a male pseudohermaphrodite. In male pseudohermaphroditism the appearance of the external genitalia varies from that of a normal female to that of a male with a penile urethra and either unilateral or bilateral cryptorchidism. Commonly there is perineal hypospadias, and the testes may be inside the abdomen, in the inguinal region, or in the labioscrotal folds.

5.28

Figure 5.28. This infant with ambiguous genitalia had an XX karyotype. Gonads present in the labial folds (note the indentations) histologically were confirmed to be ovotestes.

5.29

Figure 5.29. Ambiguous genitalia in this female pseudohermaphrodite was due to congenital virilizing adrenal hyperplasia. This female infant with 21-hydroxylase deficiency has clitoromegaly without fusion of the labial scrotal folds and separate vaginal and urethral openings. On the right the clitoris is raised to show the vaginal opening. The uterus was present on ultrasonography. Adrenogenital syndrome results from an enzymatic block of glucocorticoid biosynthesis resulting in excess secretion of androgens and masculinization of the female fetus.

5.30

Figure 5.30. Another example of a female infant with ambiguous genitalia as the result of 21-hydroxylase deficiency. In female pseudohermaphroditism (masculinization of the external genitalia) findings include clitoral hypertrophy and fusion of the labia majora and a urogenital sinus (common opening of the urethra and vagina). In 21-hydroxylase deficiency there are elevated 17-hydroxyprogesterone levels with low urinary 17-hydroxysteroids. If there is also deficiency of mineralocorticoids, there may be abnormal urinary salt loss and hyponatremia. In 11-hydroxylase deficiency, clinical virilization of the female infant can also occur, but this is usually associated with hypertension resulting from an accumulation of deoxycorticosteroid which is a potent mineralocorticoid.

5.31

Figure 5.31. Another example of congenital adrenal hyperplasia in a female infant. Note the marked labioscrotal folds; testes were absent, and a hypospadias is present. In 21-hydroxylase deficiency, genitalia are conspicuously abnormal at birth. The degree of masculinization can be judged by the size of the clitoris and the degree of labioscrotal fusion, which determines the size of the urogenital sinus. The phallus is invariably enlarged, often approximating the size of a penis. It is generally bound with chordee, behind which a perineal hypospadias is situated. Commonly the labia majora have the appearance of a bifid scrotum. The orifices of the vagina and the urethra lie within the perineal opening of the urogenital sinus.

5.32

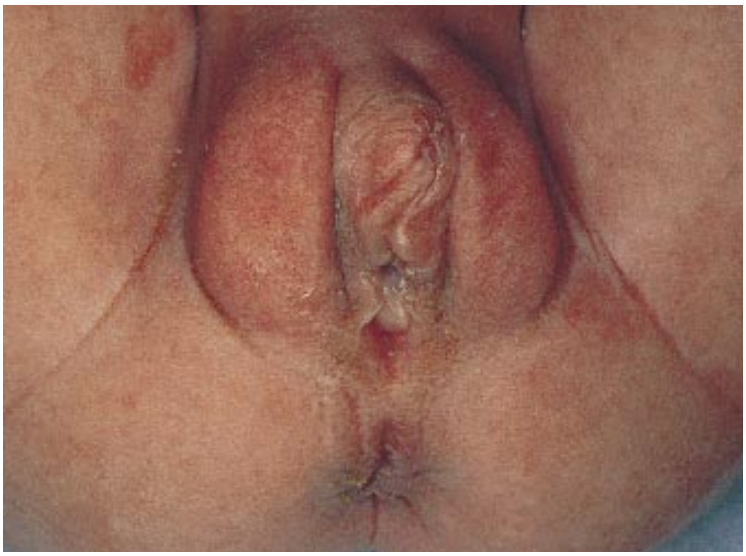

Figure 5.32. Another example of ambiguous genitalia in an infant with 21-hydroxylase deficiency. In female pseudohermaphroditism due to congenital adrenal hyperplasia, the following types of abnormalities may occur: Type I - only abnormality is an enlarged clitoris; Type II - there is partial labioscrotal fusion; Type III - a funnel-shaped urogenital sinus is present at the posterior end of a shallow vulva; Type IV - there is a very small urogenital sinus situated at the base of an enlarged phallus; Type V - a penile urethra is present.

5.33

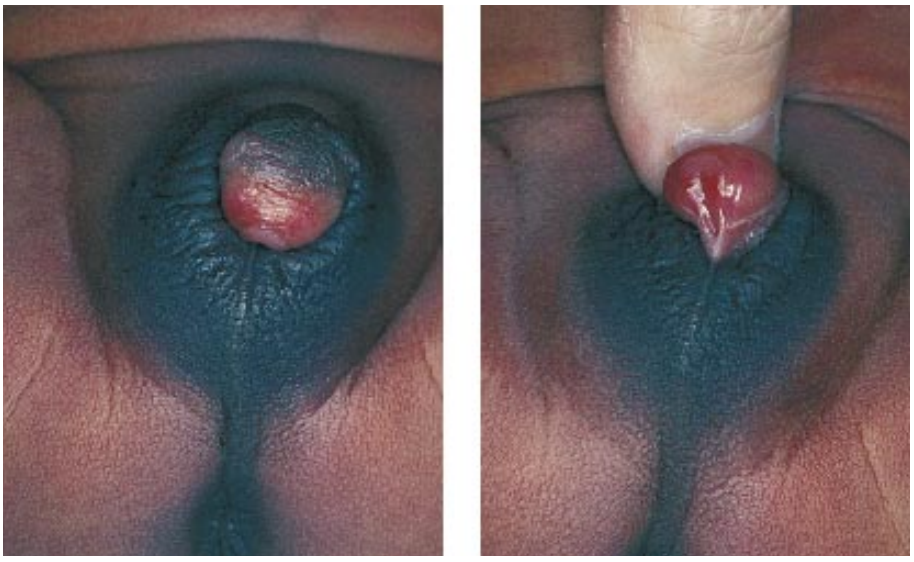

Figure 5.33. Hispanic female infant with ambiguous genitalia as a result of 21-hydroxylase deficiency. Infant presented on the 8th day of life with a serum potassium of 10 mEq/dL and a serum sodium of 108 mEq/dL due to congenital adrenal hyperplasia. Note the clitoromegaly and marked increase in pigmentation. Karyotype was 46 XX.

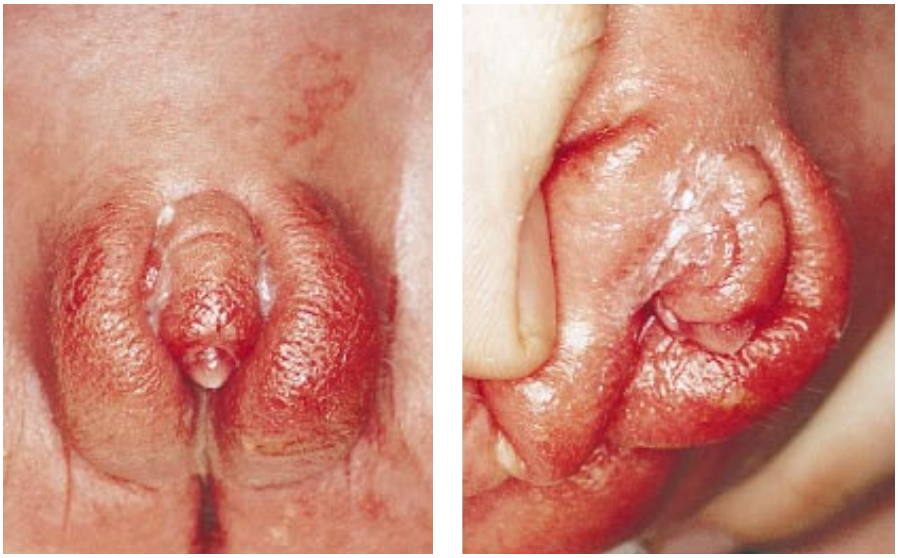

5.34

Figure 5.34. This female infant with ambiguous genitalia due to congenital adrenal hyperplasia presented in adrenal crisis at the age of 17 days with a serum potassium of 6.6 mEq/dL and a serum sodium of 117 mEq/dL. She responded rapidly to therapy.

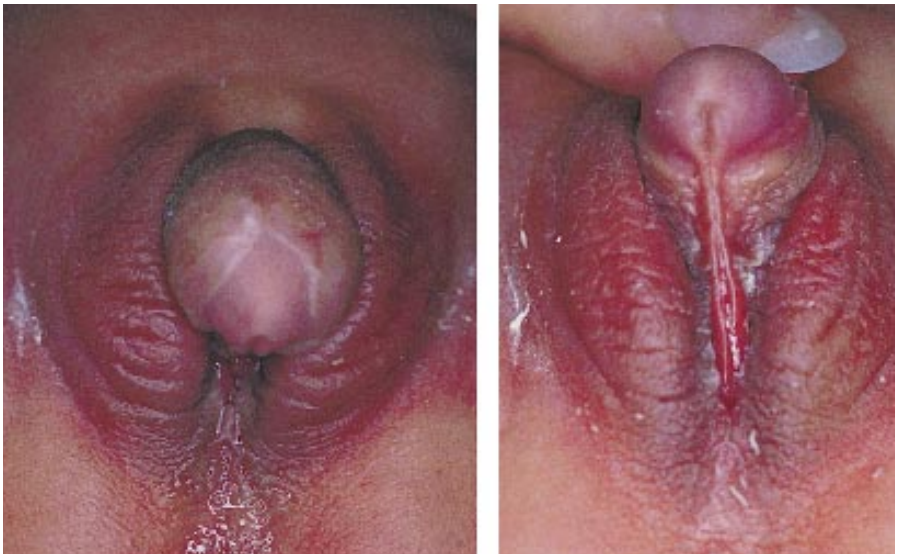

5.35

Figure 5.35. True hermaphroditism in an infant with an XX karyotype. Note the prominent phallus, lax labioscrotal folds, and urogenital sinus at the base of the phallus. Ovotestes were present in the abdomen. Most true hermaphrodites look more masculine than feminine. Cryptorchidism and inguinal herniae that contain a gonad or a vestigial uterus and fallopian tubes are present in about 50% of these infants.

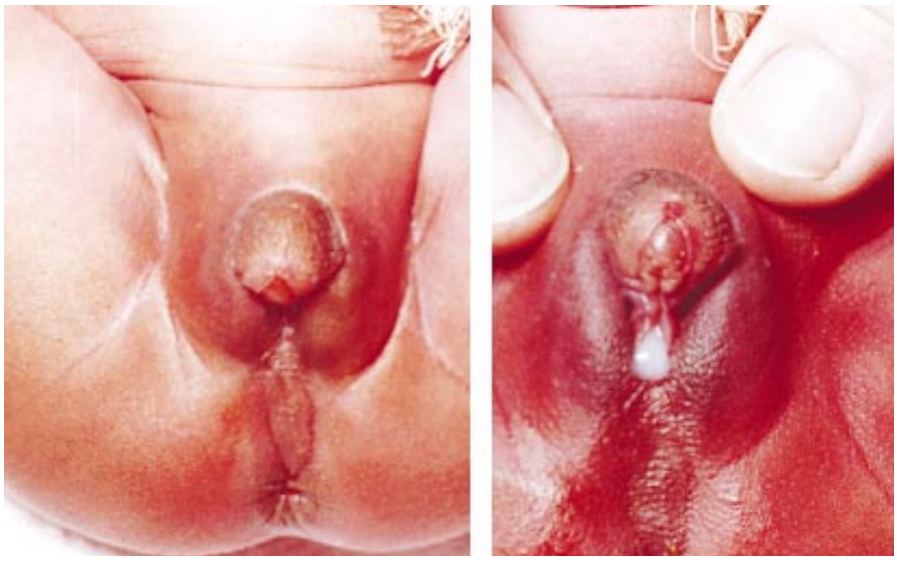

5.36

Figure 5.36. There was masculinization of this female infant following the use of diethylstilbestrol in the mother. Note the marked clitoromegaly. The presence of the vaginal secretion confirms the sex of this child. (See Volume I, Chapter 3, "Effects of Maternal Medication.")

5.37

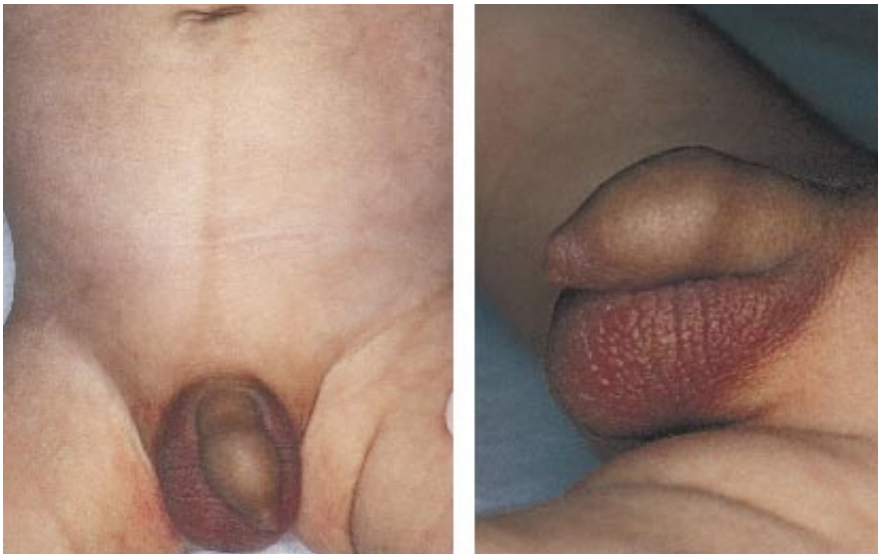

Figure 5.37. Enlarged penis and hyperpigmentation of this male infant with congenital adrenal hyperplasia. Note the prominent linea nigra.

5.38

Figure 5.38. The same infant as in Figure 5.37 with hyperpigmentation of the nipples.

5.39

Figure 5.39. Thirty-three week gestational age infant with severe intrauterine growth retardation. This Hispanic infant was born at 33 weeks gestational age. There was oligohydramnios with severe intrauterine growth retardation (birth weight 1088 g). There was marked generalized hyperpigmentation of the skin (mother is holding infant) at age 4 weeks. This infant developed adrenal failure at 1 week of age, and the diagnosis of a primary adrenal hypoplasia was confirmed. The infant responded well to therapy, started to thrive, and the pigmentation was much decreased at 4 weeks of age and continued to improve.

Metabolic Disorders

5.40

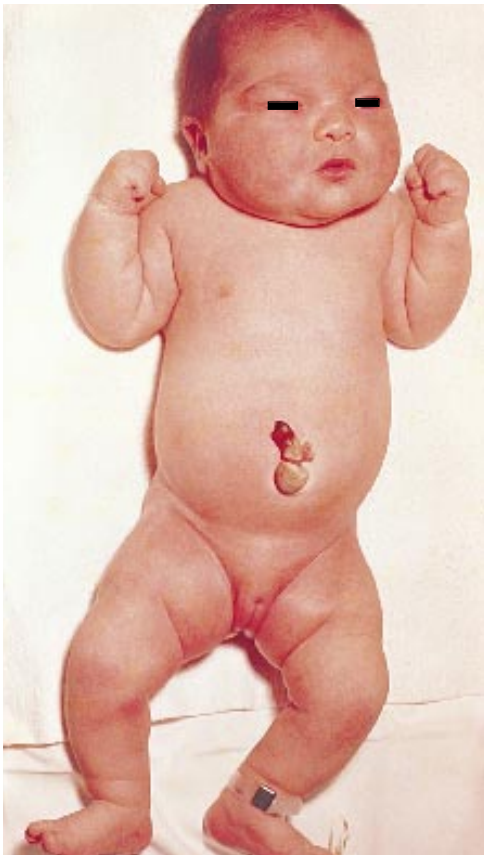

Figure 5.40. Infant of a diabetic mother. Infant is large for gestational age, has a cushingoid appearance, and is plethoric. Despite the deceptiveness of his size and appearance, the fact that the babies of diabetic mothers are often premature should not be disregarded.

5.41

Figure 5.41. Infant of a diabetic mother showing macrosomia. The birthweight and body length are in excess of infants who are appropriate for gestational age. The macrosomic head of an infant of a diabetic mother may appear disporportionately small because brain size is not increased relative to gestational age. Macrosomia is also seen in Beckwith-Wiedemann syndrome, and Sotos' syndrome. Note the hypotonia which is common in these infants.

5.42

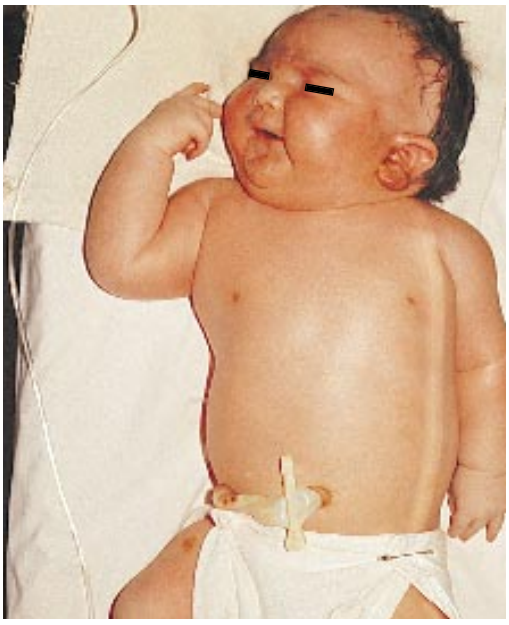

Figure 5.42. This infant of a diabetic mother has Erb's palsy of the left arm. Shoulder dystocia, which is common in these large-for-gestational-age infants, results in birth trauma such as fracture of the clavicle and brachial plexus injury. In general, there is an increased number of all congenital anomalies in infants of diabetic mothers. The caudal regression syndrome, sacral agenesis (see Volume II, Chapter 1, "Musculoskeletal Disorders"), and the small left colon syndrome (see this volume, Chapter 2) are malformations that occur almost exclusively in infants of diabetic mothers.

5.43

Figure 5.43. Classic facies of an infant of a diabetic mother. Note the shaved scalp with multiple venipuncture sites resulting from the need for intravenous glucose for hypoglycemia which occurs commonly in these infants. Therapy may also be required for hypocalcemia and hypomagnesemia.

5.44

Figure 5.44. Classic cushingoid facies of an infant of a diabetic mother. Note the "balloon cheeks," dilated capillaries over the cheeks, and eyes that appear to be small. This infant also has a small subconjunctival hemorrhage of the left eye.

5.45

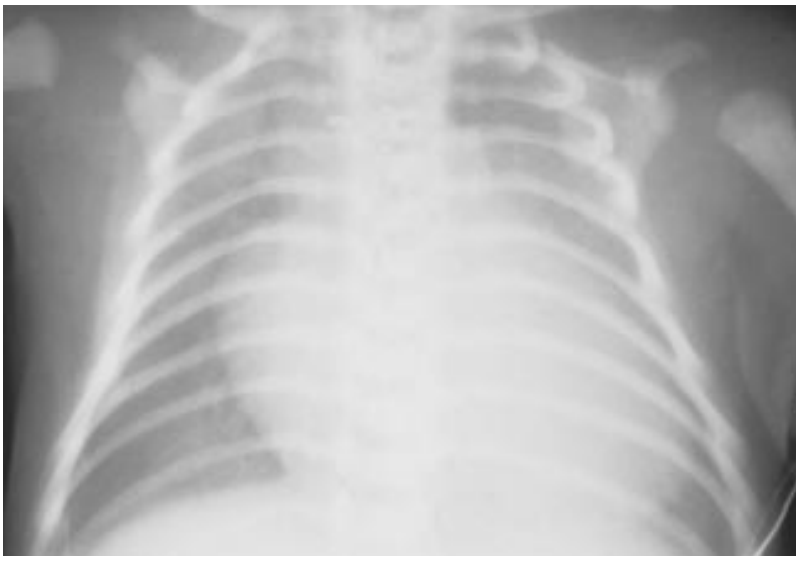

Figure 5.45. Chest radiograph of an infant of a diabetic mother presenting with tachypnea. Note the enlarged cardiac shadow. Infants of diabetic mothers may have cardiac enlargement due to a transient septal hypertrophy. The majority of these infants are asymptomatic, and the thickening is detected only by an electrocardiogram or echocardiography. With very marked septal thickening, left ventricular outflow obstruction may lead to left heart failure in the first few days after birth.

5.46

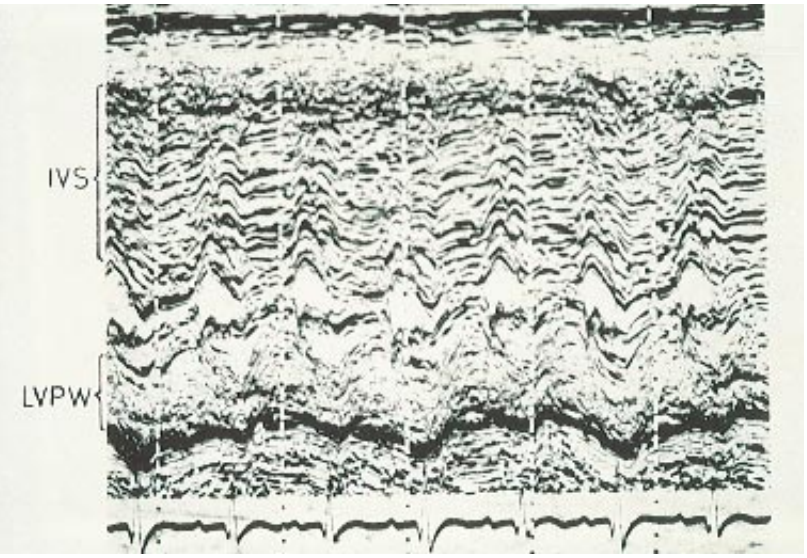

Figure 5.46. An echocardiogram of the same infant as in Figure 5.45 shows the marked thickening of the interventricular septum (interventricular septal hypertrophy). There may also be thickening of the left or right ventricular free wall. The changes generally regress after several months and the condition appears to leave no permanent effects on the myocardium. IVS interventricular septum LVPW left ventricular posterior wall.

5.47

Figure 5.47. Autopsy specimen of a heart with marked interventricular septal hypertrophy in an infant of a diabetic mother.

5.48

Figure 5.48. Infants with generalized gangliosidosis syndrome type I have a low birthweight and severe postnatal growth deficits. They have typical orofacial features and skeletal changes. The condition is autosomal recessive and has been shown to be due to a deficiency of ß-galactosidase. In this infant at the age of 16 days note the coarse features and growth deficiency.

5.49

Figure 5.49. A close-up of the face of the same infant as in Figure 5.48 shows the coarse features with frontal bossing, puffiness of eyes, low nasal bridge, anteverted nostrils, and long philtrum.

5.50

Figure 5.50. The right hand of the same infant as in Figures 5.48 and 5.49 shows the thickening of the wrists and a single palmar crease. Skeletal changes include moderate joint limitation with thick wrists, contractures at the elbows and knees, and development of a claw hand.

5.51

Figure 5.51. The feet of the same infant as in Figures 5.48–5.50 show the abnormalities of the toes. Radiologically the long bones are poorly mineralized and coarsely trabeculated, and some metaphyseal cupping and epiphyseal irregularity are usually present. The ribs are thick.

5.52

Figure 5.52. Infants with mucolipidosis type II (Leroy I-cell disease) have low birthweight and marked growth deficiency postnatally. Affected infants have the characteristic craniofacial features. There is moderate joint limitation in flexion of hips, kyphosis and broadening of the wrists and fingers. This infant at the age of 7 weeks shows the facial features and has marked ascites due to congestive cardiac failure. Death usually occurs from congestive cardiac failure.

5.53

Figure 5.53. In a lateral view of the same infant as in Figure 5.52 note the facial features, marked ascites, and labial edema.

5.54

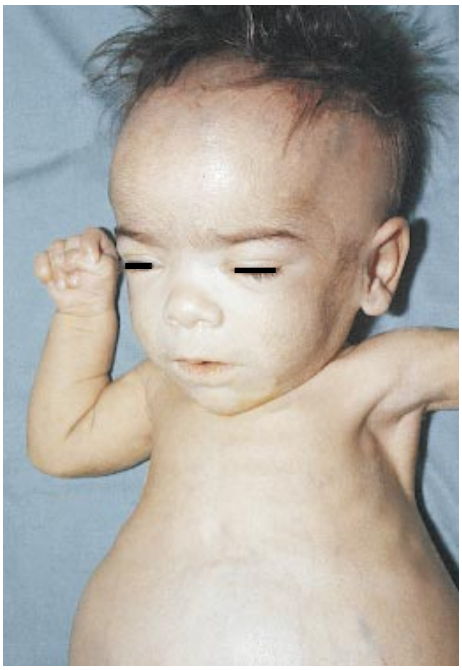

Figure 5.54. A close-up of the baby shows the typical facial features of high, narrow forehead, puffy eyelids, inner epicanthic folds, low nasal bridge, anteverted nostrils, a long philtrum, and progressive hypertrophy of the alveolar ridges.

5.55

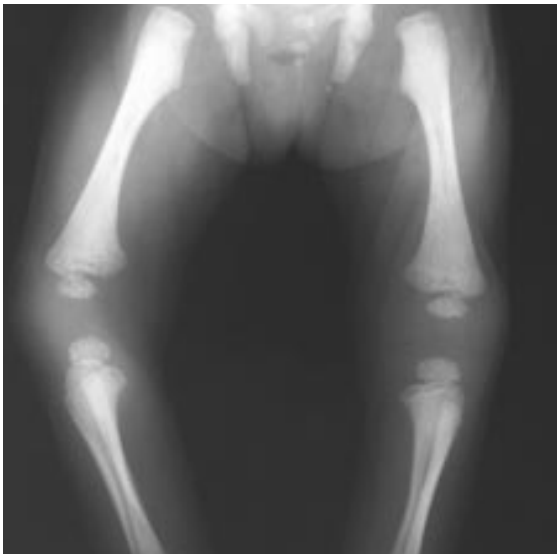

Figure 5.55. Radiograph of the lower extremities in Leroy I-cell disease shows discrete metaphyseal bands at the distal ends of the long bones.

5.56

Figure 5.56. An infant with Menke's kinky-hair syndrome ("steely-hair" syndrome; trichopilodystrophy). Note the failure to thrive, and the abnormal hair pattern and skin lesions. These infants often present with seizures. It is a sex-linked recessive neurodegenerative disorder that affects male infants as a result of a copper deficiency and results in severe progressive neurologic deficit. There are low or absent copper and ceruloplasmin levels. Radiologically there may be widening of the metaphyses with spurring and frequent fractures, particularly of the ribs and femur. These may resemble the appearance of battered-child syndrome.

5.57

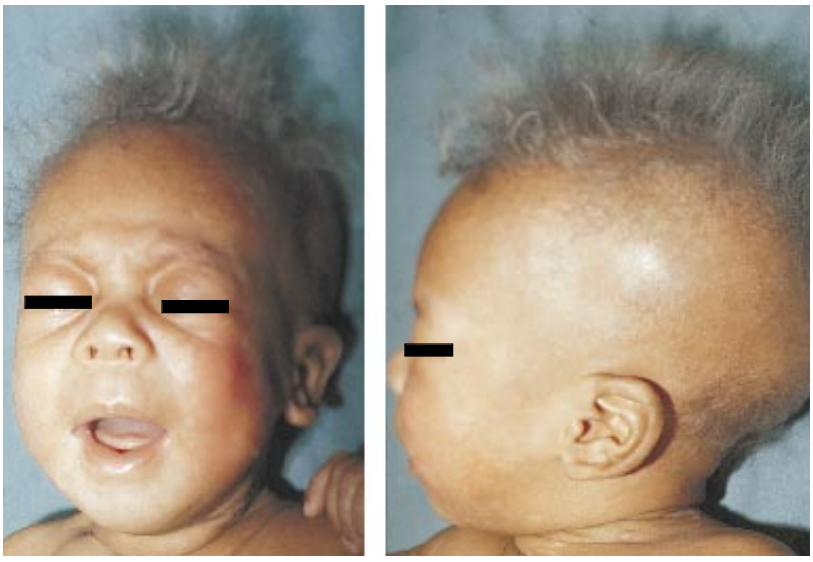

Figure 5.57. In this infant with Menke's syndrome note the pudgy cheeks, lack of expression and movement, marked areas of alopecia, and the short stubby hair which is lightly pigmented giving it a "steely" appearance.

5.58

Figure 5.58. A close-up of the hair in the same infant as in Figure 5.57 showing the "steely" appearance of the hair.

5.59

Figure 5.59. Another view of the scalp of the same infant as in Figures 5.57 and 5.58 showing hair which is fine, dull, sparse, and poorly pigmented. It stands on end and looks and feels like steel wool.

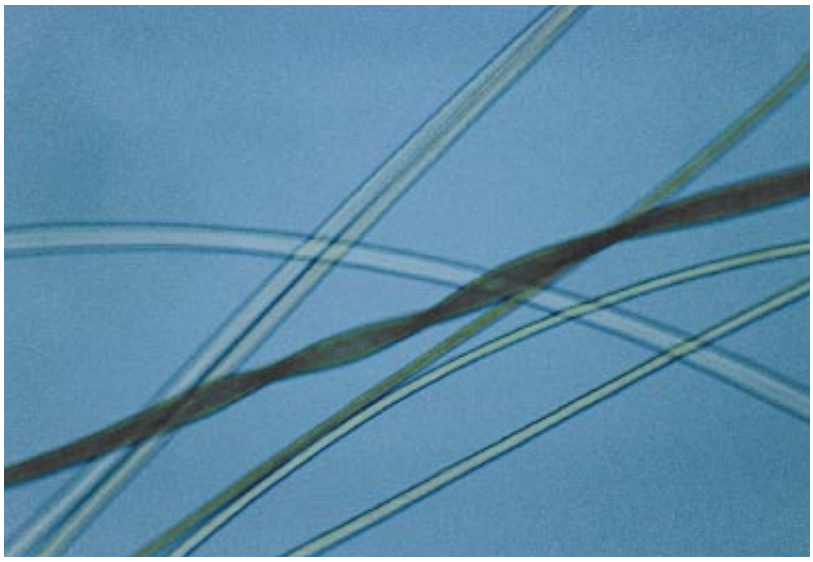

5.60

Figure 5.60. Microscopic examination of the hair shows the typical pilo torti. Note the dry fragile twisted hairs with partial breakage. This should not be confused with the apearance of the hair in argininosuccinicaciduria.

5.61

Figure 5.61. The same infant as in Figures 5.56 through 5.59 also had the typical eczema seen in infants with steely-hair syndrome. Pigmentation is often unequal and, additionally, there may be a seborrheic rash.

Chapter 6
Hematology, Jaundice, and Oncology

The neonate may suffer from hematologic conditions involving the erythrocyte, platelet, leukocyte, coagulation, and thrombosis. Many of these disturbances are life-threatening, some are primary, and some reflect other diseases. Jaundice is a common problem in the neonate, and it is rarely life-threatening or debilitating. It is of particular concern, because it frequently occurs in otherwise healthy infants, usually because the liver cannot clear sufficient bilirubin from the plasma. Neoplasias in the neonate are rare but frequently are unique in their diagnosis and treatment. They may be composed of persistent embryonal or fetal tissue, and may be associated with abnormalities of growth and congenital anomalies. The problems presented by these conditions relate to the difficulty in diagnosing a neoplasm from a poorly differentiated fetal tissue, and in the potential for long-term sequelae in the therapeutic interventions required.

6.1

Figure 6.1. This infant had blood in the stools on the first day of life. The Apt test was positive, making the diagnosis one of ingested maternal blood.

6.2

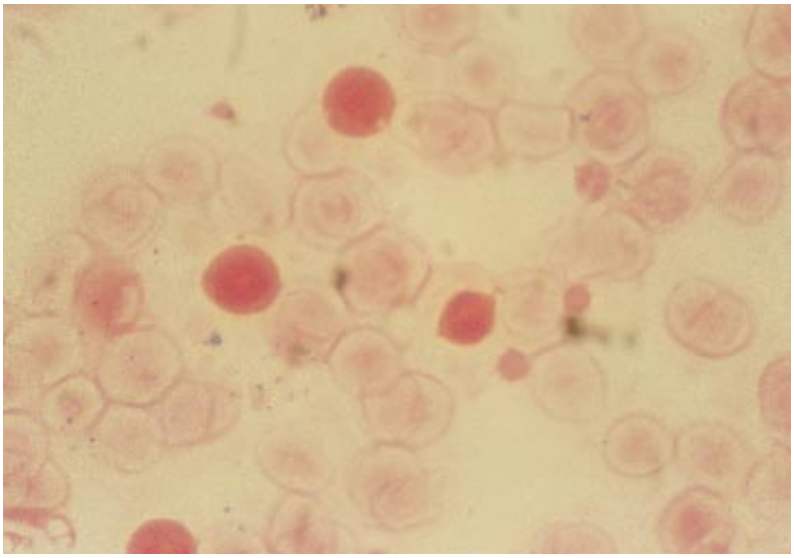

Figure 6.2. In infants with a feto-maternal hemorrhage, the Kleihauer-Betke test on maternal blood is positive as shown in this microscopic slide. Acid elution of maternal hemoglobin results in lysis of the red blood cells (creating "ghost" erythrocytes), while fetal red blood cells resist acid hydrolysis.

6.3

Figure 6.3. At the age of 3 days, this infant developed hematuria and bloody stools as a result of hemorrhagic disease of the newborn. This is due to a transitory prothrombin and vitamin K deficiency. The Apt test in such an infant would be negative for maternal blood. The condition is more common in black infants.

6.4

Figure 6.4. Hematoma of the right cheek following birth trauma. With a large hematoma there can be massive blood loss and trapping of platelets resulting in thrombocytopenia.

6.5

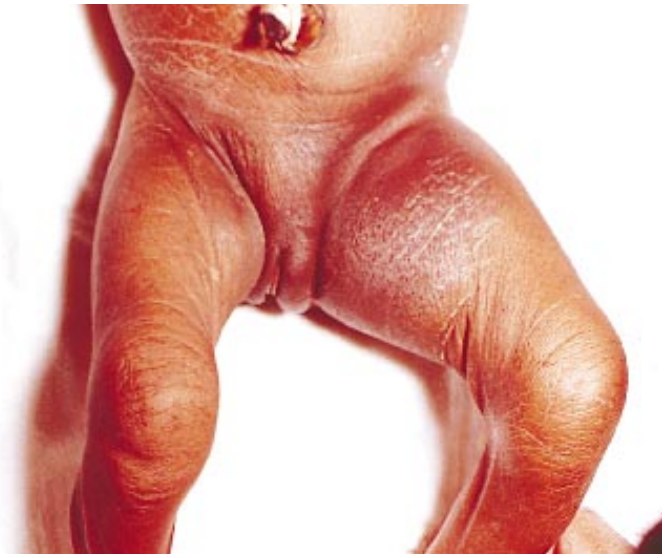

Figure 6.5. Large hematoma of the left thigh and groin.

6.6

Figure 6.6. Hematoma with ecchymosis of the neck and face of an infant following birth trauma.

6.7

Figure 6.7. Petechiae on the forearm of an infant following severe birth asphyxia. The infant's platelet count was 90,000/mm^3 and returned to normal within a week.

6.8

Figure 6.8. Note the slate gray discoloration of the skin in an infant with methemoglobinemia at the age of 9 days. Total hemoglobin was 10.4 gm/dL with 11% methemoglobin. The infant had been treated with intravenous nitrofurantoin for a urinary tract infection. There are many causes of methemoglobinemia in the neonate (see this volume, Chapter 1).

6.9

Figure 6.9. Feto-fetal (twin-twin) transfusion syndrome due to a vascular anastamosis in a monochorionic placenta. It results from abnormal placentation in identical twins in whom there is an arteriovenous anastamosis. As a result of the pressure differential, one twin becomes polycythemic and the other twin becomes anemic.

6.10

Figure 6.10. A close-up of the same infants as in Figure 6.9 shows the plethoric recipient twin on the left and pale donor twin on the right. Discordance is defined as a 20% difference in birthweight or a difference in hemoglobin of greater than 5 gm/dL. Morbidity is greater in the recipient twin. There may be intrauterine growth retardation in the donor twin due to a reduced blood supply.

6.11

Figure 6.11. Concordant female twin infants with a marked discrepancy in skin color due to a feto-fetal transfusion syndrome. The anemic twin on the right had a birthweight of 2530 g with a hemoglobin of 15.6 gm/dL and a hematocrit of 46%. The plethoric twin on the left had a birthweight of 2740 g with a hemoglobin of 27.4 gm/dL and a hematocrit of 84%.

6.12

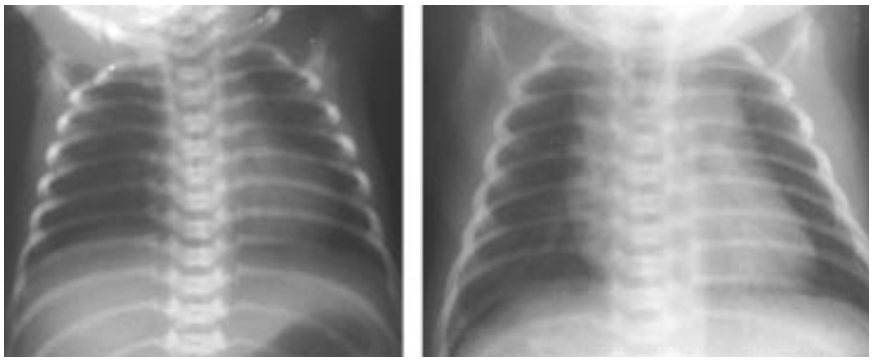

Figure 6.12. Chest radiographs of twin infants with feto-fetal transfusion syndrome. The radiograph on the left of the anemic twin is normal. The radiograph on the right of the polycythemic twin shows the increased pulmonary vascular markings with an enlarged cardiac shadow.

6.13

Figure 6.13. This is a macerated stillborn infant with its placenta markedly enlarged as a result of Rh isoimmunization. There is gross swelling and pallor of all parts of the body and hepatosplenomegaly. Whereas previously isoimmunization was the most common cause of hydrops fetalis, now with the use of Rhogam®, nonimmune causes of hydrops fetalis are much more common.

6.14

Figure 6.14. A pale hydropic newborn with Rh hemolytic disease of the newborn. Note the associated abdominal distension as a result of ascites and hepatosplenomegaly.

6.15

Figure 6.15. Nonimmune hydrops fetalis in an infant with congenital cytomegalovirus infection. Nonimmune hydrops fetalis has numerous causes including primary myocardial failure (cardiac malformation or arrhythmia), high output failure (anemia or arteriovenous malformation) and congenital infections.

6.16

Figure 6.16. Hydrops fetalis in an infant with ß-glucuronidase deficiency.

6.17

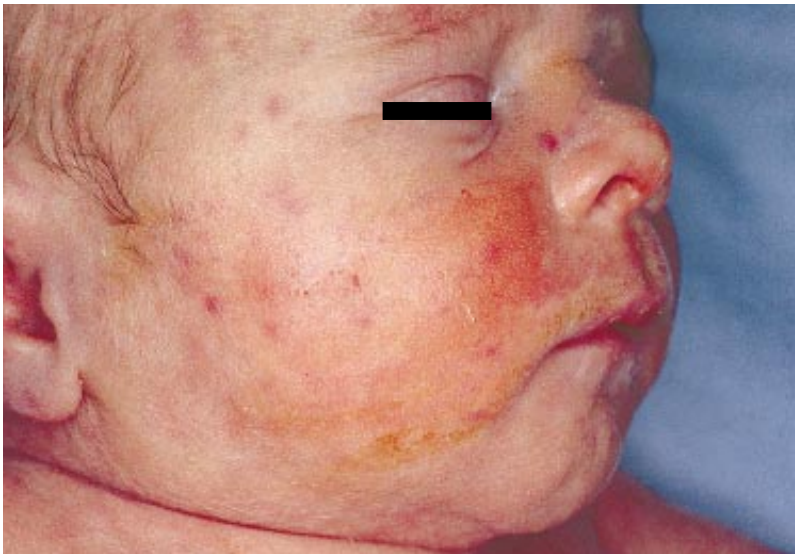

Figure 6.17. Purpuric lesions of the face and chin in an infant with Rh hemolytic disease of the newborn. Purpuric lesions represent extramedullary hematopoiesis and give rise to the "blueberry muffin" appearance. The blueberry muffin appearance may be seen in infants with other conditions. Differential diagnosis includes ABO incompatibility, TORCH infections, and isoimmune thrombocytopenia.

6.18

Figure 6.18. Purpuric lesions on the back of the same infant as in figure 6.17 with Rh hemolytic disease are the result of dermal erythropoiesis.

6.19

Figure 6.19. This infant with ABO incompatibility presented with the typical "blueberry muffin" appearance and hyperbilirubinemia. He had severe hemolysis with a bilirubin level of 18 mg/dL. The blueberry muffin appearance, due to extramedullary hematopoiesis, improved over the course of a few days.

6.20

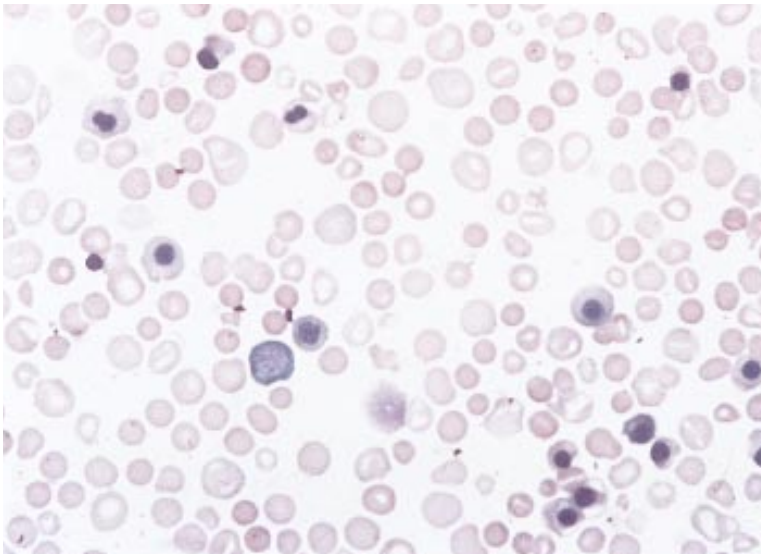

Figure 6.20. Photomicrograph of a peripheral blood smear in the same infant with a Coombs' positive ABO incompatibility. Note the microspherocytes, nucleated red blood cells, target cells, and polychromasia.

6.21

Figure 6.21. Skin coloration of infants in the first day of life who are not related. The infant on the left is jaundiced as a result of Rh hemolytic disease of the newborn. In comparison, note the normal pink skin of the infant with a large cephalhematoma on the right. The cephalhematoma can be a later cause of hyperbilirubinemia.

6.22

Figure 6.22. Markedly jaundiced appearance of the infant pictured on the left. This infant presented from home with a bilirubin of 50.6 mg/dL. Jaundice was the result of an anti-C alloimmunization. The infant on the right is normal.

6.23

Figure 6.23. The same infant as in Figure 6.22 at age 3 days had a hematocrit of 23.7% with an unconjugated bilirubin of 8.4 mg/dL and a conjugated bilirubin of 4.8 mg/dL. At 4 days of age the infant's hematocrit had fallen to 18.5% and the conjugated bilirubin had increased to 50.6 mg/dL with an unconjugated level of 4.2 mg/dL.

6.24

Figure 6.24. This infant with hemolytic disease of the newborn (left) developed persistent jaundice as a result of obstruction of bile channels (inspissated bile syndrome). Note the difference in coloration of the infant as compared to the normal infant on the right.

6.25

Figure 6.25. Opisthotonic posturing in an infant with erythroblastosis fetalis. Note the neck retraction and the hypertonic extensor spasm of the limbs with scissoring. This is the result of the development of kernicterus due to severe neonatal unconjugated hyperbilirubinemia.

6.26

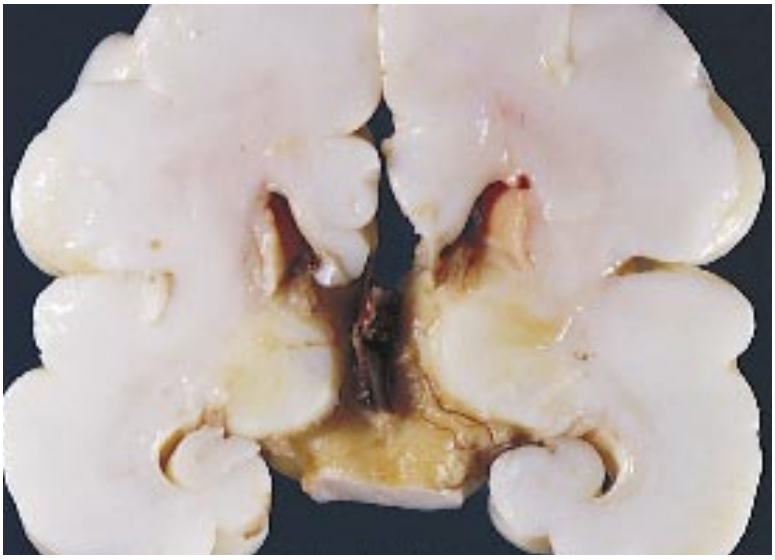

Figure 6.26. A section through the brain of a neonate who died from *Escherichia coli* sepsis shows yellow discoloration of the basal ganglia. This staining is referred to as kernicterus. Injury to the basal ganglia results in opisthotonos. Early manifestations of kernicterus are lethargy, hypotonia, poor feeding, fever, seizures, and possibly death. Late manifestations include spasticity, choreoathetosis, and deafness.

6.27

Figure 6.27. This infant with hyperbilirubinemia developed a fine erythematous maculopapular rash involving the trunk while being treated with phototherapy. This "bilirubin rash" improves rapidly. The bronze baby syndrome is a side effect of phototherapy when used in infants with an elevated direct reacting bilirubin. Natural skin color is restored after several months.

6.28

Figure 6.28. Erythema and edema of the trunk and neck of this infant with "phototherapy sunburn" as a result of placement under daylight fluorescent bulbs for hyperbilirubinemia. Phototherapy may cause hypopigmented spots in areas of the skin that are covered (for example, by electrode patches for monitoring).

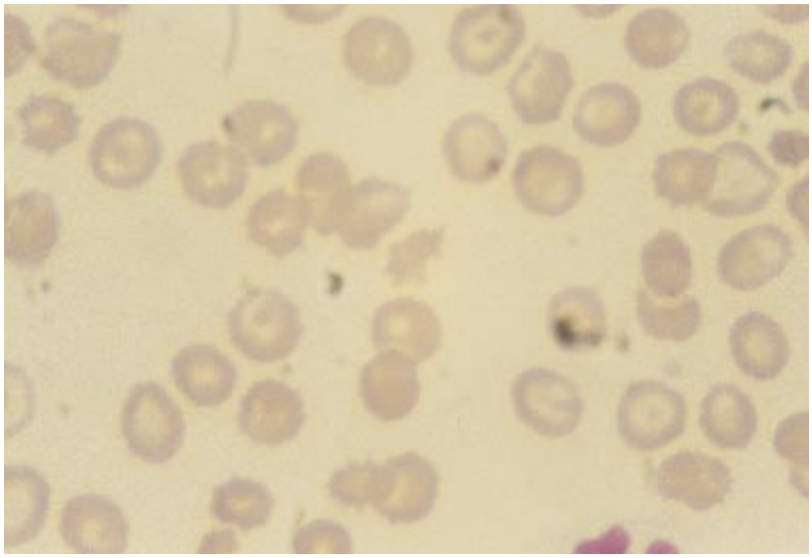

6.29

Figure 6.29. Peripheral blood smear from an infant with acanthocytosis due to vitamin E deficiency. Note the presence of target and burr cells. (Gresik, V.)

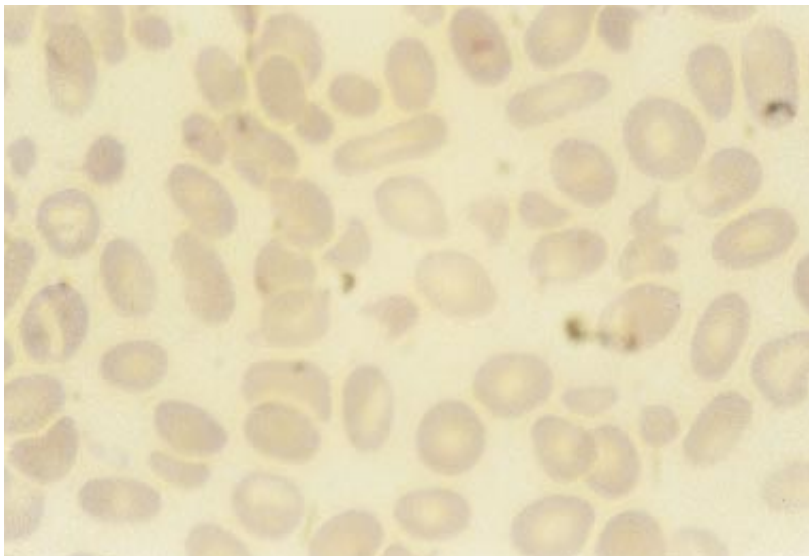

6.30

Figure 6.30. Peripheral blood smear from an infant with congenital elliptocytosis. This may be a cause of anemia or jaundice in the neonate. (Gresik, V.)

6.31

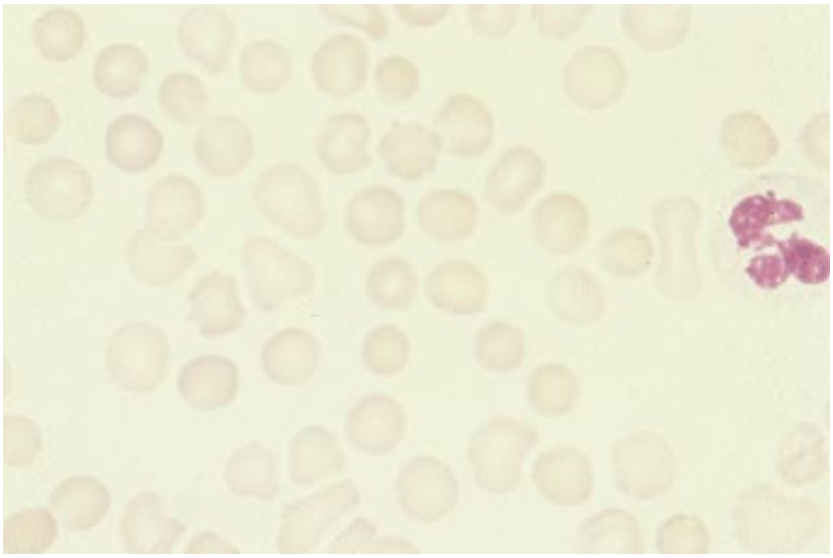

Figure 6.31. Peripheral blood smear from an infant with congenital hereditary spherocytosis. Note the microcytosis. (Gresik, V.)

6.32

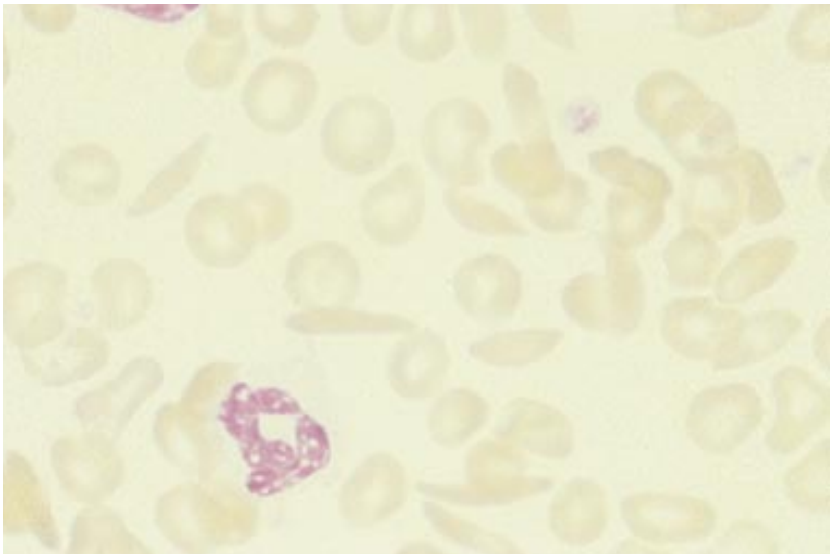

Figure 6.32. Peripheral blood smear from an older infant with sickle cell anemia. Neonates with sickle cell anemia do not have the typical sickling of cells due to the large percentage of fetal hemoglobin. (Gresik, V.)

6.33

Figure 6.33. Discoloration of the buttocks and thighs in an infant at the age of 2 days with purpura fulminans as a result of sepsis. Purpura fulminans, a nonthrombocytopenic purpura, is characterized by acute, severe, often rapidly fatal, hemorrhagic infarction and necrosis of the skin. In the neonate, acquired or congenital protein C and protein S deficiency have been shown to cause purpura fulminans. It is usually triggered by a preceding infectious process in children.

6.34

Figure 6.34. Discoloration of the face and necrosis of the fingertips in the same infant as in Figure 6.33 with purpura fulminans at the age of 10 days. Purpura fulminans is characterized by symmetrically distributed localized cutaneous ecchymoses, often with sharp irregular borders on the extremities. Lesions enlarge rapidly, coalesce, and develop central necrosis with hemorrhagic blebs and a raised edge with surrounding erythema. Visceral involvement with hematuria or gastrointestinal bleeding may occur.

6.35

Figure 6.35. This infant with congenital monocytic leukemia was admitted to the hospital at age 20 days. Leukemic lesions are visible on the face of this infant and the peripheral blood smear demonstrated a marked leukocytosis and thrombocytopenia. The bone marrow confirmed the diagnosis of congenital monocytic leukemia.

6.36

Figure 6.36. Skin lesions (leukemia cutis) on the feet and face of the same infant as in Figure 6.35 with congenital monocytic leukemia. The cutaneous lesions occur as discrete pink, red-brown, or purple macules, papules, or tumors. The tumors of monocytic leukemia tend to be large and purplish or "plum-colored," and are firm solid masses.

6.37

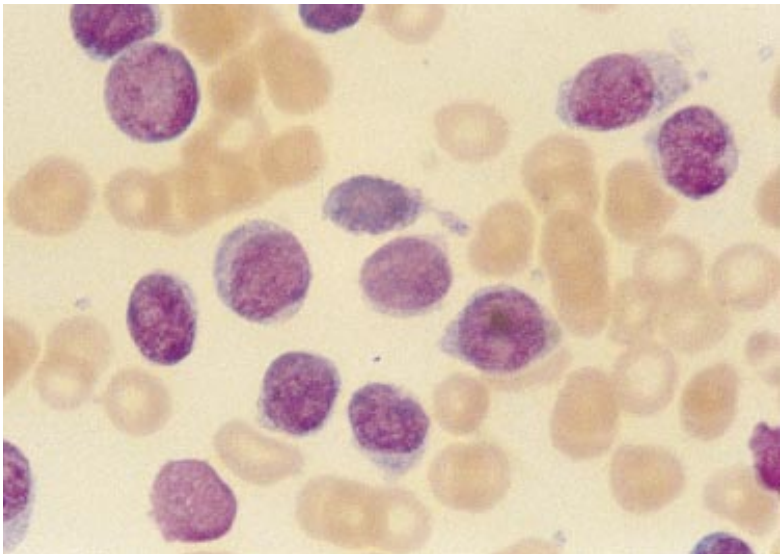

Figure 6.37. Bone marrow smear from the same infant as in Figures 6.35 and 6.36 showing numerous large immature monoblasts.

6.38

Figure 6.38. Petechiae, ecchymoses, leukemia cutis, and hepatosplenomegaly in an infant with lymphoblastic leukemia. The peripheral white blood cell count in this infant was 99,000/dL, of which 60% were blasts and the platelet count was 19,000/dL. The bone marrow confirmed the diagnosis of lymphoblastic leukemia.

6.39

Figure 6.39. Skin nodules on the leg of the same infant as in Figure 6.38 with congenital lymphoblastic leukemia. Chromosome analysis of abnormal lymphoblasts showed a translocation between chromosomes 4 and 11.

6.40

Figure 6.40. Supine and prone views of an infant with distortion of the left facial structures as the result of a large mass. Pathologic specimen confirmed the diagnosis of neuroblastoma which is the most common malignant tumor in infancy. The most common presentation is an abdominal mass. Cutaneous features are present in 50% of newborn infants with this disorder. (Cabrera-Meza, G.)

6.41

Figure 6.41. Skin metastases in the infant shown in figure 6.42 with congenital neuroblastoma at the age of six weeks. The nodules are characteristic in that they are firm, nontender, blue or grayish blue metastastic nodules that due to the release of catecholamines tend to blanch and develop a surrounding halo of erythema within 2 to 3 minutes after being palpated, stroked, or rubbed. (Cabrera-Meza, G.)

6.42

Figure 6.42. Metastases involving the orbit and scalp in the same infant as in Figure 6.41 with congenital neuroblastoma at the age of 6 weeks. The infant died at the age of 2 months. As a result of periorbital ecchymoses, which may occur from the orbital metastases, these infants may have the appearance of "raccoon eyes." (Cabrera-Meza, G.)

6.43

Figure 6.43. Midline cystic mass at the base of the spine. Surgical pathologic specimen confirmed the presence of a teratoma.

6.44

Figure 6.44. The most common solid tumor presenting in neonates at birth is a sacrococcygeal teratoma. Because the tumor arises from the coccyx, the spinal column and canal are spared. This infant has a very small midline spinal swelling. These may grow caudally, become very large, and displace the anus and genitalia. Pelvic extension may occur.

6.45

Figure 6.45. In this female infant there is a larger sacrococcygeal teratoma. These tumors are much more common in females. Differential diagnosis includes lipoma, neuroblastoma, cystic lymphangioma, and hemangioma.

6.46

Figure 6.46. This 36-week-gestation premature infant with a large sacrococcygeal teratoma was delivered vaginally. Prompt surgical excision of the mass is advisable because of possible malignant transformation. Before the 4th month of life, the malignancy rate is 6%; between the 4th month and the 5th year of life, the malignancy rate increases to 50%.

6.47

Figure 6.47. Close-up view of the same giant sacrococcygeal teratoma as in Figure 6.46 showing involvement of anus and genitalia. Pathologic specimen showed immature yolk sac elements with malignant changes.

6.48

Figure 6.48. Giant sacrococcygeal teratoma in a male infant.

6.49

Figure 6.49. Complete surgical resection of the sacrococcygeal teratoma of the same infant as in Figure 6.48. Pathologic specimen was benign and the infant did well.

6.50

Figure 6.50. This female infant presented with a midline sacral mass which proved to be a chordoma. The infant also had a lymphangioma of the left upper extremity.

6.51

Figure 6.51. The same infant as in Figure 6.50 showing the edematous left upper extremity associated with the lymphangioma.

6.52

Figure 6.52. A term infant presented at birth with a large soft tissue mass (4 cm by 4 cm) protruding from the right orbit. An MRI showed a large irregular solid soft tissue mass which appeared to arise from or encompass and largely destroy the right globe. The retrobulbar fat was preserved, and the mass did not enter the intracranial space. On pathologic examination there was a malignant, primitive, embryonic tumor that had arisen in association with a congenital hamartomatous malformation of the globe.

6.53

Figure 6.53. This neonate presented with a tumor involving the penile skin, the bladder, and the anal mucous membranes. Surgical removal showed this to be a rhabdomyosarcoma of the penis. The infant had a recurrence and died at the age of 3 years.

6.54

Figure 6.54. The left figure shows a mass involving the right ear of an infant. The biopsy diagnosis was myofibroma. The right figure is a view of the same ear 3 weeks later with regression without intervention. Congenital infantile myofibromatosis may present with multiple lesions that usually regress spontaneously or may present in a generalized form in which there is visceral involvement with a mortality of about 50%.

6.55

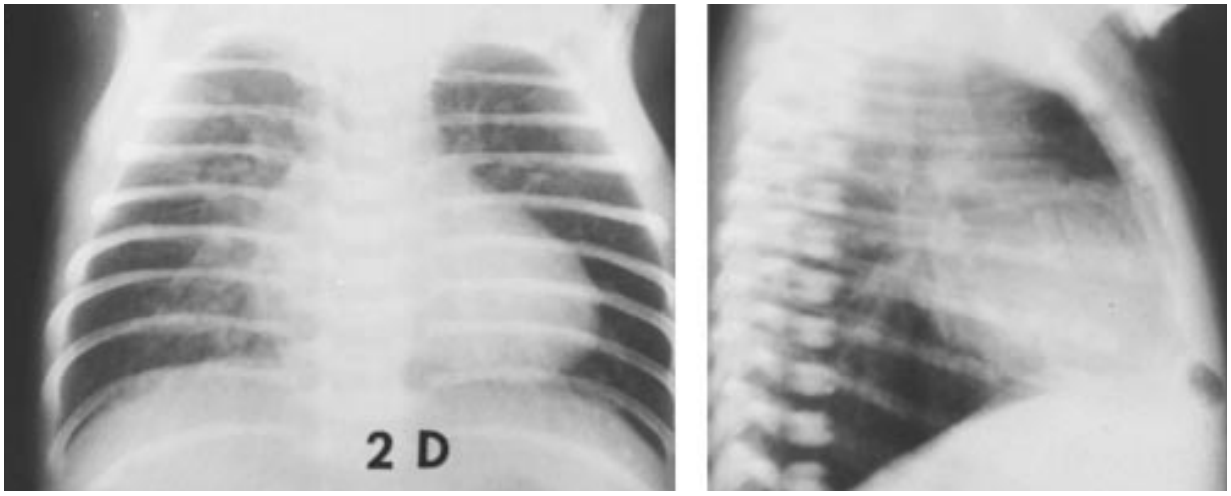

Figure 6.55. The anteroposterior and lateral chest radiographs in an infant with the DiGeorge syndrome. Note the absence of the thymic shadow on both projections. In the DiGeorge syndrome, an isolated T cell deficiency occurs as a result of a congenital malformation of the 3rd and 4th branchial arches. The acronym CATCH 22 syndrome lists the findings seen in DiGeorge syndrome: *c*ardiac defects, *a*bnormal facies, *t*hymic hypoplasia, *c*left palate, *h*ypocalcemia, and 22q11 deletion. The same chromosome abnormality—a deletion at chromosome 22q11 is manifested in velocardiofacial syndrome or Shprintzen's syndrome.

Index